

**Biofilm Engineering with a Twist: Novel Helical Polymer-based
Systems for Developing Biocatalytic *E. coli* K12 Biofilms**

by
Omar Nicholas Huneidi



**UNIVERSITY OF
BIRMINGHAM**

A thesis submitted to the University of Birmingham for the degree of
DOCTOR OF PHILOSOPHY

School of Chemistry

College of Engineering and Physical Sciences

University of Birmingham

UNIVERSITY OF
BIRMINGHAM

University of Birmingham Research Archive

e-theses repository

This unpublished thesis/dissertation is copyright of the author and/or third parties. The intellectual property rights of the author or third parties in respect of this work are as defined by The Copyright Designs and Patents Act 1988 or as modified by any successor legislation.

Any use made of information contained in this thesis/dissertation must be in accordance with that legislation and must be properly acknowledged. Further distribution or reproduction in any format is prohibited without the permission of the copyright holder.

Acknowledgements

To say that the past few years have been challenging would be a severe understatement. Numerous obstacles, big and small, presented themselves throughout where at many times the thought of reaching these final stages felt impossible. Fortunately, I have been honoured to have the pleasure to work with some amazing people throughout the years to make this seemingly impossible task a reality.

First and foremost, I am immensely grateful to my supervisors, Paco, and Tim, for their exceptional guidance, mentorship, and patience. Their expertise, insights, and dedication have been instrumental in shaping my research and intellectual growth. I am grateful for their constant encouragement and belief in my abilities, and I was incredibly lucky to have their unwavering support and understanding even at the toughest of times. I would also like to acknowledge the support and assistance provided by the faculty staff in the Departments of Chemistry (Cécile (NMR), Alan (HPLC), and Chris (MS)) and Biochemical Engineering (Ronnie, Zoe, and Adam). Their expert knowledge and support were instrumental in facilitating my research work.

Though we are now all scattered throughout the world I would like to thank former members of the Paco group; Alex, Amit, Tom, Pavan, Andrey, Sameh, Charlotte, Carlos and Teyfik. From the Overton group I would like to thank Ana, Alex, and Parissa. All the hardships were made so much easier through working with such welcoming, genuine people and I am honoured to call them my friends. I would also like to give a notable mention to Menisha, who has

continually supported every step of the way. I can say with certainty that I am only here today due to her selflessness and reassurance, and for that I will always be thankful.

Lastly, I would like to express my deepest gratitude to my family. Their unconditional love, unwavering support, and sacrifices have been the cornerstone of my academic journey from a small boy to the man I am today. I am forever grateful for their belief in me and their constant encouragement.

I am grateful to the BBSRC and MIBTP, for their financial support, which enabled me to pursue my doctoral studies and carry out the research presented in this thesis.

Abstract

In recent years, bacterial biofilms have emerged as a promising tool to exploit in biotechnology. Prospective applications include but not limited to bioremediation, agriculture, energy generation, and catalysis. Encapsulation of cells by an extracellular matrix (ECM) helps protect the cells from deleterious conditions such as pH and temperature extremes or inclusion of organic solvents. The protective nature of the ECM greatly expands the potential settings where cell-based biotechnology can be applied which will facilitate the shift towards renewable green chemical practices. As such, there is a plethora of research that focusses on optimisation of biofilm formation either through genetic engineering or development of novel materials for bacterial adhesion. The research undertaken in this thesis focusses on the development and screening of novel polymeric materials for the nucleation of *E. coli* biofilms. Recent work in our lab suggested that a biofilm phenotype is enhanced following aggregation by synthetic polymers. In this project a novel helical poly(acetylene) material – poly(propargyl hydrazine carboxamide) (P1), was synthesised as a scaffold for material library generation following reaction with aldehydes using click chemistry. Synthesis of P1 was optimised to maximise yields and the cis-character to ensure helical adoption. *E. coli* MC4100 was treated with a library of P1 derivatives to induce biofilm formation. Polymer treatment was essential to aggregate formation and aggregate size was positively correlated with polymer hydrophobicity. Generally, polymer treatment significantly enhanced curli and colanic acid production, though no notable change in PNAG was noted. Following this, the biocatalytic ability of the artificially induced *E. coli* biofilms was tested regarding the formation of 5-fluorotryptophan. Several biofilm cultures had significantly higher yields compared to equivalent planktonic cultures.

Table of Contents

Table of figures	9
Chapter 1 – Literature Review – an introduction to biofilms, their applications and, engineering strategies with polymers.	13
1.0 Project Aims	14
1.1 A brief introduction to biofilms	16
1.2 Biotechnological applications of biofilms	19
1.2.1 Agriculturally relevant biofilms	20
1.2.2 Bioremediation	20
1.2.3 Microbial fuel cells (MFCs)	22
1.2.4 Biocatalytic biofilms	25
1.3 Mechanisms of bacterial adhesion and development into biofilms	26
1.3.1 Multi-step biofilm model	26
1.3.2 Role of electrostatics in bacterial adhesion.....	28
1.3.3 Bacterial membrane components and their role in non-specific adhesion.....	33
1.3.4 Reversible cell attachment	35
1.3.5 Irreversible attachment in <i>E. coli</i>	37
1.3.6 Biofilm maturation & exopolysaccharide production	39
1.4 Engineering bacterial aggregation with polymers	42
1.4.1 Polymer-induced aggregation: Mechanisms-of-action	43
1.4.2 Aggregation by cationic polymers	46
1.4.3 Aggregation by glycopolymers	51
1.4.4 Non-specific polymer bacteria interactions	54
1.5 Conclusions	57
1.6 Bibliography	59
Chapter 2 – Synthesis, characterisation, and post-polymerisation modification of a novel poly(carbamoylhydrazine-1-carboxylate acetylene) scaffold.....	66
2.0 Introduction	67
2.1 Materials & Methods.....	71
2.1.1 General Procedures	71
2.1.2 t-butyl 2-(prop-2-yn-1-ylcarbamoyl)hydrazine-1-carboxylate (M1)	72
2.1.3 Poly(t-butyl 2-(carbamoyl)hydrazine-1-carboxylate acetylene) (P1).....	73
2.1.4 Acyl hydrazone post-polymerisation functionalisation procedures	74
2.2 Polymer design considerations and <i>in silico</i> studies	75
2.3 Monomer synthesis	78
2.4 Polymer synthesis.....	81
2.4.1 Synthetic screening	81
2.4.2 Scaled-up polymerisation & characterisation	84
2.5 Material Library generation	86
2.6 Probing polymer secondary structure	93
2.6.1 Thermochemical analyses	93
2.6.2 Temperature and solvent effects on helical adoption/ stability.....	95
2.6.3 Probing substituent effects on helical stability	98
2.7 Conclusions	100

2.8 Bibliography	101
2.9 Supplementary information.....	103
Chapter 3 – Screening <i>E. coli</i> MC4100 aggregation & biofilm development with a novel library of aldehyde functionalised poly(propargyl hydrazine carboxamide) polymers.....	120
3.0 Introduction	121
3.1 Materials & Methods.....	124
3.1.1 General polymer treatments of <i>E. coli</i> cultures	124
3.1.2 Aggregate sizing analysis assays	124
3.1.3 Turbidimetry assays	125
3.1.4 Crystal violet aggregation assay.....	125
3.1.5 <i>csgB::GFP</i> promoter activity assay	126
3.1.6 Plate surface-adherence assay.....	126
3.1.7 ECM extraction from polymer-microbe complexes:	126
3.1.8 Glucosamine quantification (MBTH) assay.....	127
3.1.9 Fucose quantification assay	128
3.1.10 Metabolic activity assays	129
3.1.11 Membrane stress assay with 1-N-phenylnaphthylamine (NPN).....	129
3.1.12 Membrane stress assay with <i>spy::gfp</i>	129
3.1.13 Phase diagram construction.....	130
3.2 Results & Discussion	132
3.2.1 Determining cell aggregation by poly(acetylenes)	132
3.2.1.2 Turbidimetric analysis of bacterial aggregates.....	136
3.2.3 Determining aggregated biomass formation in polymer-treated cultures.	143
3.2.4 Determining biofilm production in polymer-treated cultures	150
3.2.4 Curli expression	151
3.2.5 Exopolysaccharide production in bacterial aggregates.....	158
3.2.6 Probing membrane stress responses in polymer-treated cultures.....	168
3.2.7 Probing aggregative mechanism-of-action.....	181
3.3 Conclusions	190
3.4 Bibliography	192
3.5 Appendix	196
Chapter 4 – Testing biocatalytic formation of 5-fluoro-L-tryptophan with recombinant polymer-induced biofilms.....	205
4.0 Introduction	206
4.1 Experimental	211
4.1.1 Bacterial strains and plasmids	211
4.1.2 Culture set-up.....	211
4.1.3 Biocatalytic Screening	211
4.1.4 HPLC Analysis of Reaction Buffer Supernatant.....	212
4.2 Results and Discussion	213
4.3 Conclusions	224
4.4 Bibliography	225
4.5 Appendix.....	227
Chapter 5 – Conclusions & Future Work.....	235

List of abbreviations

- NMR – nuclear magnetic resonance
- HPLC – high performance liquid chromatography
- FTIR – Fourier transform infrared red spectroscopy
- UV-Vis – Ultraviolet-visible spectroscopy
- TGA – Thermal gravimetric analysis
- DSC – Differential scanning calorimetry
- PSA – Particle size analysis
- EtOAc – ethyl acetate
- DMF – dimethyl formamide
- DMSO – dimethyl sulfoxide
- DCM – dichloromethane
- THF – tetrahydrofuran
- CDI – 1,1-carbonyl diimidazole
- TFA – trifluoroacetic acid
- NaOH – sodium hydroxide
- Boc – tert-butyloxycarbonyl
- M1 – t-butyl 2-(prop-2-yn-1-ylcarbamoyl)hydrazine-1-carboxylate
- P1 – Poly(t-butyl 2-(carbamoyl)hydrazine-1-carboxylate acetylene)
- MMFF94 – Merck Molecular Forcefield
- ICA – imidazole-4-carboxaldehyde
- AFP – 2-amino-3-formyl pyridine
- IVA – isovaleraldehyde

- IND – indole-3-carboxaldehyde
- BN – benzaldehyde
- PIP – 4-formyl piperidine
- FPBA – 4-(4-formyl-3,5-dimethoxyphenoxy)butanoic acid
- UR – 5-formyluracil
- PEG4 – PEG4-aldehyde
- SAL – 5-formyl salicylic acid
- AC – acetaldehyde
- PYRR – 2-pyrrole carboxaldehyde
- THB – 2,4,6-trihydroxybenzaldehyde
- PFB – pentafluorobenzaldehyde
- PMC – polymer-microbe complex
- CV – crystal violet
- CA – colanic acid
- PNAG – poly-n-acetyl glucosamine
- MBTH – 3-Methyl-2-benzothiazolinone-hydrazonehydrochloride
- DBM – dried biomass
- GFP – green fluorescent protein
- SPY – spheroplast protein Y
- ANOVA – analysis of variance

Table of figures

FIGURE 1. 1 WORKFLOW SCHEME OF THE RESEARCH UNDERTAKEN IN THIS THESIS.	15
FIGURE 1. 2 SCHEME SHOWING VARIOUS BIOREMEDIATORY ACTIVITIES POSSIBLE IN A MIX-SPECIES BIOFILM (NOT DRAWN TO SCALE). PRODUCED IN BIORENDER.	22
FIGURE 1. 3 SCHEMATIC DIAGRAM OF A GENERAL MICROBIAL FUEL CELL (MFC) DESIGN (NOT DRAWN TO SCALE). PRODUCED IN BIORENDER.	24
FIGURE 1.4. CARTOON DIAGRAM SHOWING THE FORMATION OF DENSE COUNTER-ION (STERN) LAYER FOLLOWED AN INCREASINGLY DIFFUSE LAYER OF COUNTER IONS. THE ELECTROSTATIC POTENTIAL OF AN OBJECT (YELLOW LINE) REDUCES WITH INCREASED DISTANCE FROM THE SURFACE UNTIL REACHING EQUILIBRIUM WITH THE BULK PHASE (DEBYE LENGTH). NOT DRAWN TO SCALE. PRODUCED IN BIORENDER.	29
FIGURE 1.5 DIAGRAM REPRESENTING THE DISTANCE DEPENDENCY ON COLLOIDAL STABILITY/ BACTERIAL AGGREGATION. BLUE LINE = ELECTROSTATIC REPULSION (TOP); RED LINE = VDW ATTRACTION (BOTTOM); GREEN LINE = NET FORCE. I) PARTICLE DISTANCE TOO LARGE TO EXPERIENCE ANY INTERPARTICLE REPULSION/ ATTRACTION. II) AS DISTANCES REDUCE, PARTICLES ENTER A PRIMARY ENERGY MINIMUM CAUSING REVERSIBLE AGGLOMERATION. III) AT CLOSER PROXIMITY THE ELECTRICAL DOUBLE LAYER OVERLAP INCREASES THE REPULSIVE FORCES PRODUCING AN ENERGY BARRIER, THE SIZE OF WHICH DICTATES THE COLLOIDAL STABILITY. VARIOUS CELL SURFACE APPENDAGES LIKE PILI OR CURLI HELP OVERCOME THIS BARRIER AS THEY PROJECT FROM THE CELL WITH A SMALLER DIAMETER IV) ATTRACTIVE FORCES OVERCOME ENERGY BARRIER (E.G. KINETIC ENERGY, LIGAND BINDING OR HYDROPHOBIC INTERACTION) AND PARTICLES IRREVERSIBLY AGGLOMERATE. NOT DRAWN TO SCALE. PRODUCED IN BIORENDER.	30
FIGURE 1. 6. CARTOON DIAGRAM SHOWING THE IMPORTANCE OF CONDITIONING FILM FORMATION IN BACTERIAL ADHESION. IN THE ABSENCE OF CF FORMATION BACTERIA EXPERIENCE ELECTROSTATIC REPULSION DUE TO LIKE-CHARGES. AFTER SURFACE CONDITIONING BY PROTEINS, EXPOSURE OF INTERNAL HYDROPHOBIC RESIDUES AND/OR CATIONIC AMINO ACIDS MASK THE REPULSIVE ANIONIC CHARACTER PERMITTING SURFACE ADHERENCE.	33
FIGURE 1. 5. LEFT - CARTOON OF GRAM-NEGATIVE E. COLI CELL MEMBRANE COMPONENTS THAT ARE IMPLICATED IN BACTERIAL ADHESION/ BIOFILM FORMATION. RIGHT - DEPICTION OF THE INTERACTION BETWEEN SURFACE STRUCTURES ON A BACTERIUM AND A SURFACE. A) A SMOOTH BACTERIUM AT ITS CLOSEST PROXIMITY TO A SURFACE; B) THE SAME BACTERIA ADORNED WITH SMALLER SURFACE STRUCTURES SUCH AS CURLI OR TYPE-1 PILI. DASHED LINE = DEBYE LENGTH. NOT DRAWN TO SCALE. PRODUCED IN BIORENDER.	35
FIGURE 1.4 CARTOON SCHEMATIC OF TYPE-1 PILUS INCLUDING THE MANNOSE SPECIFIC LECTIN FIMH AT THE TERMINUS. PRODUCED IN BIORENDER.	38
FIGURE 1. 6. FLOCCULATION MECHANISMS. A) HIGH MOLECULAR WEIGHT POLYMERS CROSS-LINK INDIVIDUAL BACTERIAL TOGETHER CAUSING AGGREGATION. B) CHARGE NEUTRALISATION BY SHORT CATIONIC POLYMERS SCREENS DOUBLE-LAYER REPULSION CAUSING AGGREGATION. NOT DRAWN TO SCALE. PRODUCED IN BIORENDER.	44
FIGURE 1.7 SCHEMATIC OF POLYMER-INDUCED AGGREGATION FROM DEPLETION MECHANISM. DASHED LINES REPRESENT EXCLUSION ZONES SURROUNDING INDIVIDUAL BACTERIA AND BLACK DOTS REPRESENT POLYMER CHAINS IN SOLUTION. NOT DRAWN TO SCALE. PRODUCED IN BIORENDER.	45
FIGURE 1.8. CATIONIC POLYMERS USED FOR BACTERIAL AGGREGATION AS REPORTED IN LITERATURE AND DISCUSSED IN THIS WORK.	49
FIGURE 1.9 SCHEMATIC REPRESENTATION OF BACTERIAL INSTRUCTED POLYMERISATION AND EFFECT ON BACTERIAL AGGREGATION BEHAVIOUR. NOT DRAWN TO SCALE. PRODUCED IN BIORENDER.	50
FIGURE 1.10. AGGREGATION OF E. COLI INDUCED BY MANNOSE DERIVED GLYCOPOLYMERS (CENTRE). LITERATURE EXAMPLES OF GLYCOPOLYMERIC MATERIALS TESTED AS BACTERIAL AGGLUTINATION AGENTS. PRODUCED IN BIORENDER.	52
FIGURE 1.11. SCREENING OF BIOFILM FORMATION IN E. COLI MC4100 USING HYDROPHOBIC POLYMERS. TAKEN FROM REF ¹⁷⁴	57

FIGURE 2.1. POSSIBLE BACKBONE STEREOCHEMISTRY ADOPTED IN POLY(ACETYLENES). ONLY CIS-CIS AND CIS-TRANS POLYMERS CAN ADOPT A HELICAL SECONDARY STRUCTURE.	69
FIGURE 2.2 TWO POLYMERISATION MECHANISMS OF RH-BASED POLYMERISATION. 2,1-INSERTION PRODUCES CIS-REGULAR POLY(ACETYLENES); CARBENE METATHESIS PRIMARILY PRODUCES TRANS REGULAR POLY(ACETYLENES).	70
FIGURE 2.3 STRUCTURE OF P1 AND HYDRAZONE FUNCTIONALISED P1-R (TOP). DIAGRAM SHOWING GENERAL STRATEGY OF POST-POLYMERISATION MODIFICATION FOR MATERIAL LIBRARY GENERATION.	76
FIGURE 2.4 SIDE (LEFT) AND TOP VIEW (RIGHT) OF 3D STRUCTURE OF P1-10MER FOLLOWING MMFF94 SIMULATION IN AVOGADRO. SKELETAL STRUCTURE OF P1 SHOWING HYDROGEN BOND FORMATION BETWEEN THE POLYMER SIDE UNITS.	77
FIGURE 2.5 TESTED SYNTHETIC ROUTES FOR M1 PRODUCTION. A) TWO-STEP SYNTHESIS IN H ₂ O & ETOAC; B) ONE-POT SYNTHESIS WITH H ₂ O, ETOAC, OR DMF.	79
FIGURE 2.6 ASSIGNED ¹ H-NMR SPECTRA OF TERT-BUTYL 2-(1H-IMIDAZOLE-1-CARBONYL)HYDRAZINE-1-CARBOXYLATE INTERMEDIATE.	80
FIGURE 2.7. OVERLAYED FTIR SPECTRA OF M1, P1-BOC, AND P1.	84
FIGURE 2.8. ¹ H-NMR SPECTRA OF M1 AND P1. INTEGRATED SPECTRA GIVEN IN THE APPENDIX. (*) SOLVENT PEAKS.	86
FIGURE 2.9 CHEMICAL STRUCTURES OF THE HYDRAZONE FUNCTIONALISED ALDEHYDES COUPLED TO P1 (R) FOR LATER TESTING IN BIOFILM NUCLEATION STUDIES. HETEROCYCLIC ALDEHYDES: IMIDAZOLE-4-CARBOXALDEHYDE (ICA), 2-AMINO-3-FORMYLPYRIDINE (AFP), INDOLE-3-CARBOXALDEHYDE, 2-PYRROLECARBOXALDEHYDE (PYRR), 4-FORMYLPYPERIDINE (PIP), AND 5-FORMYLURACIL (UR). AROMATIC ALDEHYDES: 2,4,6-TRIHYDROXYBENZALDEHYDE (THB), PENTAFLUOROBENZALDEHYDE (PFB), AND BENZALDEHYDE (BN). ALIPHATIC ALDEHYDES: PEG-4-ALDEHYDE (PEG ₄), ACETALDEHYDE (AC), AND ISOVALERALDEHYDE (IVA). ACIDIC ALDEHYDES: 4-(4-FORMYL-3,5-DIMETHOXYPHENOXY)BUTANOIC ACID (FPBA) AND 5-FORMYLSALICYLIC ACID (SAL).	87
FIGURE 2.10 DSC (RED) AND TGA (BLUE) ANALYSIS OF P1-BOC	94
FIGURE 2.11 CARTOON DIAGRAM SHOWING REDUCED MOLECULAR ORBITAL OVERLAP WHEN POLY(ACETYLENES) ADOPTS A HELICAL CONFORMATION (E.G. CIS-TRANS).	96
FIGURE 2.12 TEMPERATURE-DEPENDENT UV-VIS SPECTRA OF P1-BOC IN DMF AND CHCl ₃	98
FIGURE 2.13 OVERLAYED UV-VIS SPECTRA OF P1 FORMULATIONS IN 0.1M K ₂ HPO ₄ /KH ₂ PO ₄ (PH 7) BUFFER. [P1-R] = 1 MM, BASED ON THE MOLARITY OF THE MONOMER UNITS.	98
FIGURE 2.14. ¹³ C-NMR OF P1-BOC FOLLOWING PRECIPITATION INTO HEXANE	111
FIGURE 2.15. ¹ H-NMR OF P1 FOLLOWING DIALYSIS AND LYOPHILISATION	111
FIGURE 3.1. VOLUME SIZE DISTRIBUTIONS OF E. COLI MC4100 FOLLOWING TREATMENT WITH P1 FORMULATIONS (BLUE), ALDEHYDE CONTROLS (RED), DMSO/ACOH SOLVENT (BLACK) AND UNTREATED CULTURES (BLACK). A = ICA; B = AFP; C = ICA; D = IND; E = BN; F = PIP; G = FPBA; H = UR; I = P PEG ₄ ; J = SAL; K = AC; L = PYRR; M = THB; N = PFB; O = SOLVENT TREATED CONTROLS.	133
FIGURE 3.2. CORRELATIONS BETWEEN SIZE DISTRIBUTION DX, WHERE X = 10% (BLUE); 50% (RED); 90% (GREEN) WITH PHYSICOCHEMICAL PARAMETERS OF P1 FORMULATIONS.	135
FIGURE 3.3. SCHEME REPRESENTING HOW AGGREGATION AND SEDIMENTATION OF POLYMER-INDUCED AGGREGATES EFFECTS THE AMOUNT OF TRANSMITTED LIGHT (H = PLANKS CONSTANT; N = FREQUENCY) AND CONSEQUENTLY ITS CHANGE IN OPTICAL DENSITY (OD ₆₀₀) WITH TIME (T). NOT DRAWN TO SCALE. PRODUCED IN BIOENDER.	137
FIGURE 3.4. OD ₆₀₀ MEASUREMENTS WITH TIME OF E. COLI MC4100 TREATED WITH P1 FORMULATIONS (BLUE) AND THEIR RESPECTIVE ALDEHYDE CONTROLS (RED). A = ICA; B = AFP; C = ICA; D = IND; E = BN; F = PIP; G = FPBA; H = UR; I = PEG ₄ ; J = SAL; K = AC; L = PYRR; M = THB; N = PFB. ERROR BARS = S.D. (N = 3).	138
FIGURE 3.5. IMAGES TAKEN OF BUFFERED E. COLI MC4100 CULTURES IN THE PRESENCE OF P1 FORMULATIONS 1 H AFTER INITIAL TREATMENT.	139
FIGURE 3.6. SCATTER PLOTS OF MAXIMUM OPTICAL DENSITY AT 600 NM (OD _{MAX}) AS A FUNCTION OF P1 PHYSICOCHEMICAL PROPERTIES.	142

FIGURE 3.7. CUMULATIVE BIOMASS AS MEASURED BY CRYSTAL VIOLET STAINING (ABSORBANCE @ 550 NM). ONE-WAY ANOVA PERFORMED FOR MULTIPLE PAIRWISE COMPARISONS BETWEEN POLYMER TREATMENT AND SOLVENT CONTROLS. $Q \leq 0.05$ (*); $Q < 0.021$ (**); $Q < 2 \times 10^{-4}$ (***); $Q < 1 \times 10^{-4}$ (****).	145
FIGURE 3.8. SCATTER PLOTS OF CUMULATIVE ABSORBANCE AT 500 NM AS A FUNCTION OF P1 PHYSICOCHEMICAL PROPERTIES.	147
FIGURE 3.9. TOTAL ADHERED BIOMASS ON POLYPROPYLENE MICROWELL PLATE AS MEASURED USING 0.1% CRYSTAL VIOLET.	149
FIGURE 3.10. A - M NORMALISED CURLI PRODUCTION MEASURED IN PROXY THROUGH USE OF EGFP REPORTER PLASMID PJLC-A IN P1 TREATED (0.05 MG ML ⁻¹) E. COLI MC4100 OVER 72 H. (BLUE = POLYMER & RED = ALDEHYDE). DASHED LINE = SD (N = 3). A = ICA ; B = AFP ; C = ICA ; D = IND ; E = BN ; F = PIP ; G = FPBA ; H = UR ; I = PEG4 ; J = SAL ; K = AC ; L = PYRR ; M = THB ; N = PFB ; O = SOLVENT (PINK) & UNTREATED CONTROLS (BLACK).	153
FIGURE 3.11. NORMALISED DATA WITH AVERAGE AND STANDARD DEVIATION OF CSGB ACTIVITY DETERMINED FROM THE AUC OF THE GFP FLUORESCENCE PROFILES OF THE VARIOUS POLYMER (BLUE) AND ALDEHYDE (RED) TREATMENTS. ERROR BARS = S.D. (N = 3). STATISTICAL SIGNIFICANCE TESTED FOR WITH 1-WAY ANOVA AND TUKEY'S MULTIPLE COMPARISONS POST-HOC ANALYSIS. FOR CLARITY ONLY STATISTICALLY SIGNIFICANT ($Q \leq 0.05$) PAIRWISE COMPARISONS BETWEEN THE P1 FORMULATIONS AND THEIR RESPECTIVE ALDEHYDES ARE SHOWN. ALL P1 FORMULATIONS EXCEPT P1-THB PRODUCED A STATISTICALLY SIGNIFICANT INCREASE IN CSGB PROMOTER ACTIVITY RELATIVE TO THE SOLVENT TREATED CULTURES. SEE APPENDIX FOR STATISTICAL ANALYSIS RESULTS.	156
FIGURE 3.12. LINEAR REGRESSION ANALYSES OF TOTAL NORMALISED FUCOSE PRODUCTION DETERMINED BY AUC OF THE TIME-SERIES DATA PLOTTED AS A FUNCTION OF SEVERAL PHYSICOCHEMICAL PARAMETERS OF THE P1 FORMULATIONS. A = CLOGD; B = TPSA; C = POLARISABILITY; D = PKB; E = MOLECULAR WEIGHT (MW). F = CORRELATION BETWEEN TOTAL NORMALISED CSGB ACTIVITY AND TOTAL STAINED BIOMASS (FROM CRYSTAL VIOLET STUDY IN 2.2.1).	157
FIGURE 3.13. A - M COLANIC ACID PRODUCTION IN P1 TREATED E. COLI MC4100 OVER 72 H (BLUE = POLYMER & RED = ALDEHYDE). DASHED LINE = SEM (N = 3). A = ICA ; B = AFP ; C = ICA ; D = IND ; E = BN ; F = PIP ; G = FPBA ; H = UR ; I = PEG4 ; J = SAL ; K = AC ; L = PYRR ; M = THB ; N = PFB ; O = SOLVENT (PINK) AND UNTREATED CONTROLS (BLACK).	161
FIGURE 3.14. ONE-WAY ANOVA AND TUKEY'S MULTIPLE COMPARISONS POST-HOC ANALYSIS. FOR CLARITY ONLY STATISTICALLY SIGNIFICANT ($Q \leq 0.05$) PAIRWISE COMPARISONS BETWEEN THE P1 FORMULATIONS AND THEIR RESPECTIVE ALDEHYDES ARE SHOWN. ALL P1 FORMULATIONS EXCEPT P1-ICA AND P1-THB PRODUCED A STATISTICALLY SIGNIFICANT INCREASE IN TOTAL FUCOSE COLANIC ACID PRODUCTION RELATIVE TO THE SOLVENT TREATED CULTURES. SEE APPENDIX FOR STATISTICAL ANALYSIS RESULTS. ..	162
FIGURE 3.15. LINEAR REGRESSION ANALYSES OF TOTAL NORMALISED FUCOSE PRODUCTION DETERMINED BY AUC OF THE TIME-SERIES DATA PLOTTED AS A FUNCTION OF SEVERAL PHYSICOCHEMICAL PARAMETERS OF THE P1 FORMULATIONS. A = CLOGD; B = TPSA; C = POLARISABILITY; D = PKB; E = MOLECULAR WEIGHT (MW). F = CORRELATION BETWEEN TOTAL NORMALISED FUCOSE AND TOTAL DRIED BIOMASS.	163
FIGURE 3.16. TOTAL PNAG PRODUCTION AS MEASURED IN PROXY BY GLUCOSAMINE QUANTIFICATION IN THE MBTH ASSAYS FOLLOWING TREATMENT WITH P1 FORMULATIONS (BLUE), THE RESPECTIVE ALDEHYDE CONTROLS (RED) AND THE SOLVENT (PINK) AND UNTREATED (BLACK) CONTROLS. ERROR BARS = S.D. (N = 3). ONE-WAY ANOVA AND TUKEY'S MULTIPLE COMPARISONS POST-HOC ANALYSIS, SHOWED NO STATISTICALLY SIGNIFICANT ($Q \leq 0.05$) PAIRWISE COMPARISONS BETWEEN THE P1 FORMULATIONS AND THEIR RESPECTIVE ALDEHYDES.	166
FIGURE 3.17. RESAZURIN ASSAY TO ESTIMATE E. COLI MC4100 VIABILITY IN P1 TREATED CULTURES RELATIVE TO THE UNTREATED CELL CULTURES. ERROR BARS = S.D. (N = 3). STATISTICALLY SIGNIFICANT PAIRINGS (*) DETERMINED THROUGH TUKEY'S MULTIPLE COMPARISONS TEST.	170
FIGURE 3.18. SCHEMATIC SHOWING THE ENTRY OF NPN INTO THE HYDROPHOBIC INTERMEMBRANE SPACE CAUSING FLUORESCENCE. IN THE ABSENCE OF MEMBRANE PERMEATION, NO FLUORESCENCE CAN OCCUR. PRODUCED IN BIORENDER.	173
FIGURE 3.19. NPN UPTAKE IN P1 TREATED CULTURES (BLUE) AND RESPECTIVE ALDEHYDES (RED) RELATIVE TO UNTREATED E. COLI MC4100 CULTURES (BLACK DASHED LINE).	174
FIGURE 3.20. SCREENED CONDITIONS FOR SPY::GFP CONSTRUCT IN E. COLI MC4100. A = TOTAL GFP PRODUCTION CALCULATED AS THE INTEGRAL OF FLUORESCENCE CHANGE WITH TIME; B = FLUORESCENCE CHANGE WITH TIME. ERROR BARS = SD (N = 3).	178

FIGURE 3.21. TOTAL SPY PROMOTOR ACTIVITY AS CALCULATED FROM THE AUC OF THE CHANGE IN FLUORESCENCE OVER 24 H FOR EACH TESTED TREATMENT AND CONTROL. ERROR BARS = S.D. (N = 3).	179
FIGURE 3. 22. REPRESENTATION OF CONTOUR PLOTS WITH RESPECT TO [POLYMER] (Y-AXIS), CELL DENSITY (X-AXIS), AND CELL AGGREGATION (Z-AXIS) AND HOW IT RELATES TO DIFFERENT AGGREGATIVE MECHANISMS.	183
FIGURE 3.23. CONTOUR PLOTS OF E. COLI MC4100 AGGREGATION (Z-AXIS) AT DIFFERENT INITIAL CELL DENSITIES (X-AXIS) AND POLYMER CONCENTRATIONS (Y-AXIS) FOR DIFFERENT P1 FORMULATIONS. A = ICA ; B = AFP ; C = IVA , D = IND ; E = BN ; F = PIP ; G = FPBA ; H = UR ; I = PEG₄ ; J = SAL ; L = PYRR ; M = THB ; N = PFB . ALL P1 FORMULATIONS PROCEED BY SUSPECTED BRIDGING AGGREGATION MECHANISM INDICATED BY REGIONS OF LOW CELL AGGREGATION (BLUE CONTOURS) AT HIGHER CELL DENSITY AND/OR REDUCED POLYMER CONCENTRATIONS.	185
FIGURE 4.1. NADPH-DEPENDENT REDUCTION OF ETHYL-4-CHLOROACETOACETATE BY A KETOREDUCTASE (KRED). NADPH CO-FACTOR REGENERATION BY THE SECONDARY ENZYME GLUCOSE DEHYDROGENASE (GDH) ³ .	207
FIGURE 4.2 SCHEMATIC SHOWING BIOCATALYTIC REACTION OF 5-FLUOROINDOLE AND L-SERINE TO FORM 5-FLUOROTRYPTOPHAN BY POLYMER MICROBIAL COMPLEXES OF E. COLI MC4100	209
FIGURE 4.3 PLOT OF 5-FLUOROINDOLE CONVERSION OF POLYMER TREATED CULTURES AND NON-POLYMER CONTROLS. B) PLOT OF 5-FLUOROTRYPTOPHAN CONVERSION OF POLYMER TREATED CULTURES AND NON-POLYMER CONTROLS. STATISTICAL ANALYSIS PERFORMED USING ONE-WAY ANOVA WITH TUKEY'S MULTIPLE COMPARISONS POST-HOC ANALYSIS WITH A FALSE-DISCOVERY RATE APPLIED FOR MULTIPLE COMPARISONS. STATISTICALLY SIGNIFICANT RESULTS MARKED ON PLOTS ($Q \leq 0.05$). ALL SIGNIFICANT POLYMER-ALDEHYDE COMPARISONS ALSO SHOWED A STATISTICALLY SIGNIFICANT DIFFERENCE FROM THE UNTREATED CONTROLS, THOUGH THESE HAVE BEEN OMITTED FROM THE PLOTS FOR CLARITY. NO STATISTICALLY SIGNIFICANT DIFFERENCE IN 5F-IND CONSUMPTION WAS NOTED FOR ANY OF THE TESTED CONDITIONS.	213
FIGURE 4.4 PLOT OF REACTION CONVERSION OF POLYMER TREATED CULTURES AND NON-POLYMER CONTROLS. STATISTICAL ANALYSIS PERFORMED USING ONE-WAY ANOVA WITH TUKEY'S MULTIPLE COMPARISONS POST-HOC ANALYSIS WITH A FALSE-DISCOVERY RATE APPLIED FOR MULTIPLE COMPARISONS. STATISTICALLY SIGNIFICANT RESULTS MARKED ON PLOTS ($Q \leq 0.05$). ALL SIGNIFICANT POLYMER-ALDEHYDE COMPARISONS ALSO SHOW A STATISTICALLY SIGNIFICANT DIFFERENCE FROM THE UNTREATED CONTROLS, THOUGH THESE HAVE BEEN OMITTED FROM THE PLOTS FOR CLARITY. NO STATISTICALLY SIGNIFICANT DIFFERENCE IN INDOLE CONSUMPTION WAS NOTED FOR ANY OF THE TESTED CONDITIONS.	215
FIGURE 4.5. CORRELATIONS OF 5F-TRP FORMATION WITH MEASURED BIOLOGICAL PARAMETERS FOLLOWING TREATMENT WITH P1 FORMULATIONS. A) AGGREGATE SIZING BY CRYSTAL VIOLET STAINING; B) CSGB EXPRESSION; C) CELL VIABILITY/METABOLIC ACTIVITY; D) COLANIC ACID PRODUCTION.	216
FIGURE 4.6. OVERVIEW OF POSSIBLE INDOLE AND TRYPTOPHAN IMPORT AND EXPORT MECHANISMS IN E.COLI. ARROWS REPRESENT WHETHER THE PROTEIN IS UP- (GREEN ARROW) OR DOWN-REGULATED (RED ARROW) WITHIN A BIOFILM RELATIVE TO PLANKTONIC CULTURES. THE DOUBLE GREEN ARROW ADJACENT TO TRPBA REPRESENTS CONSTITUTIVE OVEREXPRESSION BY RECOMBINANT PSTB7. PRODUCED IN BIORENDER.	220

Chapter 1 – Literature Review – an introduction to biofilms, their applications and, engineering strategies with polymers.

1.0 Project Aims

Biofilms are sessile communities of cells that are encapsulated by an extracellular matrix. Often they are detrimental to many areas of society such as healthcare, agriculture, and industrial practices. The detriment of biofilms results from their increased hardness and resistance to current anti-bacterial practices allowing them to thrive in usually inhospitable conditions. However, the same properties that make biofilms problematic can be exploited in the development of novel green industrial practices. Therefore, this thesis focussed on the study development control biofilm formation using novel helical polymers. Several objectives were sought in attempt to further this field.

The first objective of this thesis was to develop a library of poly(acetylene) materials to test in subsequent biological assays. Creation of a material library would be achieved through the synthesis of a novel polymeric scaffold; poly(hydrazine carboxamide acetylene) which on reaction with a broad range of aldehydes and ketones (**Chapter 2**). This would be the first reports of a poly(acetylene) that utilised Schiff-base chemistry for post-polymerisation modification.

The second aim of this project was to test a broad range of poly(acetylene) formulations in their ability to nucleate biofilm formation in *E. coli* MC4100 (**Chapter 3**). The scaffold poly(hydrazine carboxamide acetylene) is suited to generate a library of diverse chemical properties with such as hydrophobicity, charge, and polarity. Biofilm formation was assessed by the polymers' ability to induce bacterial aggregation and later ECM formation. Despite the plethora of literature that describes polymer-induced aggregation in bacteria, there is little-

to-no reports on the subsequent effect on ECM production within the aggregates. Furthermore, to the best of our knowledge there remains no reports of PNAG and CA production in polymer-bacteria aggregates and so it was deemed fruitful to measure these to better elucidate the role of polymeric formulation on the bacterial physiology.

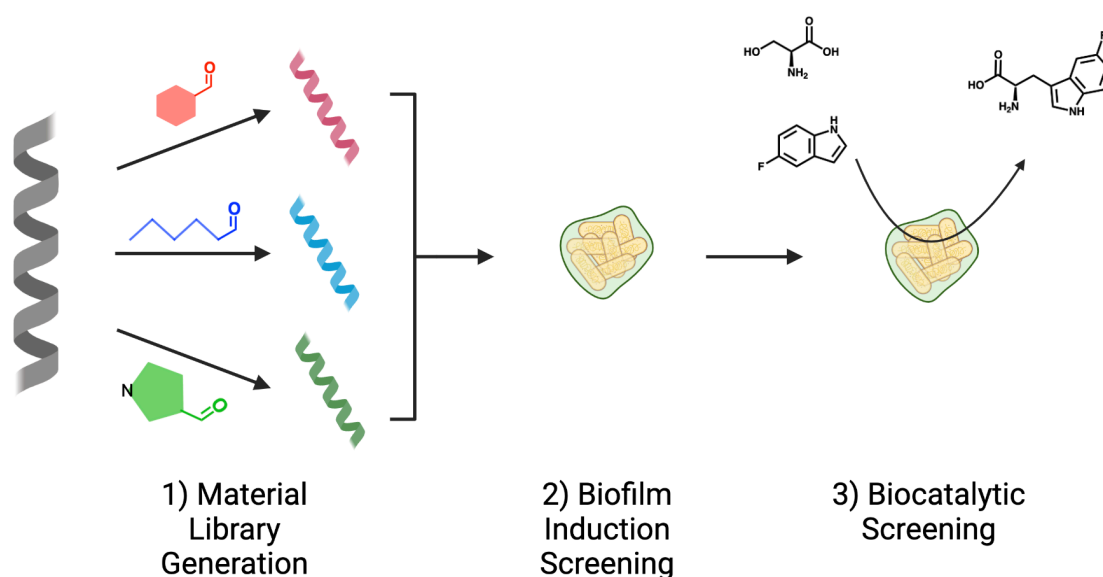


Figure 1. 1 Workflow scheme of the research undertaken in this thesis.

The final objective of this research was to test whether bacterial aggregates of *E. coli* MC4100 could be used within the sphere of biocatalysis (**Chapter 4**). Recent studies suggest that *E. coli* biofilms are well-adapted to biocatalytic applications owed to their increased hardness, longevity, and metabolic activity. Hence, to test whether biofilms produced by polymer-induced aggregation can be biocatalytically active the formation of 5-fluorotryptophan was probed as a model reaction as tested in literature.

1.1 A brief introduction to biofilms

Bacteria are extremely adaptable and versatile organisms found in a huge array of environments ranging from deep sea hydrothermal volcanic vents to glacial plateaus, as well as colonisation of almost every multicellular organism. Bacteria are typically considered to exist in a planktonic state (free swimming), where the cells freely move in the environment. Movement occurs by external forces, such as hydrodynamic forces or through cell motility from organelles such as flagella.¹ However, in nature bacteria mostly exist as biofilms; a sessile communities of cells adhered to a (a)biotic surface encapsulated by an extracellular matrix (ECM). The ECM is a highly complex structure composed of various biopolymers, such as polysaccharides, amyloid proteins, and extracellular DNA. The specific composition is highly dependent on both the bacterial species and strains in question.² Multi-species biofilms are prevalent in nature, whereby several bacterial species are present within a single biofilm structure. Cells are spatially organised to mitigate competition for nutrients, in addition to promoting co-metabolism within the biofilm.³ It is estimated that upwards to 80% of bacterial species on Earth can form biofilms.⁴ The prevalence in nature exemplifies the significant survival advantage conferred by adoption of this sessile lifestyle. In a biofilm, individual cells are localised to one another promoting horizontal gene transfer and overall population health.⁵ Moreover, ECM provides a physical 'shield' against various environmental stresses, such as pH or temperature extremes, desiccation, UV radiation, phagocytosis, and heavy metal poisoning conditions, that otherwise would be deleterious to the cells in their planktonic state.²

The increased resilience of biofilms to environmental stresses has caused growing concern in recent times due to their roles in anti-microbial resistance and chronic illnesses. Pathogenic biofilms are identified as a major detriment to societal health, where the National Institute of Health (NIH) report that 65% microbial infections are due to biofilm-related origins.⁶ Biofilms play a significant role in the development of infections due to implants in patients. Catheters are particular high risk, as bacteria can migrate along the catheter surface and bypass the dermal and subcutaneous tissues causing infection from within.⁷ ⁸The persistence of infection due to biofilms are owed to their increased resistance to antibiotics, where resistance in biofilms 10-1000-fold higher compared to their planktonic counterparts.⁹ Antibiotic resistance in biofilms differ from planktonic cells and there are several hypothesised mechanisms proposed. Bacterial cells are encapsulated by the ECM this can cause diffusion reaction inhibition. Whereby the spatiotemporal changes in antibiotic concentration within the biofilm matrix causes the required minimum inhibitory concentrations (MIC) to become insufficient to produce a bactericidal response. Furthermore, biofilms further promote antibiotic resistance due to increased population of persister cells found in biofilms compared to equivalent planktonic cultures.¹⁰ Persister cells are a sub-population of bacterial cells that are not readily killed by antibiotics, if the original persister population is cultured further then the daughter populations will possess the same increased antibiotic resistance. Persister cells are believed to play an integral role in repeated biofilm-associated infections following antibiotic treatments.¹¹ In addition, horizontal gene transfer (HGT) is believed to be the primary mechanism behind multi-drug antibiotic resistance in bacteria¹² and is found to be promoted in biofilms of different species, such as *Staphylococcus aureus* and *Escherichia coli*.^{13,14}

Asides from healthcare, biofilms pose additional significant socioeconomic burden in agriculture, industry, and the environment due to biofouling. In process industries, biofilms can form due to irregular surfaces such as pipe bends, valves, and gaskets, promoting the accumulation of difficult to clean organic matter.¹⁵ This is of particular concern in the food and dairy industry where biofilm formation can lead to food-borne diseases from contaminated food stuff or processing equipment. Common pathogens in the food industry include enterohaemorrhagic *E. coli*, *S. aureus*, *Listeria monocytogenes* and *Salmonella enterica*.¹⁶ For instance, biofilms of *S. enterica* are reported to survive on dry stainless-steel surfaces up to 1 year.¹⁷ They have the potential to contaminate thousands of food batches, where this bacterium is responsible for 50% of death in all food-associated outbreaks.¹⁶

In addition, biofouling of naval vessels is a major concern where biofilm colonisation of ship hulls is estimated to reduce a vessels' cruising speed by 86%. The increased fuel and power consumption is consequently increased by 15-20% due to increased drag. This can cause significant environmental harm and economic loss. Furthermore, biofilms are implicated in corrosion due to through extracellular electron transfer where many metal corrosive biofilm species belong to the phylum Deltaproteobacteria.¹⁸ Corrosion by biofilms in nature is likely a multi-faceted process, where in addition to bacterial redox activity the higher concentrations of organic acids within the biofilms may further expedite material corrosion. Biofilm-induced corrosion is estimated to cost 2.5 trillion dollars globally. Agricultural and aquacultural practices also suffer from biofilm-related issues, as approximately 10% of global crops are lost due to microbial pathogens.¹⁹ Additionally, the total economic loss in aquaculture, as a direct consequence of biofilm fouling, is estimated at 5-10% of total costs. Therefore, not only do

many biofilms pose as health risks to society, but also show significant detriment to both the environment and economy in many working sectors.

1.2 Biotechnological applications of biofilms

Given the considerable risks that biofilms pose in wide areas of society regarding medicine, environment, and industry, most biofilm-related research is focused on biofilm mitigation and eradication strategies. However, more recently the consensus of biofilms has shifted to realise their potential application in a transition to more sustainable industrial and agrochemical practices. The added hardiness of biofilms greatly expands both the scope and potential application, in which biotechnology can be applied. The ECM confers a significant survival advantage compared to planktonic cells, as biofilms are bestowed with considerable resistance to otherwise deleterious conditions, for example: pH and temperature extremes, the presence of toxic solvents or compounds. Furthermore, the formation of large channelled 3-dimensional structures during maturation establishes large internal diffusional gradients facilitating nutrient, metabolites, and gas transfer within the biofilm interior. Which stimulating the intracellular reaction rates compared to traditional immobilisation strategies. In addition, biofilms remain metabolically active for significantly longer time periods than planktonic bacteria, which makes them highly suited for applications continuous industrial practices, improving the process economy and efficiency. Therefore, to further develop the potential of green industrial methods, it is important to recognise the potential of biofilms and further research is needed to expand the understanding on how these biological entities can be controlled and engineered to conceive this. The following section will discuss some of the biotechnological fields biofilms have been applied to.

1.2.1 Agriculturally relevant biofilms

A major potential research area for beneficial biofilms is their use in agriculture due to the criticality of the soil microbiome to crop health. Numerous agriculturally relevant bacteria form biofilms on plant root providing critical roles, such as nitrogen fixation (e.g., *Sinorhizobium meliloti*,²⁰ *Gluconacetobacter diazotrophicus*²¹ and *Rhizobium leguminosarum*) and growth promotion (e.g., *Pseudomonas fluorescens*,^{22,23} *Azospirillum brasiliense*,²⁴ and *Bacillus subtilis*²⁵). Due to climate change, soil fertility is decreasing, leading to an increased loss of organic matter and phosphate, which further burden critical food supplies to a growing global population.²⁶

Although, using biofilms as a 'biofertiliser' can help circumvent these issues. For example, inoculation of crops with biofilm forming *Anabaena laxa* doubled chickpea crop yields compared to untreated controls.²⁷ Similarly, Prasanna *et al.* showed a statistically significant increase in cotton crop yields in *A. torulosa*–*T. viride* multi-species biofilm-treated crops relative to untreated and chemical controls.²⁸ Hence, controlled supplementation of agriculturally relevant biofilms can reduce the need for chemical pesticide and fertilisers, benefiting crop health and the surrounding biome due to reduced artificial anthropogenic interference.

1.2.2 Bioremediation

There has been a rapid increase in global pollution and environmental contamination since the advent of the industrial revolution. Industrial wastes and extensive pesticide usage has caused significant pollutant accretion due to environmental adsorption and

bioaccumulation.²⁹ One decontamination strategy is bioremediation, where microbial organisms remove pollutants from contaminated areas (Error! Reference source not found.), such as soils or waterways. Bioremediation confers several significant advantages to other remediation activities, such as high-temperature incineration or chemical decomposition procedures, as there is minimal disruption to the surrounding area and wildlife whilst remaining highly economical when applied to large land areas.^{30,31} Biofilms are well suited to bioremediation compared to planktonic microbes as the ECM confers greater resistance to the contaminants allowing them to survive in heavily polluted areas.³² Furthermore, the production of surfactants increases the bioavailability of organic compounds, enabling greater utilisation and degradation, bioavailability dictates the efficiency of bioremediation procedures.³⁰ Mixed culture biofilms of *Polaromonas* spp., *Sphingomonas* spp., *Alcaligenes* spp., *Caulobacter* and *Variovorax* spp., utilised polycyclic aromatic hydrocarbons, such as pyrene and phenanthrene. A respective 50% and 98% reduction was observed when supplemented into the liquid cultures of these mixed biofilms.³³ Various *Pseudomonas* spp. biofilms have also been demonstrated to be highly effective in the removal of halo-substituted phenols giving quantitative consumption of contaminants like tri-, tetra-, and pentachlorophenol when cultured on a fluidized bed reactor.³⁴ For example, Dasgupta *et al.* showed that crude oil degradation was nearly two-fold higher in *Pseudomonas* species biofilms compared to planktonic cells.³⁵ Inorganic heavy metals can also be removed by biomineralization or direct adsorption with the biofilm ECM. This is due to the high density of anionic functional groups that can effectively complex with metals, such as Cu, Mg, Ni and Cd.³² Where tested, biofilms achieved significantly higher pollutant removal compared to their planktonic equivalents. Similarly, the removal of heavy metals, such as Zn, Tc, U, Pb and Cr

have all been demonstrated in various biofilm composites.³⁶ Mixed *B. subtilis* and *B. cereus* biofilms immobilised on sand removed 98% of Cr(III) in a continuous flow reactor over 24 h, the primary removal mechanism was due to metal sorption to the biofilm ECM.³⁷

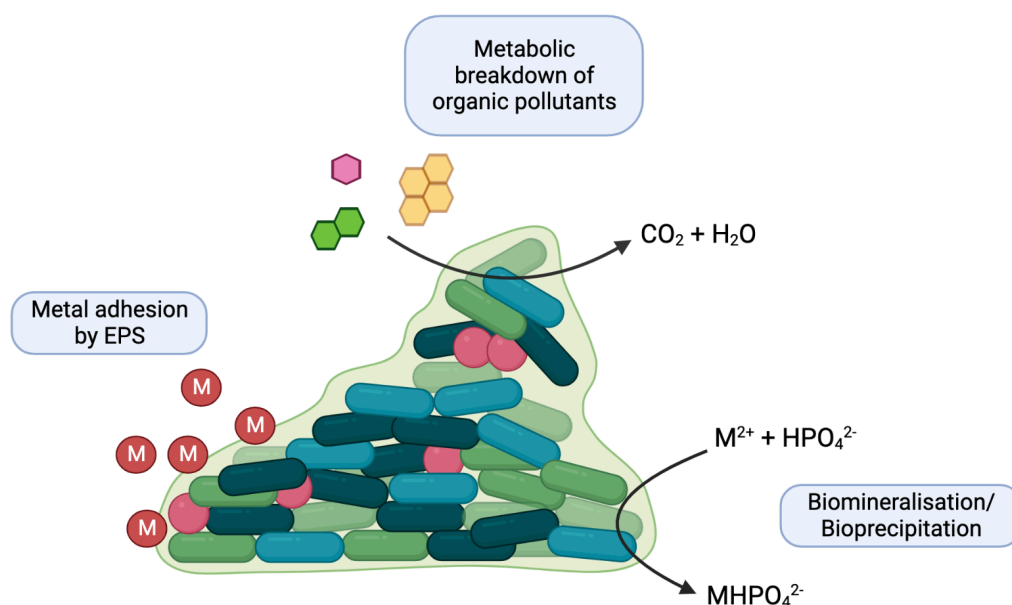


Figure 1. 2 Scheme showing various bioremediatory activities possible in a mix-species biofilm (not drawn to scale). Produced in Biorender.

1.2.3 Microbial fuel cells (MFCs)

Fuel cells convert chemical energy into electricity through redox chemical reactions, which are considered to be a cleaner energy source compared to using coal or oil fossil fuel sources. Typical fuel cells are composed of anodic and cathodic half cells containing an electrolyte solution separated by a semi-permeable proton exchange membrane. Following the reduction of a chemical species, electrons are produced causing an electron flow from the anode to cathode generating an electrical current. Microbial fuel cells (MFC) operate under the same principle, however electrogenic *Shewanella* and *Geobacter* or mixed-species biofilms thereof

are commonly used. Electrons are generated via anaerobic respiration of organic feeds like glucose, sucrose, acetic acid, ethanol etc.^{38,39} In MFCs the half-cell at which colonisation occurs becomes the anode. Electron generation on the anode creates an electrical potential difference, allowing electrons to flow from the anode to cathode to generate bioelectricity. Simultaneously, protons diffuse through the semi-permeable membrane and participate in a redox reaction within the cathodic chamber, driving electron and proton flow from the anode to cathode half-cell (Error! Reference source not found.).⁴⁰ MFCs can utilise a broad range of organic substrates as potential electron sources and are often used in conjunction with bioremediatory activities, such as waste-water treatment. For instance, benthic MFCs are researched for treatment of petrochemical waste-waters, where hydrocarbon pollutants are removed by the bacteria in the MFC whilst simultaneously generating bioelectricity.⁴¹ Liu *et al.* reported that a mixed-species biofilm of *Ralstonia* spp. YABE411 and *Pseudomonas* sp. YATO411, effectively removed 82% of benzene in waste-water in turn producing 12.7 mW/m² of power.⁴²

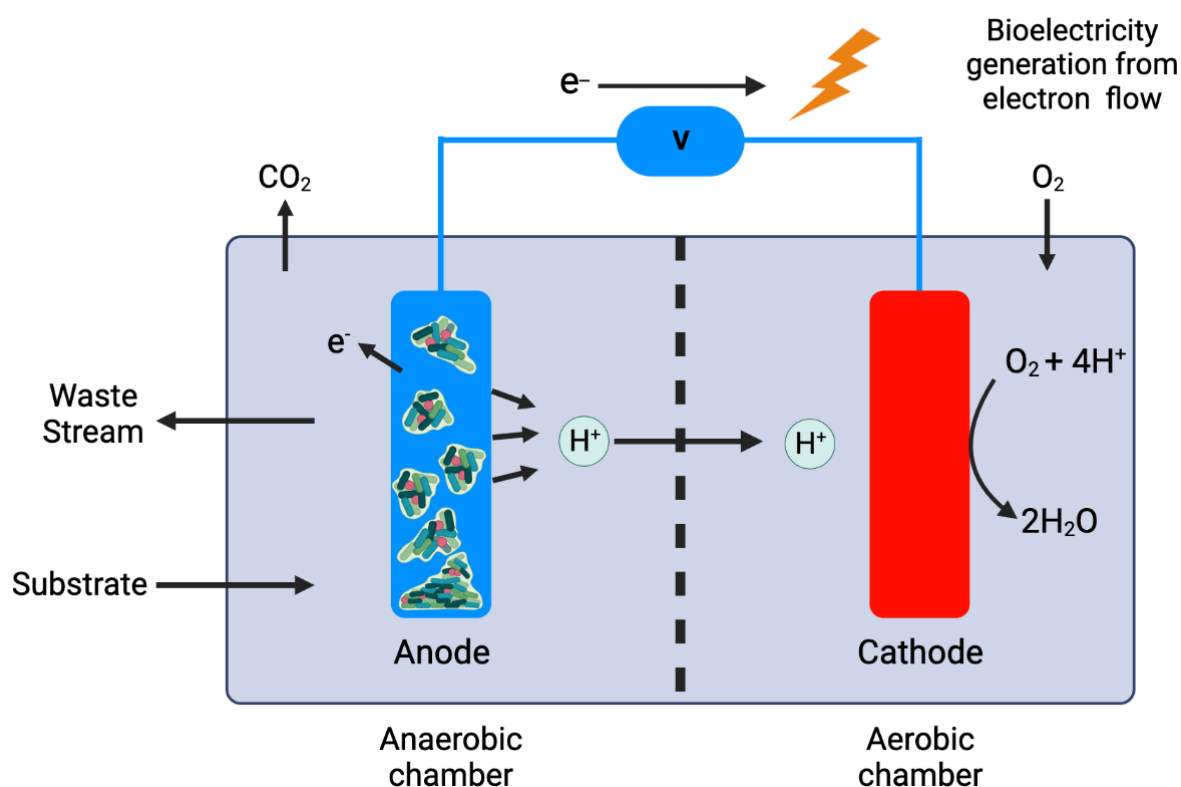


Figure 1. 3 Schematic diagram of a general microbial fuel cell (MFC) design (not drawn to scale). Produced in Biorender.

Biofilms possess several key characteristics that make them well adapted for use in MFCs. As biofilms consist of densely packed cellular communities this maximises cell density which enhances electron generation at the anode. It is also believed that the ECM of biofilms promotes extracellular electron transport by acting as a conductive-type material promoting exogenous electron flow towards the anode. Furthermore, biofilms possess excellent longevity and stability which allows the bacteria to remain electrochemically active for extended periods. This is an essential consideration if this technology is to be employed on any substantial scale.

1.2.4 Biocatalytic biofilms

Biocatalysis is the use of an organism or its components (enzymes) to catalyse a chemical reaction through reduction of its activation energy. Biocatalysis offers a considerable advantage over chemocatalysts as the latter often requires high temperatures, pressures and, organic solvent to achieve sufficient product formation. Harsher conditions employed by traditional chemocatalysts inflicts a large environmental burden, from harmful waste and increased energy demand.^{43–45} Despite the advantages traditional biocatalysts offer, they remain susceptible to denaturation due to non-native temperature or pH. Additionally, possible requirement of an organic co-solvent to aid reactant solubility further compromises the cell viability reducing catalytic activity.⁴⁶ Thus whole-cell and free-enzyme biocatalysis is limited to a narrow operating window. Using biofilms for biocatalysis is a viable strategy to overcome the above issues. The protective nature of the ECM increases resistance to adverse pH, organic solvents, and temperatures.⁴⁷ Production of porous mushroom-like structures during biofilm maturation greatly enhances the surface area-to-volume ratio. This establishes local concentration gradients within the biofilm, improving substrate diffusion into the cell to overcome mass transfer limitations at the cell surface.⁴⁸

The use of biocatalytic biofilms has been demonstrated in both bulk and fine chemical syntheses with improved productivity compared to their planktonic equivalents. Bioethanol production by *Saccharomyces cerevisiae*^{49–51} and *Zyomonas mobilis*^{49,52–54} biofilms, far outperformed their planktonic counterparts. For instance, *Z. mobilis* biofilms achieved 374 g L⁻¹ h⁻¹ ethanol production whereas planktonic cells had a maximal productivity of 124 g L⁻¹ h⁻¹. Moreover, biofilms allow for easier implementation of continuous reactors where planktonic

cells are carried through with the product. When compared to batch processes of planktonic cells, *S. cerevisiae* biofilms in continuous reactors maintained a productivity of $28.8 \text{ g L}^{-1} \text{ h}^{-1}$ compared to $3.4 \text{ g L}^{-1} \text{ h}^{-1}$ in batch planktonic cultures.⁵⁰ More hydrophobic alcohols and aldehydes, such as butanol,^{55–57} butan-2,3-diol and benzaldehyde⁵⁸ have all been synthesised using a variety of microbial biofilms. To produce (S)-styrene oxide and n-octanol, *Pseudomonas* sp. Strain VLB120 and *P. putida* biofilms were immobilised inside silicon tubing under continuous flow for 35 days. Biofilm cultures demonstrated improved volumetric productivity yielding $1.3 \text{ g L}^{-1} \text{ day}^{-1}$ compared to $1 \text{ g L}^{-1} \text{ day}^{-1}$ in free-cell batch cultures.⁵⁹ Importantly, planktonic cultures were limited to one day cultures exemplifying how biofilms can significantly enhance both process productivity and duration. Similarly, various 5-halotryptophans were synthesised in matured *E. coli* PHL644 biofilms, showing superior catalytic longevity and reactant conversion compared to planktonic cells and immobilised enzymes.⁶⁰ Further work by the same group demonstrated that the catalytic longevity of the *E. coli* biofilm was achieved through continual self-regeneration of the recombinant enzyme.⁶¹

1.3 Mechanisms of bacterial adhesion and development into biofilms

1.3.1 Multi-step biofilm model

Given the discussed applications for biofilms in biotechnology it is important to understand how bacteria naturally form biofilms to better direct novel engineering strategies for controlled biofilm growth. First described in *Pseudomonas aeruginosa*, natural biofilm formation is considered a developmental process, though occur similarly in other Gram-negative bacteria such as *E. coli* and *Vibrio cholerae* biofilm formation. In this multi-staged process cells undergo reversible attachment (1), irreversible attachment (2), maturation (3),

and dispersal (4) (Error! Reference source not found.). After the cells have irreversibly adhered to a surface, the maturation stages are associated with the development of a 3D ‘mushroom-like’ structure due to the production of various ECM components.

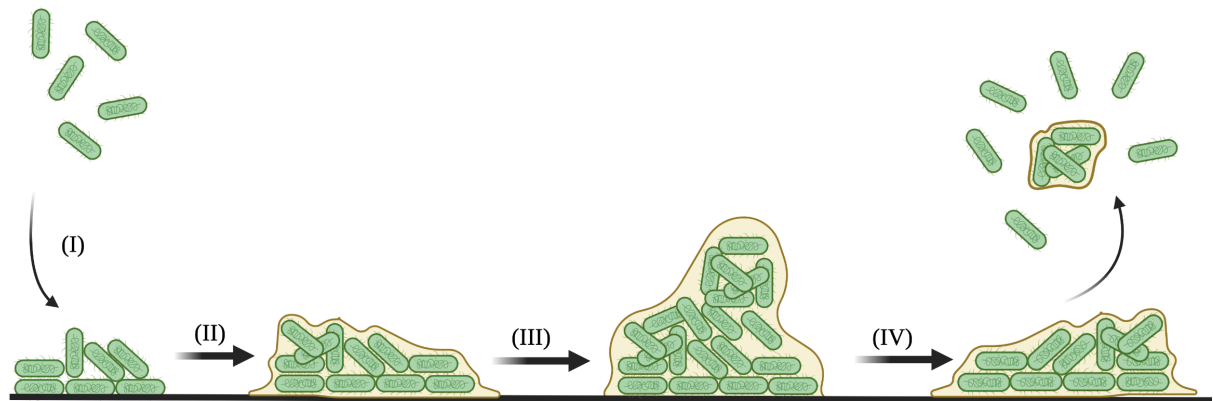


Figure 1. 3. Surface-attached biofilm formation and maturation according to the standard multi-step model. Produced in Biorender.

Although the multi-step developmental model is widely accepted as the gold standard for biofilm formation, it fails to address alternative biofilm structures.⁶² For example, at the air-liquid interface bacteria can aggregate into floating mat-like biofilms known as pellicles. These are formed in several bacterial species such as *B. subtilis*,^{63,64} *Burkholderia cenocepacia*,⁶⁴ and *Shewanella oneidensis*.⁶⁵ Recently, pellicle formation has been observed in *E. coli* K-12 strains where pellicle formation was found to be highly dependent on cell motility. Although delayed pellicle formation in non-motile *E. coli* MC4100 occurred with sufficient mixing.⁶⁶ Additionally, when subjected to hydrodynamic shear, clumps of aggregated bacteria may be removed from the biofilm structure but remain viable in a process known as sloughing. These aggregates can remain stable in solution or directly colonise other surfaces. Sloughed biofilms of *Vibrio cholerae* are implicated in higher infection rates as higher cell densities are ingested when

contaminated water is consumed. Therefore, with the change in understanding over time of biofilms it is important to redefine how they are considered. Recently, Donlan and Costerton have redefined biofilms as sessile cell communities attached to an interface and/or themselves which are encapsulated by a self-produced ECM with changes in growth rate and metabolism compared to their planktonic counterparts.⁶⁷ With respect to the research performed in this thesis, this is the definition that will be followed. The following sections will shortly review underlying principles with respect to bacterial surface attachment and biofilm formation. A focus will be placed on biofilm formation in *E. coli* as this was chosen as the model organism for the research conducted herein.

1.3.2 Role of electrostatics in bacterial adhesion.

Bacteria in solution are often considered to behave like a colloidal suspension. As such, many of the underlying physicochemical properties that dictate colloidal behaviour is applicable to bacterial surface attachment. One key principle that governs colloidal stability is the role of electrostatic or van der Waals (vdW) interactions. An electrostatic interaction can be defined as the attractive or repulsive interactive between two charged molecules or objects. These interactions maybe from permanent charge interactions, partial charges and/or induced dipole moments which cause an interaction.

In a liquid containing ions e.g. tap water, salt buffer, biological fluids etc., oppositely charged (counter) ions closely associate with a charged surface, known as the Stern layer (Figure 1.4). It is commonly accepted that most naturally occurring materials are anionic, thus the Stern layer in this instance is a densely formed cationic later. Surrounding, the Stern layer a diffuse

layer of counterions (anion) and complementary ions (cation) exist forming an electric potential. This potential decreases exponentially with distance from the charged surface. The length of this diffuse phase is known as the Debye length, which shows no influence on adhesion at equilibrium with the bulk phase. I.e. electrostatic interaction between two objects only occurs within the Debye length. These principles also govern the establishment of conditioning layers (see **1.3.1.3**).

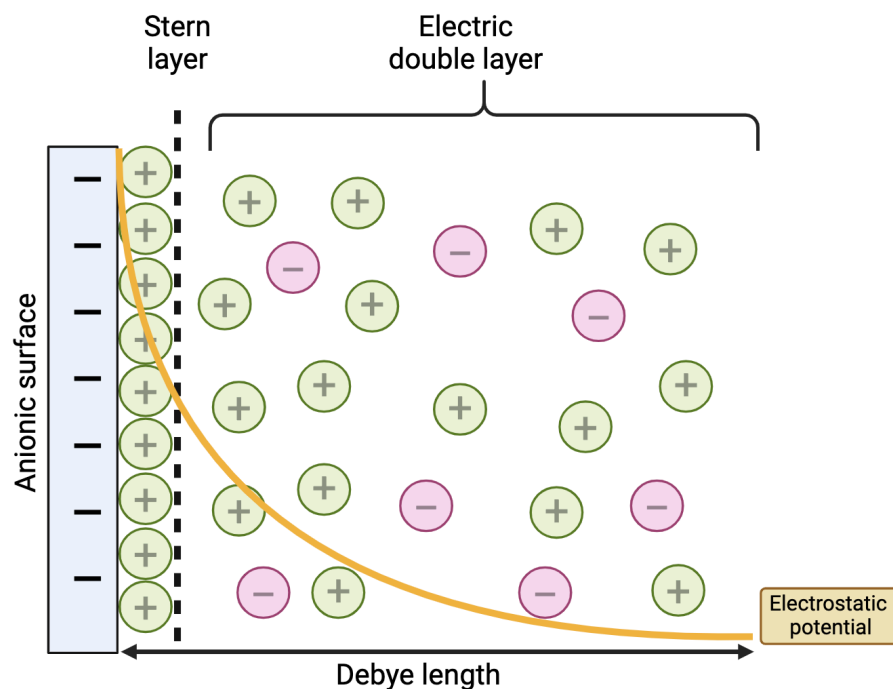


Figure 1.4. Cartoon diagram showing the formation of dense counter-ion (Stern) layer followed an increasingly diffuse layer of counter ions. The electrostatic potential of an object (yellow line) reduces with increased distance from the surface until reaching equilibrium with the bulk phase (Debye length). Not drawn to scale. Produced in Biorender.

1.3.2.1 The extended DLVO theory in the context of bacterial adhesion

Though the mechanisms responsible for bacterial adhesion to surfaces are not completely understood, they can be adequately described using the extended Derjaguin-Landau-Verwey-Overbeek (DLVO) theory.⁶⁸ Classical DLVO describes colloidal particle stabilisation in aqueous

solutions due to the contributions of the van der Waals (vdW) attraction and repulsive forces created by the electric double layer (DL) that surrounds all surfaces in solution. Therefore, the total potential energy in a system consisting of two particles or a particle and substrate can be defined as the net sum of the attraction and repulsion potentials. These respective potential forces are distance dependent. When at proximity electrostatic repulsion dominates between the particle and surface due to increased overlap of the electric double layer. However, the attractive vdW forces also increase at reduced interparticle distances and if the particles overcome the repulsive energy barrier provided, the system remains in an 'energy trap'. When in this energy minimum the attractive forces solely dominate causing irreversible aggregation or surface attachment (Error! Reference source not found.).

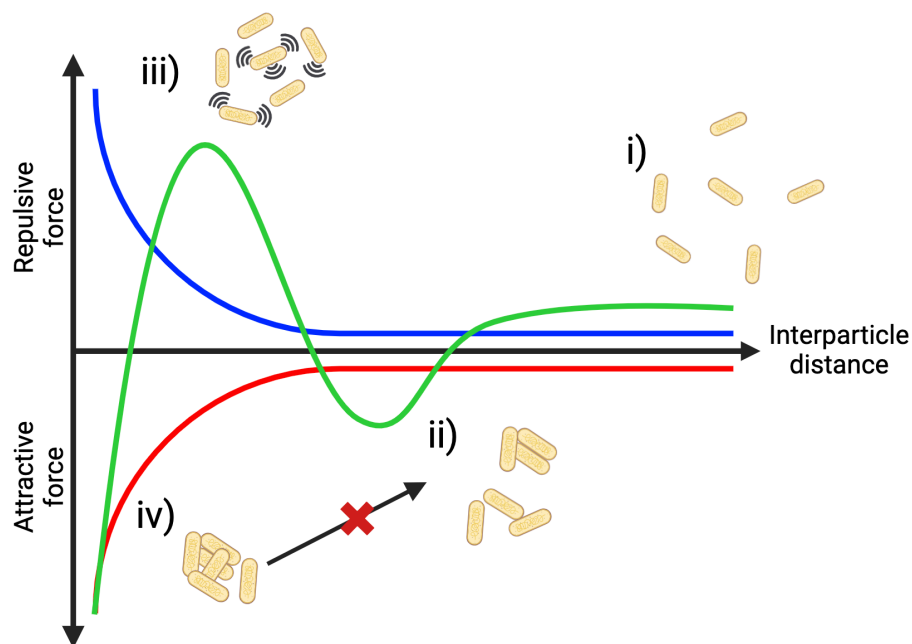


Figure 1.5 Diagram representing the distance dependency on colloidal stability/ bacterial aggregation. Blue line = electrostatic repulsion (top); Red line = vdW attraction (bottom); Green line = net force. I) Particle distance too large to experience any interparticle repulsion/ attraction. II) As distances reduce, particles enter a primary energy minimum causing reversible agglomeration. III) At closer proximity the electrical double layer overlap increases

the repulsive forces producing an energy barrier, the size of which dictates the colloidal stability. Various cell surface appendages like pili or curli help overcome this barrier as they project from the cell with a smaller diameter IV) Attractive forces overcome energy barrier (e.g. kinetic energy, ligand binding or hydrophobic interaction) and particles irreversibly agglomerate. Not drawn to scale. Produced in Biorender.

As with bacteria nearly all natural surfaces possess a net anionic charge.⁶⁹ Thus, one could expect repulsion between the bacteria and surface due to the like anionic character, thereby minimising surface colonisation; this however is not the case. Application of the DVLO theory in biological models is not suited, as it fails to address the contributions of cell surface hydrophobicity (CSH). Though bacteria are anionic, the presence of hydrophobic membrane organelles like type-1 pili, flagella, and fimbriae contribute overall to the hydrophobic character of the cell surface (see later).⁷⁰ Hydrophobicity arises from the cohesion of water molecules by preferentially forming hydrogen bonds with each other (bulk solvent) rather than the solute. Thus, hydrophobicity can be considered a Lewis acid-base interaction.⁷¹ The extended DLVO accounts for this, by inclusion of an acid-base (AB) term which is proposed to be 10-100 times stronger than the weak vdW forces, providing a significant contribution to the adhesive process.⁷² Therefore, bacterial aggregation and adhesion behaviour can be described in terms of the sum of the free energies of the vdW, DL and AB terms as described in **equation 1**.

$$\Delta G_{adh} = \Delta G_{vdW} + \Delta G_{DL} + \Delta G_{AB} \quad (1)$$

1.3.2.2 Surface chemistry and condition layer formation

When a solid is submerged in an aqueous liquid water will reach the surface within nanoseconds. The water molecules will orientate themselves dependent on material polarity and hydrophobicity/ wettability. Following this, proteins will quickly interact with the surface and their orientation will be dictated by the arrangement of water molecules adhered to the surface.⁷⁴ Quickly a layer is formed constituted primarily of proteins but also other dissolved organic matter such as amino acids and carbohydrates producing a conditioning film.⁷⁵ Conditioning films are an integral part of initial bacterial attachment. Establishment of a conditioning films aids initial attachment due to altered physicochemical properties of the surface. Generally, bacterial adhesion to hydrophobic surfaces is preferred as the surface energy of the bacteria is typically lower than that of the bulk solvent.⁷⁶ However, a conditioning film can reduce the surface energy providing a more hydrophobic surface in which the bacteria can interact.⁷⁶ For example, proteins adhered to either a charged or hydrophobic surface can misfold where protein regions normally associated with one another will instead interact with the surface.⁷⁷ Furthermore, the adhered protein can misfold to expose hydrophobic residues to the aqueous environment. This is possible as there is no energy penalty due to hydrophobic stabilisation from the surface.⁷⁸ Therefore, after forming a conditioning film protein denaturation can expose hydrophobic or charged amino acid residues changing the surfaces physicochemical properties promoting bacterial adhesion through electrostatic and/or hydrophobic attraction.

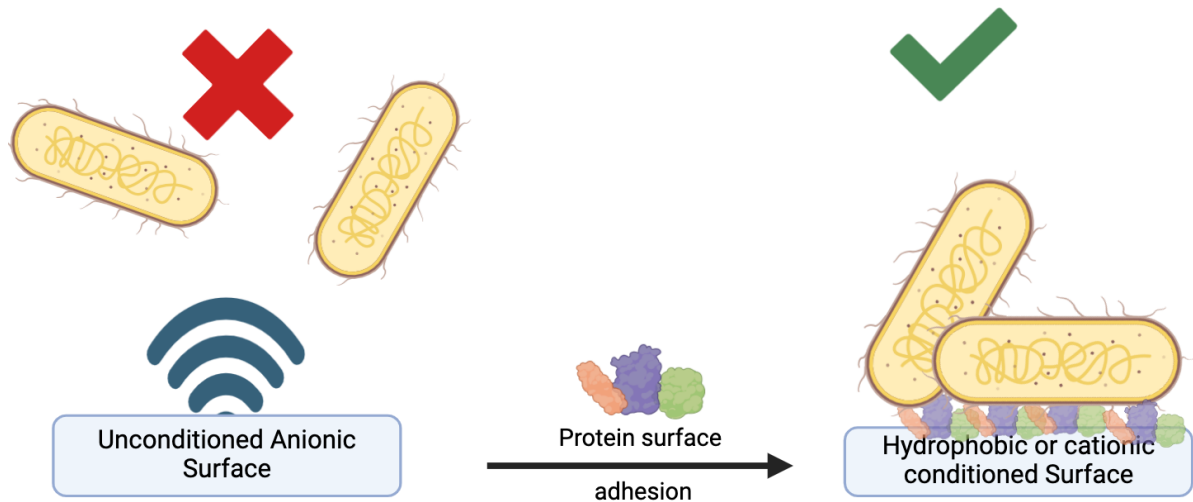


Figure 1. 6. Cartoon diagram showing the importance of conditioning film formation in bacterial adhesion. In the absence of CF formation bacteria experience electrostatic repulsion due to like-charges. After surface conditioning by proteins, exposure of internal hydrophobic residues and/or cationic amino acids mask the repulsive anionic character permitting surface adherence.

1.3.3 Bacterial membrane components and their role in non-specific adhesion

Many shortcomings in theoretical descriptions of bacterial adhesion arise from simplified assumptions of the bacterial surface, such as treating the bacteria as isotropic particles.⁷⁹ The primary constituent of the bacterial cell membrane are phospholipids that form a bilayer where the hydrophilic anionic phosphate groups are on the exterior. Embedded within the membranes are other biological structures such as lipopolysaccharides, glycolipids, pili, fimbriae and teichoic acids (in Gram-positives). The bacterial envelope is anionic at physiological pH as the number of acidic groups outnumber the amine groups at the membrane surface.⁷⁹

Bacteria are often classified as Gram-positive or Gram-negative which concerns their ability to retain crystal violet staining in the membrane. Gram-positive bacteria possess an outer membrane encapsulated by a thick peptidoglycan layer which is readily dyed. Gram-negative bacteria like *E. coli* have two distinct membranes (inner and outer) which are separated by a thin peptidoglycan layer between the cells known as the periplasmic space/ membrane (PM). The gram-negative outer membrane (OM) is covered lipopolysaccharides (LPS) that protrude from the membrane surface. The LPS consists of a hydrophobic core (lipid A) and a hydrophilic tail (O-antigen/ polysaccharide) making it highly amphiphilic. The LPS primarily serves as a permeability barrier preventing ingress of toxic molecules that may otherwise be permeable to the OM. The LPS is densely packed in the OM where adjacent chains are crosslinked by divalent cations like Mg^{2+} , it is estimated that LPS constitute approximately 80% of the OM.^{80,81} Studies have shown that LPS deficient strains of *E. coli* exhibited low surface adherence to sand and glass beads. Theoretical DLVO calculations agreed with the experimental findings, which showed a high adhesive energy barrier to LPS-deficient bacteria.⁸² Hence, the LPS also aids adhesion in that likely helps overcome short-distant repulsive forces.

The presence of membrane appendages gives the cell surface an ion-penetrable layer increasing the surface conductivity allowing the surface charge to change with external stimuli such as approaching a surface, whereby the double layer interactions cause redistribution of cell surface charge.⁹⁰ The heterogeneity that arises from this charge distribution on approach to a surface theoretically leads to a reduction in repulsion between the bacteria and surface.⁷⁹

Furthermore, organelles such as organelles like type-1 pili, flagella, and fimbriae enhance adhesion as these membrane structures help breach the repulsive energy barrier near surface proximity (**Error! Reference source not found.**). This barrier, influenced by the repulsive force between a particle and a surface, is inversely proportional to the radius of the particle. Thus, surface structures with smaller cross-sectional areas enable bacteria to interact with surfaces at shorter distances, thereby reducing the repulsive energy barrier.⁷³

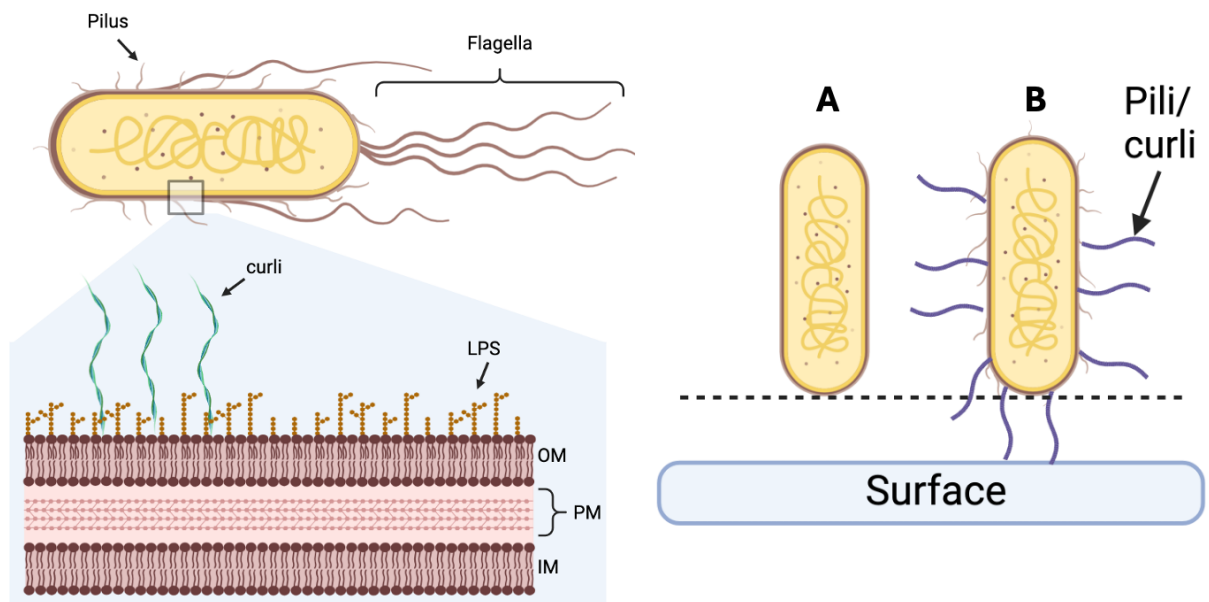


Figure 1. 7. LEFT - Cartoon of gram-negative E. coli cell membrane components that are implicated in bacterial adhesion/ biofilm formation. RIGHT - Depiction of the interaction between surface structures on a bacterium and a surface. A) A smooth bacterium at its closest proximity to a surface; B) the same bacteria adorned with smaller surface structures such as curli or type-1 pili. Dashed line = Debye length. Not drawn to scale. Produced in Biorender.

1.3.4 Reversible cell attachment

Following initial conditioning layer formation reversible attachment occurs when the cells are weakly bound to a surface primarily through electrostatic interactions (see **Error! Reference**

source not found. The weak nature of these interactions mean that cells may readily return to the bulk aqueous environment due to hydrodynamic shearing or cell motility. Attachment also remains weak as initial cell attachment occurs between the cell poles^{83,84} and the surface, limiting the direct contact area and strength of interaction. For example, biofilm formation in *P. aeruginosa* SadB199 mutants was restricted compared to non-mutant cells where polar cell attachment was associated with increased cell mobility and decreased irreversible attachment.⁸³ Initial cell-surface attachment may occur through passive mechanisms like Brownian motion. Here cell motion in the bulk phase is entirely dependent on interactions with molecules in the bulk-phase in a random-walk process.⁸⁵ Conversely, motile *E. coli* strains possess a whip-like organelle called flagella, which propels the cell through bulk solution towards regions of higher extracellular chemicals known as chemotaxis. Studies with *E. coli* 2K1056 (K-12 derived) showed that flagella enable the bacteria to overcome repulsive forces promoting abiotic surface attachment.⁸⁶ Cellular motility is found to positively correlate biofilm formation, where motility deficient *E. coli* mutants possess poorer biofilm forming capabilities.⁸⁶ Similar observations with motile *P. fluorescens* strains show that abiotic surface attachment is achieved at a four-fold higher rate and higher overall cell surface attachment compared to non-motile strains.⁸⁷ Curiously, under flow conditions motile *E. coli* MG1655 were disadvantaged in biofilm production, exhibiting delayed biofilm formation compared to the non-motile *flhD* mutants.⁸⁸ Though flagella may promote biofilm formation through enhanced cell-surface interactions they are non-essential to the process, particularly if the cells overexpress other adhesins such as curli or type-1 pili (see next).⁸⁹

1.3.5 Irreversible attachment in *E. coli*

Following reversible attachment, given favourable conditions at the substrate surface, the cells may further attach along their longitudinal axis promoting irreversible attachment. At this point motility genes *flhD* are repressed and production of 'finger-like' organelles known as fimbriae (type-1 pili and curli) is upregulated.⁹¹ In the absence of ECM production it is considered unlikely that bacteria can overcome the repulsive forces between themselves and the surface. Hence the production of fimbriae both aids in overcoming this energy barrier by further strengthening cell-surface and intercellular interactions.⁹²

1.3.5.1 Type-1 Pili

Type-1 pili is a filamentous rod-shaped protein that can grow up to 2 μm in length. Its production is controlled by the *fimAICDFGH* operon, and the type-1 pilus itself is a heteropolymer of FimA, FimF, FimG and FimH (**Figure 1.8**).^{86,93} FimA is the major protein subunit whereas FimF and FimG are minor subunits, postulated to aid FimH incorporation throughout the organelle. FimH is a 30 kD mannose-specific lectin (carbohydrate-binding sugar) primarily located at the pilus tip; however, is also believed to be located sporadically throughout. Type-1 pili aid the colonisation of eukaryotic cell tissues due to specific binding with cell-surface mannosylated glycopolymers, such as collagen and fibronectin.⁹³ Treatment of *E. Coli* cultures with the non-metabolizable α -methyl-D-mannoside is demonstrated to be an effective inhibitor of biofilm formation on a wide range of abiotic surfaces, such as poly(vinyl chloride), poly(carbonate), polystyrene and glass.⁹⁴ Type-1 pili are deemed essential to biofilm formation even in the absence of mannose-fimH interactions.⁹⁵ Production of type-1 pili reduces expression of other surface proteins, such as *OmpA*, *OmpX*, *Slp*, and *ToIC*, altering the cell envelope hydrophobicity and/or surface charge.⁹⁶ Mutations in the *N*-

terminus of type-1 pili creates an auto-aggregative response resistant to both mannose and shear disruption, suggesting a further role in surface colonisation.⁹³

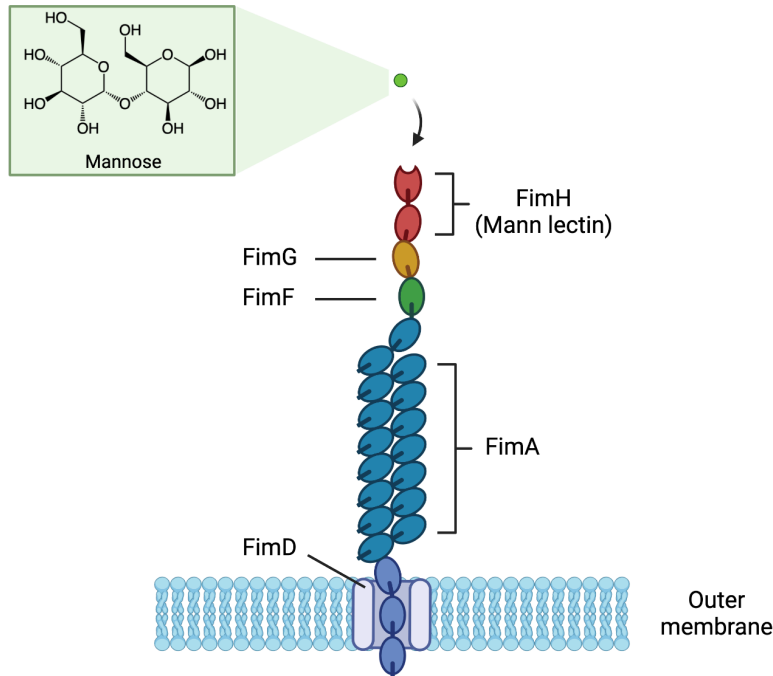


Figure 1.8 Cartoon schematic of type-1 pilus including the mannose specific lectin FimH at the terminus. Produced in Biorender.

1.3.5.2 Curli

Another fimbriae that plays a pivotal role in *E. coli* biofilm formation is the curli protein, a fibrous amyloid protein (CsgA) polymerised into a stacked β -helix by CsgB.^{97–99} Curli fibres are 4 – 6 nm wide that entangle the bacterial cell, these amyloid fibres remain highly resistant to proteinase degradation.^{98,100} Regulation of curli biosynthesis is under tight control of two transcriptionally divergent operons *csgBAC* and *csgDEFG*.⁹⁸ Polymerisation of CsgA occurs extracellularly where fibril nucleation occurs at the membrane surface.¹⁰¹ Synthesis of the amyloid polymer is regulated by the *csgBAC* operon, polymerisation of CsgA occurs extracellularly by CsgB preventing premature CsgA fibrillization and periplasmic degradation.

Curli fibrils are incapable of self-replication and their synthesis is entirely dependent on the initiator CsgB, permitting greater cellular control of the number and location of curli fibres.⁹⁷ The operon *csgDEFG* controls the translocation of CsgA and CsgB across the cell membrane, where monomeric CsgA and CsgB are chaperoned by CsgE and CsgF respectively through the porin CsgG. Secretion is greatest with a simultaneously high membrane concentration of CsgG.^{98,102} Curli fibres are considered imperative to biofilm formation, as curli facilitates cell attachment to abiotic surfaces and promotes cell-to-cell interactions via the formation of hydrophobic intercellular bundles. Additionally, curli aids attachment to extracellular mammalian proteins further implicating its role in host-tissue colonisation.⁸⁹

1.3.6 Biofilm maturation & exopolysaccharide production

The formation of ECM within biofilms is arguably its defining feature, encapsulating the cells within extracellular polysaccharides and proteins. When attached to a surface, the biofilm undergoes maturation characterised by increased exopolysaccharide biosynthesis. Here the biofilms produce 3D mushroom-like structures, forming deep channelled networks aiding oxygenation and nutrient diffusion into the film interior. Variations in ECM component alters the observed biofilm phenotype highlighting the various structural roles within the biofilm.

1.3.6.1 poly-*N*-acetyl glucosamine (PNAG)

Poly-*N*-acetyl glucosamine (PNAG) is a polymer of *N*-acetyl glucosamine (GlcNAc) formed through β -(1 \rightarrow 6) glycosidic bonds and is found in numerous microbial biofilm species like *B. subtilis*, *S. epidermis* and *A. baumannii*, as well as *E. coli*.^{103,104} PNAG is critical for biofilm maturation, though it is not essential for its formation and its necessity is highly dependent

on the bacterial species and culture conditions tested. Chemical or enzymatic treatment with periodate or dispersinB respectively, hydrolyse the β -1,6 glycoside bond causing dispersal of the biofilm, thus demonstrating the key structural role PNAG plays within the ECM.¹⁰⁵ In *E. coli*, PNAG partial deacetylation gives a partial cationic charge, which intercellular and cell-substrate interactions during tri-dimensional maturation.¹⁰⁶ In contrast to other ECM components like curli and colanic acid, it is located within the interior of the biofilm.⁶⁶ The PNAG biosynthesis enzymes are encoded by the *pgaABCD* operon, where monosaccharides are polymerised by the c-di-GMP dependent polymerases PgaC and PgaD.^{106–108} ^{107,108} The locus *pgaABCD* is under negative post-transcriptional regulation by the carbon storage regulator CsrA which represses biofilm formation and other stationary phase processes such as gluconeogenesis; whereas it is upregulated by NhaR in response to salt supplementation.¹⁰⁷ PNAG synthesis is repressed on CsrA binding to the *pgaA* transcript, this is controlled by the auto-regulatory loop of *csrB* and *csrC* which are indirectly regulated by the *barA/ UvrY* signalling pathways.¹⁰⁹ Biofilm formation is enhanced in *csrA* mutants whereas it is disrupted in *csrC*, *csrB* and *UvrY*. In addition, CsrA repression of stationary phase processes, such as gluconeogenesis and glycogen synthesis/ catabolism further repress *E. coli* biofilm formation.¹⁰⁶ It is reported that PNAG production is heavily dependent on the diguanylate cyclase activity (DGC; c-di-GMP synthases) like YddV rather than c-di-GMP itself, where it is suggested that DGCs like YddV act as ‘triggers’ for ECM components like PNAG.^{107,110}

1.3.6.2 Colanic Acid

Colanic acid (CA) is an anionic branched polysaccharide comprised of glucose, galactose, fucose and glucuronic acid in a 1:2:2:1 ratio.¹¹¹ CA is considered non-essential regarding initial

attachment and formation of sessile cell communities. However, like PNAG it is critical for 3D structure formation as well as maintaining the integrity of the biofilm.^{89,94,112} Due to its hydrophilic character CA is believed to act synergistically with the other ECM components like curli and type-1 pili.¹¹² Biosynthesis of CA in *E. coli* demonstrates temperature dependence where higher CA production is observed at 30 °C in contrast to 37°C. This suggests that CA production may aid environmental rather than host colonisation.¹¹³ CA is typically located to the exterior of the ECM, and CA deficient strains produce biofilms of limited thickness.⁸⁹ Overexpression of CA hinders biofilm formation due to increased cell surface hydrophilicity. For instance, the CA overproducer *E. coli* RcsF⁺ shows minimal attachment to hydrophobic VDF, MCE and PTFE membranes.¹¹⁴ CA synthesis and secretion is performed by the genes contained within the *wca* cluster. Upregulation of *wca* genes is not fully characterised but is thought to be triggered by a myriad of stimuli such as changes in osmolarity, cell envelope stress and desiccation due to a response by the sensor kinase *rscC*.^{115,116} CA synthesis and regulation is a highly complicated and not fully understood yet; though it is believed that the three-component *rscC/yojN/rscB* system regulates its synthesis through stimulation by low temperature and limited glucose concentrations.¹¹⁷

1.3.6.3 Cellulose

Cellulose is a linear polysaccharide chain composed of D-glucose repeat units linked by a β -1,4-glycosidic bond that associate into cable-like fibres.¹¹⁸ Recently, it was discovered that bacterial cellulose in biofilms contains a phosphoethanolamine modification promoting host tissue adhesion.¹¹⁹ In *Enterobacteriaceae* cellulose interacts with curli to give the *rdar*¹ colony

¹ Rdar = rough, dry, and red; red colouring comes from CongoRed staining of the amyloid curli protein

phenotype and is believed to add elasticity to the bulk biofilm. Cellulose production is dependent on the *yhjR-bcsQABZC* and *bcsEFG* operons.¹²⁰ Though cellulose is produced in several *E. coli* strains, K-12 derived strains are incapable of cellulose production owed to a mutation within *bcsQ* causing premature transcription termination.¹²¹ However, as cellulose deficient *E. coli* strains can still form biofilms this highlights that cellulose is not a necessity for biofilm formation.

1.4 Engineering bacterial aggregation with polymers

Biofilms may be used for a series of biotechnological applications such as (bio)chemical synthesis, MFCs and agriculture. The realisation of these potential applications is dependent on the selection of a suitable substrate for bacterial adhesion and growth, where initial attachment and biofilm maturation is dependent on surface hydrophobicity, electrostatics, topography and stiffness.^{122–124} In industrial settings, biofilms have been cultured on a variety of materials ranging from natural derived supports, such as sugarcane molasses¹²⁵ and vermiculite,¹²⁶ to synthetic materials like cation exchange resins¹²⁷ and po¹²⁸ However this prior research fails to address the significance of the material support on biofilm productivity or the implication of material type on development and/or composition of the ECM.

To further advance the industrial potential of biofilms, controlled ECM production is paramount to ensure biofilms do not become diffusion-limited.¹²⁹ A potential solution to controlled ECM production maybe through the development and application of synthetic polymers as scaffolds for biofilm growth. The physicochemical properties of synthetic polymers can be controlled through selection and modification of monomer composition.

Furthermore, polymers can be formulated into a solid surface such as hydrogels which that bacteria can adsorb directly to or exist a 'free' chain in suspension acting like a net to capture and aggregate the bacteria. As the research performed in this project is focused on the use of linear polymers in solution, the following literature discussions will primarily focus on 'free polymers' that employ various chemistries that cause polymer-induced aggregation.

1.4.1 Polymer-induced aggregation: Mechanisms-of-action

There are two mechanisms-of-action of bacterial aggregation by polymer treatment: flocculation and depletion aggregation. Flocculation is a well-studied process in engineering that can be described as destabilisation of colloidal matter due to the addition of a coagulant (often a polymer) causing sedimentation known as a floc. In biotechnological contexts, flocculation has found widespread use in industrial processes such as clarification of crude cell lysates or whole-cell recovery. Typically employing cationic polymers, such as chitosan or poly(ethylene) imine (PEI), that directly adsorb with the anionic cell membrane constituents.^{130,131} Flocculation may occur through either a polymer-bridging or charge-neutralisation mechanism.¹³² In the former, a polymer simultaneously interacts and bridge multiple colloidal particles, overcoming the electric double layer repulsions causing colloidal destabilisation and consequent aggregation.¹³³ Charge neutralisation occurs when the polymer encapsulates the oppositely charged particle, effectively shielding the particles net charge. The loss of like-charged repulsive forces leads to agglomeration and subsequent flocculation.¹³⁴

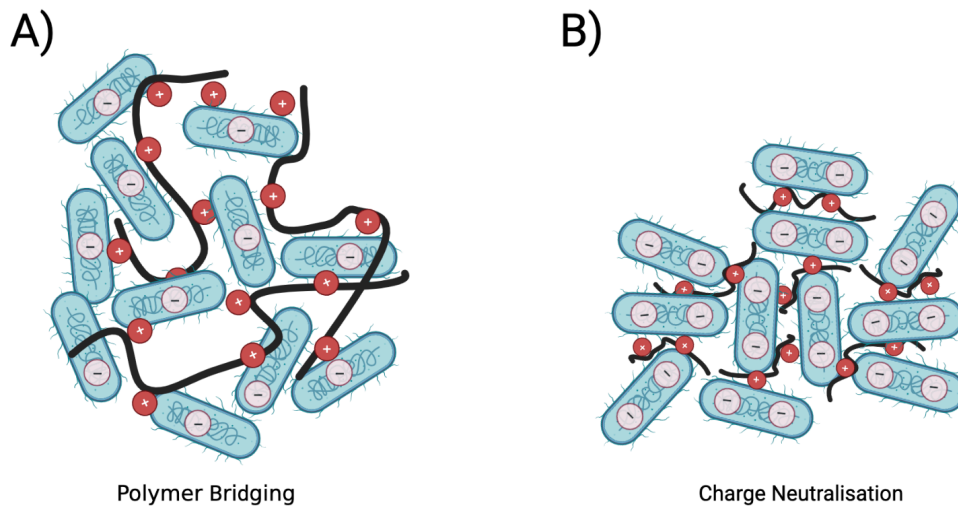


Figure 1. 9. Flocculation mechanisms. A) High molecular weight polymers cross-link individual bacterial together causing aggregation. B) Charge neutralisation by short cationic polymers screens double-layer repulsion causing aggregation. Not drawn to scale. Produced in Biorender.

Alternatively, non-adsorbing polymers can cluster bacteria via depletion aggregation (DA). A thermodynamic process whereby the polymer chain is excluded from the intercellular space or 'depletion zones' in an entropic process (**Figure 1.10**). As independent cells approach one another, this creates a localised osmotic pressure differential driving aggregation between cells.^{135,136} In contrast to bridging or neutralisation mechanisms reliance on polymer and bacterial surface chemistries, DA is instead highly dependent on polymer concentration, molecular weight, and cell morphology. At sufficiently high polymer concentrations, colloidal re-stabilisation may occur due to complete surface coverage of the particle/ bacteria giving electrostatic repulsion. Hence, a polymer length must exceed the Debye length to ensure exclusion of the polymer when in proximity to the bacteria. To summarise the range of depletion forces is dependent on polymer size whereas interaction strength is dictated by its concentration.¹³⁵

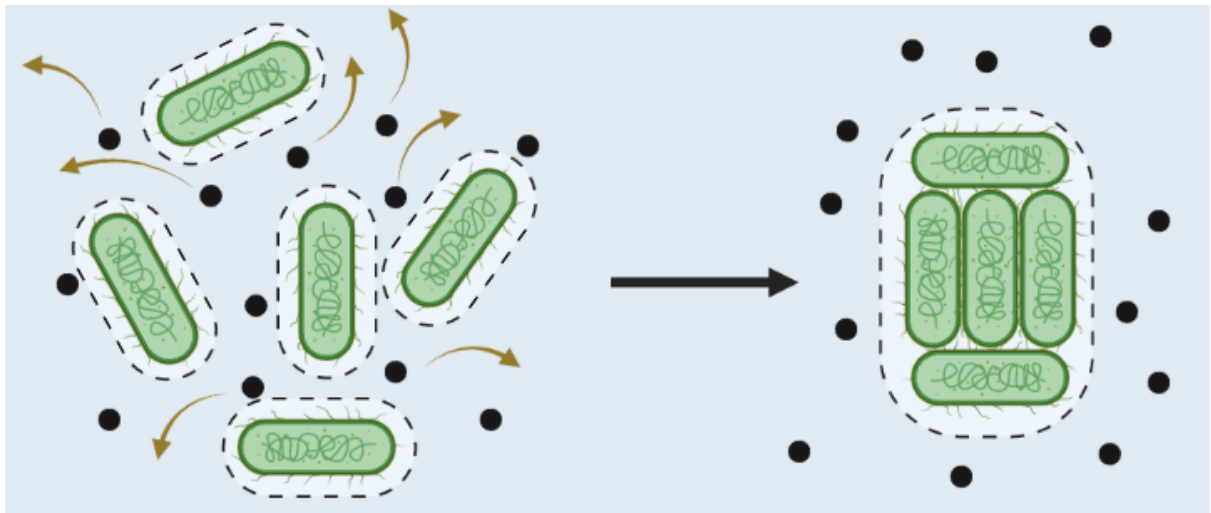


Figure 1.10 Schematic of polymer-induced aggregation from depletion mechanism. Dashed lines represent exclusion zones surrounding individual bacteria and black dots represent polymer chains in solution. Not drawn to scale. Produced in Biorender.

Interestingly, depletion aggregation appears to be a natural process that bacteria exploit to aid surface colonisation and biofilm formation. The production of hydrophilic exopolymers like cellulose or succinoglycan by soil bacteria like *Agrobacterium tumefaciens*, *Sinorhizobium meliloti* and *Xanthomonas campestris* show increased biofilm formation due to depletion effects.¹³⁷ Similarly, biofilm formation in opportunistic pathogens such as *P. aeruginosa* may be potentiated by depletion interactions. Biofilms associated with chronic infections like cystic fibrosis are usually found suspended in solution, it is believed that high concentrations of mucin and DNA leads to bacterial aggregation and biofilm formation.¹³⁸ Wound infections typically have high concentrations of hydrophilic biopolymers such as glycosaminoglycans, glycoproteins and collagen that can promote biofilm formation wound sites.¹³⁹ Both *P. aeruginosa* and *E. coli* aggregates formed by depletion mechanisms show increased anti-biotic resistance.¹³⁹ Synthetic non-adsorptive polymers like poly(ethylene glycol) (PEG), cellulose nanoparticles and polystyrene sulfonate are proven to cause phase induced separation on

both Gram-negative and positive bacteria, though a more detailed review regarding synthetic polymers is given later (see 1.4.4.1 Depletion Aggregation by synthetic polymers).

1.4.2 Aggregation by cationic polymers

The surface of cell envelopes of prokaryotic cells is anionic due to the presence of phospholipids, lipopolysaccharides, and teichoic acids in Gram-negative and Gram-positive cells, respectively. Therefore, one logical strategy in the design of novel bacterial aggregators is the use of cationic polymers. The electrostatic attraction with an oppositely charged polymer leads to bridging of the cells and subsequent aggregation. Cationic polymers, such as polyethylene imine (PEI) and chitosan have already found use in biotechnology as flocculating agents. Furthermore, amphiphilic polycations are well reported anti-microbial agents whereby the bacteria are clustered by electrostatic attraction whilst the hydrophobic portion inserts into the hydrocarbon tail of the outer membrane causing lysis.¹⁴⁰ Peng and co-authors demonstrated through surfactant-like poly(ester urethanes) that increased polymer hydrophobicity amplifies membrane disruption thereby improving anti-microbial activity against Gram-negative bacteria, such as *S. aureus*, *P. aeruginosa* and, *E. coli*.¹⁴¹ However, given that this project is not focussed on the development of anti-microbial polymers and the abundance of literature that pertains to this, these literature reports will not be discussed herein.

More recently, cationic polymers have been studied as potential non-biocidal bacteriostatic materials that effectively sequester the bacteria due to aggregation (**Figure 1.11**). The quaternary cationic polymer poly(*N*-[3-(dimethylamino)propyl] methacrylamide) (pDMAPMA)

and derivatives thereof are documented as effective aggregators of a wide range of bacteria such as *V. harveyi*, *V. cholerae*, *E. coli* and, *S. mutans*. In many cases, they have secondary influences on biofilm formation due to changes in QS behaviour when the bacteria are clustered together. Lui *et al.* first reported that when *V. harveyi* was clustered by pDMPMA, there was increased autoinducer-2 (AI-2) production.¹⁴² Further tests showed a poly(*N*-dopamine methacrylamide-co-*N*-[3-(dimethylamino)propyl] methacrylamide) (pDMPMA-co-pDMPMA) co-polymer effectively aggregated bacteria and sequestered AI-2 production, suggesting that the polymer-induced aggregation was responsible for this increased QS phenotype.¹⁴² In addition, pDMPMA and pDMPMA have been demonstrated to repress cholera toxin production in *V. cholerae* due to increased biofilm production. Colonisation of zebrafish larvae by *V. cholerae* was limited in the presence of pDMPMA and pDMPMA and so the zebrafish experienced less toxicity due to both reduced cell numbers and cholera toxin production.¹⁴³ Further works in the same group showed QS induction in *V. cholerae* by pDMPMA and pDMPMA occurred earlier with a 5-fold increase in peak auto-inducer production relative to untreated cultures. The enhanced QS in polymer treated cultures leads to induction of the biofilm master regulator VpsR and the downstream biofilm structural protein RbmA.¹⁴⁴

Additional cationic QS modulators have been demonstrated with other polymer morphologies such as dendrimers. For instance, gallic acid triethylene glycol (GATG) dendrimers containing amine functional groups effectively aggregate *V. harveyi*, showing improved aggregation compared to the model linear polymer pDMPMA.¹⁴⁵ Furthermore, bacterial clustering was highly dependent on polymer generation whereby only 2nd and 3rd generation (G2 & G3)

dendrimers could cluster bacteria and increased aggregate sizes were observed with the latter. In addition, generational dependence was observed in membrane permeation and AI-2 production, where G3 dendrimers showed the highest response in both, whereas G1 remained the lowest. Similarly, dendritic polyfluorene decorated with terminal amine increased biofilm production in *E. coli* by 55%, due to increased AI-2 production and duration.¹⁴⁶ The authors also note a generational dependence on the polymer action signalling that a minimum size is required for effective intercellular bridging.

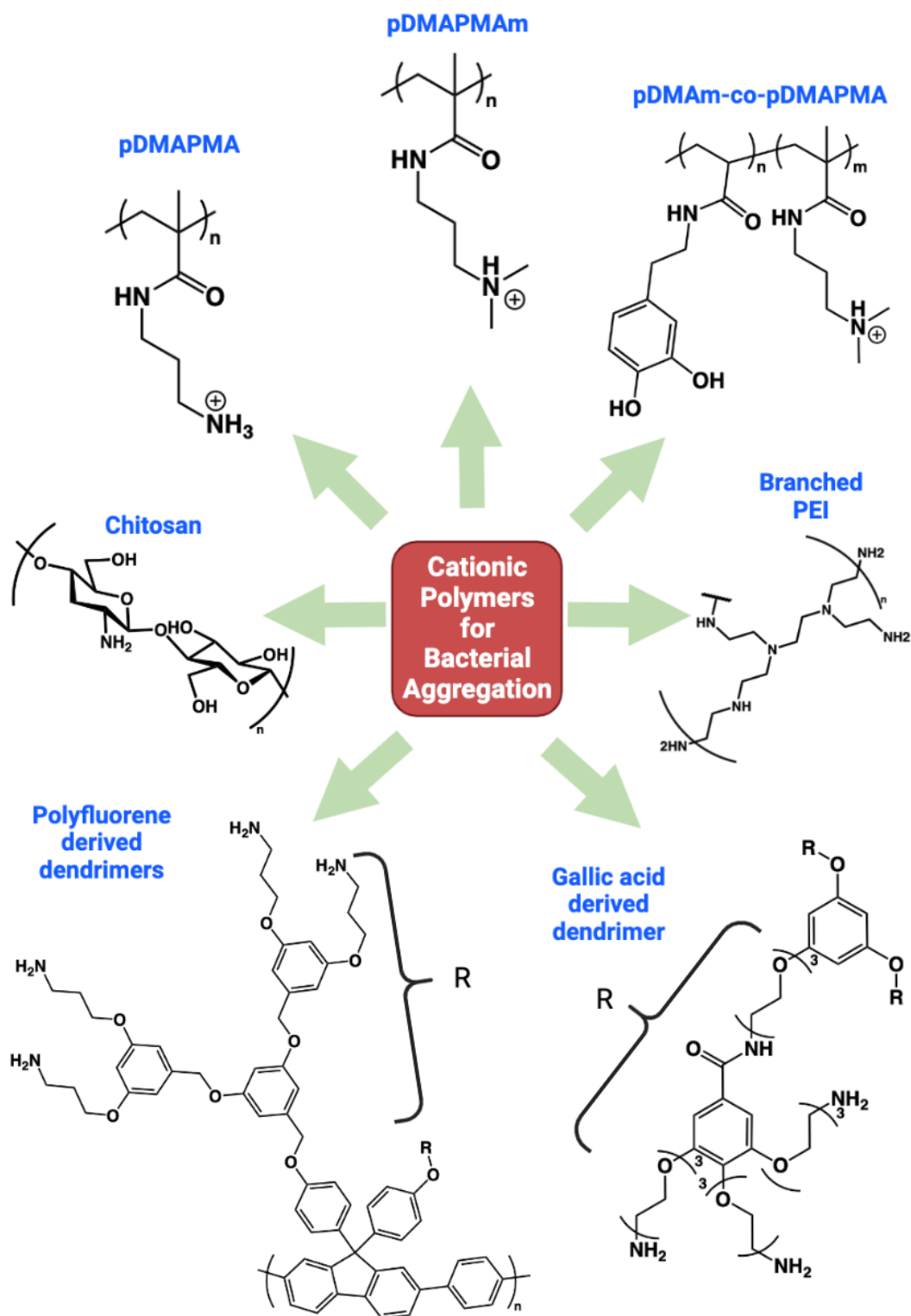


Figure 1.11. Cationic polymers used for bacterial aggregation as reported in literature and discussed in this work.

Polymer-induced aggregation of bacteria may be improved through control of the monomer composition through the synthesis of co-polymers, which can further enhance specificity. Cationic co-polymers are attractive as aggregation will primarily proceed via electrostatic interactions. However, this can be further tuned with the inclusion of other secondary monomers. For example, pDMAM-co-pDMAPMA copolymers increase aggregation of *P. aeruginosa*, *E. coli*, *V. harveyi* and, *S. aureus* to the sole cationic pDMAPMA polymer, with the greatest aggregation observed with *S. aureus*. The presence of dopamine units within the polymer were hypothesised to enhance aggregation due to a synergistic effect of electrostatics and secondary interactions with bacterial siderophores.¹⁴⁷ Similarly, derivatives of poly(2-(dimethylamino ethyl)methacrylate) (pDMAEMA) co-polymerised with either N,N,N-trimethylethanaminium (cationic) or sulfobetaine (zwitterionic) demonstrated differing binding affinities towards *S. mutans* or *E. coli*. Increasing zwitterionic character of the polymer showed preferential binding towards *S. mutans* even when applied in mixed co-cultures with *P. aeruginosa* or *E. coli*.

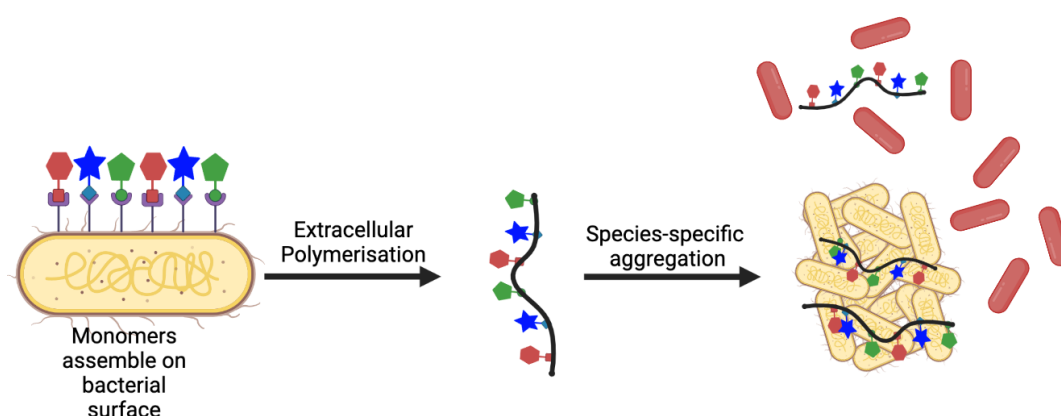


Figure 1.12 Schematic representation of bacterial instructed polymerisation and effect on bacterial aggregation behaviour. Not drawn to scale. Produced in Biorender

1.4.3 Aggregation by glycopolymers

Many *E. coli* strains possess the lectin (carbohydrate-binding protein) *fimH* on the end of the type-1 pili that is highly specific towards mannose. This enables bacterial adherence to host cells and as such is considered a crucial feature in *E. coli* related pathogenesis.¹⁵⁰ The specificity of this interaction makes it a highly attractive feature to exploit in the design of novel materials, for example glycopolymers (**Figure 1.13**).

Numerous glycopolymer designs and morphologies have been developed for improved bacterial agglutination. Yan *et al.* designed several linear and star-shaped polymers decorated with heptyl mannose moieties to agglutinate *E. coli*.¹⁵³ The bacteriostatic ability of the polymers increased with chain length in the linear polymer but addition of more arms in the star polymers slightly reduced it. Though when compared to monovalent heptyl α -D-mannose (HM), both polymer structures produced a 100-fold increase in potency.¹⁵³ Similar works studied the roles of polymer microstructure and pendant motifs on bacterial aggregation a library of RAFT co-polymers (block and statistical) of glycidyl methacrylate (GMA) and *N*-[7-(α -D-mannopyranosyloxy) heptyl] methacrylamide (HMM) were synthesised and further modified with either ethanolamine, (2-amino-ethyl)trimethylammonium chloride or taurine. Although there was no clear correlation between polymer microstructure and aggregation through the co-polymers were more effective agglutination agents compared to the homopolymer.¹⁵⁴

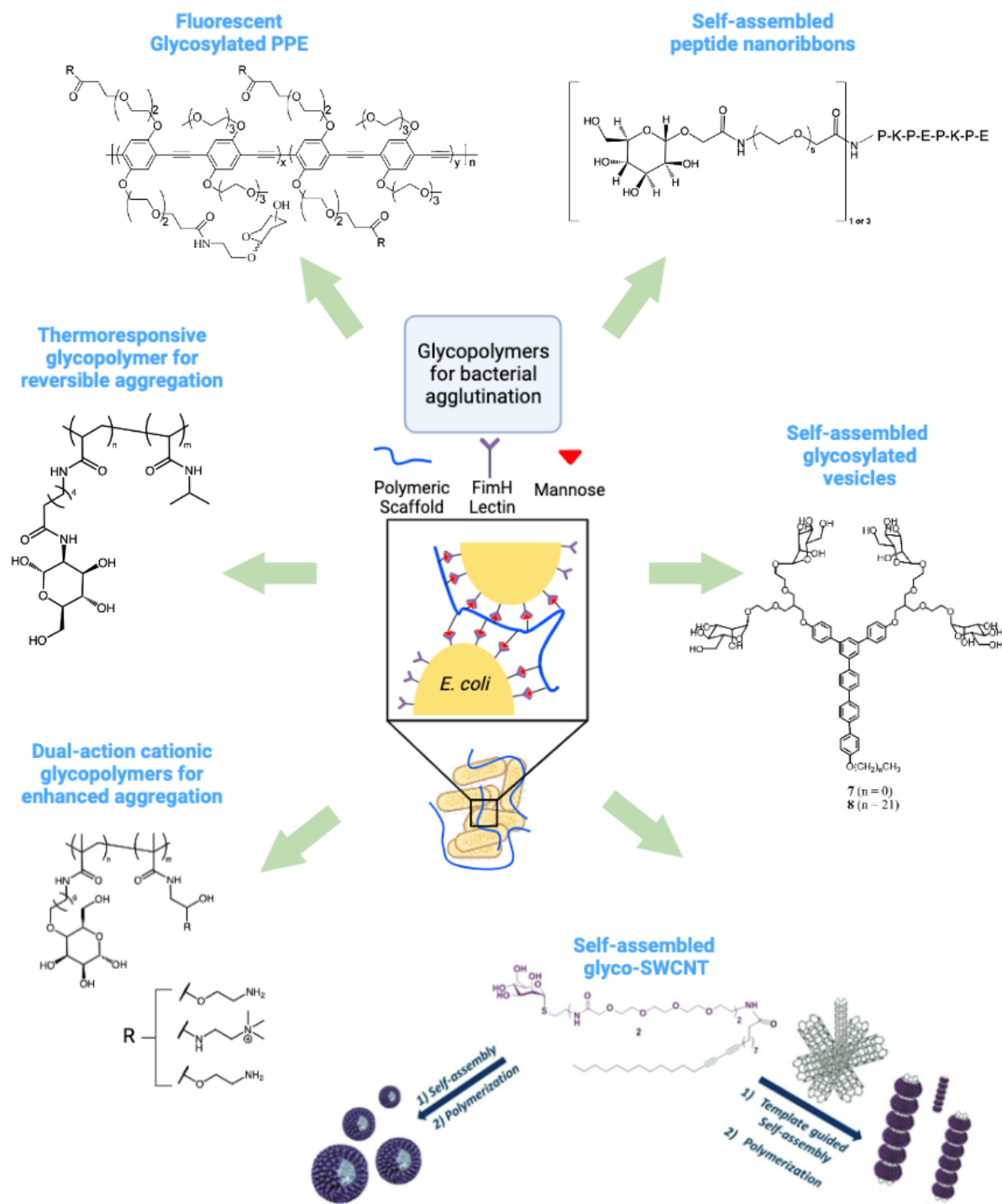


Figure 1.13. Aggregation of *E. coli* induced by mannose derived glycopolymers (centre). Literature examples of glycopolymeric materials tested as bacterial agglutination agents. Produced in Biorender.

For dual detection and capture, conjugated polymers such as poly(p-phenylene ethynylene) (PPE) and poly(phenylene) (PE) and poly(thiophenes) decorated with sugar and moieties have been proven effective in the agglutination of *E. coli*.^{155–158} Tethering the polymers with oligo(ethylene glycol) chains allows these highly hydrophobic polymers to become water soluble permitting their use in biological applications. These polymers show selective fluorescence only in the presence of *fimH* positive strains, such as *E. coli* ORN178, highlighting their potential as biosensors. Further developments in agglutinating polymers saw the creation of thermoresponsive poly(NIPAm-st-HEMide) decorated with glucose which was shown to effectively agglutinate *E. coli* MG1655. Most interestingly, agglutination was shown to be reversible as a function of temperature. At temperatures exceeding the lower critical solution temperature (LCST), no aggregation occurred as the polymer existed as a collapsed globule which prevented effective sugar-lectin association. However, the opposite occurred at temperatures below the LCST as the polymer is in an extended chain increasing the association of the sugar-lectin interaction. The authors demonstrated this reversible process could be cycled three times before loss of activity.¹⁵⁹

Bacterial agglutination has also been demonstrated with self-assembled materials. Polymeric self-assembly can be considered the ordered arrangement of monomers from a disordered state due to favourable interactions, such as hydrophobic or hydrogen bonding. Consequently, a broad range of morphologies and sizes can be achieved through altered polymer crystallinity. Much like traditional polymers, these self-assembled polymers can contain sugar functional groups permitting the agglutination of bacteria, such as *E. coli*. The effect of particle topology is deemed to be a critical aspect in successful bacterial inhibition, where research is

under the consensus that self-assembled systems must be of sufficient size and/or dimensions to achieve intercellular bridging and thereby aggregation. Lim *et al.*, demonstrated that in glycosylated β -sheet peptide nanoribbons bacterial inhibition was positively correlated with nanoribbon stability due to PEG length used.^{151,160} Interestingly, spherical vesicles are poorer agglutination agents compared to rod-like morphologies such as single-walled carbon nanotubes (SW-CNT), nanocylinders and/or ribbons.^{151,160–165} A common feature regarding agglutination by glycopolymeric materials is that the polymers must be of sufficient length to cause intercellular bridging. Therefore, the poor agglutination behaviour by spherical vesicles is likely due to the insufficient dimensions capable to achieve intercellular bridging.¹⁶⁶

1.4.4 Non-specific polymer bacteria interactions

Though cationic and glycopolymers dominate in prior published works regarding bacterial aggregation/ agglutination there are other polymeric material types that are reported to be effective in the bacterial aggregation. This section will discuss various ‘non-specific’ polymers and their potential uses; non-specific polymers in this sense are used to describe polymer-induced aggregation that cannot be directly explained by electrostatics or sugar-lectin interactions.

1.4.4.1 Depletion Aggregation by synthetic polymers

Non-adsorptive synthetic polymers like poly(styrene sulfonate) (PSS) induce bacterial aggregation through polymer-driven depletive forces. Depletion aggregation is dependent on numerous factors, such as: polymer concentration, polymer molecular weight, cell densities and cell physiology; all of which influence one another to dictate the observed aggregation

behaviours. Bacterial physiology is dependent on its growth phase, for instance *E. coli* cell electrophilic mobility is increased in later growth phases due to changes in cell surface charge, which elevates the PSS concentration required to aggregate the bacteria.¹⁶⁷ Both increased molecular weight and chain stiffness positively effect depletion aggregation lowering the required polymer concentrations.^{135,168} Similar effects are observed in depletion aggregation of *B. subtilis* by PEG. Cell cluster sizes were positively correlated with PEG concentration and the cells began to cluster in longitudinal chains typically seen in the initial stages of *Bacilli* biofilm formation. For aggregation to occur, the depletive forces in the system must dominate the shear forces, otherwise cell clusters disperse leading to a reduction in cell culture viscosity.¹⁶⁹

More recently, Sun *et al.* reported rod-shaped cellulose nanocrystal particles (CNC) as effective depletive agents of both *E. coli* and *P. aeruginosa* in concentrations as low as 0.1%. The authors believe the efficacy of CNCs is due to their highly negative zeta (ζ)-potential in conjunction with stationary phase ECM production which minimises the effective polymer concentration required.¹⁷⁰ This was corroborated further when studying the effect of CNCs on normal and overproducing ECM *P. fluorescens* strains (CHA0 and CHA19 respectively). Large dense aggregates were seen in CHA19 following CNC addition compared to small loose aggregates in CHA0.¹⁷¹ Similarly, bacterial colonisation of silica surfaces is reduced in the presence of CNCs. It is postulated that either reduced convective-diffusive transport or larger aggregates formation causes increased hydrodynamic shear thereby elevating surface detachment.^{171,172} A series of thermo- and salt responsive vitamin B5 derived polymers are also reported to induce significant aggregation of *E. coli* and *B. subtilis* by depletive forces¹⁷³

independent of molecular weight, concentration, and crosslinking density. The aggregative effect was hypothesised to be a consequence of competition between the polymer and bacteria for aqueous solute interactions to maintain polymer chain flexibility causing bacterial aggregation.

1.4.4.2 Hydrophobic polymers for bacterial aggregation

Though it is widely recognised that bacteria readily colonise hydrophobic surfaces there are few reports of hydrophobic polymer materials for bacterial aggregation. A poly(acryloyl hydrazide) polymer scaffold was functionalised with a series of hydrophobic aldehydes generating a library of materials to test the role of hydrophobicity in biofilm formation in *E. coli* MC4100 and its daughter strain PHL644 (curli overproducer) (**Figure 1.14**).¹⁷⁴ Functionalisations of increasing hydrophobicity were shown to enhance aggregate formation and curli production in both strains, where following polymer treatment curli production in MC4100 could be increased to levels like PHL644. This work is one of the first works to definitively show that polymer-induced aggregation alters the bacterial physiology to initiate ECM biofilm formation. The subsequent biocatalytic activity of the polymer-induced aggregates was strongly correlated with degree-of-aggregation, furthermore the polymer-induced biofilms displayed greater solvent tolerance and productivity compared to their planktonic counterparts.

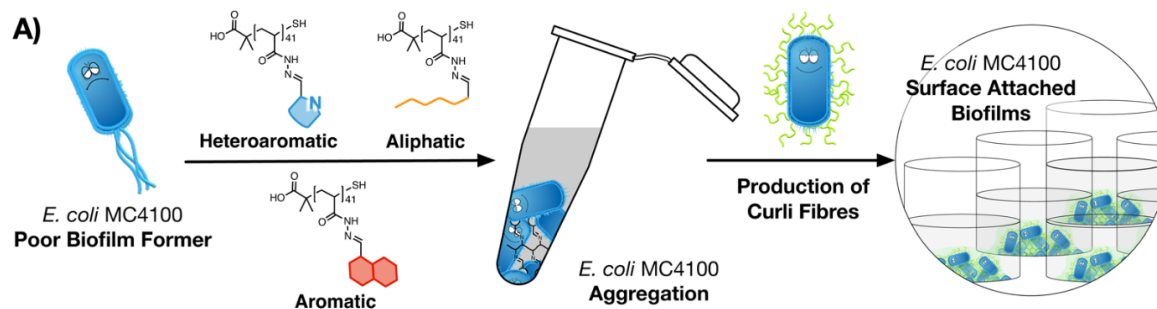


Figure 1.14. Screening of biofilm formation in *E. coli* MC4100 using hydrophobic polymers.

Taken from ref ¹⁷⁴.

High-throughput screenings also show that hydrophobicity greatly influences biofilm formation. Screening of hundreds of polyurethanes and polyacrylates and copolymer derivatives thereof, show that polymer surfaces increased with more hydrophobic formulations. Further studies suggest that bacterial attachment to polymers is a subtle blend of polymer hydrophobicity and chain flexibility. It was discovered that surface attachment of *P. aeruginosa* is greatly reduced in the presence of poly(methacrylates) co-polymers with a rigid hydrophobic pendant (e.g., cyclohexane) when partnered with a hydrophilic ester co-monomer.¹⁷⁵

1.5 Conclusions

Biofilms are typically surface associated cells that are defined by the production of an ECM which bestows the multicellular community with increased resistance to mechanical, physical, and chemical stresses. Previously, biofilms have often been considered as a societal detriment due to their increased antibiotic resistance leading to chronic infection, increased survival of foodborne pathogens as well as their significant role in industrial fouling. However, the very properties that make it difficult to eradicate harmful biofilms have proved useful in several

biotechnological applications, expanding the potential scope of novel green technologies. Previous studies have shown that polymers are useful materials to effectively sequester bacteria where monomer composition can be altered to target bacteria in a variety of mechanisms, such as: hydrophobic interaction, electrostatics, agglutination, or depletive effects. Further research demonstrated that certain Gram-negative bacteria like *V. cholerae* or *E. coli* produce a biofilm-like response following polymer-induced aggregation. However, the understanding of polymer-bacteria interaction remains incomplete. The main limitation of current literature is the lack of reports of polymer-induced aggregation and ECM formation. Much of the literature report polymers as effective sequestrants of bacteria, except for a select handful there are no reports on subsequent changes to bacterial physiology, such as ECM production. Physiological changes are a critical consideration for use of artificial biofilms in biotechnological and biomedical applications as this can greatly affect how bacteria interacts with its environment. As well as its supposed function due to possible mass-transfer limitations or changes in metabolic activity following adoption of a sessile lifestyle. Therefore, this work looks to expand on the prior literature and address some of the current limitations by probing how polymer formulation/ composition influences biofilm formation. The work presented in this thesis represents a multi-disciplinary approach to explore controlled biofilm formation in the biotechnologically relevant strain *E. coli* MC4100. The overview of this research was to evaluate the use of poly(acetylene) based materials as a simultaneous platform for post-polymerisation modification and biofilm formation screening. A more detailed outline of the objectives is given in the following section.

1.6 Bibliography

- 1 M. Berlanga and R. Guerrero, *Microb Cell Fact*, 2016, **15**, 165.
- 2 S. Pandit, M. Fazilati, K. Gaska, A. Derouiche, T. Nypelö, I. Mijakovic and R. Kádár, *Int J Mol Sci*, 2020, **21**, 6755.
- 3 R. V. Joshi, C. Gunawan and R. Mann, *Front Microbiol*, , DOI:10.3389/fmicb.2021.635432.
- 4 H.-C. Flemming and S. Wuertz, *Nat Rev Microbiol*, 2019, **17**, 247–260.
- 5 T. Stalder and E. Top, *NPJ Biofilms Microbiomes*, 2016, **2**, 16022.
- 6 M. Jamal, W. Ahmad, S. Andleeb, F. Jalil, M. Imran, M. A. Nawaz, T. Hussain, M. Ali, M. Rafiq and M. A. Kamil, *Journal of the Chinese Medical Association*, 2018, **81**, 7–11.
- 7 M. Cámara, W. Green, C. E. MacPhee, P. D. Rakowska, R. Raval, M. C. Richardson, J. Slater-Jefferies, K. Steventon and J. S. Webb, *NPJ Biofilms Microbiomes*, 2022, **8**, 42.
- 8 M. Gominet, F. Compain, C. Beloin and D. Lebeaux, *APMIS*, 2017, **125**, 365–375.
- 9 D. Sharma, L. Misba and A. U. Khan, *Antimicrob Resist Infect Control*, 2019, **8**, 76.
- 10 K. Lewis, 2008, pp. 107–131.
- 11 S. M. Amato, C. H. Fazen, T. C. Henry, W. W. K. Mok, M. A. Orman, E. L. Sandvik, K. G. Volzing and M. P. Brynildsen, *Front Microbiol*, , DOI:10.3389/fmicb.2014.00070.
- 12 M. Barlow, 2009, pp. 397–411.
- 13 J. E. Król, A. J. Wojtowicz, L. M. Rogers, H. Heuer, K. Smalla, S. M. Krone and E. M. Top, *Plasmid*, 2013, **70**, 110–119.
- 14 V. J. Savage, I. Chopra and A. J. O'Neill, *Antimicrob Agents Chemother*, 2013, **57**, 1968–1970.
- 15 T. Mattila-Sandholm and G. Wirtanen, *Food Reviews International*, 1992, **8**, 573–603.
- 16 S. Galié, C. García-Gutiérrez, E. M. Miguélez, C. J. Villar and F. Lombó, *Front Microbiol*, , DOI:10.3389/fmicb.2018.00898.
- 17 Y. MORITA, E. KOMODA, K. ONO and S. KUMAGAI, *Food Hygiene and Safety Science (Shokuhin Eiseigaku Zasshi)*, 2011, **52**, 299–303.
- 18 P.-Y. Qian, A. Cheng, R. Wang and R. Zhang, *Nat Rev Microbiol*, 2022, **20**, 671–684.
- 19 S. Tousehik, A. Roy, M. Alam, U. Rahman, N. Nath, S. Nahar, B. Matubber, M. Uddin and P. Roy, *Microorganisms*, 2022, **10**, 2348.
- 20 F. G. Sorroche, M. B. Spesia, Á. Zorreguieta and W. Giordano, *Appl Environ Microbiol*, 2012, **78**, 4092–4101.
- 21 C. H. S. G. Meneses, L. F. M. Rouws, J. L. Simões-Araújo, M. S. Vidal and J. I. Baldani, *Molecular Plant-Microbe Interactions®*, 2011, **24**, 1448–1458.
- 22 A. Gaballa, P. D. Abeyasinghe, G. Urich, S. Matthijs, H. De Greve, P. Cornelis and N. Koedam, *Appl Environ Microbiol*, 1997, **63**, 4340–4345.
- 23 A. Rincón, B. Ruiz-Díez, S. García-Fraile, J. A. L. García, M. Fernández-Pascual, J. J. Pueyo and M. R. Felipe, *FEMS Microbiol Ecol*, 2005, **51**, 303–311.
- 24 S. Burdman, Y. Okon and E. Jurkevitch, *Crit Rev Microbiol*, 2000, **26**, 91–110.
- 25 H. P. Bais, R. Fall and J. M. Vivanco, *Plant Physiol*, 2004, **134**, 307–319.
- 26 C. Alewell, B. Ringeval, C. Ballabio, D. A. Robinson, P. Panagos and P. Borrelli, *Nat Commun*, 2020, **11**, 4546.
- 27 N. Bidyarani, R. Prasanna, S. Babu, F. Hossain and A. K. Saxena, *Microbiol Res*, 2016, **188–189**, 97–105.
- 28 R. Prasanna, B. Ramakrishnan, K. Ranjan, S. Venkatachalam, A. Kanchan, P. Solanki, D. Monga, Y. S. Shivay and S. Kranthi, *Journal of Phytopathology*, 2016, **164**, 1030–1042.
- 29 S. Bajaj and D. K. Singh, *Int Biodeterior Biodegradation*, 2015, **100**, 98–105.

- 30 A. Mitra and S. Mukhopadhyay, *AIMS Bioeng*, 2016, **3**, 44–59.
- 31 M. Vidali, *Pure and Applied Chemistry*, 2001, **73**, 1163–1172.
- 32 T. Biswal and J. A. Malik, in *Microbes and Microbial Biotechnology for Green Remediation*, ed. J. A. Malik, Elsevier, 2022, pp. 205–225.
- 33 M. Eriksson, G. Dalhammar and W. W. Mohn, *FEMS Microbiol Ecol*, 2002, **40**, 21–27.
- 34 Jaakko A. Puhakka, Esa S. Melin, Kimmo T. Järvinen, Päivi M. Koro, Jukka A. Rintala, Päivi Hartikainen, Wen K. Shieh and John F. Ferguson, *Water Science and Technology*, , DOI:10.1016/0273-1223(95)00170-R.
- 35 D. Dasgupta, R. Ghosh and T. K. Sengupta, *ISRN Biotechnol*, 2013, **2013**, 1–13.
- 36 S. Mishra, Y. Huang, J. Li, X. Wu, Z. Zhou, Q. Lei, P. Bhatt and S. Chen, *Chemosphere*, 2022, **294**, 133609.
- 37 K. Sundar, I. M. Sadiq, A. Mukherjee and N. Chandrasekaran, *J Hazard Mater*, 2011, **196**, 44–51.
- 38 B. H. Kim, T. Ikeda, H. S. Park, H. J. Kim, M. S. Hyun, K. Kano, K. Takagi and H. Tatsumi, *Biotechnology Techniques*, 1999, **13**, 475–478.
- 39 D. R. Lovley, *Curr Opin Biotechnol*, 2008, **19**, 564–571.
- 40 J. Greenman, I. Gajda, J. You, B. A. Mendis, O. Obata, G. Pasternak and I. Ieropoulos, *Biofilm*, 2021, **3**, 100057.
- 41 M. F. Umar, M. Rafatullah, S. Z. Abbas, M. N. Mohamad Ibrahim and N. Ismail, *Int J Environ Res Public Health*, 2021, **18**, 3811.
- 42 S.-H. Liu, C.-Y. Lai, J.-W. Ye and C.-W. Lin, *J Clean Prod*, 2018, **194**, 78–84.
- 43 E. M. M. Abdelraheem, H. Busch, U. Hanefeld and F. Tonin, *React Chem Eng*, 2019, **4**, 1878–1894.
- 44 R. A. Sheldon and J. M. Woodley, *Chem Rev*, 2017, **118**, 801–838.
- 45 P. N. Devine, R. M. Howard, R. Kumar, M. P. Thompson, M. D. Truppo and N. J. Turner, *Nat Rev Chem*, 2018, **2**, 409–421.
- 46 R. A. Sheldon and D. Brady, *Chemical Communications*, 2018, **54**, 6088–6104.
- 47 L. Hall-Stoodley, J. W. Costerton and P. Stoodley, *Nat Rev Microbiol*, 2004, **2**, 95–108.
- 48 M. Winn, J. M. Foulkes, S. Perni, M. J. H. Simmons, T. W. Overton and R. J. M. Goss, *Catal Sci Technol*, 2012, **2**, 1544.
- 49 M. R. Kunduru and A. L. Pometto, *J Ind Microbiol*, 1996, **16**, 241–248.
- 50 R. D. Tyagi and T. K. Ghose, *Biotechnol Bioeng*, 1982, **24**, 781–795.
- 51 G. Izmirliloglu and A. Demirci, *Fuel*, 2016, **181**, 643–651.
- 52 R. R. Bland, H. C. Chen, W. J. Jewell, W. D. Bellamy and R. R. Zall, *Biotechnol Lett*, 1982, **4**, 323–328.
- 53 T. Todhanakasem, O. Salangsing, P. Koomphongse, S. Kaewket, P. Kanokratana and V. Champreda, *Front Microbiol*, 2019, **10**, 1777.
- 54 T. A. Krug and A. J. Daugulis, *Biotechnol Lett*, 1983, **5**, 159–164.
- 55 B. Halan, I. Vassilev, K. Lang, A. Schmid and K. Buehler, *Microb Biotechnol*, 2017, **10**, 745–755.
- 56 J. Lienhardt, J. Schripsema, N. Qureshi and H. P. Blaschek, *Appl Biochem Biotechnol*, 2002, **98–100**, 591–598.
- 57 D. Liu, Y. Chen, F.-Y. Ding, T. Zhao, J.-L. Wu, T. Guo, H.-F. Ren, B.-B. Li, H.-Q. Niu, Z. Cao, X.-Q. Lin, J.-J. Xie, X.-J. He and H.-J. Ying, *Biotechnol Biofuels*, 2014, **7**, 5.
- 58 X. Z. Li, J. S. Webb, S. Kjelleberg and B. Rosche, *Appl Environ Microbiol*, 2006, **72**, 5678–5678.
- 59 R. Gross, K. Buehler and A. Schmid, *Biotechnol Bioeng*, 2012, **110**, 424–436.

- 60 A. N. Tsoligkas, M. Winn, J. Bowen, T. W. Overton, M. J. H. Simmons and R. J. M. Goss, *ChemBioChem*, 2011, **12**, 1391–1395.
- 61 X. Tong, T. T. Barberi, C. H. Botting, S. V Sharma, M. J. H. Simmons, T. W. Overton and R. J. M. Goss, *Microb Cell Fact*, 2016, **15**, 180.
- 62 K. Sauer, P. Stoodley, D. M. Goeres, L. Hall-Stoodley, M. Burmølle, P. S. Stewart and T. Bjarnsholt, *Nat Rev Microbiol*, 2022, **20**, 608–620.
- 63 K. Kobayashi, *J Bacteriol*, 2007, **189**, 4920–4931.
- 64 A. Sass, I. Vandenbussche, B. Bellich, P. Cescutti and T. Coenye, *J Bacteriol*, , DOI:10.1128/jb.00017-22.
- 65 Y. Liang, H. Gao, J. Chen, Y. Dong, L. Wu, Z. He, X. Liu, G. Qiu and J. Zhou, *BMC Microbiol*, 2010, **10**, 291.
- 66 S. R. Golub and T. W. Overton, *J Biosci Bioeng*, 2021, **131**, 381–389.
- 67 R. M. Donlan and J. W. Costerton, *Clin Microbiol Rev*, 2002, **15**, 167–193.
- 68 M. Hermansson, *Colloids Surf B Biointerfaces*, 1999, **14**, 105–119.
- 69 B. A. Jucker, H. Harms and A. J. Zehnder, *J Bacteriol*, 1996, **178**, 5472–5479.
- 70 J. M. Meinders, H. C. van der Mei and H. J. Busscher, *J Colloid Interface Sci*, 1995, **176**, 329–341.
- 71 C. J. van Oss, *Colloids Surf B Biointerfaces*, 1995, **5**, 91–110.
- 72 C. J. Van Oss, *Cell Biophys*, 1989, **14**, 1–16.
- 73 C. J. van Oss, *Journal of Molecular Recognition*, 2003, **16**, 177–190.
- 74 B. Kasemo, *Surf Sci*, 2002, **500**, 656–677.
- 75 G. S. Lorite, C. M. Rodrigues, A. A. de Souza, C. Kranz, B. Mizaikoff and M. A. Cotta, *J Colloid Interface Sci*, 2011, **359**, 289–295.
- 76 H. H. Tuson and D. B. Weibel, *Soft Matter*, 2013, **9**, 4368.
- 77 M. Stefani, *Int J Mol Sci*, 2008, **9**, 2515–2542.
- 78 A. Sethuraman and G. Belfort, *Biophys J*, 2005, **88**, 1322–1333.
- 79 A. T. Poortinga, R. Bos, W. Norde and H. J. Busscher, *Surf Sci Rep*, 2002, **47**, 1–32.
- 80 E. D. Avila-Calderón, M. del S. Ruiz-Palma, Ma. G. Aguilera-Arreola, N. Velázquez-Guadarrama, E. A. Ruiz, Z. Gomez-Lunar, S. Witonsky and A. Contreras-Rodríguez, *Front Microbiol*, , DOI:10.3389/fmicb.2021.557902.
- 81 J. Sun, S. T. Rutherford, T. J. Silhavy and K. C. Huang, *Nat Rev Microbiol*, 2022, **20**, 236–248.
- 82 N. I. Abu-Lail and T. A. Camesano, *Environ Sci Technol*, 2003, **37**, 2173–2183.
- 83 N. C. Caiazza and G. A. O’Toole, *J Bacteriol*, 2004, **186**, 4476–4485.
- 84 O. E. Petrova and K. Sauer, *J Bacteriol*, 2012, **194**, 2413–2425.
- 85 G. Li, L.-K. Tam and J. X. Tang, *Proceedings of the National Academy of Sciences*, 2008, **105**, 18355–18359.
- 86 L. A. Pratt and R. Kolter, *Mol Microbiol*, 1998, **30**, 285–293.
- 87 D. R. Korber, J. R. Lawrence and D. E. Caldwell, *Appl Environ Microbiol*, 1994, **60**, 1421–1429.
- 88 W. Benyoussef, M. Deforet, A. Monmeyran and N. Henry, *Front Cell Infect Microbiol*, 2022, **12**, 896898.
- 89 C. Prigent-Combaret, G. Prensier, T. T. Le Thi, O. Vidal, P. Lejeune and C. Dorel, *Environ Microbiol*, 2000, **2**, 450–464.
- 90 M. L. Grant and D. A. Saville, *J Colloid Interface Sci*, 1995, **171**, 35–45.
- 91 D. Ren, L. A. Bedzyk, S. M. Thomas, R. W. Ye and T. K. Wood, *Appl Microbiol Biotechnol*, 2004, **64**, 515–524.
- 92 K. C. Marshall, *ASM News*, 1992, 202–207.

- 93 M. A. Schembri, G. Christiansen and P. Klemm, *Mol Microbiol*, 2001, **41**, 1419–1430.
- 94 P. N. Danese, L. A. Pratt and R. Kolter, *J Bacteriol*, 2000, **182**, 3593–3596.
- 95 M. A. Lasaro, N. Salinger, J. Zhang, Y. Wang, Z. Zhong, M. Goulian and J. Zhu, *Appl Environ Microbiol*, 2009, **75**, 246–251.
- 96 K. Otto, J. Norbeck, T. Larsson, K.-A. Karlsson and M. Hermansson, *J Bacteriol*, 2001, **183**, 2445–2453.
- 97 E. P. DeBenedictis, Y. Zhang and S. Keten, *Macromolecules*, 2020, **53**, 6123–6134.
- 98 E. A. Epstein and M. R. Chapman, *Cell Microbiol*, 2008, **10**, 1413–1420.
- 99 Q. Shu, S. L. Crick, J. S. Pinkner, B. Ford, S. J. Hultgren and C. Frieden, *Proceedings of the National Academy of Sciences*, 2012, **109**, 6502–6507.
- 100 A. Olsén, M. J. Wick, M. Mörgelin and L. Björck, *Infect Immun*, 1998, **66**, 944–949.
- 101 M. Andreasen, G. Meisl, J. D. Taylor, T. C. T. Michaels, A. Levin, D. E. Otzen, M. R. Chapman, C. M. Dobson, S. J. Matthews and T. P. J. Knowles, *mBio*, 2019, **10**, e02279–18.
- 102 S. A. Tursi and Ç. Tükel, *Microbiology and Molecular Biology Reviews*, , DOI:10.1128/mmbr.00028-18.
- 103 C. Beloin, A. Roux and J.-M. Ghigo, *Curr Top Microbiol Immunol*, 2008, 249–289.
- 104 D. Roux, C. Cywes-Bentley, Y.-F. Zhang, S. Pons, M. Konkol, D. B. Kearns, D. J. Little, P. L. Howell, D. Skurnik and G. B. Pier, *Journal of Biological Chemistry*, 2015, **290**, 19261–19272.
- 105 J. B. Kaplan, K. Velliyagounder, C. Ragunath, H. Rohde, D. Mack, J. K.-M. Knobloch and N. Ramasubbu, *J Bacteriol*, 2004, **186**, 8213–8220.
- 106 X. Wang, J. F. Preston and T. Romeo, *J Bacteriol*, 2004, **186**, 2724–2734.
- 107 C. Goller, X. Wang, Y. Itoh and T. Romeo, *J Bacteriol*, 2006, **188**, 8022–8032.
- 108 Y. Itoh, J. D. Rice, C. Goller, A. Pannuri, J. Taylor, J. Meisner, T. J. Beveridge, J. F. Preston and T. Romeo, *J Bacteriol*, 2008, **190**, 3670–3680.
- 109 X. Wang, A. K. Dubey, K. Suzuki, C. S. Baker, P. Babitzke and T. Romeo, *Mol Microbiol*, 2005, **56**, 1648–1663.
- 110 R. Hengge, M. Y. Galperin, J.-M. Ghigo, M. Gomelsky, J. Green, K. T. Hughes, U. Jenal and P. Landini, *J Bacteriol*, 2016, **198**, 7–11.
- 111 C. Wang, H. Zhang, J. Wang, S. Chen, Z. Wang, L. Zhao and X. Wang, *Microbiol Res*, 2020, **239**, 126527.
- 112 T. May and S. Okabe, *J Bacteriol*, 2008, **190**, 7479–7490.
- 113 X. Nassif, N. Honoré, T. Vasselon, S. T. Cole and P. J. Sansonetti, *Mol Microbiol*, 1989, **3**, 1349–1359.
- 114 K. Yoshida, Y. Tashiro, T. May and S. Okabe, *Water Res*, 2015, **76**, 33–42.
- 115 M. Ionescu and S. Belkin, *Appl Environ Microbiol*, 2009, **75**, 483–492.
- 116 B. Obadia, S. Lacour, P. Doublet, H. Baubichon-Cortay, A. J. Cozzone and C. Grangeasse, *J Mol Biol*, 2007, **367**, 42–53.
- 117 D. Hagiwara, M. Sugiura, T. Oshima, H. Mori, H. Aiba, T. Yamashino and T. Mizuno, *J Bacteriol*, 2003, **185**, 5735–5746.
- 118 D. H. Limoli, C. J. Jones and D. J. Wozniak, *Microbiol Spectr*, , DOI:10.1128/microbiolspec.MB-0011-2014.
- 119 J. Jeffries, W. Thongsomboon, J. A. Visser, K. Enriquez, D. Yager and L. Cegelski, *Biopolymers*, 2021, **112**, e23395.
- 120 U. Römling and M. Y. Galperin, *Trends Microbiol*, 2015, **23**, 545–557.
- 121 D. O. Serra, A. M. Richter and R. Hengge, *J Bacteriol*, 2013, **195**, 5540–5554.
- 122 R. Bos, H. C. van der Mei and H. J. Busscher, *FEMS Microbiol Rev*, 1999, **23**, 179–230.

- 123 M. Katsikogianni and Y. Missirlis, *Eur Cell Mater*, 2004, **8**, 37–57.
- 124 V. D. Gordon and L. Wang, *J Cell Sci*, , DOI:10.1242/jcs.227694.
- 125 R. D. Tyagi and T. K. Ghose, *Biotechnol Bioeng*, 1982, **24**, 781–795.
- 126 R. R. Bland, H. C. Chen, W. J. Jewell, W. D. Bellamy and R. R. Zall, *Biotechnol Lett*, 1982, **4**, 323–328.
- 127 T. A. Krug and A. J. Daugulis, *Biotechnol Lett*, 1983, **5**, 159–164.
- 128 M. R. Kunduru and A. Pometto, *J Ind Microbiol*, 1996, **16**, 241–248.
- 129 Yu. G. Maksimova, *Appl Biochem Microbiol*, 2014, **50**, 750–760.
- 130 G. P. Treweek and J. J. Morgan, *J Colloid Interface Sci*, 1977, **60**, 258–273.
- 131 J. Hughes, D. K. Ramsden and K. C. Symes, *Biotechnology Techniques*, 1990, **4**, 55–60.
- 132 J. Chen, A. Eraghi Kazzaz, N. AlipoorMazandarani, Z. Hosseinpour Feizi and P. Fatehi, *Molecules*, 2018, **23**, 868.
- 133 S. P. Strand, M. S. Vandvik, K. M. Vårum and K. Østgaard, *Biomacromolecules*, 2001, **2**, 126–133.
- 134 T. Suopajärvi, H. Liimatainen, O. Hormi and J. Niinimäki, *Chemical Engineering Journal*, 2013, **231**, 59–67.
- 135 J. Schwarz-Linek, G. Dorken, A. Winkler, L. G. Wilson, N. T. Pham, C. E. French, T. Schilling and W. C. K. Poon, *EPL (Europhysics Letters)*, 2010, **89**, 68003.
- 136 J. Schwarz-Linek, A. Winkler, L. G. Wilson, N. T. Pham, T. Schilling and W. C. K. Poon, *Soft Matter*, 2010, **6**, 4540–4549.
- 137 G. Dorken, G. P. Ferguson, C. E. French and W. C. K. Poon, *J R Soc Interface*, 2012, **9**, 3490–3502.
- 138 T. Bjarnsholt, M. Alhede, M. Alhede, S. R. Eickhardt-Sørensen, C. Moser, M. Kühl, P. Ø. Jensen and N. Høiby, *Trends Microbiol*, 2013, **21**, 466–474.
- 139 P. R. Secor, L. A. Michaels, A. Ratjen, L. K. Jennings and P. K. Singh, *Proceedings of the National Academy of Sciences*, 2018, **115**, 201806005.
- 140 H. Qiu, Z. Si, Y. Luo, P. Feng, X. Wu, W. Hou, Y. Zhu, M. B. Chan-Park, L. Xu and D. Huang, *Front Bioeng Biotechnol*, , DOI:10.3389/fbioe.2020.00910.
- 141 C. Peng, A. Vishwakarma, S. Mankoci, H. A. Barton and A. Joy, *Biomacromolecules*, 2019, **20**, 1675–1682.
- 142 L. T. Lui, X. Xue, C. Sui, A. Brown, D. I. Pritchard, N. Halliday, K. Winzer, S. M. Howdle, F. Fernandez-Trillo, N. Krasnogor and C. Alexander, *Nat Chem*, 2013, **5**, 1058–1065.
- 143 N. Perez-Soto, L. Moule, D. N. Crisan, I. Insua, L. M. Taylor-Smith, K. Voelz, F. Fernandez-Trillo and A. M. Krachler, *Chem Sci*, 2017, **8**, 5291–5298.
- 144 N. Perez-Soto, O. Creese, F. Fernandez-Trillo and A.-M. Krachler, *ACS Chem Biol*, 2018, **13**, 3021–3029.
- 145 E. Leire, S. P. Amaral, I. Louzao, K. Winzer, C. Alexander, E. Fernandez-Megia and F. Fernandez-Trillo, *Biomater Sci*, 2016, **4**, 998–1006.
- 146 P. Zhang, H. Lu, H. Chen, J. Zhang, L. Liu, F. Lv and S. Wang, *Anal Chem*, 2016, **88**, 2985–2988.
- 147 I. Louzao, C. Sui, K. Winzer, F. Fernandez-Trillo and C. Alexander, *European Journal of Pharmaceutics and Biopharmaceutics*, 2015, **95**, 47–62.
- 148 E. P. Magennis, F. Fernandez-Trillo, C. Sui, S. G. Spain, D. J. Bradshaw, D. Churchley, G. Mantovani, K. Winzer and C. Alexander, *Nat Mater*, 2014, **13**, 748–755.
- 149 G. Qi, F. Hu, Kenry, K. C. Chong, M. Wu, Y. H. Gan and B. Liu, *Adv Funct Mater*, 2020, **30**, 2001338.

- 150 P. Magala, R. E. Klevit, W. E. Thomas, E. V. Sokurenko and R. E. Stenkamp, *Proteins: Structure, Function, and Bioinformatics*, 2020, **88**, 593–603.
- 151 Y. Lim, S. Park, E. Lee, H. Jeong, J.-H. Ryu, M. S. Lee and M. Lee, *Biomacromolecules*, 2007, **8**, 1404–1408.
- 152 J. Bouckaert, J. Berglund, M. Schembri, E. De Genst, L. Cools, M. Wuhrer, C.-S. Hung, J. Pinkner, R. Slättegård, A. Zavialov, D. Choudhury, S. Langermann, S. J. Hultgren, L. Wyns, P. Klemm, S. Oscarson, S. D. Knight and H. De Greve, *Mol Microbiol*, 2004, **55**, 441–455.
- 153 X. Yan, A. Sivignon, N. Yamakawa, A. Crepet, C. Travelet, R. Borsali, T. Dumych, Z. Li, R. Bilyy, D. Deniaud, E. Fleury, N. Barnich, A. Darfeuille-Michaud, S. G. Guin, J. Bouckaert and J. Bernard, *Biomacromolecules*, 2015, **16**, 1827–1836.
- 154 X. Yan, A. Sivignon, N. Barnich, S. G. Guin, J. Bouckaert, E. Fleury and J. Bernard, *Polym Chem*, 2016, **7**, 2674–2683.
- 155 M. D. Disney, J. Zheng, T. M. Swager and P. H. Seeberger, *J Am Chem Soc*, 2004, **126**, 13343–13346.
- 156 R. L. Phillips, I.-B. Kim, B. E. Carson, B. Tidbeck, Y. Bai, T. L. Lowary, L. M. Tolbert and U. H. F. Bunz, *Macromolecules*, 2008, **41**, 7316–7320.
- 157 M.-G. Baek, R. C. Stevens and D. H. Charych, *Bioconjug Chem*, 2000, **11**, 777–788.
- 158 C. Xue, S. Velayudham, S. Johnson, R. Saha, A. Smith, W. Brewer, P. Murthy, S. T. Bagley and H. Liu, *Chemistry - A European Journal*, 2009, **15**, 2289–2295.
- 159 G. Pasparakis, A. Cockayne and C. Alexander, *J Am Chem Soc*, 2007, **129**, 11014–11015.
- 160 Y. Lim, S. Park, E. Lee, J.-H. Ryu, Y.-R. Yoon, T.-H. Kim and M. Lee, *Chem Asian J*, 2007, **2**, 1363–1369.
- 161 J. J. Cid Martín, M. Assali, E. Fernández-García, V. Valdivia, E. M. Sánchez-Fernández, J. M. Garcia Fernández, R. E. Wellinger, I. Fernández and N. Khair, *J Mater Chem B*, 2016, **4**, 2028–2037.
- 162 D.-W. Lee, T. Kim, I.-S. Park, Z. Huang and M. Lee, *J Am Chem Soc*, 2012, **134**, 14722–14725.
- 163 G. Yu, Y. Ma, C. Han, Y. Yao, G. Tang, Z. Mao, C. Gao and F. Huang, *J Am Chem Soc*, 2013, **135**, 10310–10313.
- 164 M. K. Müller and L. Brunsveld, *Angewandte Chemie International Edition*, 2009, **48**, 2921–2924.
- 165 J.-H. Ryu, E. Lee, Y. Lim and M. Lee, *J Am Chem Soc*, 2007, **129**, 4808–4814.
- 166 G. Yu, Y. Ma, C. Han, Y. Yao, G. Tang, Z. Mao, C. Gao and F. Huang, *J Am Chem Soc*, 2013, **135**, 10310–10313.
- 167 K. E. Eboigbodin, J. R. A. Newton, A. F. Routh and C. A. Biggs, *Langmuir*, 2005, **21**, 12315–12319.
- 168 J. Schwarz-Linek, A. Winkler, L. G. Wilson, N. T. Pham, T. Schilling and W. C. K. Poon, *Soft Matter*, 2010, **6**, 4540.
- 169 X. Wang, X. Shen, Z. Wang and Y. Kong, *European Biophysics Journal*, 2019, **48**, 599–608.
- 170 X. Sun, C. Danumah, Y. Liu and Y. Boluk, *Chemical Engineering Journal*, 2012, **198–199**, 476–481.
- 171 X. Sun, Y. Shao, Y. Boluk and Y. Liu, *Colloids Surf B Biointerfaces*, 2015, **136**, 570–576.
- 172 X. Sun, Q. Lu, Y. Boluk and Y. Liu, *Soft Matter*, 2014, **10**, 8923–8931.
- 173 N. Nazeer and M. Ahmed, *Eur Polym J*, 2019, **119**, 148–154.
- 174 P. Adoni, A. Romanyuk, T. W. Overton and P. Fernandez-Trillo, *Mater Horiz*, 2022, **9**, 2592–2602.

- 175 A. A. Dundas, O. Sanni, J. Dubern, G. Dimitrakis, A. L. Hook, D. J. Irvine, P. Williams and M. R. Alexander, *Advanced Materials*, 2019, **31**, 1903513.

Chapter 2 – Synthesis, characterisation, and post-polymerisation
modification of a novel poly(carbamoylhydrazine-1-carboxylate
acetylene) scaffold

2.0 Introduction

The helix is considered a fundamental structure in nature appearing as an abundant secondary structure in proteins, nucleic acids, and polysaccharides and most famously DNA.¹ Synthetic polymer chemistry has flourished in the past century birthing a wide range of materials finding potential biotechnological and biomedical applications such as tissue engineering, drug delivery vectors and anti-microbials.^{1,2} The abundance of helical structures throughout nature have made it a highly attractive structure to mimic by scientists in the development of more advanced materials. The design and application of synthetic polymeric helices is a growing field in drug delivery and cell engineering, where the helix potentiates the biological activity of the material. For example, siRNA transfection into HeLa cells by poly[5-(4-formylbenzyl)-L-glutamic acid] was effective only when the polymeric vector was helical. It was hypothesised that helicity enhanced permeation through the cell membrane.³

There are several reported classes of synthetic helical polymers such as poly(amino acids)/polypeptides, poly(isocyanides), and poly(acetylenes). Synthetic poly(amino acids) commonly synthesised through ring opening polymerisations of N-carboxyanhydride derived amino acids. Helical formation is dependent on the amino acid composition of the polymer chain, whereby amino acids such as alanine, glutamic acid and leucine promote formation of α -helices. Poly(isocyanides) are synthesised from substituted isocyanide monomers using group-10 catalysts, most commonly Ni(II). The polymer backbone consists entirely of substituted isocyanides stabilised by steric and electronic effects due to formation of local energy minima.

These classes of materials were not chosen for several reasons. Firstly, the susceptibility of poly(amino acids) by bacterial proteases was unknown, which could limit its long-term application in *in-vitro* experiments. Thus, given the infancy of the project it was considered more appropriate to use a polymer with a stable backbone resistant to possible biological activity. Ultimately, poly(acetylenes) were chosen over poly(isocyanides). Despite their similarities, poly(acetylenes) were chosen due to their facile synthesis and purification. Furthermore, the polymerisations are tolerance of a wide range of functional groups greatly expanding possible material designs.

Poly(acetylenes) and poly(phenylacetylenes) are synthesised from alkyne monomers resulting in a conjugated backbone with alternating carbon-carbon double bonds. Poly(acetylenes) can exist in one of four stereochemistries; cis-cisoid, cis-transoid, trans-cisoid and trans-transoid (Error! Reference source not found.). Due to the restricted bond rotation around the single C-C bond in cis-cisoid and cis-transoid polymers the backbone is constrained to a helical structure.^{4,5} Non-covalent interactions such as intramolecular hydrogen bonding, π - π stacking and steric repulsions between the polymer side chains further stabilises the helical secondary structure.¹ Simionescu *et al.*, first deduced that successful helical adoption by poly(acetylenes) is highly dependent on the stereoregularity of the backbone where high cis- contents favoured the adoption of helical secondary structures.⁶

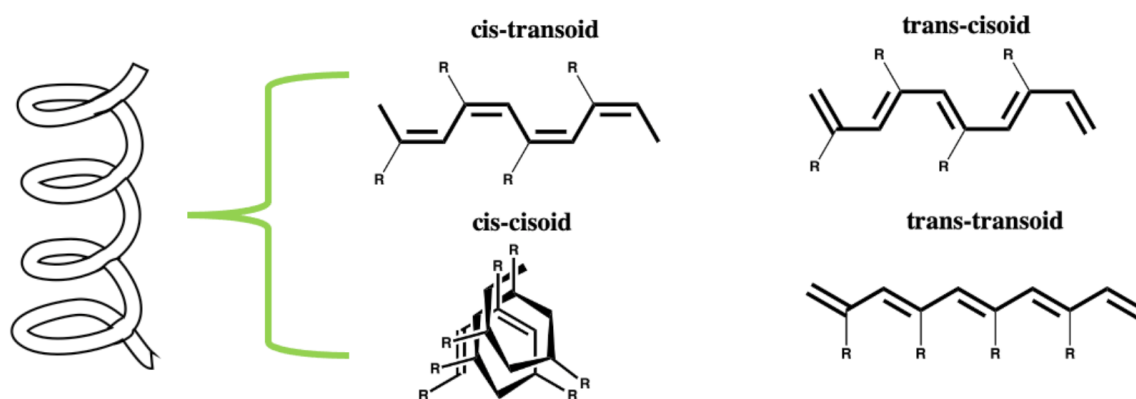
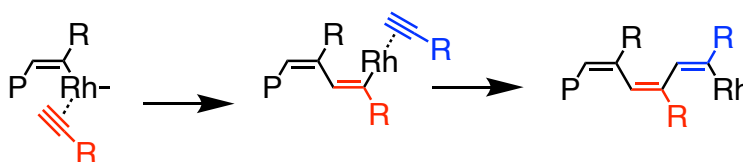


Figure 2.1. Possible backbone stereochemistry adopted in poly(acetylenes). Only cis-cis and cis-trans polymers can adopt a helical secondary structure.

Stereochemical control of the polymer backbone is achieved through metal catalyst choice. Group 5, 6 and 8 transition metal-based catalysts polymerise various mono- and disubstituted alkynes with varying success. Masuda *et al.* first proposed that the polymerisation mechanism of alkynes with Mo occurs akin to olefin co-ordination polymerisation whereby the polymer is formed through a metal-carbene complex (**Figure 2.2**).⁷ Poly(acetylenes) synthesised with metathesis catalysts generally have low cis content and therefore will not form helical secondary structures due to the unrestricted rotation in the C-C bond.⁸ Alternatively, Rh-based catalysts produce almost exclusively stereoregular, predominantly cisoid polymers. Noyori *et al.*, demonstrated that the cis stereoregularity was a product of a 2,1-insertion mechanism between the monomer and metal-olefin complex (**Figure 2.2**).⁹ Although, metathesis polymerisation is theoretically possible using Rh catalysts it is highly energetically unfavourable with respect to initiation and propagation. For instance, activation enthalpy of a metathesis transition state and subsequent ring opening needs to overcome an energy barrier of 18.7 kcal mol⁻¹ and 24.9 kcal mol⁻¹ respectively. In contrast, an insertion mechanism would require an energetic barrier of only 13.3 kcal mol⁻¹ and 9.4 kcal mol⁻¹ for respective

initiation and propagation.¹⁰ Therefore, Rh catalysts thermodynamically favour insertion polymerisation mechanisms, leading to extremely high cis-character polymers. Furthermore, Rh catalysts show much greater stability in with polar solvents and functional groups whilst metathesis catalysts are prone to fouling. Hence, the improved reaction stability is a considerable advantage in the synthesis of highly functionalised polymers due to the wider scope of materials that can be synthesised.^{9,11,12}

2,1 Insertion mechanism



Carbene metathesis mechanism

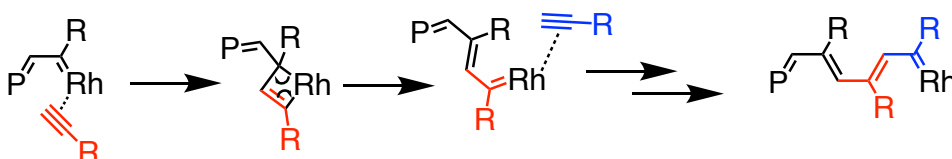


Figure 2.2 Two polymerisation mechanisms of Rh-based polymerisation. 2,1-insertion produces cis-regular poly(acetylenes); carbene metathesis primarily produces trans regular poly(acetylenes).

Cis-regular PA and PPA materials often form helical structures in solution, stabilised by intramolecular non-covalent interactions. Reported polyacetylenes such as N-propargylamides,^{13,14} N-propargyl alkylamides,^{15,16} N-propargylcarbamates,¹⁷ N-propargylurea,^{18,19} and methyl propargyl esters^{20–22} all form stable helices due to intramolecular hydrogen bonding between the side chains. Tang et al., showed that helix stability varied with spacer length in the side chains. Here, increased pendant length reduced stereoregularity in the polymer backbones effecting the conformational coil-to-helix

transition. Stable helices were only observed at low temperatures in polymers with lower cis regularity showing that stereoregularity and stability were dependent on monomer bulk.^{23,24}

Although poly(acetylenes) form helices their utility in biological applications remains largely unexplored. This work was interested in the use of helical polymers for controlled biofilm formation in *E. coli* (see Chapter 3). It was hypothesised that a helical structure would enhance bacterial association from improved ligand surface presentation (due to restricted backbone mobility). Previous studies showed cylindrical nanoparticles were more effective agglutination agents than spherical nanoparticles.^{25–28} It is expected that a helical polymer would form a rod-shape which was postulated to enhance aggregation in these systems rather than a random coil polymer. In addition, Kolewe et al., showed that bacterial adhesion was enhanced by increased chain/material stiffness in polymer-coated surfaces. Given the restricted rotation in helical polymers, it was believed that this added stiffness may also promote bacterial aggregation in our tested systems.²⁹ To the best of our knowledge there have been no reports of helical polymers as nucleation agents for biofilm formation; therefore, this is an extremely novel area in which to expand our understandings. ³The work presented herein focussed on the design, synthesis, characterisation, and modification of a novel poly(acetylene; poly(carbamoylhydrazine-1-carboxylate acetylene).

2.1 Materials & Methods

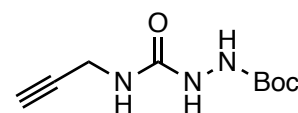
2.1.1 General Procedures

Nuclear Magnetic Resonance (NMR) spectra were recorded on either a Bruker Advance III 300 MHz or a Bruker Advance III 400 MHz spectrometer. Chemical shifts are reported in ppm (units) referenced to TMS (0 ppm). Gel Permeation Chromatography (GPC) was performed

with a Shimadzu Prominence LC-20A fitted with a ThermoFisher Refractomax 521 Detector and a SPD20A UV-vis Detector. DMF was used as the eluent at a flow rate of 1 mL min⁻¹. The instrument was fitted with an Agilent PLGel PL1110-6540 columns (300 × 7.5 mm, 5 μm) column and run at 35 °C. Molecular weights were calculated based on a standard calibration method using poly(ethylene oxide). All FTIR measurements were performed in the solid phase using a PerkinElmer UATR2 spectrometer. Ultraviolet/visible (UV-vis) measurements were performed using a Cary 5000 spectrophotometer using a 1 cm pathlength quartz cuvette. All circular dichroism measurements were performed using a Jasco J-810 CD Spectrometer with a 0.1 mm pathlength quartz cuvette. All chemicals were purchased from either Sigma-Aldrich®, Fisher Scientific®, VWR® or Acros®, and used without further purification unless otherwise stated. All solvents were Reagent grade or above, purchased from Sigma-Aldrich®, Fisher Scientific® or VWR®, and used without further purification.

2.1.2 t-butyl 2-(prop-2-yn-1-ylcarbamoyl)hydrazine-1-carboxylate (M1)

1,1-carbonyl diimidazole was first recrystallised from hot anhydrous THF under N₂ prior to reaction. Solutions of 0.44M 1,1-

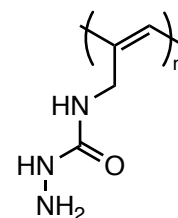


CDI (3.68 g) and 0.44 M t-butyl carbazate (3.0 g) were respectively dissolved in DMF and degassed for 20 mins. The solution of t-butyl carbazate was added dropwise to CDI over the course of 30 mins and then allowed to react for a further 15 mins at 30 °C. 1 equivalent of propargyl amine (1.251 g) was then added dropwise to the stirred solution over 30 mins left to react for an additional 1 h. The solvent was removed under vacuum and the resultant residue was dissolved in ethyl acetate. The organic layer was washed with 5% HCl (3 x 50 mL), deionised water (3 x 50 mL), and then saturated brine. The organic phase was dried with

anhydrous Na₂SO₄, filtered, and concentrated in vacuo to yield a pure product as an off-white solid and stored in a desiccator prior to use. Yield = 2.91 g (60%). ¹H NMR (400 MHz, DMSO-*d*₆) δ 8.52 (s, 1H), 7.76 (s, 1H), 6.64 (s, 1H), 3.79 (dd, *J* = 5.8, 2.5 Hz, 2H), 3.03 (t, *J* = 2.5 Hz, 1H), 1.40 (s, 9H). ¹³C NMR (400 MHz, DMSO-*d*₆) δ 158.34, 156.38, 82.79, 79.45, 72.86, 29.18, 28.56. FTIR (cm⁻¹): 3298.3, 2981.2, 2050.5, 1725.0, 1642.9, 1490.3, 1366.1, 1280.8, 1101.3, 940.44, 793.9, 665.41, 534.25. [M+Na]⁺ calculated for C₉H₁₅N₃O₃ Na 236.1011; found 236.1013.

2.1.3 Poly(*t*-butyl 2-(carbamoyl)hydrazine-1-carboxylate acetylene) (P1)

M1 (2.9 g) was suspended in 60 mL CHCl₃ and degassed with nitrogen, the mixture was heated to 30 °C and stirred until complete dissolution of the monomer. A solution of [Rh(nbd)BPh₄]⁰ (0.01 equiv.) in CHCl₃ was added via syringe to the reaction mixture and then reacted at 30 °C for 24h. The polymerisation mixture was transferred to a dropping funnel and was precipitated dropwise into a large excess of hexane. The polymer precipitate was filtered, and the solids were collected and dried under vacuum to yield P1-Boc as a brown solid (2.85 g). P1-Boc was dissolved in neat TFA (30 mg mL⁻¹) and stirred for 24 h, after which TFA removed under a continuous N₂ stream, and the resultant oil was carefully neutralised with 8M NaOH. The neutralised mixture was dialysed (Spectra/Por 6 1kDa MWCO; 38 mm width) against a deionised water for 24 h (5 × water changes in this time) and the dialysed suspension was lyophilised to yield P1 as a static beige powder. Yield = 1.43 g (92%). ¹H NMR (400 MHz, Deuterium Oxide) δ 6.77 – 5.34 (br. s, 1H), 3.81 (br. s, 2H). ¹³C NMR (101 MHz, Chloroform-*d*) δ 82.28, 28.79. FTIR (cm⁻¹): 3254.3, 3009.2, 2879.4, 1635.9, 1525.1, 1490.3, 1374.1, 1230.6, 1101.3, 991.17. GPC: M_w = 4.1 × 10⁴ g mol⁻¹; M_n = 2.4 × 10⁴; Đ_M = 1.70.



2.1.4 Acyl hydrazone post-polymerisation functionalisation procedures

Separate stock solutions of P1 (0.0884 M) in deuterated 0.2M acetic acid and 0.0884 M aldehydes stock solutions in DMSO-d₆ were prepared separately. The aldehyde stock solutions are added in equal volume to the polymer stock solutions (1 mol equiv.) and reacted at 30 °C for 24 h. Degree-of-functionalisation (DF %) is measured by quantitative ¹H-NMR using dimethyl sulfone as an internal standard and calculated according to equation 1.

$$DF = 1 - \left[\frac{\left(\frac{I_{ald}}{\#H_{ald}} \right)}{\left(\frac{I_{stand}}{\#H_{stand}} \right)} \right] \times 100 \quad (1)$$

2.2 Polymer design considerations and *in silico* studies

The aim of this thesis was to probe the effect of polymer structure and chemistry on *E. coli* biofilm formation. To undertake this, it was desirable to develop a material library for screening in later biological assays. Rather than synthesise multiple unique polymers, it was considered more attractive to create a reactive polymer scaffold which could be modified post-polymerisation. Pursuing post-polymerisation modification simplifies material synthesis as optimisation is only required for one polymer scaffold rather than many. Furthermore, the post-polymerisation reactions can be performed in identical conditions allowing rapid creation of a material library. There are numerous reaction types reported for post-polymerisation modifications such as amide coupling, copper-azide click chemistry, Michael-type addition reactions, anhydride additions, and thiol exchanges.³⁰ One post-polymerisation modification strategy that has garnered a lot of attraction in bio-conjugative chemistry is Schiff bases. The general chemical structure $R^1R^2C=NR^3$ (R^3 = alkyl or aryl) can be used to broadly describe a range of functional groups such as imines, ketimines, hydrazones and oximes due to the high yields attained and biorthogonality of these reactions.³¹ Compared to other imines and hydrazones, acyl hydrazones possess superior resistance to hydrolysis in both acid and neutral pH.³² Minimising acyl hydrazone hydrolysis is highly advantageous in biological environments given the extended exposure to aqueous environments; hence limited aldehyde reformation should occur with the use of polymeric acyl hydrazone materials. Poly(acryloyl hydrazone) was shown to effectively conjugate a wide range of hydrophilic and hydrophobic aldehydes demonstrating it to be an effective transfection screening agent for siRNA delivery.³³ Furthermore, the same polymer scaffold was shown to be effective in the aggregation and subsequent biofilm formation in *E. coli* PHL644. The broad range of possible

applications successfully performed by the same polymer scaffold is possible due to the altered physicochemical properties following post-polymerisation modification. Therefore, for the work described herein the polymer poly(hydrazine carboxamide acetylene) (**P1**) was synthesised, where the polymer side chains possess an acyl hydrazones terminus that would readily react with aldehydes under mildly acidic conditions (*Figure 2.3*).

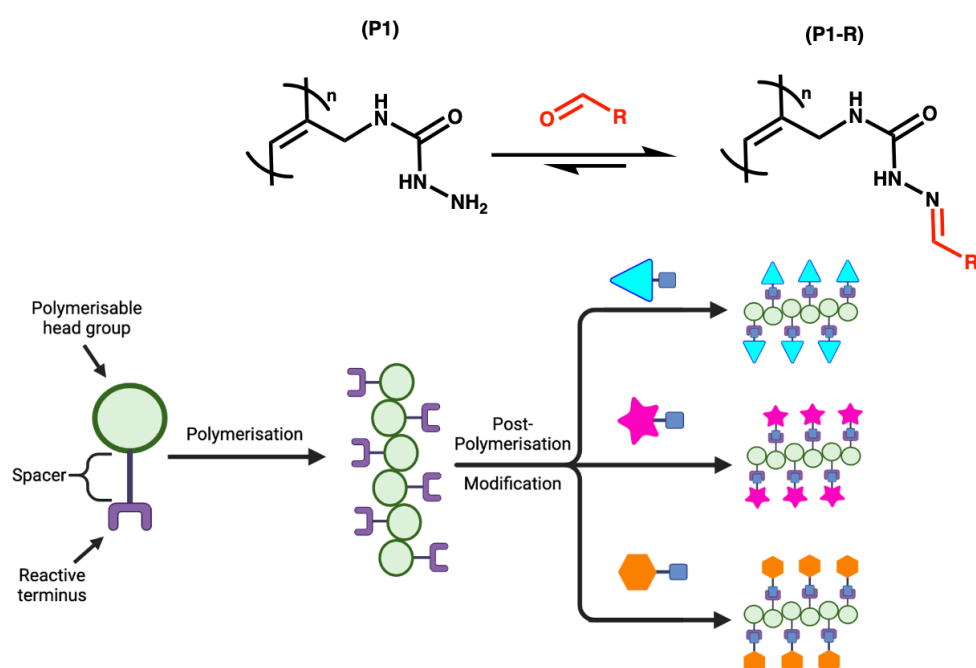


*Figure 2.3 Structure of **P1** and hydrazone functionalised **P1-R** (top). Diagram showing general strategy of post-polymerisation modification for material library generation.*

Inclusion of the carbamoyl fragment in the design considerations was two-fold. Firstly, previous poly(acetylene materials) synthesised within the group included a structurally similar carbamate hydrazide derivative of **P1**. This however suffered from poor solubility in both organic and aqueous solvents therefore a change to the more hydrophilic urea/carbamate motif was hypothesised to improve solubility. In addition, it was hypothesised that the carbamoyl moiety would stabilise a helical secondary structure through extensive hydrogen

bonding (N-H---O=C) between adjacent side chains (Figure 2.4). To test this an oligomeric structure of **P1** (10mer) was imported into Avogadro® and an MMFF94 energy minimisation simulation was performed using a steepest descent gradient algorithm.

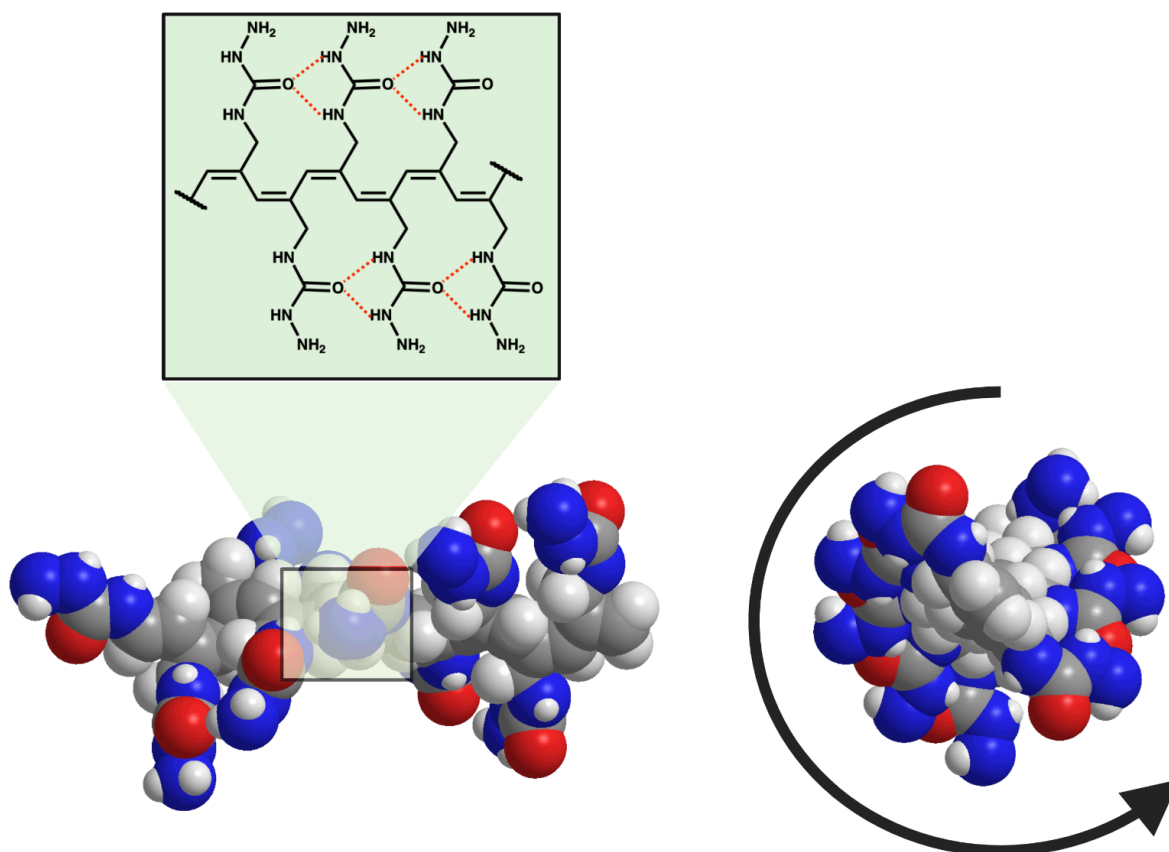


Figure 2.4 Side (left) and top view (right) of 3D structure of P1-10mer following MMFF94 simulation in Avogadro. Skeletal structure of P1 showing hydrogen bond formation between the polymer side units.

The energy minimised structure (Figure 2.4) showed **P1** adopted a helical configuration. The P1 backbone possessed an average torsional bond angle (φ) of $138^\circ \pm 12^\circ$ equivalent to what is found in poly(acetylenes) with *cis-transoid*. A more powerful simulation would include varied torsional angles in the polymer backbone with subsequent energy minimisations performed to identify conformations with the lowest local energy minima. Unfortunately,

such procedures were not possible with the software available. Though limited in scope the initial MMFF94 simulation proved that helical adoption of **P1** was theoretically possible.

2.3 Monomer synthesis

To synthesise **P1**, the corresponding monomer *t*-butyl 2-(prop-2-yn-1-ylcarbamoyl)hydrazine-1-carboxylate (**M1**) was first synthesised. There are numerous synthetic strategies for the synthesis of asymmetric ureas; however, many of these involves the use of toxic reagents such as phosgene and derivatives thereof.(ref) An alternative acylating agent is the non-toxic, commercially available 1,1-carbonyldiimidazole (CDI). CDI has been successfully used in the synthesis of (a)symmetric carbamates, thiocarbamates and ureas with a broad range of substrates.(ref) Padiya *et al.*, synthesised a library of asymmetric ureas as one-pot synthesis using water as a solvent.³⁴ A key advantage given is that water is non-toxic and cheap with the additional benefit that in many cases the product precipitates out allowing easy isolation by vacuum filtration. Initial attempts to synthesise **M1** involved direct replication of the literature procedure outlined by Padiya *et al.* as a one-pot reaction in water. Here CDI was sequentially reacted with *t*-butyl carbazate, followed by propargyl amine but proved unfruitful. **M1** could not be synthesised with this strategy, but formation of the intermediate *t*-butyl 2-(1*H*-imidazole-1-carbonyl)hydrazine-1-carboxylate was confirmed by NMR (Figure 2.6) and isolated as a white solid in low yields (20-30%).

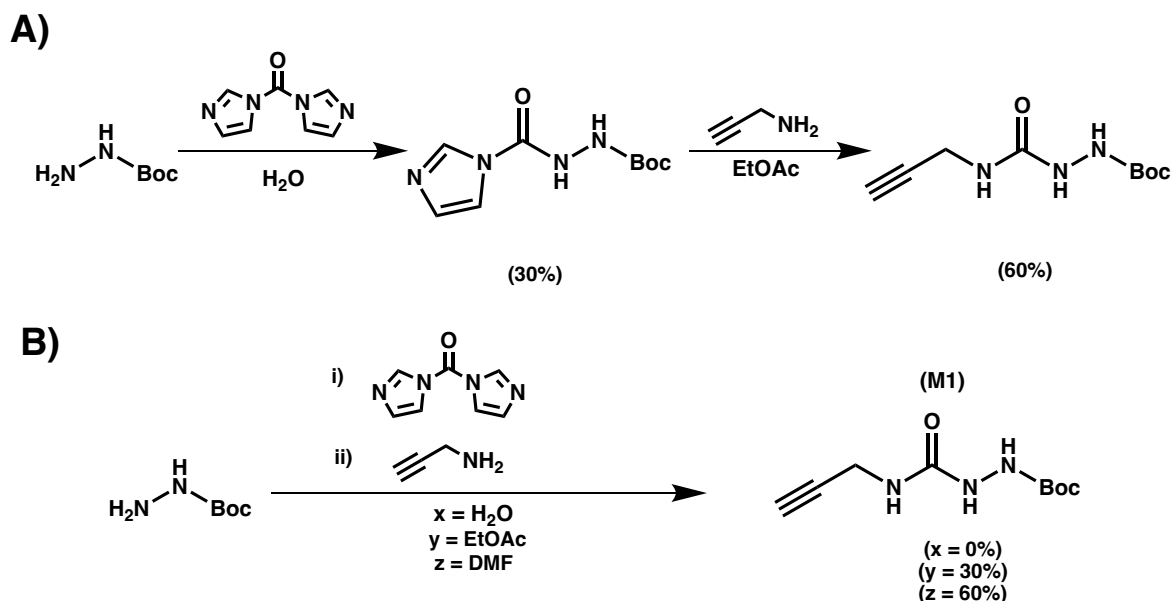


Figure 2.5 Tested synthetic routes for M1 production. A) Two-step synthesis in H₂O & EtOAc; B) One-pot synthesis with H₂O, EtOAc, or DMF.

Attempts to further react this intermediate in water remained unsuccessful, however successful reaction of the intermediate with propargyl amine was possible on changing to EtOAc, where M1 was isolated in moderate yields (60% yield: 15% across two steps). Increased reaction time and reversal of addition order (amine then carbazate) showed negligible product formation in water still. The lack of product formation in water was suspected to be a consequence of reactant solubility rather than reactivity. Thus, the one-pot reaction strategy was repeated using EtOAc or DMF as reaction solvents. **M1** was successfully synthesised in a one-pot reaction with both EtOAc and DMF increasing the yields to 30% and 60% respectively.

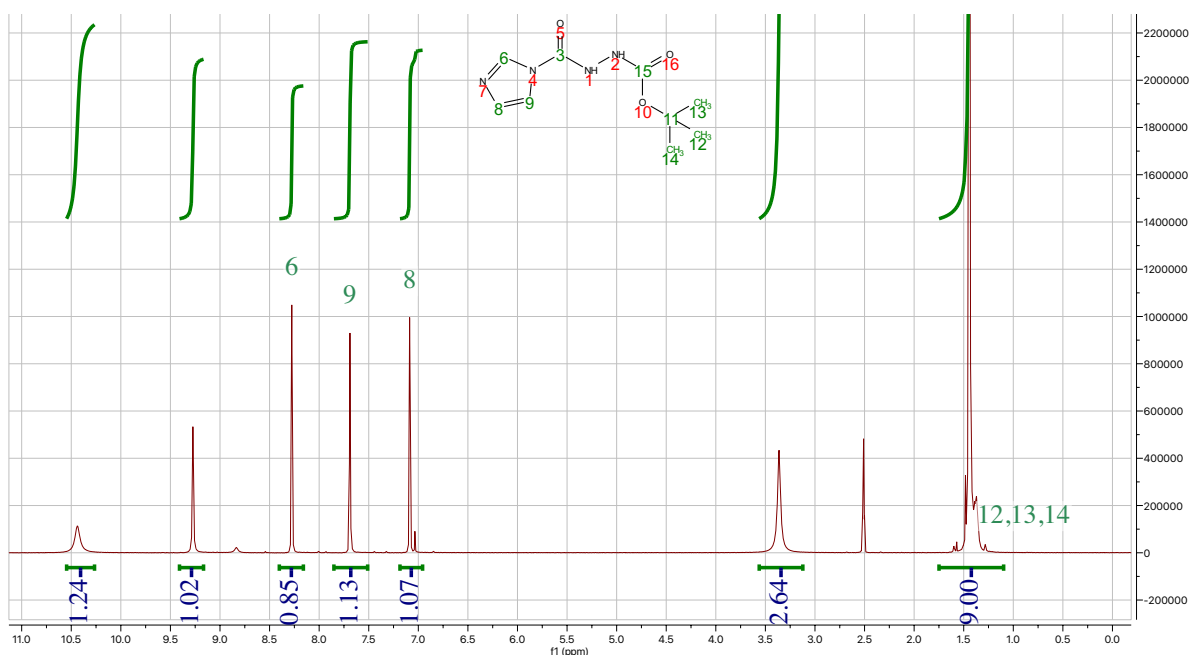


Figure 2.6 Assigned ¹H-NMR spectra of tert-butyl 2-(1H-imidazole-1-carbonyl)hydrazine-1-carboxylate intermediate.

The bottleneck in the aqueous synthetic route is low yield of the intermediate giving overall poor atom economy. CDI shows complete decomposition to imidazole at 0 °C within 10 minutes,³⁴ however amine nucleophilicity is reportedly much higher in water compared to organic solvent.³⁵ The presence of the adjacent N-atom in t-butyl carbazate should increase the nucleophilicity and thus reactivity of the carbazate's terminal N-atom through the α -effect. Under the tested conditions one should expect the rate of nucleophilic attack at the carbonyl to exceed that of CDI hydrolysis giving product formation though this is not the case. As t-butyl carbazate has limited solubility in water it creates a highly heterogenous system lowering reaction rates. When using water as a solvent, rate of CDI hydrolysis may exceed the reaction rate; therefore, decomposition to imidazole is favoured limiting intermediate formation. This hypothesis is somewhat substantiated as performing the same reaction in either EtOAc or DMF results in successful isolation of **M1** though with differing yields. The

original paper states that hydrogen bonding between water molecules and the imidazole rings lowers the ring electron density increasing its nucleofugality and thus improves its leaving group ability.³⁴ Therefore, the greater yields observed in DMF compared to EtOAc maybe due to increased hydrogen bonding to the imidazole thereby improving its leaving group ability and subsequent M1 yields.

2.4 Polymer synthesis

2.4.1 Synthetic screening

The polymerisation conditions were screened² with respect to solvent (CHCl_3 , DCM, DMF and THF) and catalyst choice ($[\text{Rh}(\text{nbd})\text{BPh}_4]^0$ and $\text{Rh}(\text{nbd})\text{Cl}_2$) in an orthogonal design, where each catalyst was tested in each solvent. Rh catalysts were chosen as they are highly selective in forming cis-cisoid and cis-transoid stereoisomers due to the polymerisation occurring through a 2,1-insertion mechanism. In Rh-catalysed syntheses, polymerisation rate is affected by electron density of the metal centre, where reduced electron density positively affects polymerisation rates of acetylenes.¹¹ Compared to other ligands like cyclooctadiene (cod), norbornadiene (nbd) experiences reduced sterics which enhances its electron withdrawing abilities due to improved π -back bonding.³⁶ Therefore, catalysts with nbd ligands were selected due to their reported high catalytic activity, commercial availability or ease of synthesis.

Screening reactions that used the dimeric rhodium species (Cat 2) were performed in the presence of Et_3N co-catalyst, which coordinates to the metal centre and cleaves the $\mu\text{-Cl}$ bridges to form the monomeric and catalytically active $\text{Rh}^{(I)}$ species.³⁷ Other amine co-

² Screening experiments were performed by AD – data shown and discussed with their permission.

catalysts like n-BuNH₂, Et₂NH have been shown to influence both polymerisation rates and molecular weights of poly(acetylenes) due to differences in basicity and steric bulk of the amine.³⁸ Given that Et₃N is reported to give high yields and its commonality in the published literature it was selected as the choice co-cocatalyst for all screening reactions. Reaction conversions were calculated by ¹H-NMR, taken as the ratio of the integral vinyl proton in the polymer backbone and the acetylene proton as described by **Equation 1**. Similarly cis-character was calculated by ¹H-NMR (**Equation 2**).³⁹ Integral of the cis vinyl proton is taken as a ratio of the sum of all other integrals (excluding exchangeable protons) divided by the total number of protons (3). However, cis-character could not be calculated for most reactions due to either poor M1 conversion or overlap of the methylene and solvent peaks.

$$Conv. (\%) = \left(\frac{\int H_{6.2 \text{ ppm}}}{\int H_{3.1 \text{ ppm}}} \right) \times 100 \quad (1)$$

$$Cis(\%) = \left(\frac{\int H_{6.2 \text{ ppm}}}{\frac{\int H_{total}}{3}} \right) \times 100 \quad (2)$$

Table 1. Result of polymerisation screening of M1

Solvent	Catalyst	Conv (%)
THF	[Rh(nbd)BPh ₄] ⁰ (Cat. 1)	37.5
DMF		1.96
CHCl ₃		97.1
DCM		100
THF	[Rh(nbd)Cl] ₂ (Cat. 2)	26.5
DMF		0.00
CHCl ₃		52.4
DCM		0.00

In all tested solvents significantly higher monomer consumption was observed with catalyst 1. It is proposed with dimeric Rh catalysts like 2 used in this work, polymerisation is initiated by Et₃N coordination promoting the dissociation into the active monomeric species

[Rh(L)ClNEt₃].³⁷ Given that catalyst 1 is monomeric it does not require prior dissociation to be catalytically active thereby increasing reaction rates and yields. Moreover, the BPh₄ ligand further reduces the Rh electron density promoting coordination with the acetylene monomers further enhancing polymerisation rates. Degree-of-polymerisation is solvent-dependent generally following the order DCM ~ CHCl₃ > THF > DMF. The significantly poor polymerisations of both catalysts in DMF and THF were surprising given that the monomer and catalysts were completely soluble in this solvent. Prior literature showed that acetylene polymerisation varies with solvent choice dependent on the monomer and catalyst in question. Although it is accepted that solvent affects polymerisation there remains to be an underlying mechanistic understanding of solvent involvement. Research into the polymerisation of propiolate derived acetylenes, showed poor polymerisation performance in THF.²⁰ It was argued that THF coordinates with the metal promoting premature termination of the propagating chain. In addition, the acidity of the acetylene proton permits hydrogen bonding with the bulk solvent further reducing polymerisations due to reduced coordination to the metal centre.²⁰ A similar process may occur in the systems tested herein, which could explain why non-hydrogen bonding solvents DCM and CHCl₃ considerably outperform DMF and THF with respect to monomer conversion. However, given that THF and DMF have reported success in other reported acetylene polymerisations no definitive conclusions can be made in the absence of any mechanistic understandings.

2.4.2 Scaled-up polymerisation & characterisation

The optimal polymerisation conditions of **M1** were identified as 1% [Rh(nbd)BPh₄]⁰ in chloroform these conditions were used for all subsequent polymerisations. The protected polymer (**P1-Boc**) was precipitated into hexane, filtered, and washed with hexane to yield a red-brown solid. To yield produce the reactive polymer scaffold **P1**, **P1-Boc** was deprotected using neat trifluoroacetic acid (TFA) for 24h. Neutralisation, dialysis, and lyophilisation yielded pure **P1** as light yellowish powder. The deprotection procedure appeared to have little effect on the cis content of the polymer with only a 2% reduction, though this may arise from measurement variance. In contrast to **P1-Boc**, **P1** remains insoluble in all tested organic solvents at room temperature (CHCl₃, DCM, DMF, DMSO and toluene). The polymer is soluble in acidic solvents (0.1M acetic acid and 0.1M HCl) but at higher concentrations (> 5 mg mL⁻¹) **P1** is only partially soluble and instead forms a stable suspension.

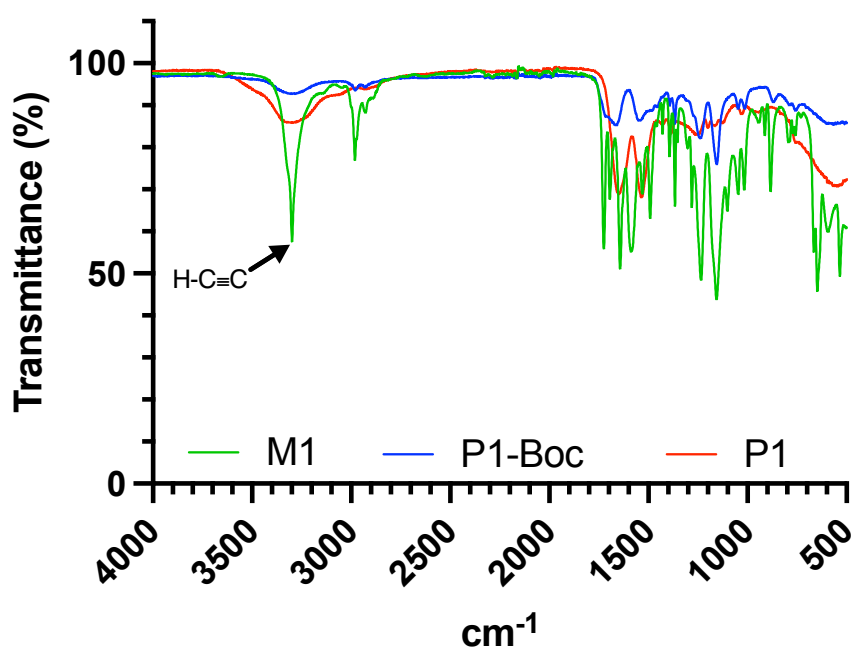


Figure 2.7. Overlaid FTIR spectra of M1, P1-Boc, and P1.

FTIR spectroscopy (**Figure 2.7**) confirmed the successful polymerisation of **P1**. FTIR analysis where the spectra showed the loss of a sharp signal at $\sim 3300\text{ cm}^{-1}$ which corresponds to the CH alkyne stretch, though it is not immediately apparent due to the overlap with the N-H amine stretch peak. This amine-stretch peak also becomes broadened in the polymers suggesting intramolecular hydrogen bonding between the side chains. $^1\text{H-NMR}$ (**Figure 2.8**) confirmed the disappearance alkyne proton signal at 3.01 ppm and the corresponding appearance of a new broad singlet at 6.2 ppm. This indicated the formation of an olefinic alkene in the polymer backbone.⁴⁰ Furthermore, the chemical shift of this new singlet confirms the backbone of **P1** is in a cis configuration. The broadened vinyl (6.2 ppm) and methylene (3.6 ppm) signals suggest restricted motion within the polymer chain.^{41–43} The cis content was calculated as 100% showing that **P1** was highly stereoregular. GPC analysis shows the **P1** to be a high molecular weight with moderate dispersity ($4.1 \times 10^4\text{ g mol}^{-1}$; $\mathcal{D}_M = 1.70$) (see *S.I. Figure 2.15*). The moderate \mathcal{D}_M of **P1-Boc** suggested that polymerisation proceeds by a non-living mechanism.

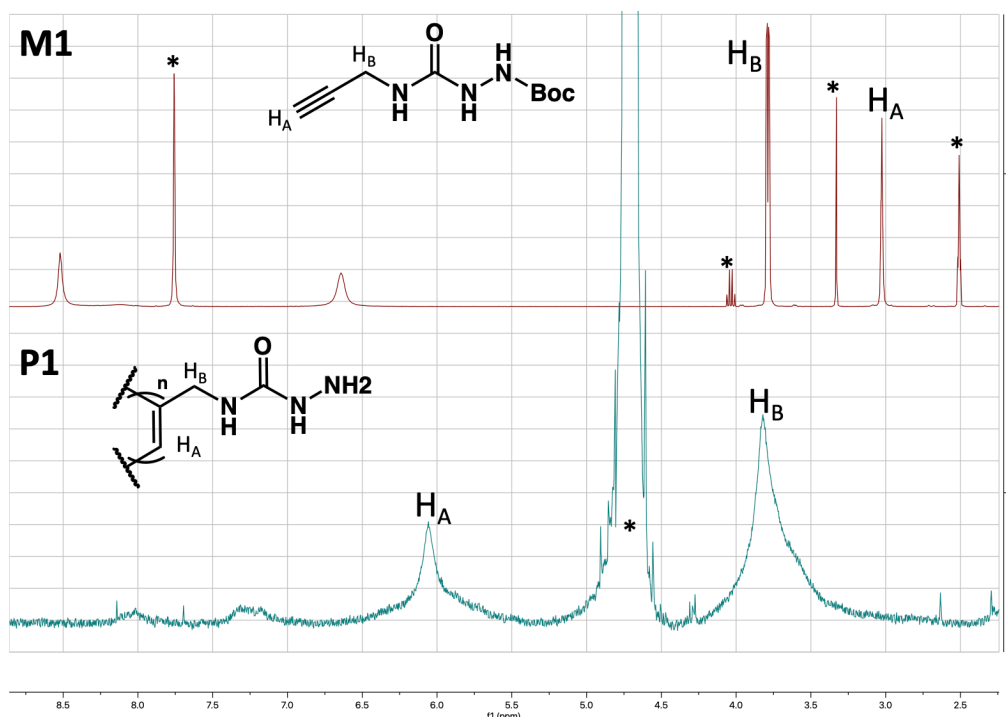


Figure 2.8. ¹H-NMR spectra of M1 and P1. Integrated spectra given in the appendix. (*) solvent peaks.

2.5 Material Library generation

Our group previously pioneered the design and synthesis of poly(hydrazide) based polymers as basis for post-polymerisation modification. With this strategy a large library of materials can be rapidly generated from a single scaffold greatly increasing throughput.^{33,44,45} It was hypothesised that **P1** would readily undergo condensation reactions with aldehydes and ketones to form the corresponding hydrazone products. Previous research within group demonstrated that structurally similar poly(acryloyl hydrazide) (pAH) was an effective scaffold for screening biofilm formation in *E. coli*. Hydrophobic formulations induced bacterial aggregation with a concomitant increase in EPS (curli) production.⁴⁶ Adoni et al. found that heterocyclic and aromatic compounds produced the largest biofilm response with respect to aggregation and curli production.⁴⁶

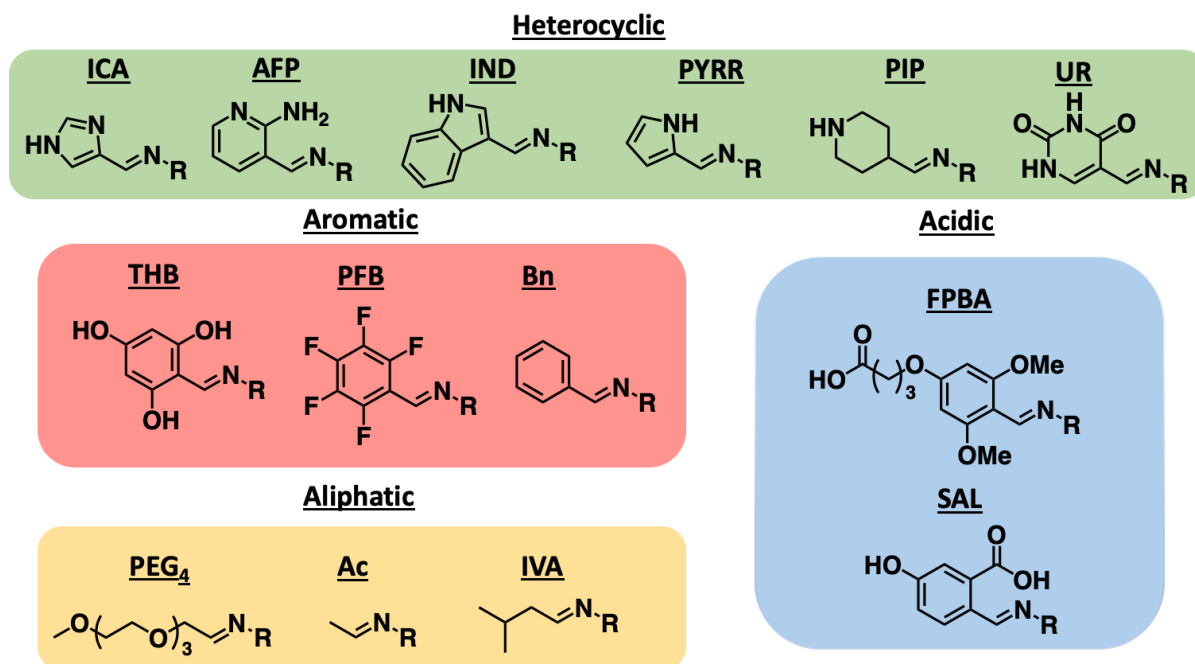


Figure 2.9 Chemical structures of the hydrazone functionalised aldehydes coupled to P1 (R) for later testing in biofilm nucleation studies. Heterocyclic aldehydes: imidazole-4-carboxaldehyde (ICA), 2-amino-3-formylpyridine (AFP), indole-3-carboxaldehyde, 2-pyrrolicarboxaldehyde (PYRR), 4-formylpiperidine (PIP), and 5-formyluracil (UR). Aromatic aldehydes: 2,4,6-trihydroxybenzaldehyde (THB), pentafluorobenzaldehyde (PFB), and benzaldehyde (Bn). Aliphatic aldehydes: PEG-4-aldehyde (PEG₄), acetaldehyde (Ac), and Isovaleraldehyde (IVA). Acidic aldehydes: 4-(4-formyl-3,5-dimethoxyphenoxy)butanoic acid (FPBA) and 5-formylsalicylic acid (SAL).

This work aimed to include and expand upon the previous chemical space used to assess biofilm formation in *E. coli* through the creation of a polyacetylene material library (Figure 2.9). It is widely accepted that bacterial adhesion is enhanced on hydrophobic and/or cationic surfaces. Therefore, many of selected functionalisations were chosen to exploit these interactions associated with bacterial adhesion. Heteroaromatic formulations were most numerous in the library which includes the previously tested imidazole-4-carboxaldehyde

(ICA), 2-amino-3-formyl pyridine (AFP), and indole-3-carboxaldehyde (IND). In addition, the novel choices of pyrrole-2-carboxaldehyde (PYRR), 4-formyl piperidine (PIP), and 5-formyluracil (UR) were included to probe new (non-) aromatic heterocycles. These formulations vary with respect to both hydrophobicity and electrostatics, where all were expected to be at least partially protonated at pH 7. Thus, these formulations were hypothesised to enhance adhesion through a synergistic effect of both hydrophobicity and electrostatic attraction. To probe the effect of aromatic substitution the highly hydrophobic formulations, 2,4,6-trihydroxybenzene (THB) and pentafluorobenzaldehyde (PFB) were included in addition to benzaldehyde (Bn). Previous research included polyaromatic formulations like anthracene and naphthaldehyde which had a propensity to aggregate in aqueous solvents.⁴⁶ Given the often-high insolubility of poly(acetylenes) it was deemed beneficial to avoid using with large molecular weight hydrophobic aldehydes to minimise this. Furthermore, using substituted aromatics would alter the electronic properties of the ring which would influence induced dipole formation and potentially bacterial aggregation. Aliphatic isovaleraldehyde (IVA) was selected due to its moderate hydrophobicity but is joined with hydrophilic PEG₄ aldehyde and acetaldehyde (Ac). Part of this research was interested in how these materials can influence biofilm formation and surface adhesion. Hence, hydrophilic formulations like PEG₄ and Ac were included to possibly elucidate differences in aggregation and subsequent biofilm phenotypes. The acidic formulations, 5-formylsalicylic acid (SAL) and 4-(4-formyl-3,5-dimethoxyphenoxy)butanoic acid (FPBA) were included as no acidic or anionic polymer formulations had been tested prior with regards to biofilm formation in *E. coli*. Furthermore, many carboxylic acids are anti-microbial due membrane permeation activity. When administered in sub-inhibitory concentrations these induce cell membrane stress

pathways many of which are also involved in biofilm pathways. Therefore, we were interested to see if anionic polymers could still elicit a biofilm response due to increased stress although they were hypothesised to be poor aggregators. The physicochemical properties of these formulations were calculated with chemometric software (Chemaxon). Calculations were performed to probe the effect of the formulations' physicochemical properties on biofilm formation in *E. coli*. Ideally, a much larger library would be generated for screening but without automation this would be difficult to effectively study in the given timeframe.

Previous, polyhydrazone coupling reactions used a 95:5 mixture of 0.1M acetic buffer (pH 5) and DMSO, where inclusion of organic solvent permits coupling of hydrophobic aldehydes to the otherwise hydrophilic polymer.^{33,44,45} However, the insolubility of **P1** in aqueous solvents prevents usage of identical conditions. Consequently, all hydrazone reactions with **P1** were performed using a 1:1 deuterated mixture of DMSO and 0.1 M AcOH. Inclusion of DMSO promoted reaction with hydrophobic aldehydes and aid **P1** solubility. The reaction was also performed in a more acidic system (pH ~3), **P1** has an estimated $pK_b = 3.1$ hence at pH ~3 approximately 55% of the monomer units in the polymer are protonated to ensure sufficient solubility of the polymer scaffold. Formation of acylhydrazones is a reversible pH dependent reaction proceeding by acid or base-catalysed mechanisms.⁴⁷ However, if pH is too extreme then the equilibrium shifts to favour hydrolysis of the hydrazone and the reactants are reformed.^{31,32,47} Therefore, pH 3 was chosen as a suitable compromise between polymer solubility and reactivity.

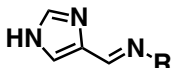
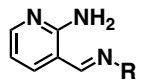
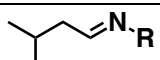
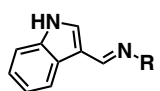
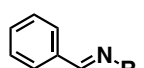
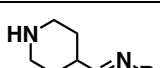
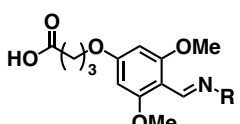
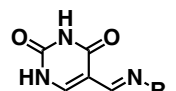
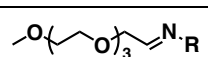
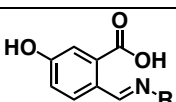
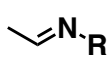
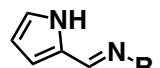
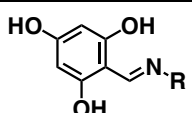
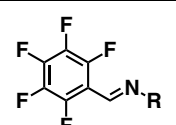
As outlined in

Table 2, all aldehydes were effectively coupled to **P1** in good yields, with the lowest degree-of-functionalisation (DoF) of 60% with PYRR. In general, common aldehydes used for hydrazone formation in **P1** is significantly higher than previous reports.⁴⁵ The more acidic conditions employed in this work may catalyse the hydrazone coupling more effectively leading to higher yields. The aliphatic aldehydes tested herein showed near quantitative conversions for all tested aldehydes. The generally higher DoF observed with aliphatic reactants is likely due to a mixture of reduced steric hindrance and lack of structural resonance. As the aliphatic carbonyl experiences less steric hindrance repulsion is minimised with the nucleophile (hydrazide monomer unit) promoting successful coupling. Aromatic carbonyls generally experience lower reaction rates due to π -electron delocalisation from the ring into the carbonyl increasing the electron density at the carbon centre, consequently reaction rates are reduced due to its reduced electrophilicity. Conjugation in aryl aldehydes also disrupts the formation of the tetrahedral intermediate, further slowing reaction rates.⁴⁸

The effect of chemical structure and substituents on reaction yield is readily visualised in Table 2. DoF in heteroaromatic aldehydes (ICA, IND and PYRR) does not exceed 77% likely due to said resonance effects. Conversions between the heterocycles PIP and UR were 100% and 69% respectively. The carbon-carbon double bond adjacent to the carbonyl in UR likely lowers reaction rates due to conjugation, whereas no resonance occurs in PIP leading to quantitative conversions. The aromatic aldehydes (including acidic FPBA and SAL for ease of discussion) experienced a broad range of measured DoF. Relative to BN (DoF = 87%) coupling with THB and FPBA is less effective. Given that both aldehydes are double *ortho*-substituted the reactive carbonyl experiences increased steric hindrance.⁴⁸ Furthermore, both hydroxyl and methoxy

functional groups are electron donating. Electron donation increases electron density in the ring further decreasing reactivity due to delocalisation. In contrast, the increased DoF of SAL relative to BN is due to the electron withdrawing groups on the aromatic ring. Electron withdrawal increases the electrophilicity of the carbonyl thereby increasing reaction rates.³¹ This is most pronounced with PFB, where pentafluoro substitution makes the ring highly electron deficient overcoming the limited reaction rate due to resonance effects. Despite the varied DoF, the moderate to excellent yields demonstrate the suitability of reaction conditions chosen as well as the suitability of poly(acetylene) materials for post-polymerisation modification reactions by hydrazone click chemistry.

Table 2. Total acyl hydrazone (%) achieved by **P1** in the presence of aldehydes. Aldehyde reacted with one equivalent of **P1** in 0.1M AcOH/DMSO at 30 °C for 24 h. Degree-of-functionalisation (DoF) calculated using ¹H-NMR using a dimethyl sulfone internal standard added. † DoF of acyl hydrazone formation with poly(acryloyl hydrazide) using 95:5 DMSO-Acetic buffer as reported in literature.⁴⁵

Formulation		DoF (%)	† Lit. DoF (%) ⁴⁵
ICA		77	74
AFP		71	N/A
IVA		100	82
IND		72	52
BN		87	64
PIP		100	N/A
FPBA		75	N/A
UR		69	65
PEG ₄		97	N/A
SAL		92	75
Ac		100	89
PYRR		61	N/A
THB		75	50
PFB		94	56

2.6 Probing polymer secondary structure

Adoption of a helical secondary structure is well documented for poly(acetylenes) that possess a cis-cis or cis-trans backbone. Chiral monomers polymerise into optically active polymers as the helix possesses either a left or right-handed turn dependent on monomer chirality. However, if the monomer is achiral and no chiral agents are used during polymerisation, like in **M1**, the poly(acetylene) is a racemic mixture of helices and therefore optically inactive. Because **P1** is achiral, the secondary structure cannot be studied using circular dichroism. In the absence of available CD studies additional analytical procedures such as UV-Vis spectroscopy, differential scanning calorimetry (DSC) and thermal gravimetric analysis (TGA) were performed to further probe whether **P1** adopts a helical secondary structure.

2.6.1 Thermochemical analyses

As discussed prior, a high cis content within the polymer backbone is critical for adoption of a helical secondary structure in poly(acetylenes). **P1** was estimated to have quantitative cis-content, which should promote helical formation. To further corroborate these findings and deduce the stereochemistries of **P1**-Boc both differential scanning calorimetry (DSC) and thermogravimetric analysis (TGA) were performed to deduce the respective thermal isomerisation and thermal degradation of the polymers ().

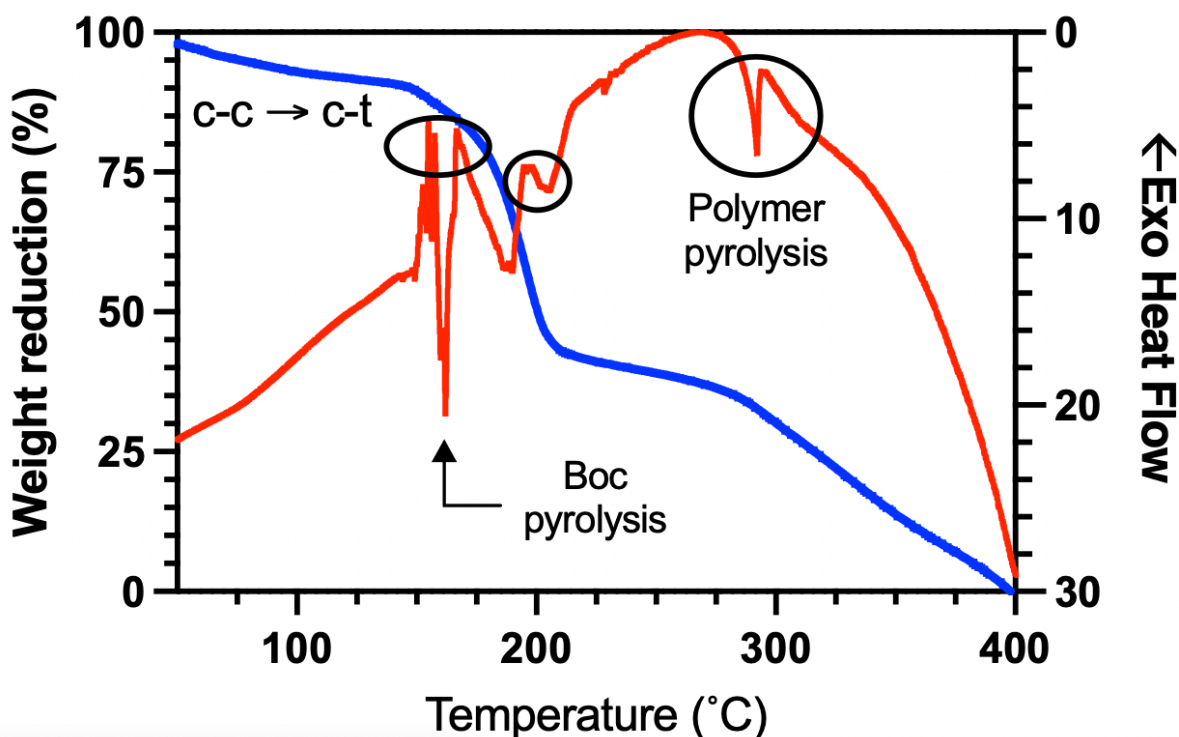


Figure 2. 10 DSC (red) and TGA (blue) analysis of P1-Boc

DSC has been applied in the study of poly(acetylenes) to probe the liquid-crystalline properties and thermal isomerism of the polymer main chain.^{49–52} Previous studies state that two exothermic peaks are associated with c-t to c-c isomerism and with further heating additional isomerism to t-t occurs. For instance, Nakako *et al.*, showed the polymerisation of (-)-menthyl propiolate catalysed by $[\text{Rh}(\text{nbd})\text{Cl}]_2$ produced high cis-regular polymer whereas polymers produced by $\text{MoOCl}_4\text{-n-Bu}_4\text{Sn}$ did not.⁴³ Low cis-content in poly(acetylenes) cause the formation of amorphous sterically irregular polymers which do not display any large exothermic shifts in their DSC profiles, whereas crystalline polymers do.⁴³ Similar observations have been made with a wide range of different poly(acetylenes) and poly(phenylacetylene) materials as they all display this highly similar two shoulder peaks.^{52–55} The DSC analysis of **P1-Boc** shows two exo heat flow peaks at approximately between 150–180 °C, which can likely be ascribed from cis to trans thermal isomerism. This is not immediately apparent due to overlap

with a large endothermic peak at $\sim 150^\circ\text{C}$ associated with a 50% weight reduction in TGA. The Boc protecting group shows spontaneous thermal degradation at 150°C , which occurs at a near identical temperature to backbone isomerism. There is an additional exothermic peak at 205°C which may be due to further isomerism to a fully transoid polymer backbone or possible changes in crystallinity. It is difficult to comment with certainty due to conflicting interpretations of DSC analysis in the context of polyacetylenes. At 290°C there is a second endothermic peak, which continues with increased temperature. This second endotherm is associated with a second mass loss in TGA which is likely due to pyrolysis of the polymer backbone and its degradation.

2.6.2 Temperature and solvent effects on helical adoption/ stability

UV-spectroscopy is a demonstrated technique to measure helicity in achiral poly(acetylene)s.

The poly(acetylene) main chain is comprised of alternating C=C bonds. In an idealised planar conformation, there is increased conjugation due to overlap between adjacent π - π orbitals (*Figure 2.11*). Increased orbital overlap decreases the π - π^* (HOMO-LUMO) energy gap, which shifts the absorbance to lower energy, higher wavelengths (red-shift). If the poly(acetylene) adopts a twisted/helical conformation (as in a cis-transoid or cis-cisoid polymer), the π -orbitals will move out of plane with respect to one another. This reduces the effective conjugative length of the backbone. Hence, the π - π^* energy gap increases and absorbance maximum are blue shifted due to higher energy transitions.¹⁷ Polyacetylenes with tight helical conformations are reported to be more blue-shifted compared to 'relaxed' helices due to this decreased orbital overlap.¹⁶ Similarly, the polyacetylene may be disordered and form a random coil. π -orbital overlap is even worse and will produce an even greater blue shift relative to an ordered helix.

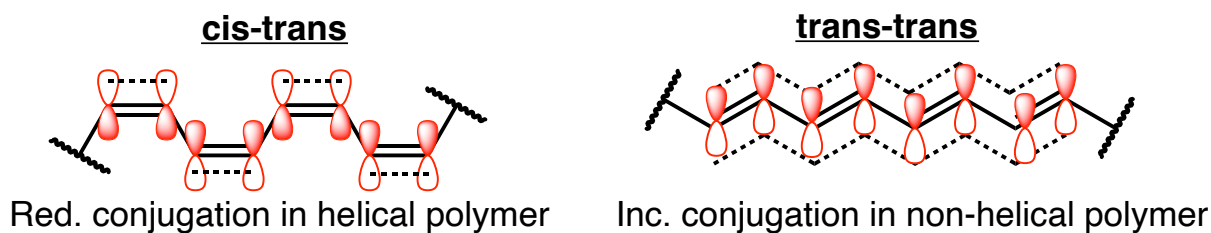


Figure 2.11 Cartoon diagram showing reduced molecular orbital overlap when poly(acetylenes) adopts a helical conformation (e.g. cis-trans).

The stability of helical structures in poly(acetylenes) is believed to be primarily due to a synergistic effect of intramolecular hydrogen bonding and sterics. Hydrogen bonding is critical as it compensates for the loss of entropy due to formation of an ordered helix.¹⁷ Reported helical poly(acetylenes) materials like poly(propargyl amides),^{56–59} alkylamides,⁴¹ sulfamides,^{60,61} carboxamides, propiolic esters,⁶² and ureas all generally absorb between 350 – 420 nm. Discrepancies in absorbance values likely result from different helical ‘tightness’, whereby compressed helices show increased blue shift. These polymers are all stabilised by intramolecular hydrogen bonding and so are vulnerable to polar solvents. Increased methanol titration compromises helical character which is associated with a blue shift to ~ 320 nm due to a helix-to-random coil transition. However, there are some conflicting reports regarding this. Sanda *et al.*, reported a series of helical poly(propargyl amides) derived from lactic acid which showed a λ_{max} of ~300 nm like **P1-Boc** (Figure 2.12).¹³ As the polymers displayed chiroptical properties at this wavelength, the blue-shifted absorbance was reasoned to be caused by increased helical tightness rather than a random coil. Likewise, poly(propargyl carbamates) bearing an isopentane R-group absorbed at 300 nm. In contrast to other reported propargyl(amides), treatment with methanol caused a red-shift due to adoption of a looser helical structure.¹⁷

Therefore, to probe helix formation in organic solvents the UV-spectra for **P1-Boc** was recorded in DMF and CHCl₃ (**Figure 2.12**). These solvents were selected as anti-HB and pro-HB solvents. The UV-spectra were recorded at several temperatures for each solvent to probe the helical stability of **P1-Boc**. Elevated temperatures were hypothesised to give a red-shift due to reduced intramolecular hydrogen bonding. Reduced intramolecular hydrogen bonding would likely reduce helical tightness which increases the effective conjugative length of the polymer. Relative to CHCl₃, there was a slight red-shift when the polymer was dissolved in DMF the (λ_{max} = 295 nm and 305 nm respectively). Neither solvent nor temperature change produced any significant changes in spectra. The minimal influence of solvent polarity and/or temperature may indicate that helicity **P1-Boc** is primarily stabilised by steric repulsion rather than hydrogen bonding. The blue-shifted λ_{max} in **P1-Boc** in conjunction with the high cis-content (98%) may suggest that **P1-Boc** forms a cis-cisoid helix. The large size of the Boc group, and the capability to form 2 hydrogen bonds with adjacent side chains makes this a reasonable hypothesis. Nomura *et al.*, found that introduction of α -branched alkyl substituents greatly enhanced helical stability in poly(n-propargyl alkylamides).^{41,56} Thus, the large steric bulk of the Boc-protected semi-carbazide may have a similar effect. It would be useful to expand the range of solvents, temperatures and include titrations to further probe the polymer helical structure.

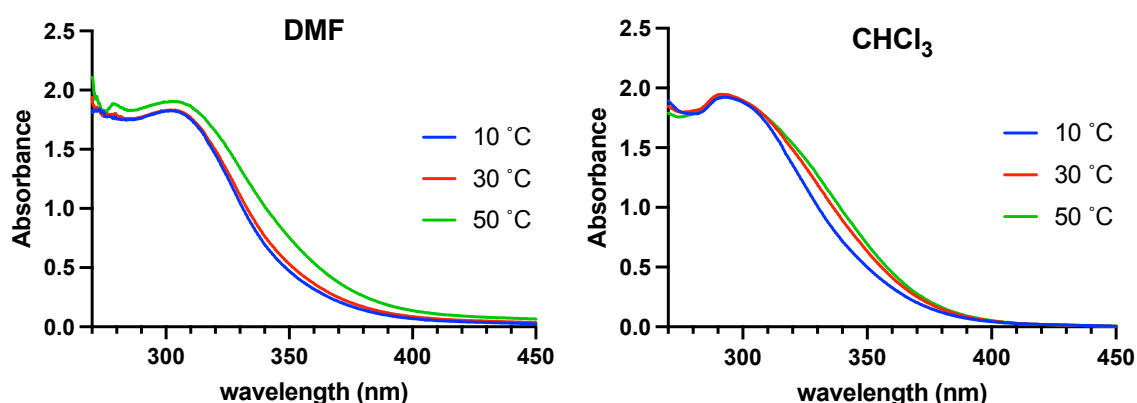


Figure 2.12 Temperature-dependent UV-vis spectra of **P1-Boc** in DMF and CHCl_3

2.6.3 Probing substituent effects on helical stability

Initial UV-Vis studies tentatively suggested that **P1-Boc** likely exists as a cis-cisoid polymer in organic solvent. The secondary structure of the functionalised **P1** library was the probed to determine the effects of functionalisation on helical character. Following post-polymerisation modification of **P1**, the polymers were added to 0.1M $\text{K}_2\text{HPO}_4/\text{KH}_2\text{PO}_4$ (pH 7) buffer (as used in subsequent biological assays) and the UV-spectra were recorded for each formulation. As stated prior, a red-shift would be due to looser helical tightness. Helical induction would be through increased steric hindrance and/or changes to intramolecular hydrogen bonding.

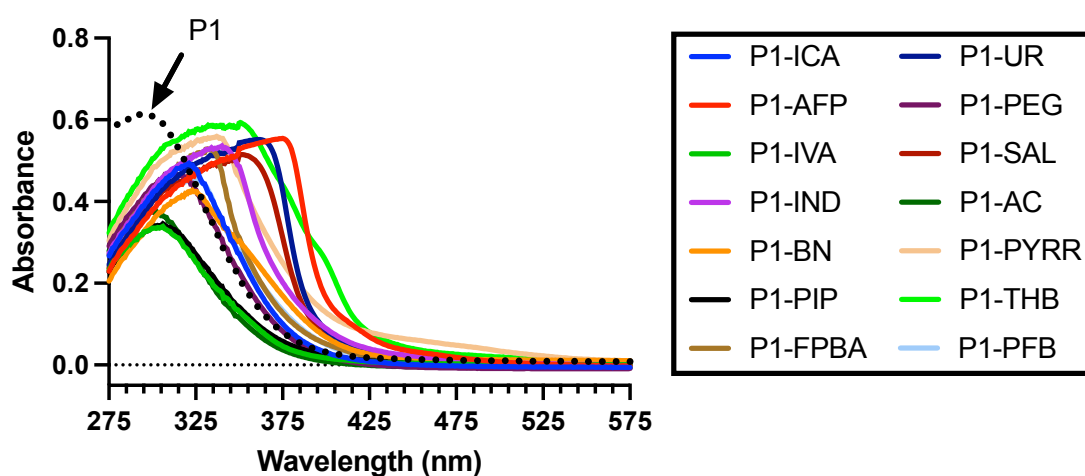


Figure 2.13 Overlaid UV-Vis spectra of **P1** formulations in 0.1M $\text{K}_2\text{HPO}_4/\text{KH}_2\text{PO}_4$ (pH 7) buffer. $[\text{P1-R}] = 1 \text{ mM}$, based on the molarity of the monomer units.

As shown in Figure 2.13 for **P1**, $\lambda_{\text{max}} = 295 \text{ nm}$ which suggested it may form a tight cis-cisoid helix like **P1-Boc**. All functionalisations showed a $\lambda_{\text{max}} < 400 \text{ nm}$, although the absorbance was red-shifted for all formulations except **P1-PIP**, **P1-IVA**, **P1-PEG₄**, and **P1-AC**. All except **P1-PIP** are aliphatic functionalisations which may limit the role of steric stabilisation. Increased mobility/ flexibility in the side chains permits increased helical compression as the side chains can orientate to minimise steric repulsion between themselves with a minimal change to the backbone. Despite the steric bulk of **P1-PIP**, there is no observed red-shift. **P1-PIP** is a non-aromatic heterocycle which cannot form any intramolecular π -stacking; moreover, it is incapable intramolecular hydrogen bond formation as it is protonated at pH 7. Helix formation is dependent on the balance of enthalpic and entropic contributions.¹⁷ Furthermore, as **P1-PIP** is cationic it was expected that electrostatic repulsion would cause helical relaxation to minimise this repulsion. Future work should look to research possible effect of pH and ionic strength on the charged polyacetylenes like **P1-PIP**. All remaining formulations except **P1-UR** are aromatic; therefore, additional stabilisation may be provided through π - π stacking between the side chains. Steric bulk would likely further stabilise helix formation and/or additional hydrogen bonding in the cases of heteroaromatic compounds or substituted benzenes. Furthermore, increased steric bulk would likely decrease helical tightness in the backbone. The largest red-shifts were observed in **P1-AFP**, **P1-UR**, and **P1-THB**.¹⁷ Given that the aldehydes **P1-PIP**, **P1-IVA**, **P1-PEG₄**, and **P1-AC** lack any chromophores it is possible that the lack of red-shift is due to this. Although limited studies showed aromatic acyl hydrazones primarily absorbed under 335 nm.⁶³⁶³ Hence, helix induction by functionalisation remains a possibility. For future work, it would be good to resolve this question. This could be achieved by reaction of a chiral aldehydes with P1 to assess whether induced circular dichroism (ICD)

was possible. If ICD occurs at similar wavelengths as the achiral aldehydes, then this would support the claim that post-polymerisation functionalisation aids helix formation in **P1**.

2.7 Conclusions

This work shows the successful synthesis of the novel urea-based polymer, poly(carbamoylhydrazine-1-carboxylate acetylene) (**P1**). Synthesis of the monomer was achieved in respectable yields (60%) in a one-pot synthesis in DMF and could be purified with ease from simple acidic washes. The protected polymer **P1-Boc** was synthesised in quantitative yields in CHCl_3 , and the polymer showed extremely high stereoregularity with an approximate 100% cis-content in the polymer backbone. Following deprotection, **P1** was successfully coupled in high yields with a library of aldehydes and ketones via hydrazone click chemistry to produce a novel library of poly(acetylenic) materials. None of the functional groups proves significantly detrimental to the overall reaction conversion although much higher degree-of-functionalisation was achieved with aliphatic or electron deficient aromatic aldehydes. UV-spectroscopic studies suggest that **P1** may exist as a cis-cisoid polymer in CHCl_3 and DMF given by the blue-shifted spectra. The marked red-shift following post-polymerisation modification suggested possible helix relaxation and the formation of cis-transoid geometry due to increased enthalpic stabilisations and steric repulsion.

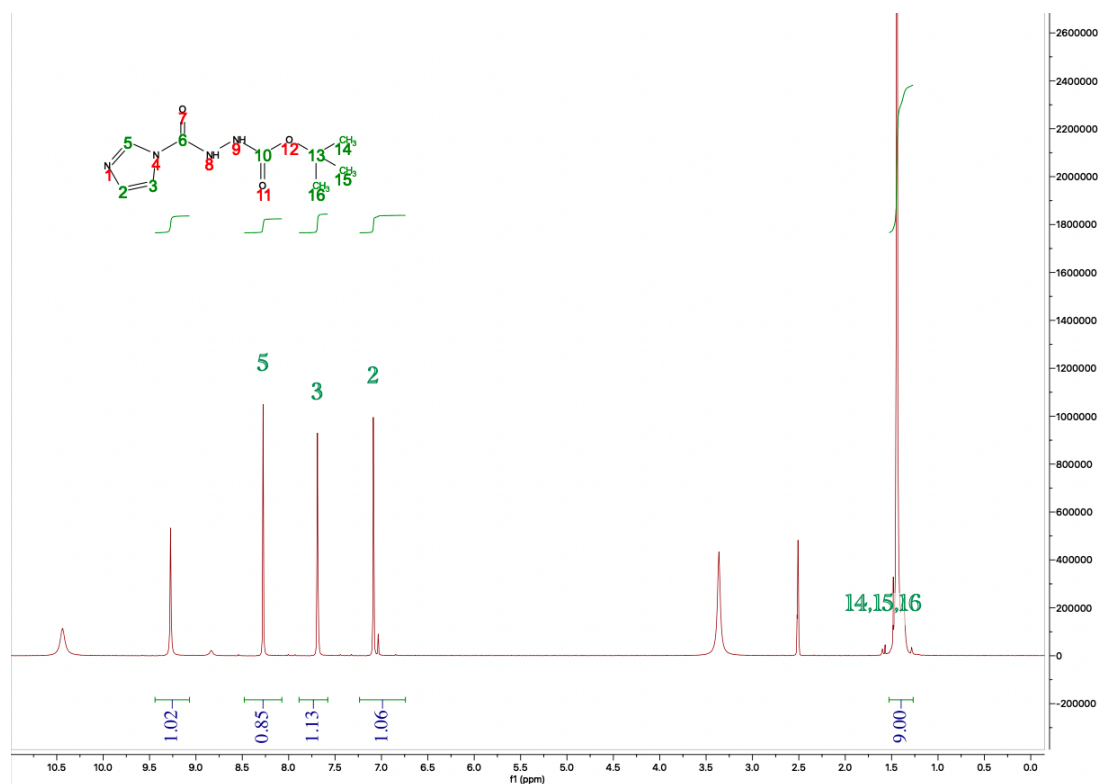
2.8 Bibliography

- 1 T. Leigh and P. Fernandez-Trillo, *Nat Rev Chem*, 2020, 1–20.
- 2 A. K. Bajpai, J. Bajpai, R. Saini and R. Gupta, *Polymer Reviews*, 2011, **51**, 53–97.
- 3 N. P. Gabrielson, H. Lu, L. Yin, K. H. Kim and J. Cheng, *Molecular Therapy*, 2012, **20**, 1599–1609.
- 4 R. J. Kern, *J Polym Sci A1*, 1969, **7**, 621–631.
- 5 J. Sedláček and H. Balcar, *Polymer Reviews*, 2016, **57**, 1–21.
- 6 C. I. Simionescu, V. Percec and S. Dumitrescu, *Journal of Polymer Science: Polymer Chemistry Edition*, 1977, **15**, 2497–2509.
- 7 T. Masuda, N. Sasaki and T. Higashimura, *Macromolecules*, 1975, **8**, 717–721.
- 8 T. Masuda, *Polymer Reviews*, 2016, **57**, 1–14.
- 9 Y. Kishimoto, P. Eckerle, T. Miyatake, M. Kainosho, A. Ono, T. Ikariya and R. Noyori, *J Am Chem Soc*, 1999, **121**, 12035–12044.
- 10 Z. Ke, S. Abe, T. Ueno and K. Morokuma, *J Am Chem Soc*, 2011, **133**, 7926–7941.
- 11 Y. Kishimoto, M. Itou, T. Miyatake, T. Ikariya and R. Noyori, *Macromolecules*, 1995, **28**, 6662–6666.
- 12 T. Masuda, *Polymer Reviews*, 2017, **57**, 1–14.
- 13 F. Sanda, T. Fujii, M. Shiotsuki and T. Masuda, *Polym J*, 2008, **40**, 768.
- 14 X. Bu, Z. Zhang, Z. Hang, Y. Huang and Y. Zhou, *J Appl Polym Sci*, , DOI:10.1002/app.44824.
- 15 M. Teraguchi, D. Tanioka, T. Kaneko and T. Aoki, *ACS Macro Lett*, 2012, **1**, 1258–1261.
- 16 Y. Suzuki, Y. Miyagi, M. Shiotsuki, Y. Inai, T. Masuda and F. Sanda, *Chemistry*, 2014, **20**, 15131–15143.
- 17 R. Nomura, S. Nishiura, J. Tabei, F. Sanda and T. Masuda, *Macromolecules*, 2003, **36**, 5076–5080.
- 18 M. Su, W. Wan, X. Yong, X. Lu, R. Liu and J. Qu, *Chinese Journal of Polymer Science*, 2013, **31**, 620–629.
- 19 J. Deng, X. Luo, W. Zhao and W. Yang, *J Polym Sci A Polym Chem*, 2008, **46**, 4112–4121.
- 20 Y. Yoshida, Y. Mawatari and M. Tabata, *Polymers (Basel)*, 2019, **11**, 93.
- 21 H. Nakako, Y. Mayahara, R. Nomura, M. Tabata and T. Masuda, *Macromolecules*, 2000, **33**, 3978–3982.
- 22 X. A. Zhang, M. R. Chen, H. Zhao, Y. Gao, Q. Wei, S. Zhang, A. Qin, J. Z. Sun and B. Z. Tang, *Macromolecules*, 2011, **44**, 6724–6737.
- 23 J. Liu, J. W. Y. Lam and B. Z. Tang, *Chem Rev*, 2009, **109**, 5799–5867.
- 24 J. W. Y. Lam and B. Z. Tang, *Acc Chem Res*, 2005, **38**, 745–754.
- 25 J. J. Cid Martín, M. Assali, E. Fernández-García, V. Valdivia, E. M. Sánchez-Fernández, J. M. Garcia Fernández, R. E. Wellinger, I. Fernández and N. Khair, *J Mater Chem B*, 2016, **4**, 2028–2037.
- 26 Y. Lim, S. Park, E. Lee, J.-H. Ryu, Y.-R. Yoon, T.-H. Kim and M. Lee, *Chem Asian J*, 2007, **2**, 1363–1369.
- 27 Y. Lim, S. Park, E. Lee, H. Jeong, J.-H. Ryu, M. S. Lee and M. Lee, *Biomacromolecules*, 2007, **8**, 1404–1408.
- 28 J.-H. Ryu, E. Lee, Y. Lim and M. Lee, *J Am Chem Soc*, 2007, **129**, 4808–4814.
- 29 K. W. Kolewe, J. Zhu, N. R. Mako, S. S. Nonnenmann and J. D. Schiffman, *ACS Appl Mater Interfaces*, 2018, **10**, 2275–2281.

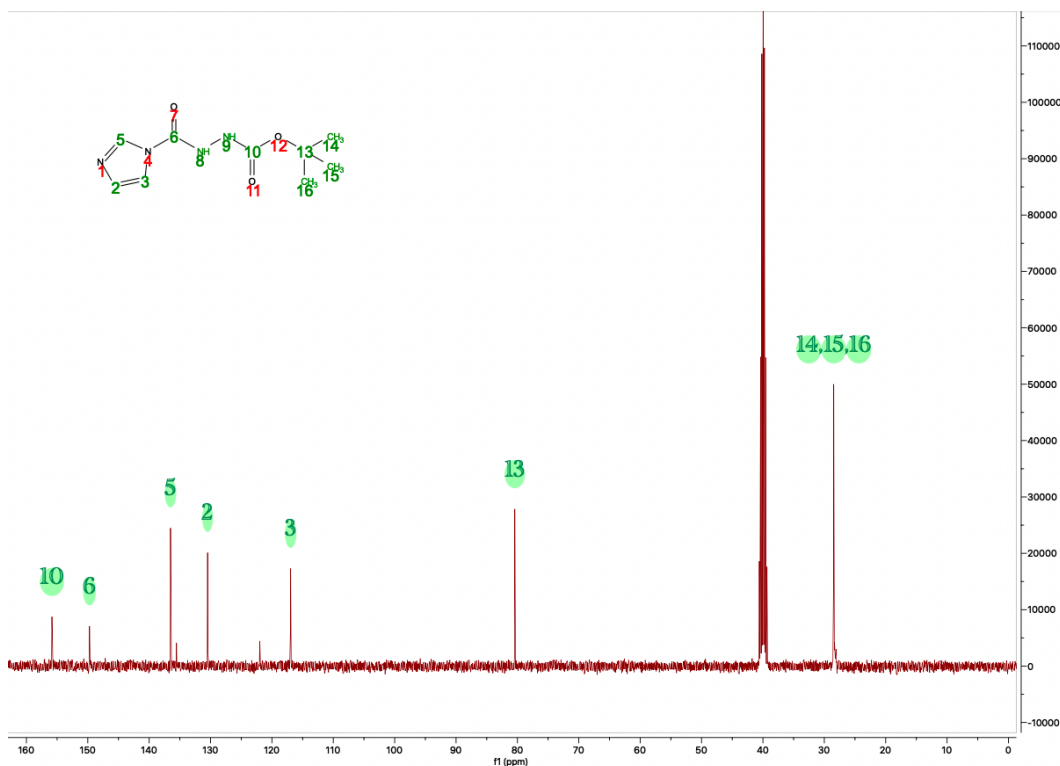
- 30 M. A. Gauthier, M. I. Gibson and H.-A. Klok, *Angewandte Chemie International Edition*, 2009, **48**, 48–58.
- 31 D. K. Kölmel and E. T. Kool, *Chem Rev*, 2017, **117**, 10358–10376.
- 32 J. Kalia and R. T. Raines, *Angewandte Chemie International Edition*, 2008, **47**, 7523–7526.
- 33 J. M. Priegue, I. Lostalé-Seijo, D. Crisan, J. R. Granja, F. Fernández-Trillo and J. Montenegro, *Biomacromolecules*, 2018, **19**, 2638–2649.
- 34 K. J. Padiya, S. Gavade, B. Kardile, M. Tiwari, S. Bajare, M. Mane, V. Gaware, S. Varghese, D. Harel and S. Kurhade, *Org Lett*, 2012, **14**, 2814–2817.
- 35 F. Brotzel, Y. C. Chu and H. Mayr, *J Org Chem*, 2007, **72**, 3679–3688.
- 36 H. C. Volger, Mrs. M.M.P. Gaasbeek, H. Hogeveen and K. Vrieze, *Inorganica Chim Acta*, 1969, **3**, 145–150.
- 37 W. Yang, M. Tabata, S. Kobayashi, K. Yokota and A. Shimizu, *Polym J*, 1991, **23**, 1135–1138.
- 38 A. Nakazato, I. Saeed, T. Katsumata, M. Shiotsuki, T. Masuda, J. Zednik and J. Vohlidal, *J Polym Sci A Polym Chem*, 2005, **43**, 4530–4536.
- 39 J. W. Y. Lam, X. Kong, Y. Dong, K. K. L. Cheuk, K. Xu and B. Z. Tang, *Macromolecules*, 2000, **33**, 5027–5040.
- 40 Y. Okano, T. Masuda and T. Higashimura, *Journal of Polymer Science: Polymer Chemistry Edition*, 1985, **23**, 2527–2537.
- 41 R. Nomura, J. Tabei and T. Masuda, *Macromolecules*, 2002, **35**, 2955–2961.
- 42 R. Nomura, H. Nakako and T. Masuda, *J Mol Catal A Chem*, 2002, **190**, 197–205.
- 43 H. Nakako, R. Nomura, M. Tabata and T. Masuda, *Macromolecules*, 1999, **32**, 2861–2864.
- 44 M. Juanes, O. Creese, P. Fernández-Trillo and J. Montenegro, *Medchemcomm*, 2019, **10**, 1138–1144.
- 45 D. N. Crisan, O. Creese, R. Ball, J. L. Brioso, B. Martyn, J. Montenegro and F. Fernandez-Trillo, *Polym Chem*, 2017, **8**, 4576–4584.
- 46 P. Adoni, A. Romanyuk, T. W. Overton and P. Fernandez-Trillo, *Mater Horiz*, 2022, **9**, 2592–2602.
- 47 R. N. Huc and Ivan, *Chemical Communications*, 2003, **0**, 942–943.
- 48 E. T. Kool, D.-H. Park and P. Crisalli, *J Am Chem Soc*, 2013, **135**, 17663–17666.
- 49 J. W. Y. Lam, Y. Dong, K. K. L. Cheuk, J. Luo, Z. Xie, H. S. Kwok, Z. Mo and B. Z. Tang, *Macromolecules*, 2002, **35**, 1229–1240.
- 50 J. W. Y. Lam, J. Luo, Y. Dong, K. K. L. Cheuk and B. Z. Tang, *Macromolecules*, 2002, **35**, 8288–8299.
- 51 H. Nakako, R. Nomura and T. Masuda, *Macromolecules*, 2001, **34**, 1496–1502.
- 52 S. Leiras, F. Freire, J. M. Seco, E. Quiñoá and R. Riguera, *Chem Sci*, 2013, **4**, 2735–2743.
- 53 R. Rodríguez, E. Quiñoá, R. Riguera and F. Freire, *J Am Chem Soc*, 2016, **138**, 9620–9628.
- 54 S. Arias, F. Freire, M. Calderón and J. Bergueiro, *Angew Chem Int Ed Engl*, 2017, **56**, 11420–11425.
- 55 V. Percec, J. G. Rudick, M. Peterca, M. Wagner, M. Obata, C. M. Mitchell, W.-D. Cho, V. S. K. Balagurusamy and P. A. Heiney, *J Am Chem Soc*, 2005, **127**, 15257–15264.
- 56 J. Tabei, R. Nomura and T. Masuda, *Macromolecules*, 2002, **35**, 5405–5409.
- 57 J. Deng, B. Chen, Z. Zhang and W. Yang, *Polym Int*, 2007, **56**, 1247–1253.
- 58 J. Deng, W. Zhao, J. Wang, Z. Zhang and W. Yang, *Macromol Chem Phys*, 2007, **208**, 218–223.
- 59 J. Deng, J. Wang, W. Zhao, Z. Zhang and W. Yang, *Macromol Chem Phys*, 2007, **208**, 316–323.
- 60 Z. Zhang, J. Deng, W. Zhao, J. Wang and W. Yang, *J Polym Sci A Polym Chem*, 2007, **45**, 500–508.

- 61 J. Deng, J. Li, W. Yang and Z. Zhang, *Polym J*, 2008, **40**, 436–441.
 62 E. Yashima, H. Goto and Y. Okamoto, *Polym J*, 1998, **30**, 69–71.
 63 R. L. HINMAN, *J Org Chem*, 1960, **25**, 1775–1778.

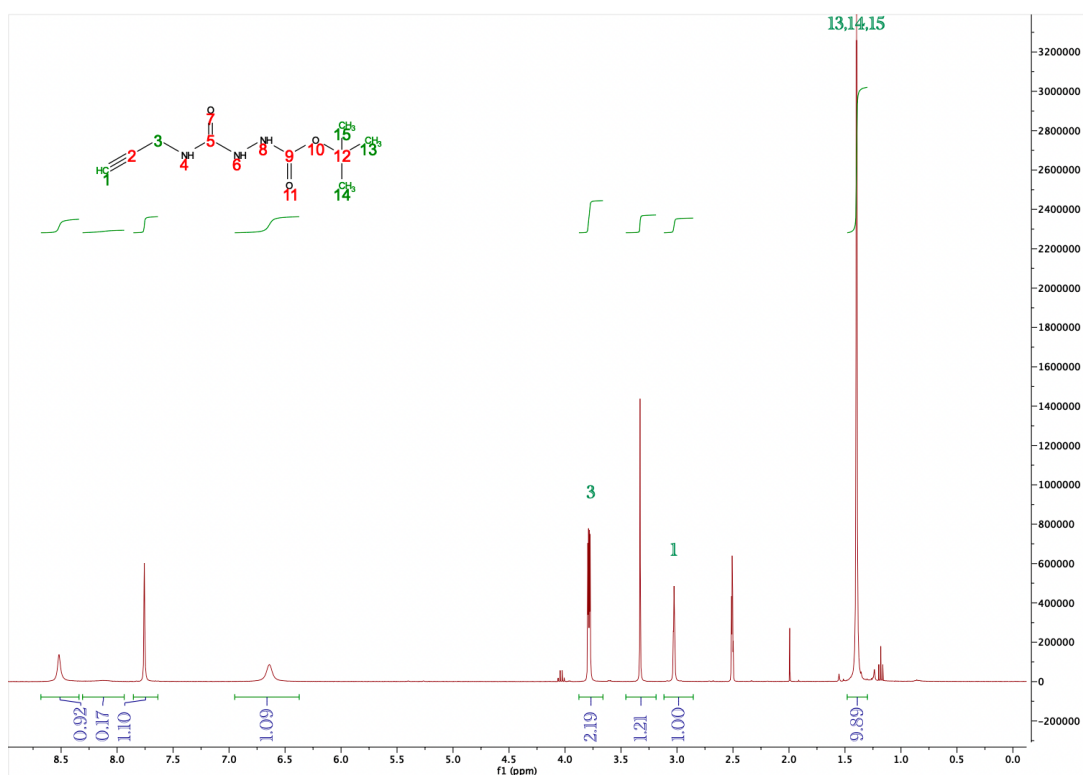
2.9 Supplementary information



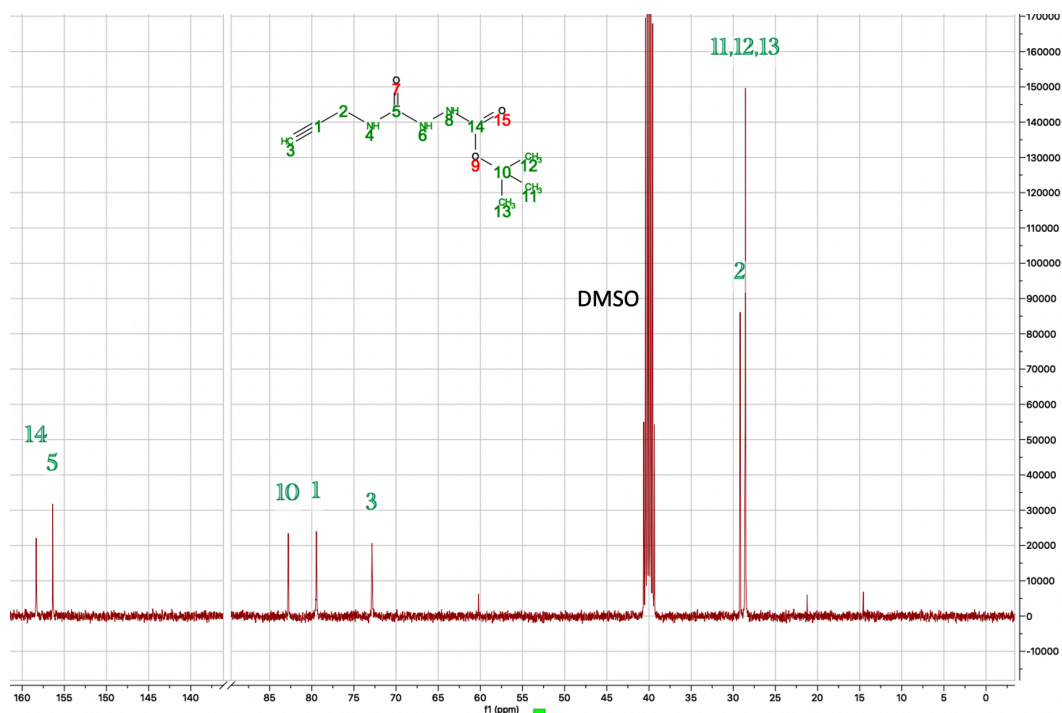
S.I. Figure 2.1 . ¹H-NMR of tert-butyl 2-(1H-imidazole-1-carbonyl)hydrazine-1-carboxylate intermediate isolated from monomer synthesis in water.



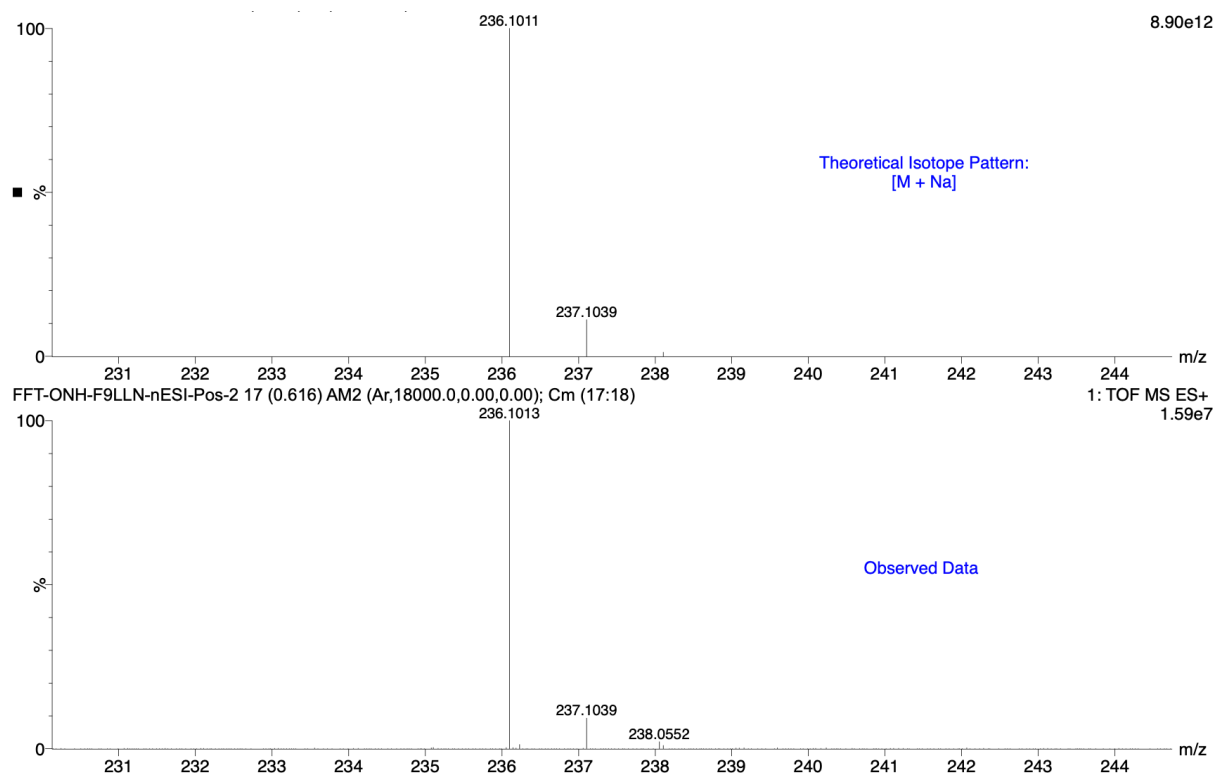
S.I. Figure 2.2 ^{13}C -NMR of *tert*-butyl 2-(1H-imidazole-1-carbonyl)hydrazine-1-carboxylate intermediate isolated from monomer synthesis in water.



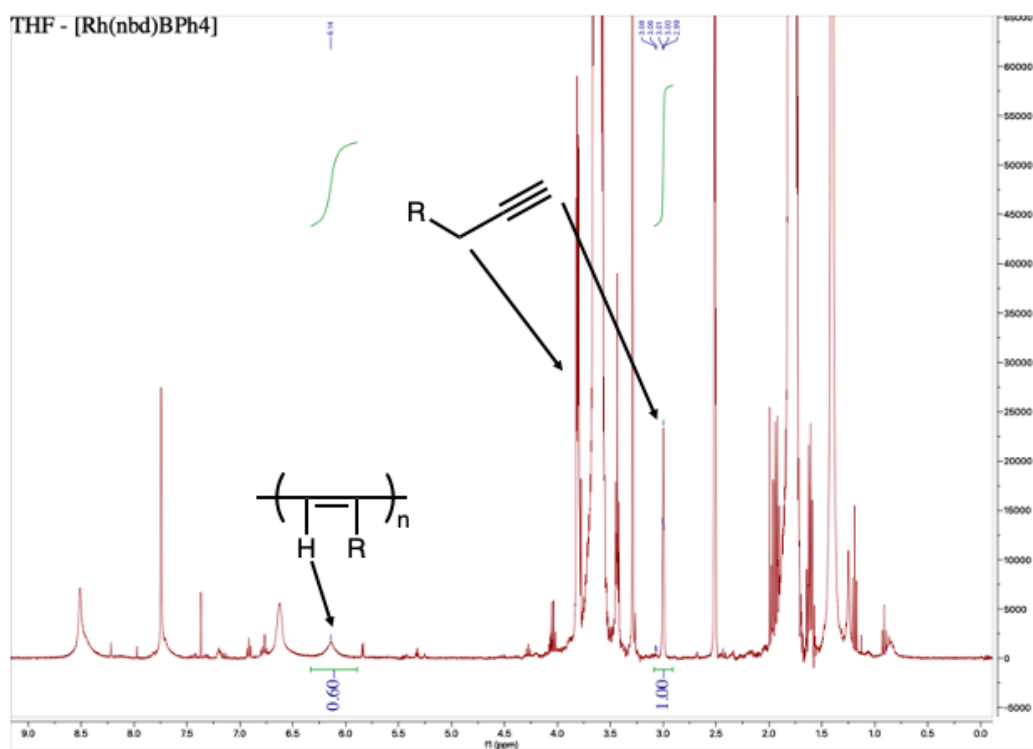
S.I. Figure 2.3. ^1H -NMR of *tert*-butyl 2-(prop-2-yn-1-ylcarbamoyl)hydrazine-1-carboxylate (M1)



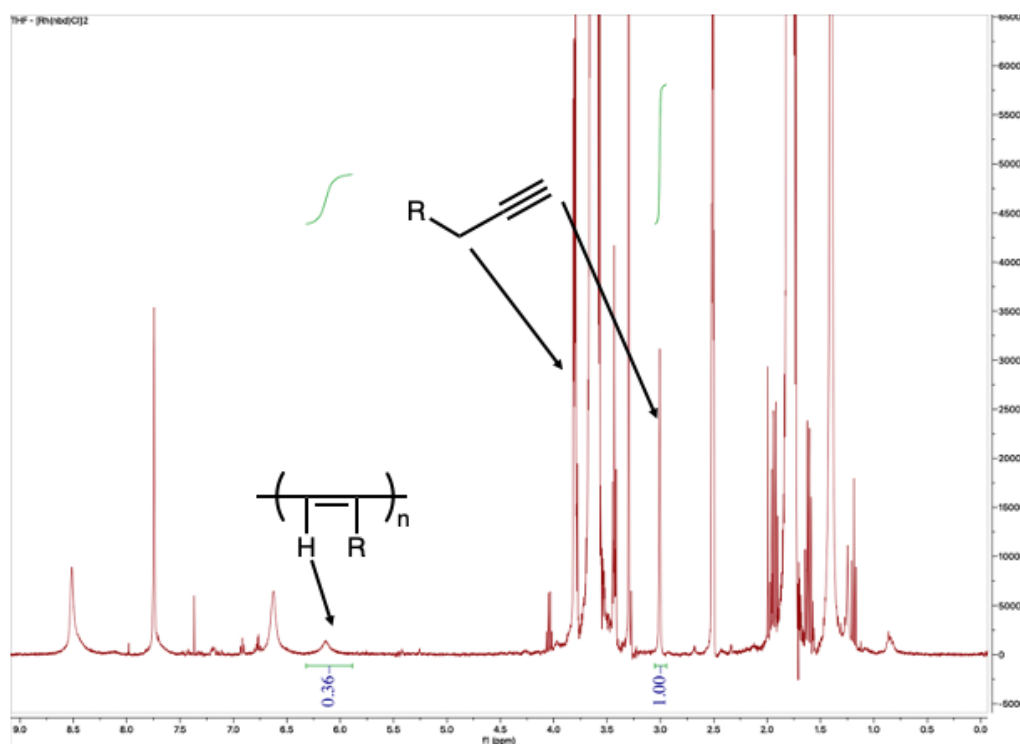
S.I. Figure 2.4 ¹³C-NMR of *tert*-butyl 2-(prop-2-yn-1-ylcarbamoyl)hydrazine-1-carboxylate (M1)



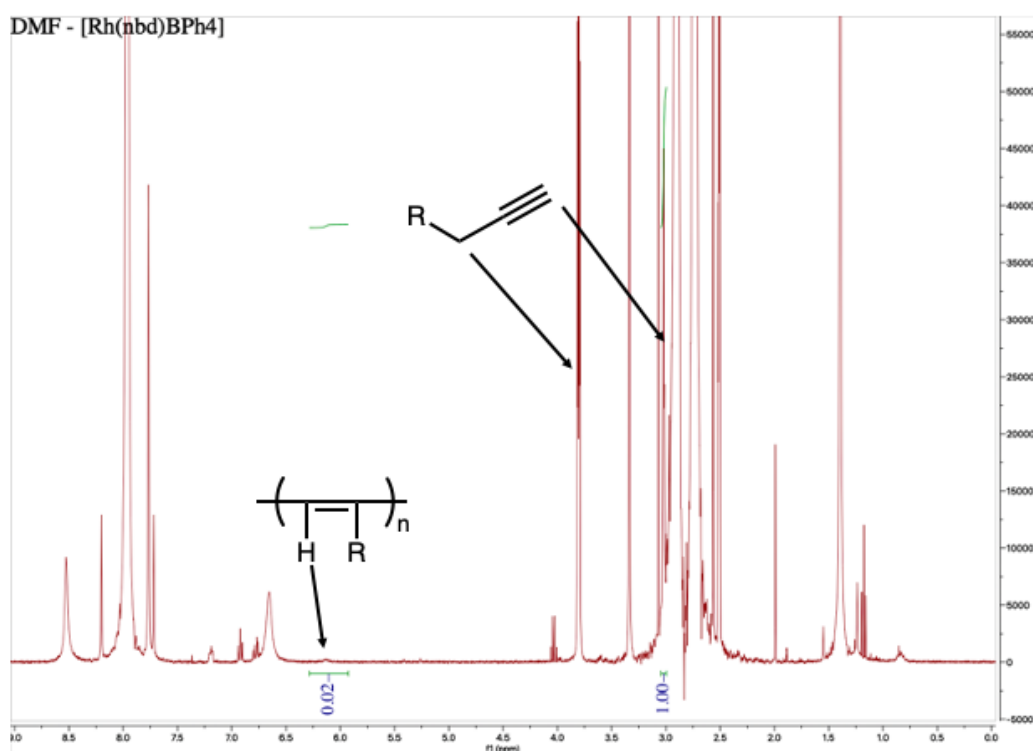
S.I. Figure 2.5. Mass spectrometry spectra for of *tert*-butyl 2-(prop-2-yn-1-ylcarbamoyl)hydrazine-1-carboxylate (M1)



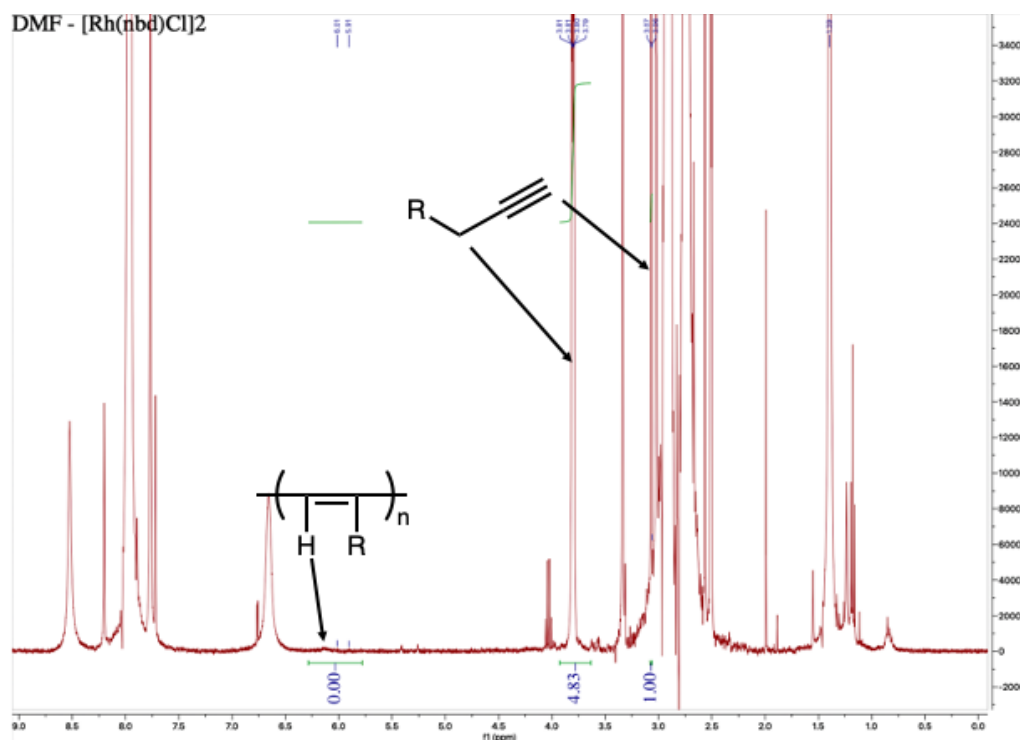
S.I. Figure 2.6. ¹H-NMR analysis of polymerisation screening of M1. Performed at 30 °C in THF with 0.01 equivalents of [Rh(nbd)BPh₄]



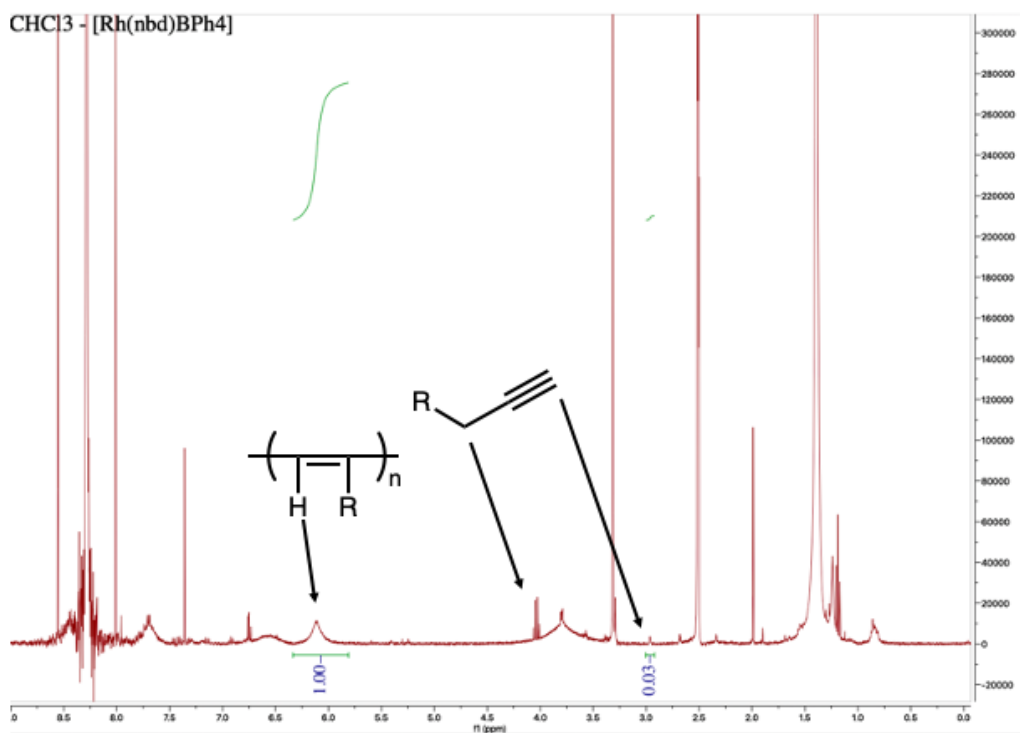
S.I. Figure 2.7. ¹H-NMR analysis of polymerisation screening of M1. Performed at 30 °C in THF with 0.01 equivalents of [Rh(nbd)Cl]₂.



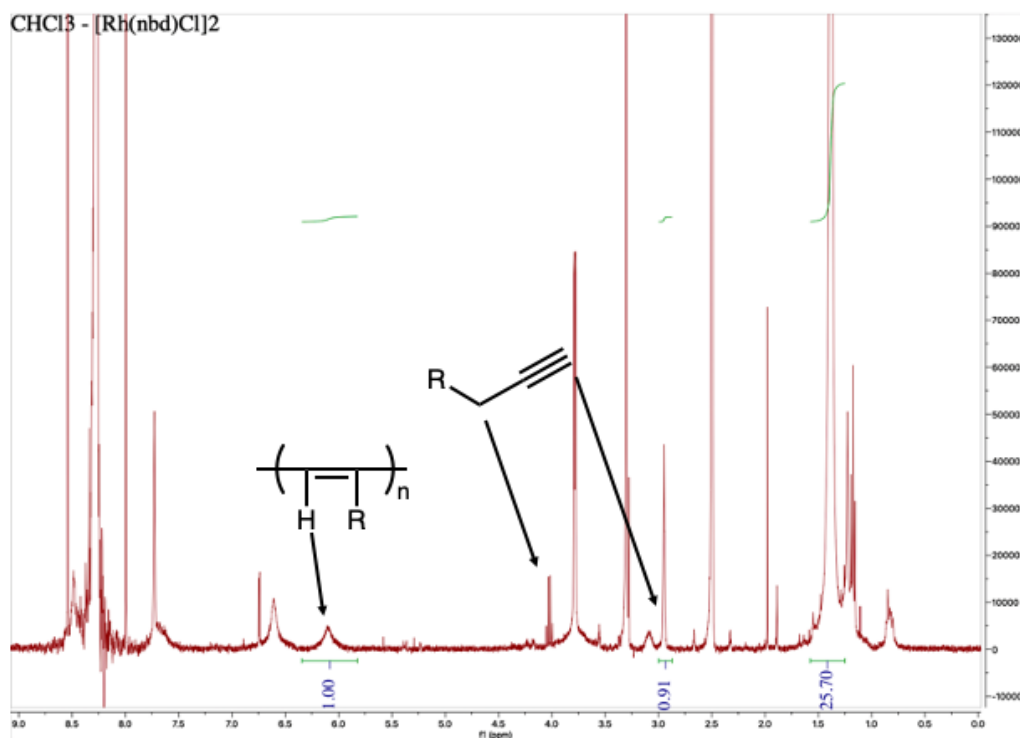
S.I. Figure 2.8. ¹H-NMR analysis of polymerisation screening of M1. Performed at 30 °C in DMF with 0.01 equivalents of [Rh(nbd)BPh₄]



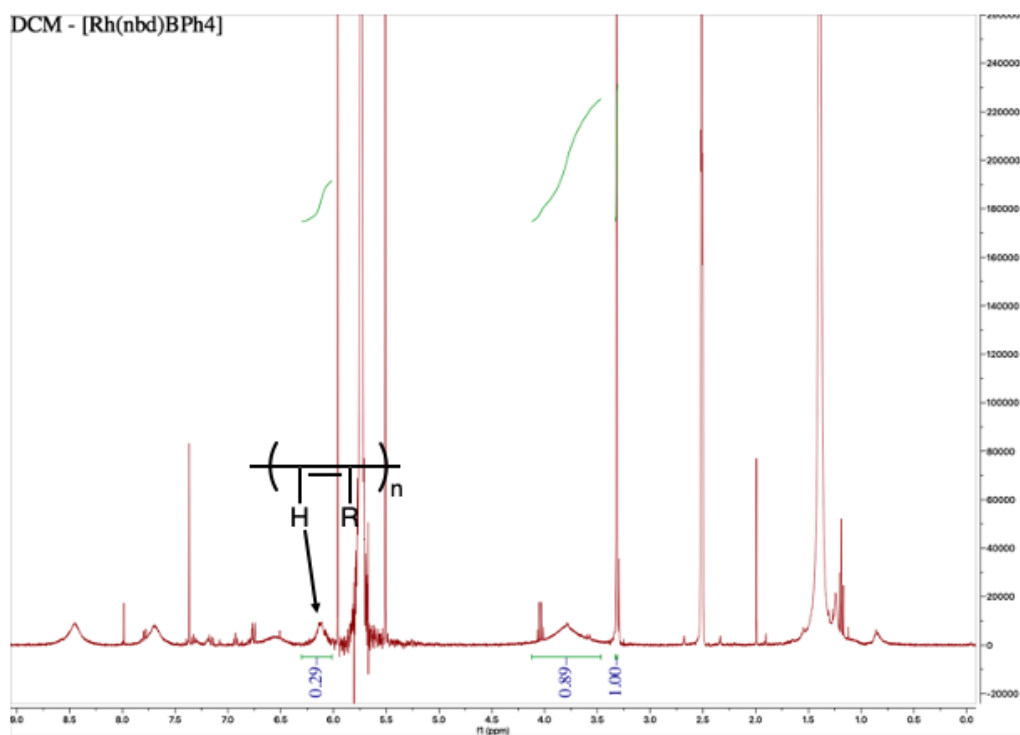
S.I. Figure 2.9. ¹H-NMR analysis of polymerisation screening of M1. Performed at 30 °C in DMF with 0.01 equivalents of [Rh(nbd)Cl]₂.



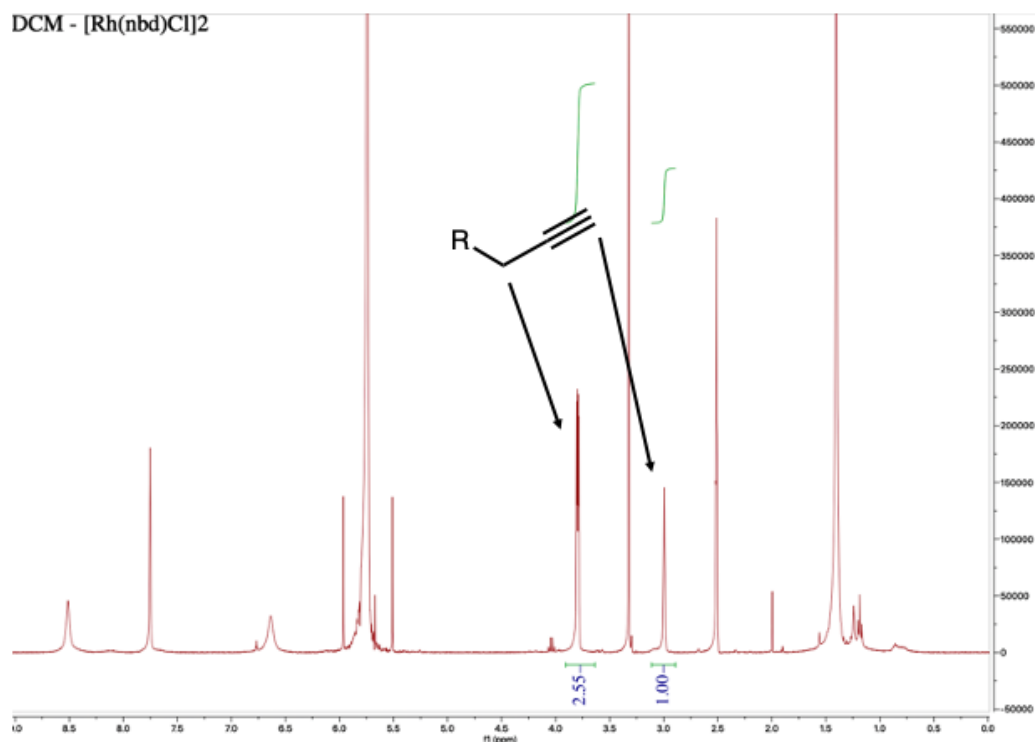
S.I. Figure 2.10. ¹H-NMR analysis of polymerisation screening of M1. Performed at 30 °C in CHCl₃ with 0.01 equivalents of [Rh(nbd)BPh₄]



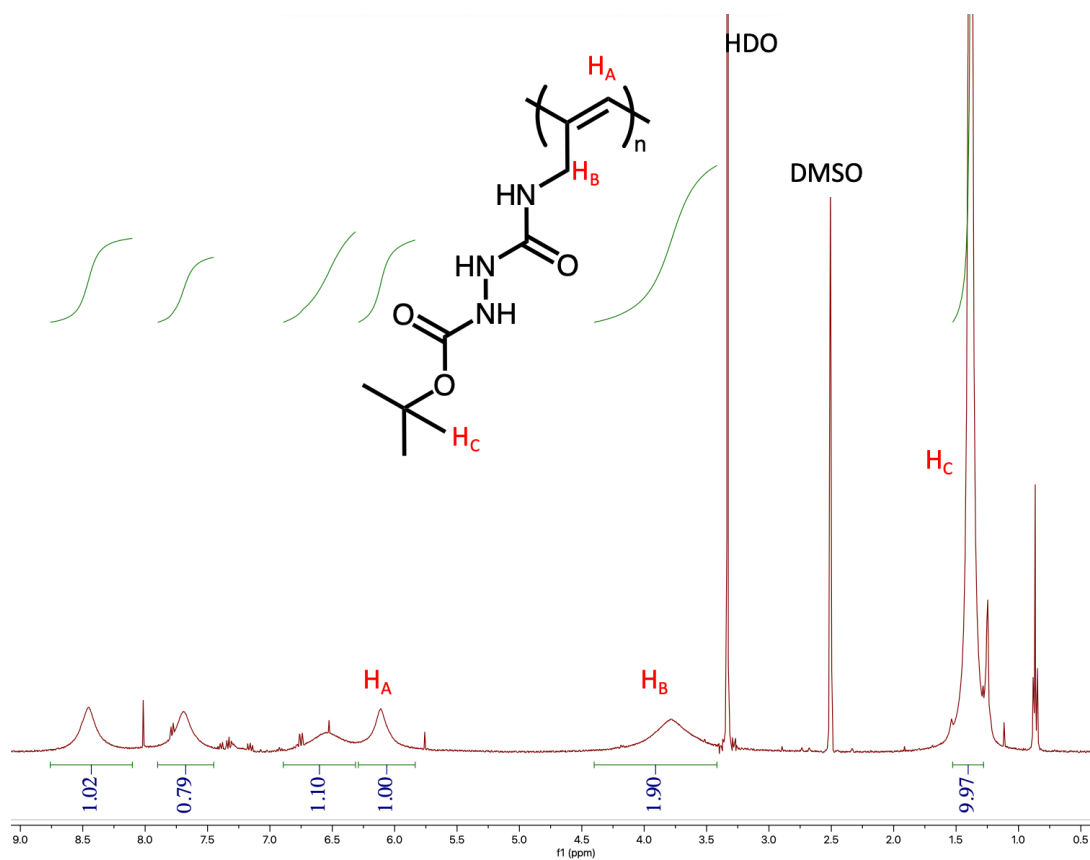
S.I. Figure 2.11. ¹H-NMR analysis of polymerisation screening of M1. Performed at 30 °C in CHCl₃ with 0.01 equivalents of [Rh(nbd)Cl]₂.



S.I. Figure 2.12. ¹H-NMR analysis of polymerisation screening of M1. Performed at 30 °C in DCM with 0.01 equivalents of [Rh(nbd)BPh₄]



S.I. Figure 2.13. ¹H-NMR analysis of polymerisation screening of M1. Performed at 30 °C in DCM with 0.01 equivalents of [Rh(nbd)Cl]₂.



S.I. Figure 2.14. ¹H-NMR of P1-Boc following precipitation into hexane

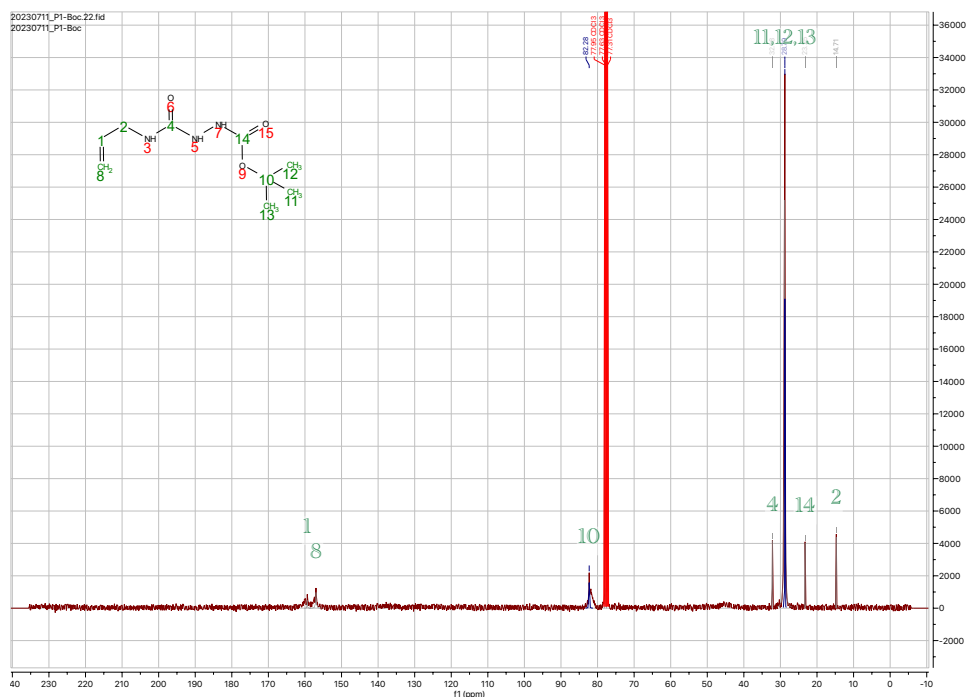


Figure 2.14. ¹³C-NMR of P1-Boc following precipitation into hexane

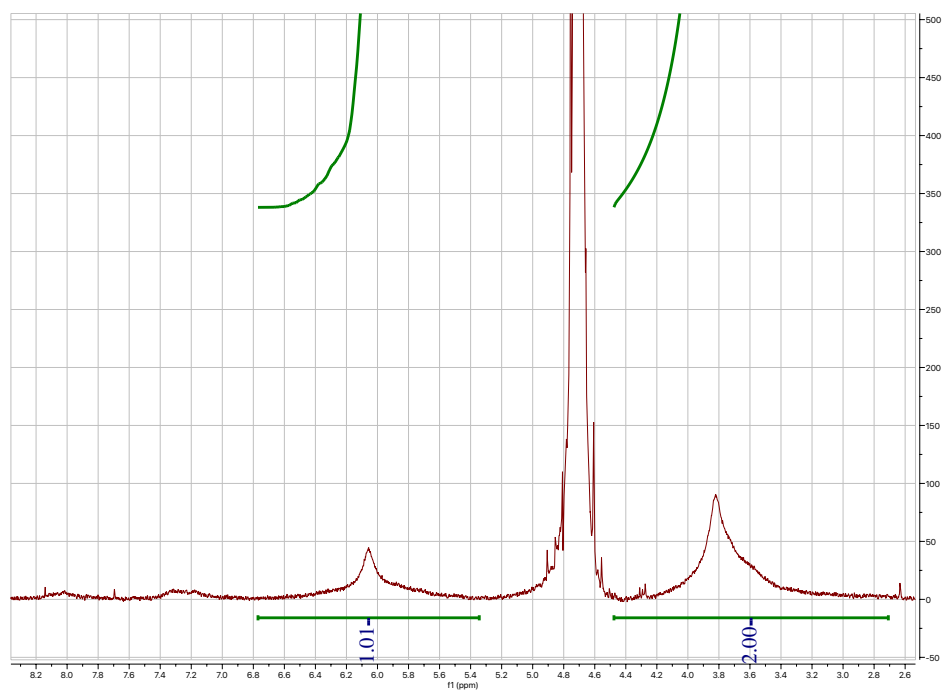
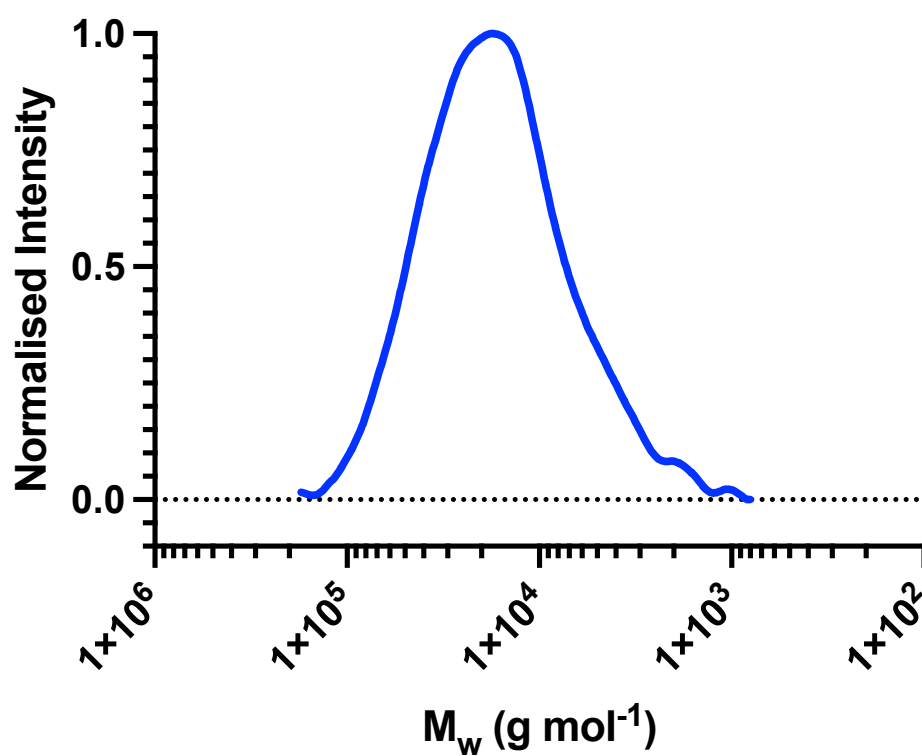
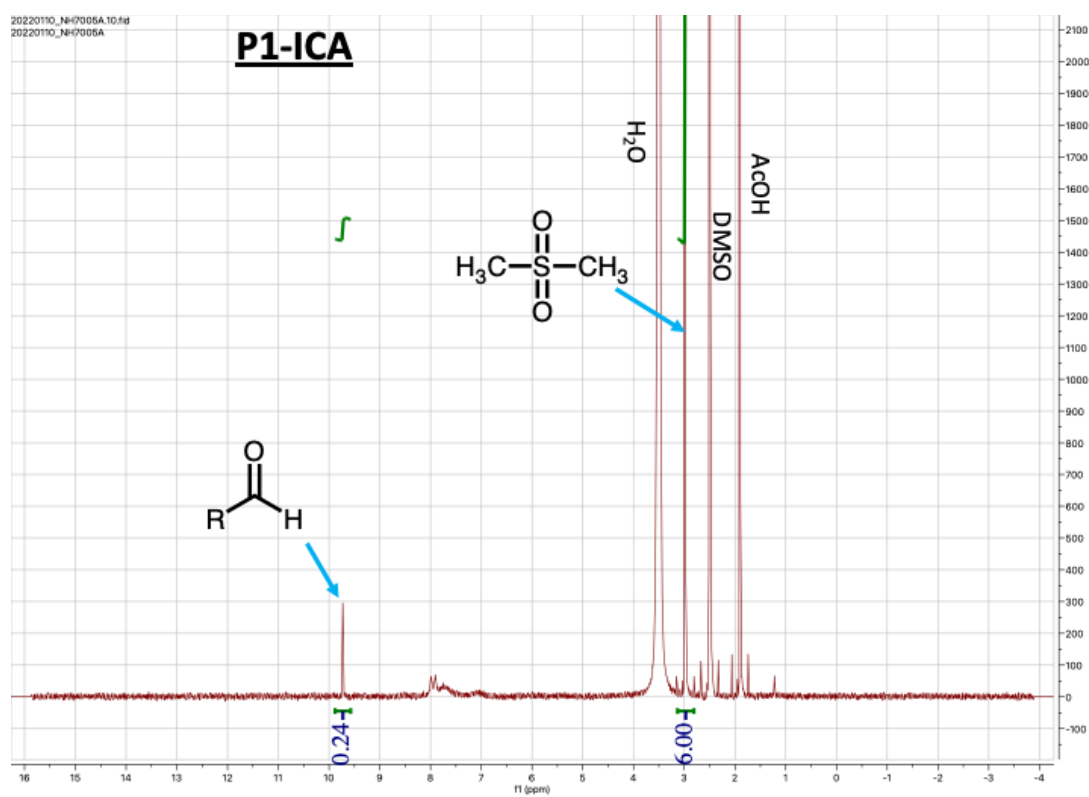


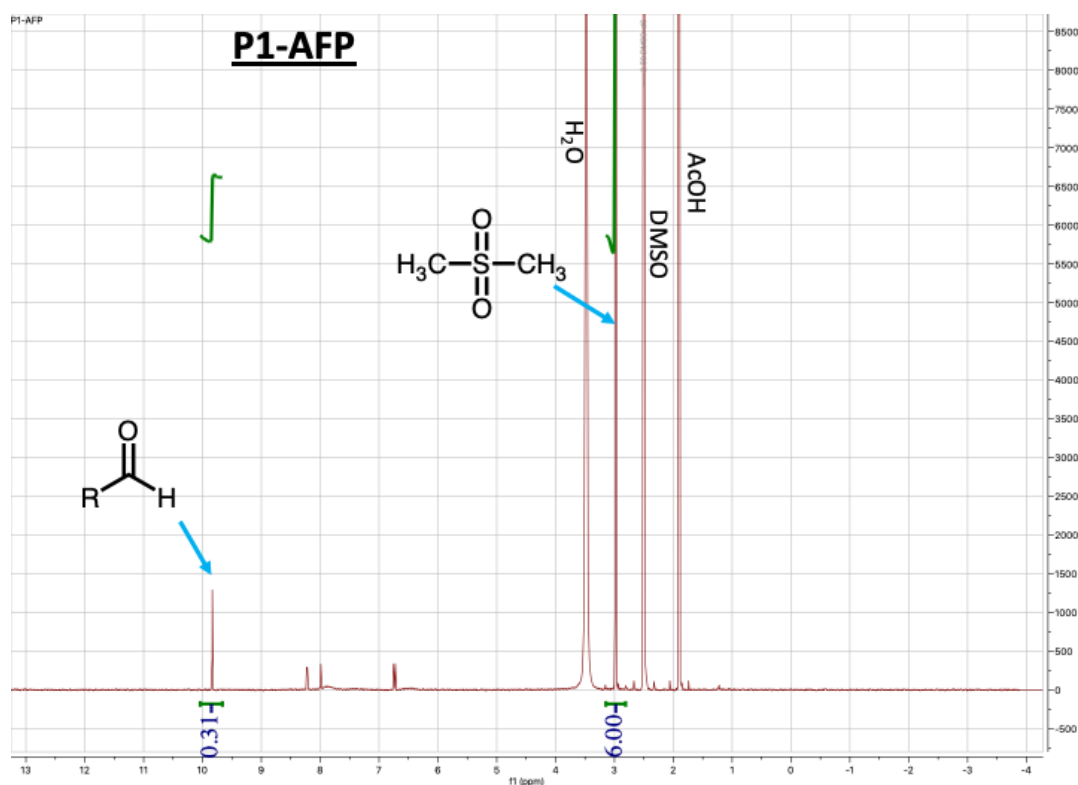
Figure 2.15. ¹H-NMR of P1 following dialysis and lyophilisation



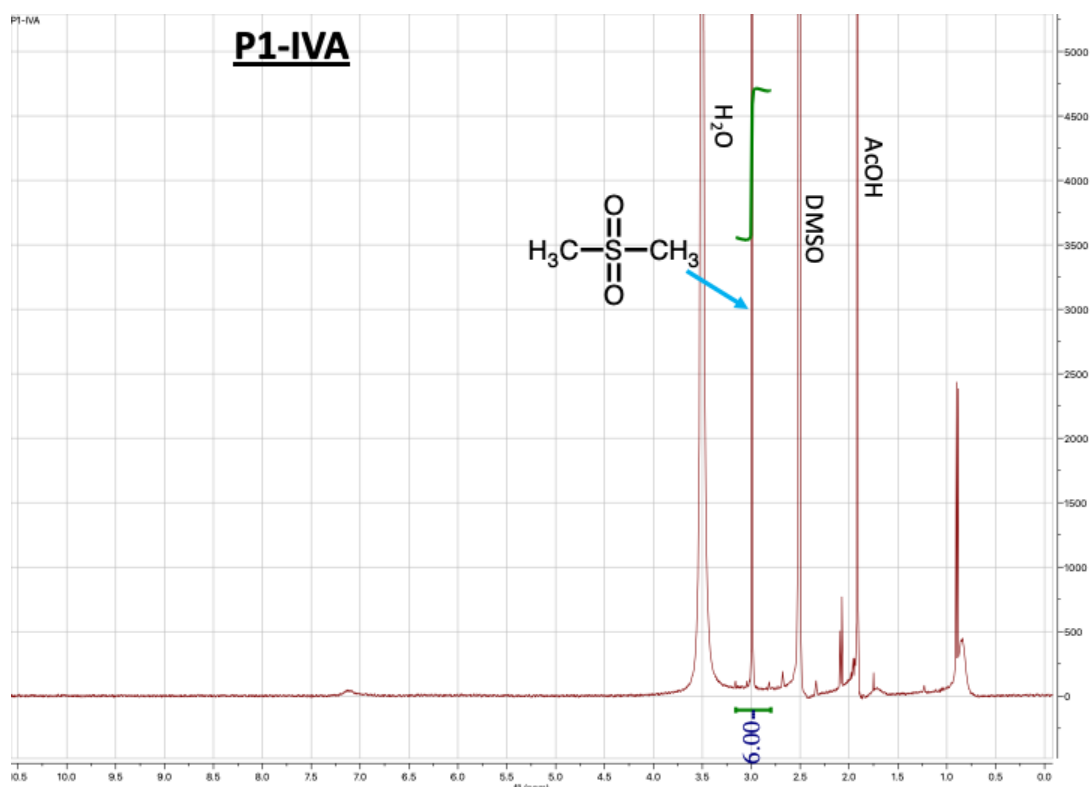
S.I. Figure 2.15. GPC trace for P1 from scaled-up polymerisation.



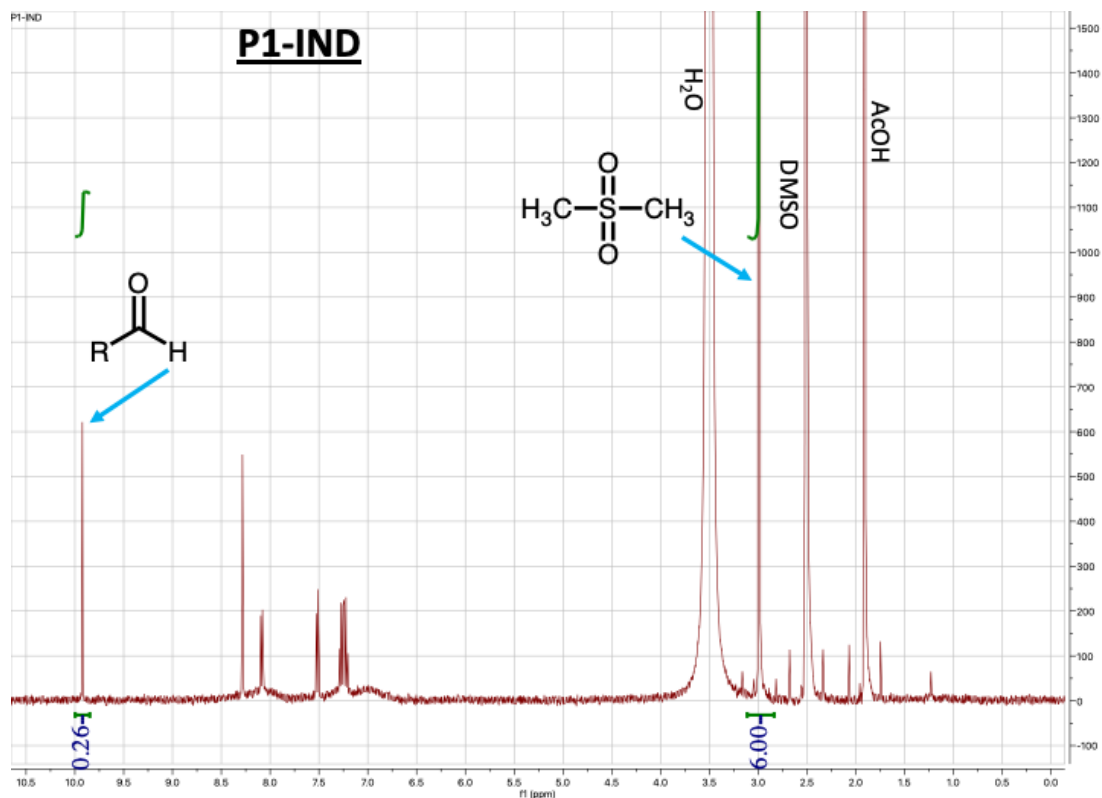
S.I. Figure 2.16. Quantitative ^1H -NMR analysis of ICA functionalisation with P1. Unreacted aldehyde signal ($\sim 9.8 \text{ ppm}$) measured against internal dimethyl sulfone standard (s, 3.1 ppm)



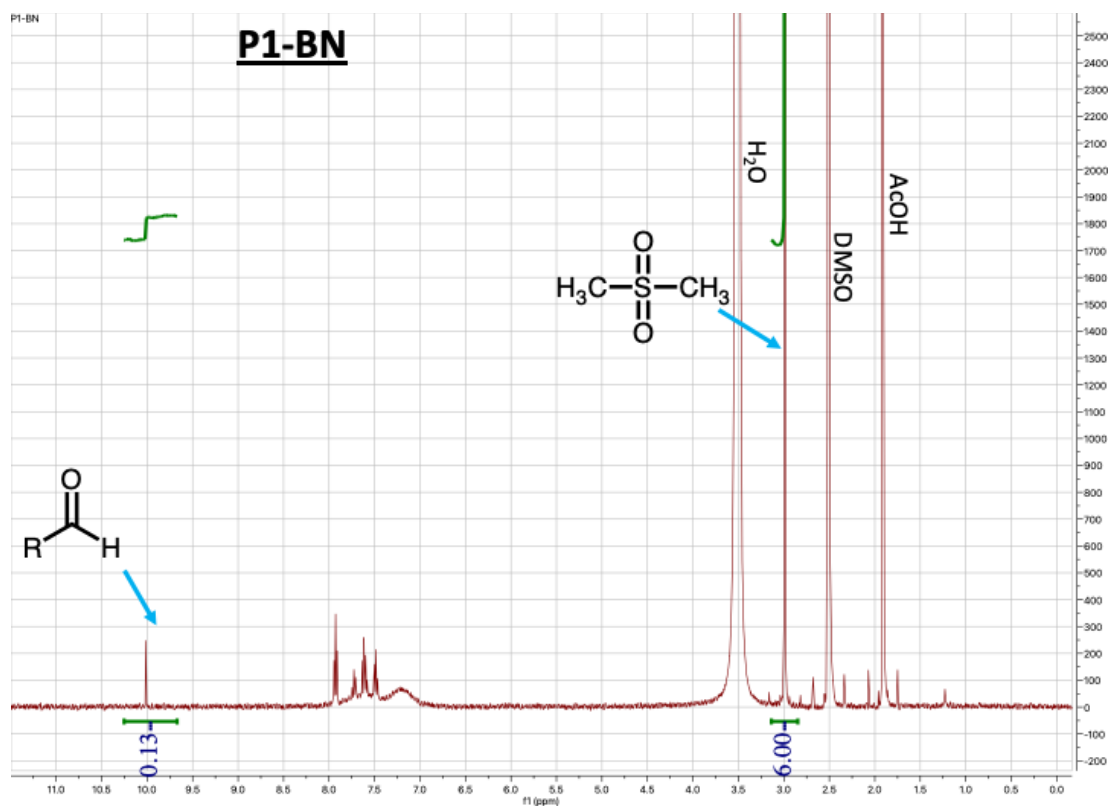
S.I. Figure 2.17. Quantitative ^1H -NMR analysis of AFP functionalisation with P1. Unreacted aldehyde signal (~ 9.8 ppm) measured against internal dimethyl sulfone standard (s, 3.1 ppm)



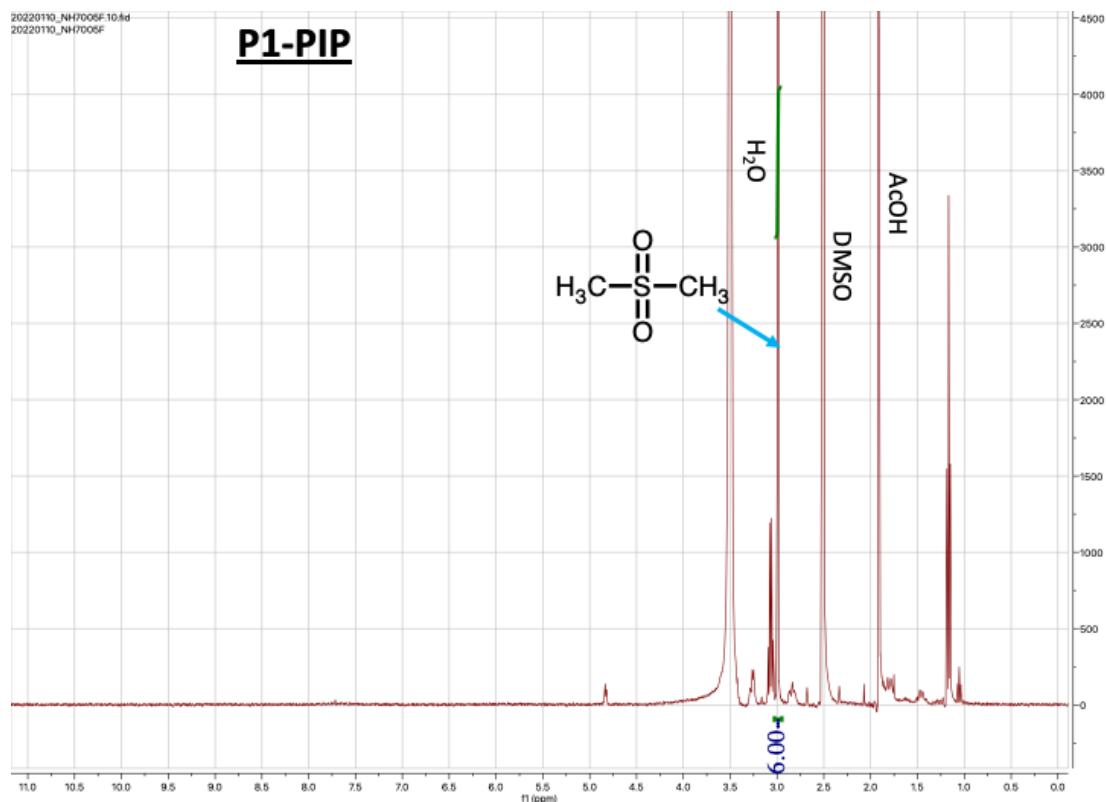
S.I. Figure 2.18. Quantitative ^1H -NMR analysis of IVA functionalisation with P1. Unreacted aldehyde signal (~ 9.8 ppm) measured against internal dimethyl sulfone standard (s, 3.1 ppm)



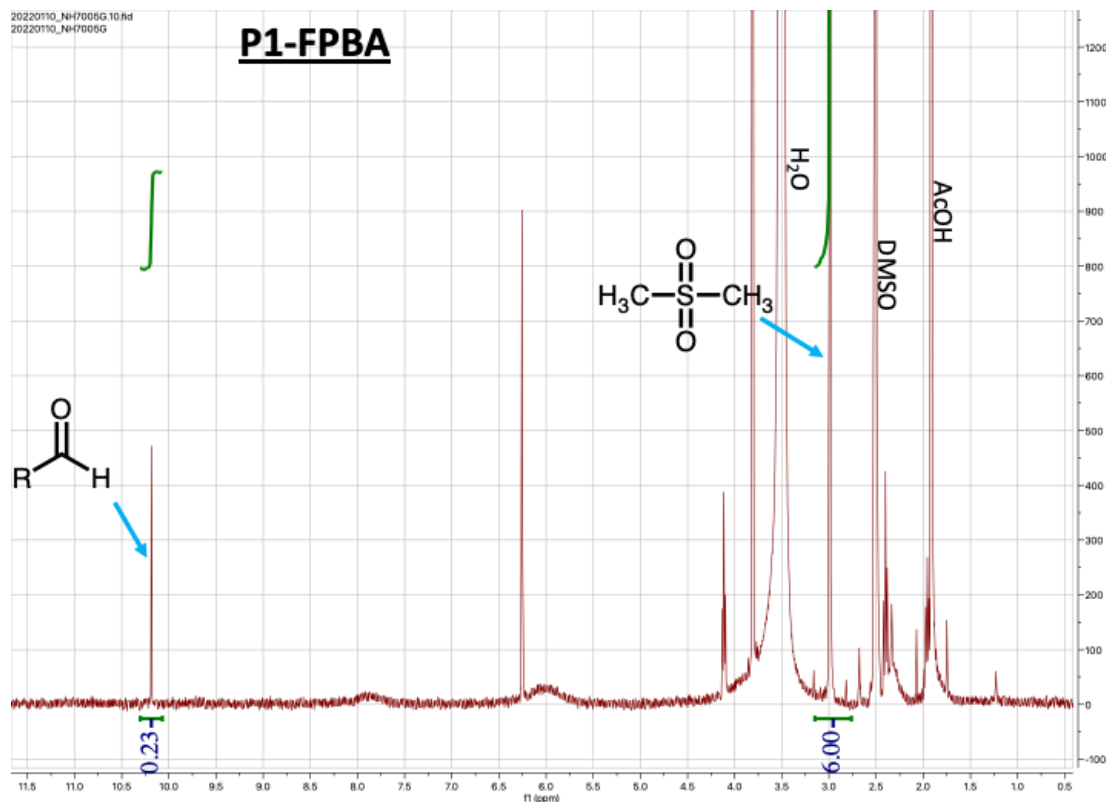
S.I. Figure 2.19. Quantitative ¹H-NMR analysis of IND functionalisation with P1. Unreacted aldehyde signal (~ 9.8 ppm) measured against internal dimethyl sulfone standard (s, 3.1 ppm)



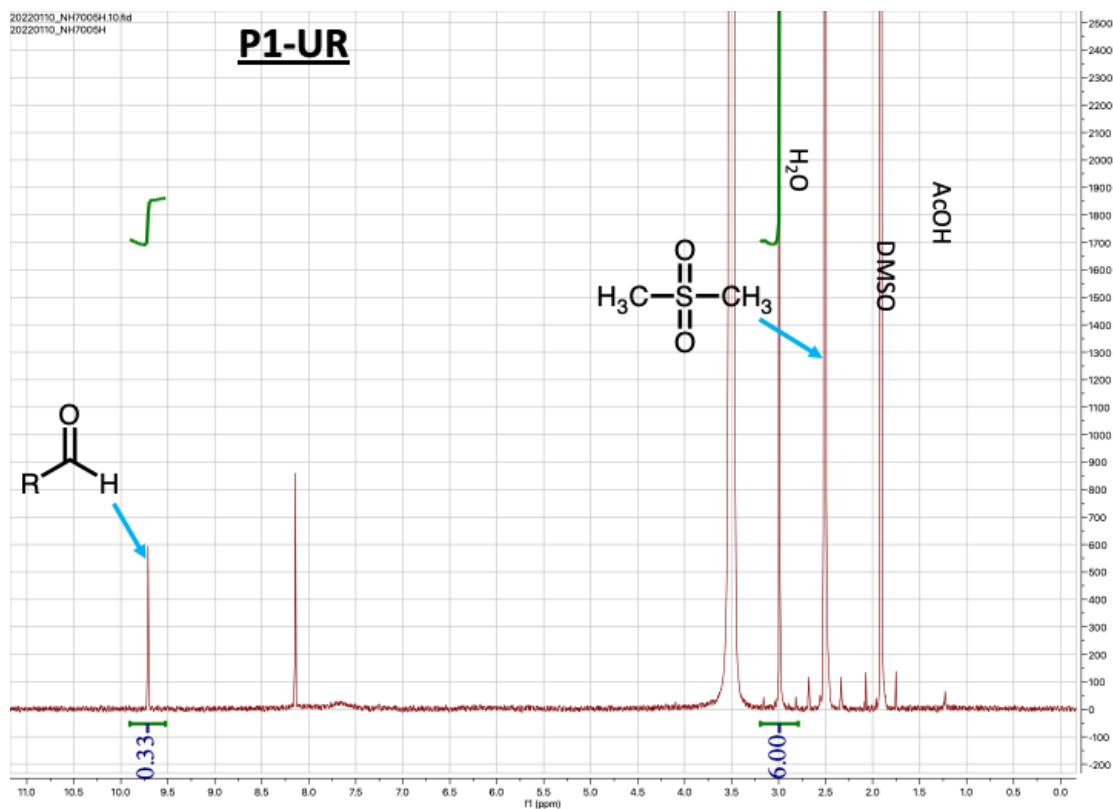
S.I. Figure 2.20. Quantitative ¹H-NMR analysis of BN functionalisation with P1. Unreacted aldehyde signal (~ 9.8 ppm) measured against internal dimethyl sulfone standard (s, 3.1 ppm)



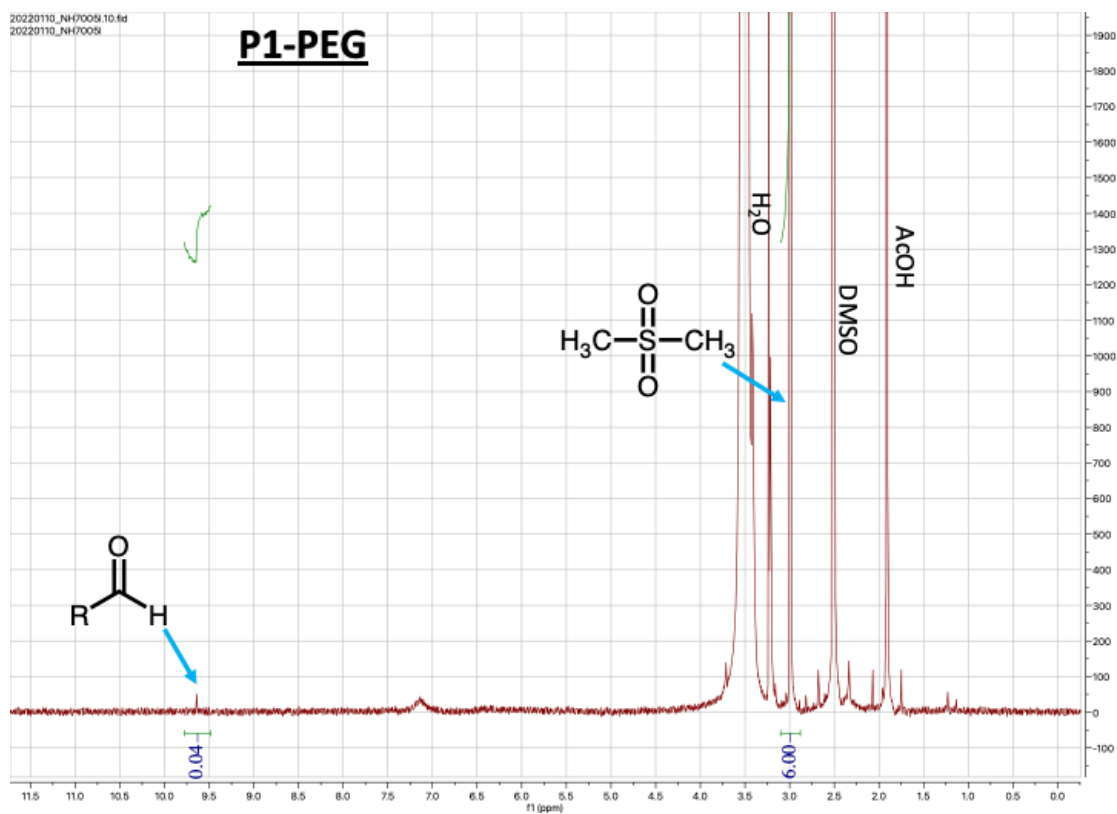
S.I. Figure 2.21. Quantitative ^1H -NMR analysis of PIP functionalisation with P1. Unreacted aldehyde signal (~ 9.8 ppm) measured against internal dimethyl sulfone standard (s, 3.1 ppm)



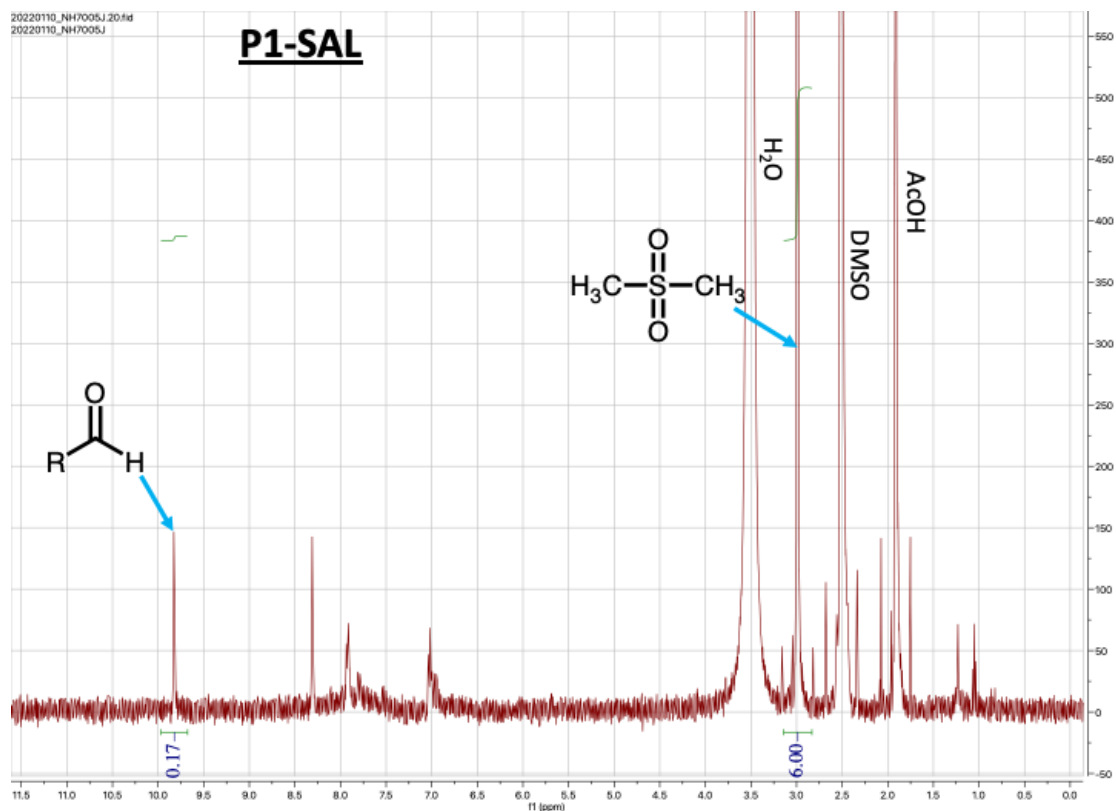
S.I. Figure 2.22. Quantitative ^1H -NMR analysis of FPBA functionalisation with P1. Unreacted aldehyde signal (~ 9.8 ppm) measured against internal dimethyl sulfone standard (s, 3.1 ppm)



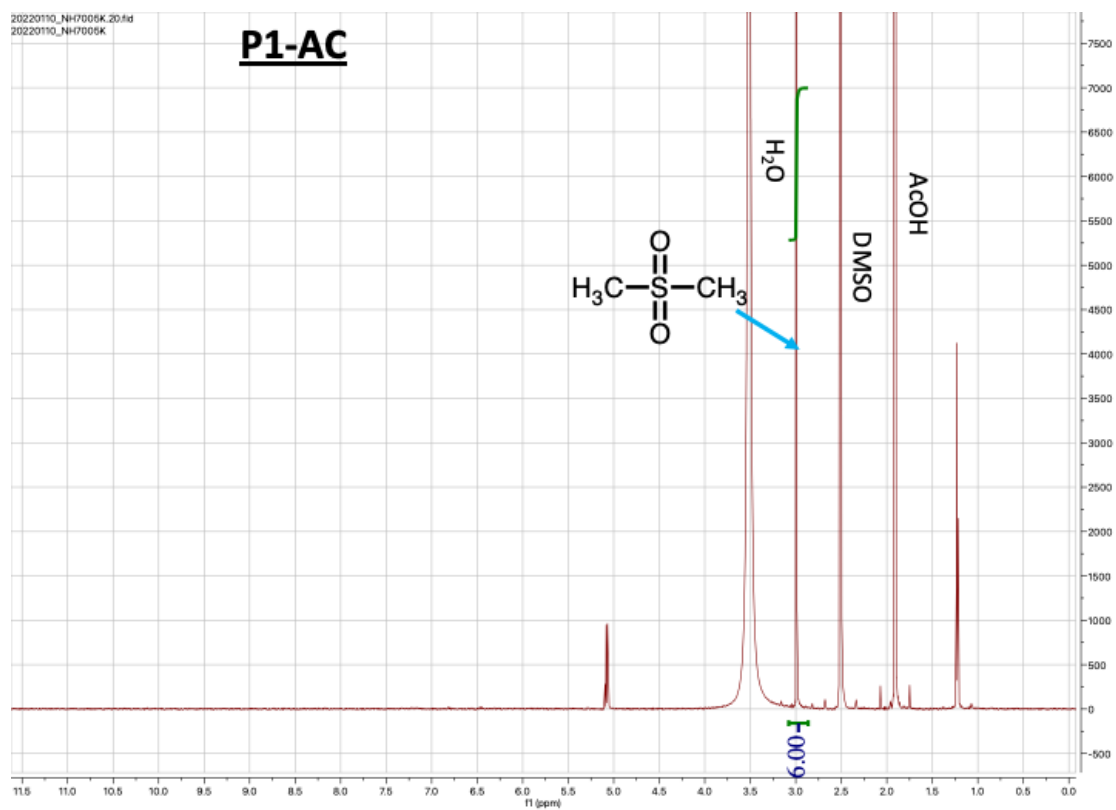
S.I. Figure 2.23. Quantitative ¹H-NMR analysis of UR functionalisation with P1. Unreacted aldehyde signal (~ 9.8 ppm) measured against internal dimethyl sulfone standard (s, 3.1 ppm)



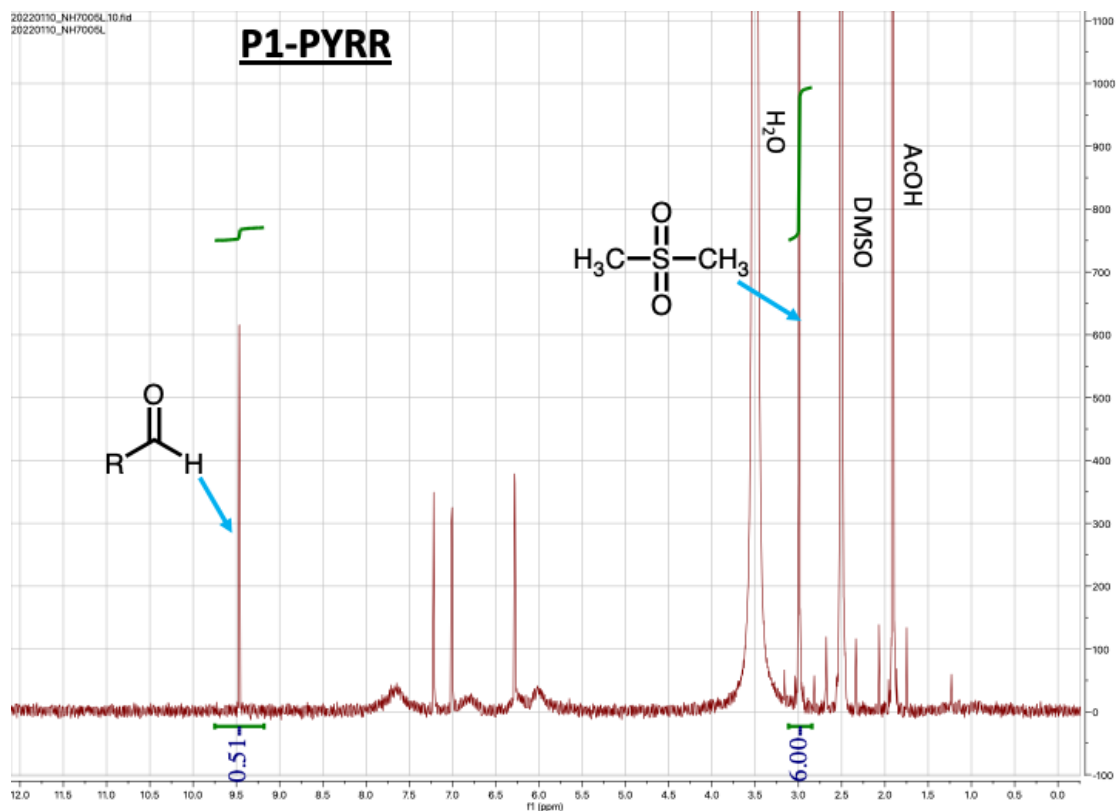
S.I. Figure 2.24. Quantitative ¹H-NMR analysis of PEG functionalisation with P1. Unreacted aldehyde signal (~ 9.8 ppm) measured against internal dimethyl sulfone standard (s, 3.1 ppm)



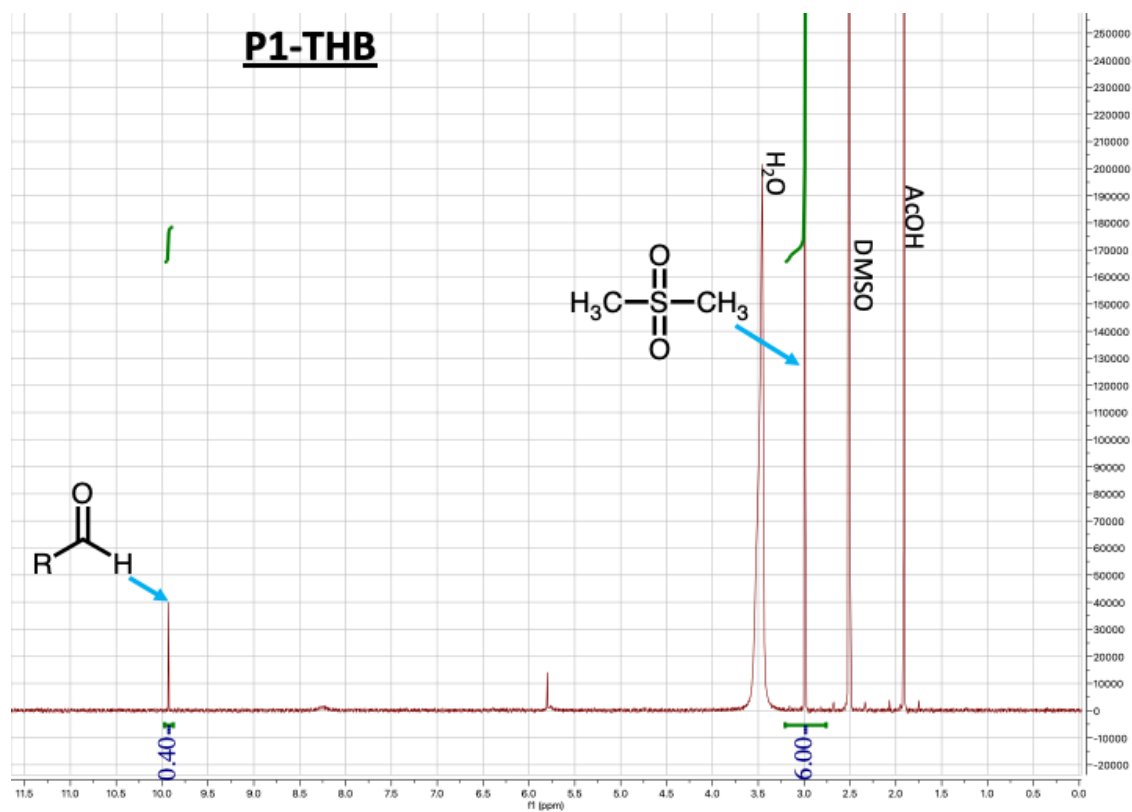
S.I. Figure 2.25. Quantitative ^1H -NMR analysis of SAL functionalisation with P1. Unreacted aldehyde signal (~ 9.8 ppm) measured against internal dimethyl sulfone standard (s, 3.1 ppm)



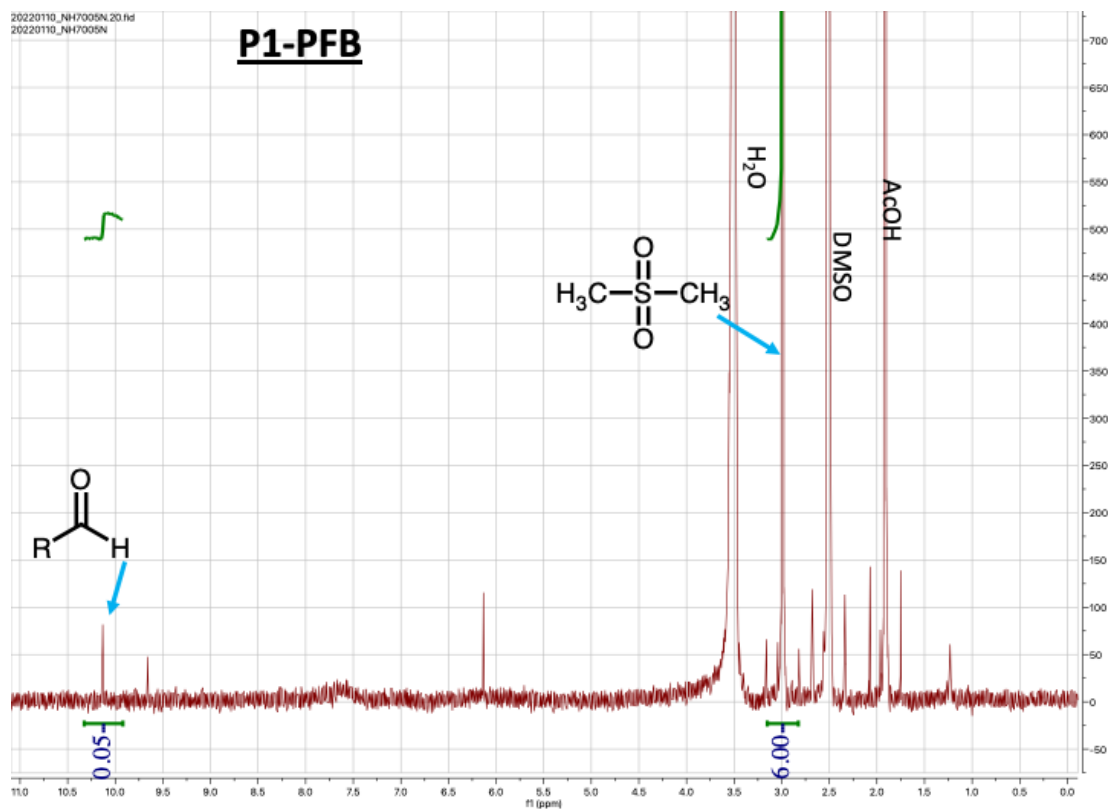
S.I. Figure 2.26. Quantitative ^1H -NMR analysis of AC functionalisation with P1. Unreacted aldehyde signal (~ 9.8 ppm) measured against internal dimethyl sulfone standard (s, 3.1 ppm)



S.I. Figure 2.27. Quantitative ^1H -NMR analysis of PYRR functionalisation with P1. Unreacted aldehyde signal (~ 9.8 ppm) measured against internal dimethyl sulfone standard (s, 3.1 ppm)



S.I. Figure 2.28. Quantitative ^1H -NMR analysis of THB functionalisation with P1. Unreacted aldehyde signal (~ 9.8 ppm) measured against internal dimethyl sulfone standard (s, 3.1 ppm)



S.I. Figure 2.29. Quantitative ¹H-NMR analysis of PFB functionalisation with P1. Unreacted aldehyde signal (~ 9.8 ppm) measured against internal dimethyl sulfone standard (s, 3.1 ppm)

Chapter 3 – Screening *E. coli* MC4100 aggregation & biofilm development with a novel library of aldehyde functionalised poly(propargyl hydrazine carboxamide) polymers

3.0 Introduction

The field of biotechnology has grown rapidly over the past five decades with an estimated global biotechnology market size of one trillion USD in 2021, projected to increase to 3.8 trillion by 2030.¹ At the forefront of this, is the use of biological organisms for the development of biopharmaceuticals and other fine chemicals.² *E. coli* is commonly considered to be the workhorse of biotechnology due to its well characterised genome, rapid growth rate and facile growth requirements.³ It has found use in the production of bulk and fine chemicals in whole-cell biocatalysis. However, these processes are limited by its susceptibility to unnatural conditions and the presence of organic solvents, reducing catalytic activity due to diminished cell viability. Although strategies such as immobilisation and encapsulation of microbes by polymers exist, these can create mass transfer limitations limiting process efficiency. An alternative approach is to exploit the protective ability of the biofilm, where the plaque-like extracellular matrix (ECM) confer a significant survival advantage to biofilms compared to their planktonic counterparts.^{4–6} As biofilms mature, they can produce channelled 3D mushroom-like structures promoting solute diffusion to the interior thereby overcoming mass-transfer limitations typically associated with artificial immobilisation strategies.^{7,8}

Although biofilms are an attractive alternative to traditional immobilisation techniques, many industrially relevant *E. coli* laboratory strains are typically poor biofilm producers, limiting their use in engineered biofilms. This thesis looks to address this issue, by using a library of novel synthetic poly(acetylene)s derived from **P1** (as prepared in **Chapter 2**) to study the effect of polymer physicochemical properties on biofilm formation in the model organism *E. coli* MC4100 (*araD139Δ(argF-lac)U169 rpsL150relA1 flbB5301 deoC1 ptsF25 rbsR*). Compared to

other *E. coli* K12 strains that are poor biofilm producers, MC4100 is a particularly poor biofilm producer as this strain is incapable of producing cellulose and type-1 pili. Cellulose deficiency arises due to a mutant stop codon at the start of the *bcsQ* causing premature termination of transcription and expression of downstream cellulose synthase proteins.⁹ MC4100 is also incapable of type-1 pili synthesis due to a deletion within the open reading frame deletion of the recombinase *fimB*.¹⁰

As such MC4100 only produces three extracellular matrix components (ECM): poly-N-acetyl glucosamine (PNAG), colanic acid (CA) and curli. Therefore, it was hypothesised that it would be easier to deduce the role of the polymer materials on bacterial physiology. The impact of polymer treatment on bacterial aggregation and subsequent ECM production was determined in several assays. Attempts were made to quantify the biofilm response against the formulated polymers' physicochemical properties. It is previously reported that surfaces modified with hydrophobic polymers promote cell attachment and biofilm formation.^{11–13} Adoni *et al.*, demonstrated that poly(acryloyl hydrazide) modified with hydrophobic aldehydes stimulated biofilm formation with enhanced aggregation and curli production in *E.coli* both MC4100 and its daughter strain PHL644.¹³ Where PHL644 is a curli overproducer due to a mutation within the OmpR regulator.¹⁴

To expand on this work, it was deemed pertinent to expand the chemical space previously explored using a novel poly(acetylene) derived scaffold (**P1**). Fourteen aldehydes were selected with a broad range of hydrophobicity and various functional groups to probe the effects on biofilm formation in *E. coli* MC4100. Poly(acetylenes) like **P1** are defined by their

characteristic conjugated main chain. Restricted rotation around the C=C double bond permit the polymers to adopt a helical secondary structure if the backbone possesses cis-transoid or cis-cisoid stereochemistry. In the previous chapter, characterisation and *in silico* studies showed **P1** potentially adopted a helical conformation, to the best of our knowledge there have been no published works using poly(acetylene) or helical polymers to induce biofilm formation in *E. coli*. Additional research has focused on trying to elucidate the aggregative mechanisms of **P1** and its respective formulations.

3.1 Materials & Methods

3.1.1 General polymer treatments of *E. coli* cultures

E. coli MC4100 was grown on Luria-Bertani-agar (LB) plates (10 g/L tryptone, 5 g/L yeast extract, 10 g/L NaCl, 15 g/L bacteriological agar) (Sigma, UK). Cultures were prepared by selecting a single colony from the plate of the required strain and grown overnight at 30 °C in 10 mL LB broth (5 g/L tryptone, 2.5 g/L yeast extract, 5 g/L NaCl (Sigma, UK). For experiments monitoring curli expression, *E. coli* MC4100 was transformed with the reporter plasmid pJLC-T using standard heat shock methods. Growth media was supplemented with 10 µg/mL tetracycline. Cells were reinoculated in fresh LB media (1% inoculum) and grown until the mid-exponential phase. The cells were pelleted by centrifugation (10 mins at 3200 × *g*) and washed thrice in sterile 0.1 M KH₂PO₄/K₂HPO₄ (pH 7) buffer. The cell-buffer suspension was then diluted to optical density, OD₆₀₀ = 0.2 with additional 0.1 M KH₂PO₄/K₂HPO₄ (pH 7). The cells were then treated with 0.1 mg mL⁻¹ polymer and relevant controls, followed an equal volume of 1 × M63 media (0.1M KHPO₄, 15 mM (NH₄)₂SO₄, 1 mM MgSO₄, 1.8 µM FeSO₄, 10 mM glucose, 0.5% thiamine, 40 µg mL⁻¹ L-cysteine adjusted to pH 7 using 5M NaOH). Therefore, final [P1] = 0.05 mg/mL in 1:1 (v/v) 0.1 M KH₂PO₄/K₂HPO₄ and 1×M63. Unless otherwise stated, cell cultures were incubated at 30 °C, 150 rpm for the required time, after which analysis would be performed.

3.1.2 Aggregate sizing analysis assays

General cell culture and polymer treatment performed as described in **Section 3.1.1**. *E. coli* MC4100 was cultured in 1:1 (v/v) 0.1 M KH₂PO₄/K₂HPO₄ (1mL) and 1×M63 at 30 °C, 150 rpm for 72 h. The cultures were then carefully added dropwise to Mastersizer2000 (Malvern Instruments, UK) dispersion chamber filled with 100 mL deionised (DI) water (at 150 rpm) with care taken to not disrupt any formed aggregates. Particle size distributions were obtained with

the General-Purpose Model for irregular non-spherical particle sizes with an obscuration limit set to 1%. Each sample was measured thrice to obtain the reported volume size distributions.

3.1.3 Turbidimetry assays

General cell treatment performed as described in **Section 3.1.1**. Cells were treated with 0.5 mg mL⁻¹ polymer treatment with an initial OD₆₀₀ = 0.5 in a standard 1cm plastic cuvette with a 1 mL total culture volume. Cells were cultured in 0.1 M KH₂PO₄/K₂HPO₄ (pH 7) alone. Following treatment, the cells were cultured for 4 h at 30 °C at 150 rpm. In this period the OD₆₀₀ of the treated cultures were then recorded every 30 minutes (Jenway 635 001 Benchtop UV/Vis) This was performed with three independent biological controls.

3.1.4 Crystal violet aggregation assay

General cell treatment performed as described in **Section 3.1.1**. Cells were cultured in sterile 1.5 mL Eppendorf tubes. From the same initial culture, the cells separate tubes were used for 1 h, 24 h, 48 h and 72 h timepoints. Cells were cultured in 1:1 (v/v) 0.1 M KH₂PO₄/K₂HPO₄ (1mL) 30 °C, 150 rpm for the desired time. At each timepoint the cell aggregates were first carefully washed by removing 900 µL culture media and replaced with 900 µL fresh 0.1 M KH₂PO₄/K₂HPO₄ (pH 7) buffer, this was performed twice. The cell aggregates were centrifuged (1 min at 14000 × *g*), the supernatant discarded and then the aggregates were resuspended in 1% crystal violet solution and left to stain at room temperature for 1 h. After staining the aggregates were again centrifuged (1 min at 14000 × *g*) and the supernatant was discarded. The stained pellet was dissolved in 33% acetic acid and 200 µL aliquots were transferred to a 96-well plate with triplicate wells used for each culture. Absorbance values were recorded at 550 nm using a CLARIOstar PLUS plate reader. This was performed with three independent biological controls.

3.1.5 *csgB::GFP* promoter activity assay

General cell treatment performed as described in **Section 3.1.1**. Cells were cultured in sterile 96-well plates in 1:1 (v/v) 0.1 M KH₂PO₄/K₂HPO₄ (300 µL). *E. coli* MC4100 was incubated at 30 °C for 72 h with orbital shaking (100 rpm) in a BMG Clariostar microplate reader with absorbance (600 nm) and fluorescence measurements (536 nm) taken hourly throughout this duration. This was performed with three independent biological controls. Fluorescence intensity (*F*) of treated cultures at time, *t*, was normalised to the maximum fluorescence value of the untreated cell cultures as described by **Equation 1**.

$$F = \frac{GFP_t - GFP_0}{GFP_{max}} \quad (1)$$

3.1.6 Plate surface-adherence assay

General cell treatment performed as described in **Section 3.1.1**. Cells were statically incubated in sterile 96-well plates in 1:1 (v/v) 0.1 M KH₂PO₄/K₂HPO₄ (300 µL) for 72 h. Non-adhered bacteria were removed by inversion of the plate and the remaining adhered biomass was carefully washed with sterile 0.1 M KH₂PO₄/K₂HPO₄ (pH 7). Total adhered biomass was determined by staining with 0.1% crystal violet (300 µL) for 1 h. The crystal violet was removed by inversion and the wells carefully washed thrice with DI water, the stained biomass was dissolved in 33% acetic acid and 200 µL aliquots were transferred to a 96-well plate with triplicate wells used for each condition. Absorbance values were recorded at 550 nm using a CLARIOstar PLUS plate reader. This was performed with three independent biological controls.

3.1.7 ECM extraction from polymer-microbe complexes:

General cell treatment performed as described in **Section 3.1.1**. Cells were cultured in sterile 50 mL Falcon tubes in 1:1 (v/v) 0.1 M KH₂PO₄/K₂HPO₄ (15 mL) at 30 °C, 150 rpm for 72 h. At

each timepoint the culture media was first removed, resuspended in 2 mL DI water and then cell cultures were pelleted (10 min at $3214 \times g$), the supernatant discarded and replaced with 1 mL sterile deionised water, vortexed and transferred to a 1.5 mL Eppendorf tube. The concentrated cell suspensions were heated to 80°C (Grant, BT5D High Temp. Dry Block Heater) for 30 min to denature intracellular enzymes and liberate membrane-bound PNAG and CA. Following heat treatment, the cell suspensions were sonicated for 10 mins at room temperature in a sonication bath (Ultrasonic Bath XUBA3) and then centrifuged (30 min at $14000 \times g$) and the supernatant was dialysed for a minimum 12 h with a Pur-a-Lyzer® Maxi 3.5 kD dialysis membrane to remove monomeric sugars and other intracellular contaminants. Dialysed solutions were transferred to sterile 1.5 mL Eppendorf tubes and stored at -20°C until quantification experiments were performed. The pellet was dried at 60°C for 24 h and the total dried biomass (DBM) was recorded. This was performed with three independent biological controls.

3.1.8 Glucosamine quantification (MBTH) assay

Following from **3.1.7**. Samples (500 μL) were thawed on ice and 98% H_2SO_4 (1.785 mL) was added to give a 72% (w/v) working H_2SO_4 concentration. Samples were vortexed and left to hydrolyse at room temperature for 3 h. Samples were diluted with DI water to 2N and heated to 100°C for 4h. Following the second hydrolysis step, 60 μL aliquots were taken and added to a polystyrene 96-well plate in triplicate for each tested condition. Next, 5% (w/v) NaNO_2 (60 μL) was added to each well and thoroughly mixed by pipetting and then allowed to react for 30 mins at 200 rpm. Next, 12.5% $\text{NH}_4\text{SO}_3\text{NH}_2$ (40 μL) was slowly added to each well and mixed, then incubated for 5 mins at room temperature. After, 0.5% MBTH (40 μL) was added

to each well and mixed by pipetting, the 96-well plate was covered and heated at 90 °C for 20 minutes. After cooling to room temperature, 0.5% FeCl₃ (40 µL) was added to each well and mixed as before and incubated for 15 minutes. Absorbance measurements were performed at 656nm/630nm and subtracted from the blanks (no sugar present). GluN content was determined from a 6-point calibration plot and then normalised to DBM as described by **Equation 2**. Standards were prepared fresh by dissolution in 2N H₂SO₄ and treated in an identical procedure to the unknown samples. This was performed with three independent biological controls. All absorbance measurements were performed using a CLARIOstar PLUS plate reader.

$$[GluN](\mu g mL^{-1} mg^{-1}) = \frac{(A_t^{656} - A_0^{656})}{DBM} \quad (2)$$

3.1.9 Fucose quantification assay

Following from **3.1.7**. The frozen dialysed samples were thawed on ice and 35.8 µL of sample was transferred to a 96-well plate in triplicates wells per sample. Samples were treated with 160.8 µL H₂SO₄/H₂O mixture (6:1 v/v) and hydrolysed at 100 °C for 12 minutes in a microwell plate heater (VWR Digital Heatblock). The plate was cooled to room temperature and the absorbance measured at 396 nm and 427 nm in . Next, 3.4 µL 3% L-cysteine hydrochloride (w/v) was added and mixed thoroughly via pipetting. Absorbance measurements were repeated at 396 nm and 427 nm. A 6-point calibration curve of fucose standards treated in an identical procedure to the samples were used to quantify the fucose concentration. Fucose concentrations were reported as normalised to DBM according to **Equation 3**. This was performed with three independent biological controls. All absorbance measurements were performed using a CLARIOstar PLUS plate reader.

$$[Fuc] (\mu g mL^{-1} mg^{-1}) = \frac{((A_{post}^{396} - A_{pre}^{396}) - (A_{post}^{427} - A_{pre}^{427}))}{DBM} \quad (3)$$

3.1.10 Metabolic activity assays

General cell treatment performed as described in **Section 3.1.1**. *E. coli* MC4100 was in cultured in 1:1 (v/v) 0.1 M KH₂PO₄/K₂HPO₄ (1 mL) in sterile 1.5 mL Eppendorf tubes. At each timepoint the polymer-bacteria aggregates were centrifuged (1 min x 3200 × *g*) the supernatant was discarded. After, the aggregates were resuspended in sterile 0.1 M KH₂PO₄/K₂HPO₄ (pH 7) containing 20 μM resazurin (0.6 mL) and incubated in the dark for 3 h at 37 °C. Following incubation, 3×200 μL aliquots were taken from each well and transferred to a black polystyrene 96-well plate and the fluorescence was recorded at 640 nm with a BMG Clariostar microplate reader in 5×5 well scan mode. This was performed with three independent biological controls.

3.1.11 Membrane stress assay with 1-N-phenylnaphthylamine (NPN)

General cell treatment performed as described in **Section 3.1.1**. Buffered *E. coli* MC4100 suspensions (200 μL, OD = 0.1) were treated with 0.1 mg mL⁻¹ polymer and/or aldehyde formulations in a black opaque 96-plate. NPN (20 μM working conc.) was immediately added, and the fluorescence measured at 426 nm in a with a BMG Clariostar microplate reader. Measurements were performed over a 10-minute period and then averaged to give a single measure. This was performed with two biological repeats.

3.1.12 Membrane stress assay with *spy::gfp*

General cell treatment performed as described in **Section 3.1.1**. *E. coli* MC4100 was cultured in 1:1 (v/v) 0.1 M KH₂PO₄/K₂HPO₄ (300 μL) for 24h at 30 °C, 100 rpm in a BMG Clariostar microplate. Absorbance (600 nm) and fluorescence measurements (536 nm) taken hourly

throughout this duration. Additional validation experiments were performed at higher cell concentrations (OD = 0.4) in LB media alone and cultured with the same parameters above. This was performed with three independent biological controls.

3.1.13 Phase diagram construction

General cell treatment performed as described in **Section 3.1.1**. *E. coli* MC4100 in 0.1 M KH₂PO₄/K₂HPO₄ were diluted in 1.5 mL cuvettes to give four initial cell densities (1 mL; OD = 0.25, 0.5, 1.0 & 2.0). Each dilution was treated with four different polymer concentrations (0.05, 0.25, 0.5 & 0.1 mg mL⁻¹) in an orthogonal design to give 16 different conditions for each tested polymer formulation. The OD₆₀₀ was measured immediately (Jenway 635 001 Benchtop UV/Vis) following polymer treatment (A_0), and incubated for 24 h at 30 °C, 150 rpm. At 24 h the OD₆₀₀ measurements were repeated (A_{24}) and the percentage of aggregated bacteria (Agg%) according to equation 4.

$$Agg(\%) = \left(\frac{A_0 - A_{24}}{A_0} \right) \times 100 \quad (4)$$

3.1.14 Statistical Analyses

All statistical analyses and data presented was performed in GraphPad9. For all comparative statistics of the polymer treatments against a single control group , an ordinary one-way analysis of variance (ANOVA) was performed. A Tukey's multiple pairwise comparisons post-hoc analysis was performed to test for significance between numerous pairs of interest. To account for multiple comparison testing (limit Type-1 errors/false negatives), a two-stage step-up method of Benjamini, Krieger, and Yekutieli was chosen to control the false discovery rate (FDR (Q) = 0.05). A comparison was deemed a statistically significant result/ discovery when the FDR-*adjusted* p-values (q) \leq 0.05. If all the null hypotheses are true, there will be only a Q% chance of finding one or more discoveries. For time-series data, a Two-way ANOVA

was performed. Again, a Tukey's multiple pairwise comparisons post-hoc analysis was performed and corrected for with an FDR (Q) = 0.05.

3.2 Results & Discussion

3.2.1 Determining cell aggregation by poly(acetylenes)

3.2.1.1 Particle size analysis

To probe the aggregation process between **P1** formulations and MC4100, the size of the polymer-microbial complexes (PMCs) was measured using a Mastersizer2000. According to the Mie theory, the amount of light scattered by a particle is proportional to its size.¹⁵ Therefore, the size and distributions of PMCs in suspension can be determined by the amount of scattered light detected from this. The Mastersizer is well-suited for the analysis of PMCs compared to dynamic light scattering, as it can measure much larger particle sizes ($\leq 2000\ \mu\text{m}$). As well as deal effectively with irregularly shaped particles, which would be highly likely in the tested conditions. All results reported herein are volume weighted distributions, where the percentage volume can be interpreted as the percentage of space/volume occupied by an individual particle of a certain size. The cumulative particle size distributions are shown in the appendix (**S.I. Figure 3.1**). All measurements were performed after *E. coli* MC4100 was cultured in a 1:1 mixture of 0.1 M $\text{K}_2\text{HPO}_4/\text{KH}_2\text{PO}_4$ and 1×M63 media for 72 h in the presence of **P1**. Additional controls included the unreacted aldehydes (added in the same molar ratio as the polymers), the polymers' reaction solvent (0.1 M AcOH/DMSO) and a negative untreated control of *E. coli* MC4100 was also included. The inclusion of the controls confirmed that any change relative to the untreated cultures is due to the polymer rather than the aldehyde or solvents used in the formulation.

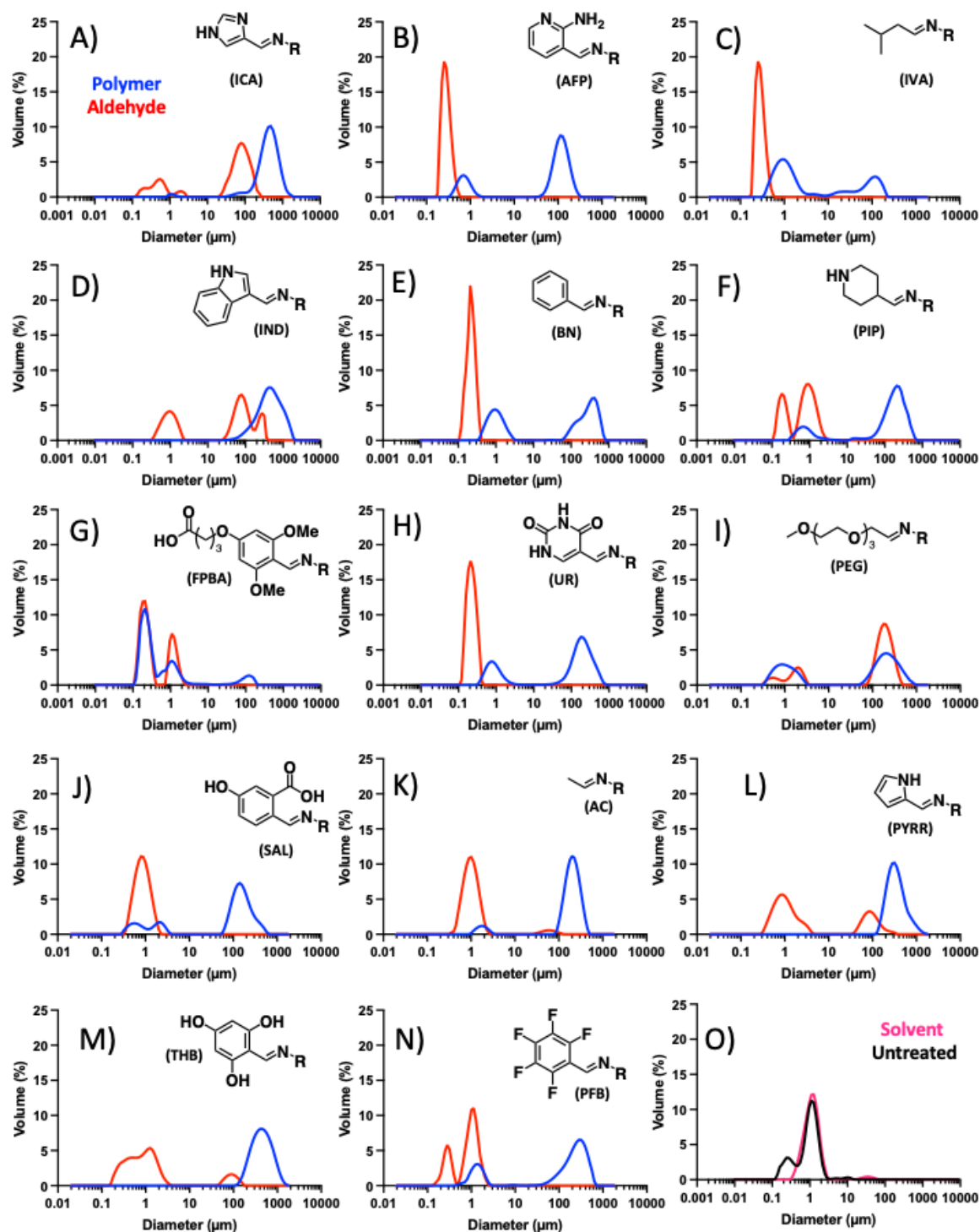


Figure 3.1. Volume size distributions of *E. coli* MC4100 following treatment with P1 formulations (blue), aldehyde controls (red), DMSO/AcOH solvent (black) and untreated cultures (black). A = ICA; B = AFP; C = ICA; D = IND; E = BN; F = PIP; G = FPBA; H = UR; I = P PEG_4 ; J = SAL; K = AC; L = PYRR; M = THB; N = PFB; O = solvent treated controls.

The untreated cultures were strictly monomodal, whereby only a single particle size population ($\sim 1 \mu\text{m}$) was recorded, suggesting that untreated *E. coli* MC4100 was incapable of

auto-aggregation under these experimental conditions (*Figure 3.1*). Polymer treatment generally produced a bimodal distribution of unaggregated individual cells ($\sim 1 \mu\text{m}$) and polymer-induced aggregates ($100 - 500 \mu\text{m}$) dependent on the treatment in question. Moreover, all aldehyde treated cultures (red) except **ICA**, **PIP**, **PEG4₄**, and **PYRR** and the solvent treated cultures (*Figure 3.10*; pink) gave near identical particle size distributions as the untreated controls. This suggested that in the absence of polymers there are no observed large macroscopic clusters due to the lack of intercellular bridging. Prior literature shows that the molecular weight or size, as well as the shape of a polymer is critical in its effectiveness as an aggregating agent. For instance, dendrimers with increased generation size (i.e. number of 'arms') could more effectively cluster a range of bacterial species compared to smaller dendrimers.^{16,17} Likewise, linear glycopolymers were also shown to be much more efficient agglutinating agents compared to spherical vesicle formulations of the same polymer with a smaller hydrodynamic radius.¹⁸ Therefore, given that aldehydes are small molecules, their size is insufficient to produce any crosslinking between the multiple bacterial cells and so little macroscopic aggregate formation is observed. However, some aldehydes (**ICA**, **IND**, **PEG4₄**, and **PYRR**) formed smaller aggregates in suspension, likely due to passive settling and adherence to the tube surface. Why these compounds produce a larger aggregative effect compared to the others remains unknown and no obvious trend is apparent. **ICA**, **IND**, and **PYRR** are heterocyclic, and **IND** is believed to negatively affect biofilms. In the **P1** treated cultures, the larger particle size distributions ($\geq 100 \mu\text{m}$) which were assigned to be the polymer-induced aggregates, produced a monomodal distribution in all formulations except **P1-PIP** and **P1-IVA**. Although the produced particles sizes are polymer-dependent, the observed monomodal distributions for each treatment suggest that the formed aggregates

are homogeneous within their population size, which is an important characteristic for future application. To screen the possible role of the physicochemical properties of the **P1** formulations on polymer-driven aggregation, several physicochemical parameters (clogD, topological surface area (tPSA), strongest basic pK_A , polarisability, and molecular weight (M_w)) were predicted using Chemaxon chemoinformatic software. They were then plotted as a function of particle size distributions (d_x) (Figure 3.2), where x equals the percentile population of size, for example d_{50} means that 50% of the particle population is equivalent to a certain size or lower. No significant correlations were observed with any calculated physicochemical parameters of the polymer. There is a possible correlation regarding the 90% particle distribution size (D_{90}) with clogD and polarisability, suggesting that increased polymer hydrophobicity promotes larger aggregate formation.

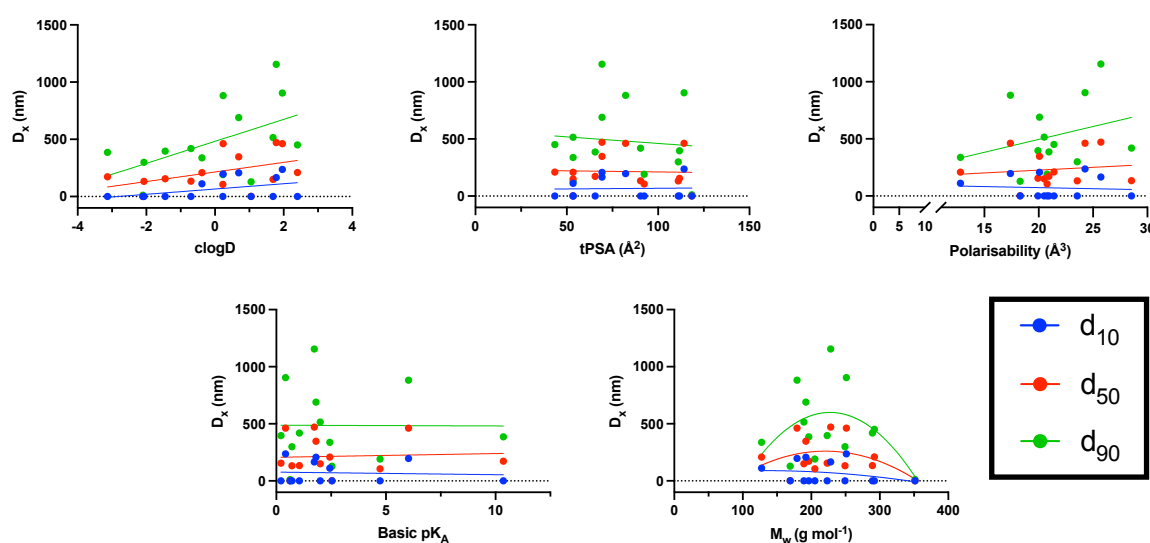


Figure 3.2. Correlations between size distribution d_x , where $x = 10\%$ (blue); 50% (red); 90% (green) with physicochemical parameters of P1 formulations.

However, the increased variability when looking at these models may be due to the PMCs disintegrating during the measurements due to high hydrodynamic shear in from mixing within the system. Similar observations have been made previously,¹³ where MC4100

aggregates were too weak to withstand the shear mixing in the Mastersizer leading to aggregate break-up. Therefore, it is probable that the measurements reported herein are under-representations of the true value due to this breakdown and only polymers that interact strongly with the bacteria give rise to mechanically robust PMCs. Visual observations of the polymer treated aggregates showed macroscopic clustering clearly visible by eye. The measured particle volumes are much lower than these qualitative observations further supporting possible aggregate breakdown during measurement. Shearing of the bacterial aggregates may explain why there is seemingly no significant correlations with any physicochemical parameters of **P1**. Therefore, to further corroborate the particle size analysis alternative less destructive quantitative measurements were used to determine bacterial clustering by **P1**.

3.2.1.2 Turbidimetric analysis of bacterial aggregates

Due to increased measurement variability and possible aggregate breakdown with the Mastersizer, alternative non-destructive analytic techniques were sought to support these initial findings. Growth in planktonic bacterial cell cultures is typically measured by turbidimetry, which is the loss of transmitted light through a suspension due to absorption by particles contained within. In the context of microbial growth, at 600 nm (OD_{600}) higher cell densities reduce the amount of transmitted light increasing absorbance/OD which indicates higher cell numbers. Furthermore, the presence of large particles or aggregate in suspension increases light scattering and thereby increases absorbance. Consequently, turbidimetric analysis of the polymer-induced aggregate produced in this work would initially show an increase in OD_{600} approximately proportional aggregate size. As shown in *Figure 3.3.*,

aggregates of sufficient mass will sediment from the bulk suspension increasing the amount of transmitted light as the particles sediment out of the light path. A continued reduction in absorbed light occurs as sedimentation continues reaching an eventual minimum.

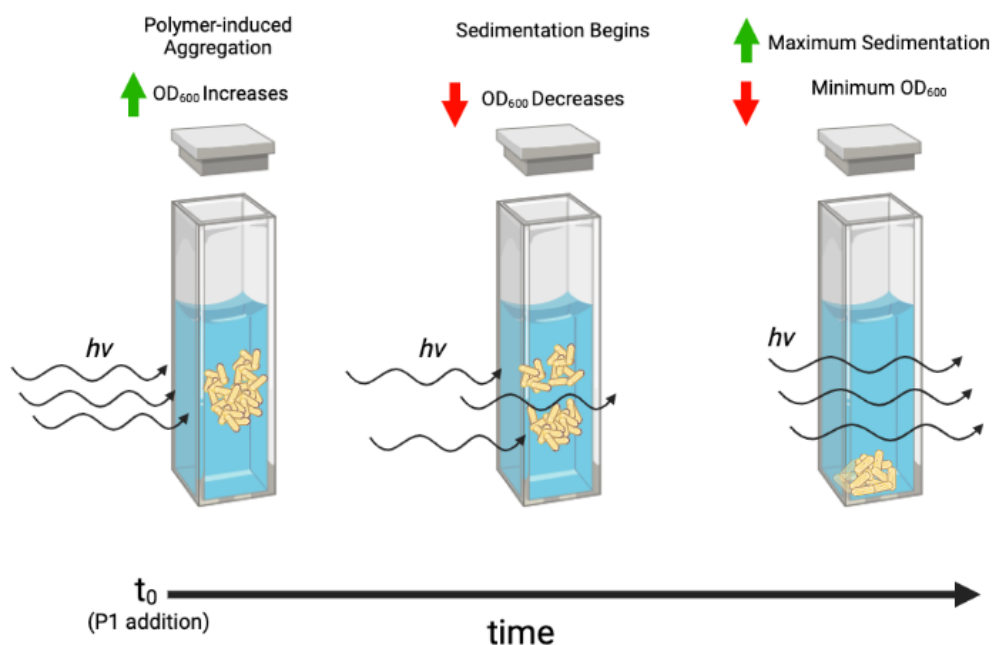


Figure 3.3. Scheme representing how aggregation and sedimentation of polymer-induced aggregates effects the amount of transmitted light (h = Planks constant; ν = frequency) and consequently its change in optical density (OD_{600}) with time (t). Not drawn to scale. Produced In Biorender.

Buffered cell suspensions ($OD = 1$) were treated with the functionalised P1 formulations produced in **Chapter 2** and their respective aldehydes (as controls). Turbidity (OD_{600}) was recorded every 30 mins for 5.5 h for all conditions to determine how the clustering behaviour of the bacteria was altered in the presence of polymers (**Figure 3.4**). All polymers except **P1-SAL** show a large increase in OD_{600} indicative of the formation of large clusters following polymer treatment (**Figure 3.4**). No increase in OD_{600} was observed for any aldehyde or solvent controls. Non-polymer treatments were like the untreated negative control, which suggested

that no aggregation had occurred. Though a slight decrease in OD₆₀₀ was noted with time this was likely due to passive settling in the planktonic cultures, as MC4100 is a non-motile strain.

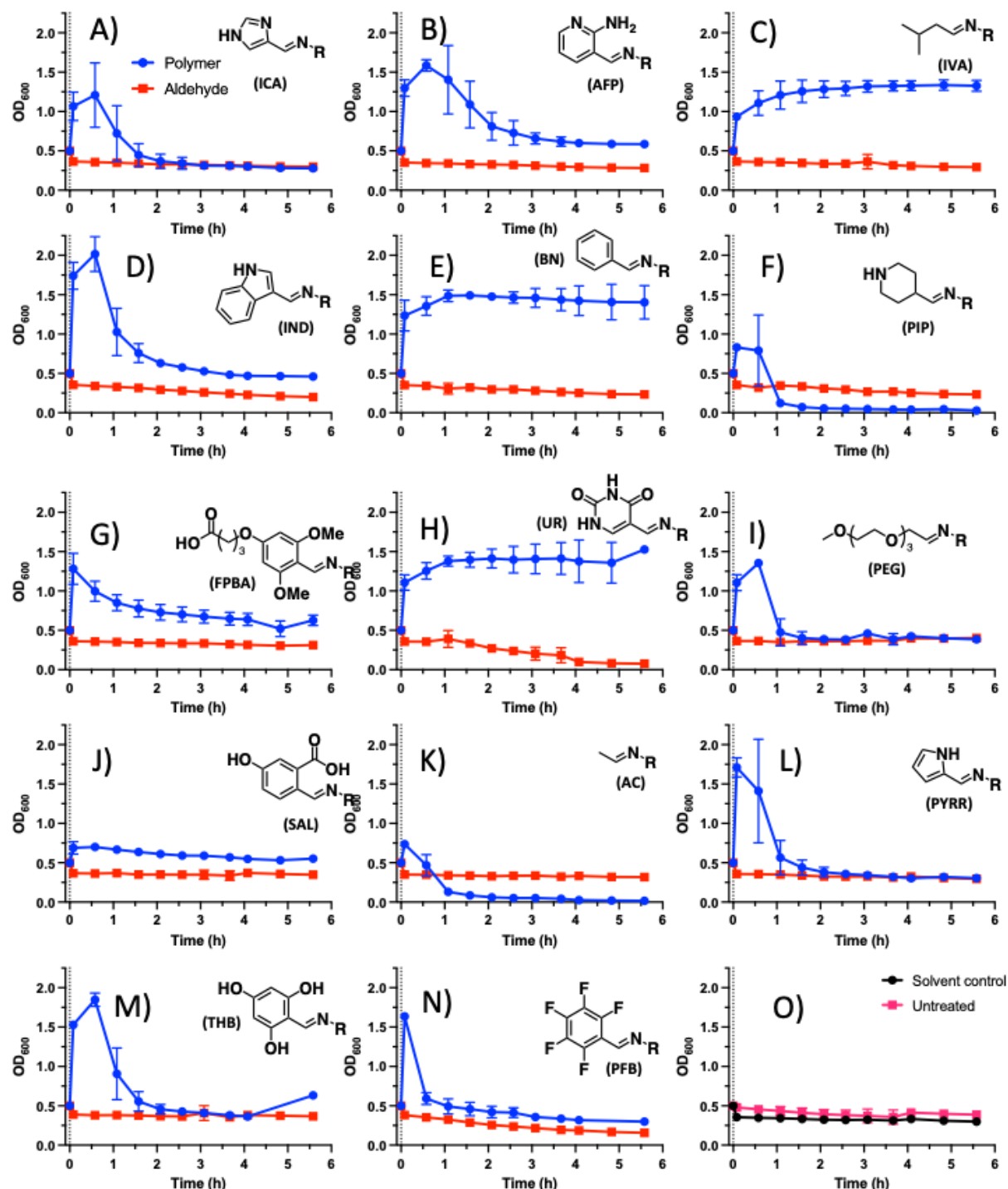


Figure 3.4. OD₆₀₀ measurements with time of *E. coli* MC4100 treated with P1 formulations (blue) and their respective aldehyde controls (red). A = ICA; B = AFP; C = ICA; D = IND; E = BN; F = PIP; G = FPBA; H = UR; I = PEG₄; J = SAL; K = AC; L = PYRR; M = THB; N = PFB. Error bars = s.d. (n = 3)

Therefore, as insinuated by the initial particle size analyses (**Figure 3.1**), only polymeric formulations can induce macroscopic aggregation in bacteria. Only polymers are of sufficient size to effectively cross-link the bacterial cells together causing aggregation. All formulations except **P1-IVA**, **P1-BN**, and **P1-UR** exhibited similar aggregative behaviour. Typically, OD₆₀₀ peaked within 1 h of polymer addition; followed by a decrease in absorbance due to sedimentation (*Figure 3.4*). Visual inspection of the aggregates relating to **P1-IVA**, **P1-BN**, and **P1-UR** show aggregates that are much larger and diffuse in contrast to the remaining formulations (**Figure 3.5**). Therefore, it is possible that the aggregates produced by these formulations are less dense, which diminishes the sedimentation rate to the point that no sedimentation is observed within the time frame of this experiment. The exact cause behind this observation remains elusive. A possible hypothesis is that initial interaction with the cell wall is slower with these formulations. Therefore, crosslinking between cells also occurs at a lower rate leading more diffuse particles than possess lower sedimentation rates.

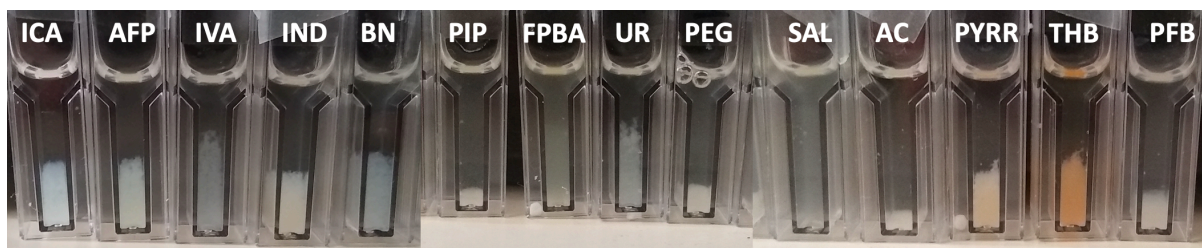


Figure 3.5. Images taken of buffered E. coli MC4100 cultures in the presence of P1 formulations 1 h after initial treatment.

In addition, both **P1-PIP** and **P1-AC** showed minimal increase in maximum measured optical density (OD_{max}) followed by rapid sedimentation. Majority of all the bacteria had settled out of solution 1h following treatment. Additionally, **P1-SAL** showed a minimal increase in OD_{max}, though unlike **P1-PIP** and **P1-AC** there is also minimal settling within the experimental timeframe. This implied that there is low aggregation occurring (**Figure 3.4**) in P1-SAL. The

different recorded OD_{max} for each polymer treatment are well visualised when looking at images taken of the cultures at 1h (**Figure 3.5**). For instance, **P1-SAL** produced a negligible change in OD, which can be clearly displayed in its respective image (**Figure 3.5**). The treated culture remains a homogenous turbid mixture, showing that minimal aggregation has occurred following treatment with **P1**. In contrast, the other formulations that produced a profound increase in OD_{600} showed distinct macroscopic clustering indicative of bacterial aggregation.

An alternative hypothesis is that the different behaviours observed amongst the polymer formulations are due to different mechanisms-of-action. For instance, the hydrophilic nature of **P1-Ac** and **P1-PEG₄** formulations may cause the aggregation to proceed by depletive mechanisms. Although the less pronounced effect with **P1-PEG₄** maybe due to lower hydrazone formation from the aldehyde coupling reactions. This would increase the polymer hydrophobicity, thereby reducing the possible depletive effect. Likewise, both **P1-FPBA** and **P1-SAL** share an anionic charge with the bacterial cell surface and are expected to be non-adherent, also possible depleting agents. Interestingly, **P1-PIP** despite being cationic at pH 7, behaved like **P1-Ac** with respect to OD_{max} and settling behaviour. Given its cationic character it is highly improbable that aggregation by **P1-PIP** proceeds by depletion aggregation. However, it is possible that the aggregation may occur due to charge neutralisation of the cell surface by the polymer leading to colloidal destabilisation and thus aggregation. A preliminary experimental investigation of this was performed later (see **Section 2.6**).

As with the particle sizing analyses, the OD_{max} measured for each treatment was plotted as functions of the physicochemical parameters of the **P1** formulations. This was to determine whether any physicochemical properties affected the observed aggregative behaviour with the bacteria (**Figure 3.6**). Supporting the data gathered from the particle sizing analysis, there is a significant positive linear correlation with polymer hydrophobicity ($clogD$, $R^2 = 0.461$) and maximum OD_{600} which agrees with the literature.¹³ The aromatic (**P1-BN**, **P1-THB**, and **P1-PFB**) and heteroaromatic (**P1-IND** and **P1-PYRR**) formulations produced the largest increase in OD_{max} . **P1-IVA** has similar $clogD$ to **P1-THB** and **P1-PYRR** yet has a significantly lower OD_{max} . This suggested that aromaticity may enhance association with the bacterial membrane by possibly through cation- π interactions in which full or partial positive charges such as cations embedded in the cell membrane could induce a complementary dipole in an aromatic system. No other significant correlations were identified from the regression analyses, although there is a possible positive linear correlation with polarisability on exclusion of ionic formulations (**P1-PIP**, **P1-FPBA**, and **P1-SAL**). Here the ionic formulations also show a similarly significant positive correlation when the regression is performed separate to their non-ionic counterparts. Polarisability pertains to how strongly the electrons are held by atomic nuclei, when subjected to an electric field this distorts the electron cloud producing a dipole moment in the molecule. the greater the deformation, the larger the dipole moment and thus, the greater the polarisability. The bacterial cell membrane is a highly heterogenous surface due to its net anionic charge but also hydrophobic to a certain extent due to surface proteins. Theoretical studies suggest that bacterial surface charge shifts on approach to a surface.¹⁹ Therefore, in the presence of polymers with high polarisability it is possible that ion-dipole or dipole-dipole interactions are established between the polymer and outer cell membrane

further driving bacterial aggregation. This may explain why some aggregation is observed **P1-FPBA** but not **P1-SAL**.

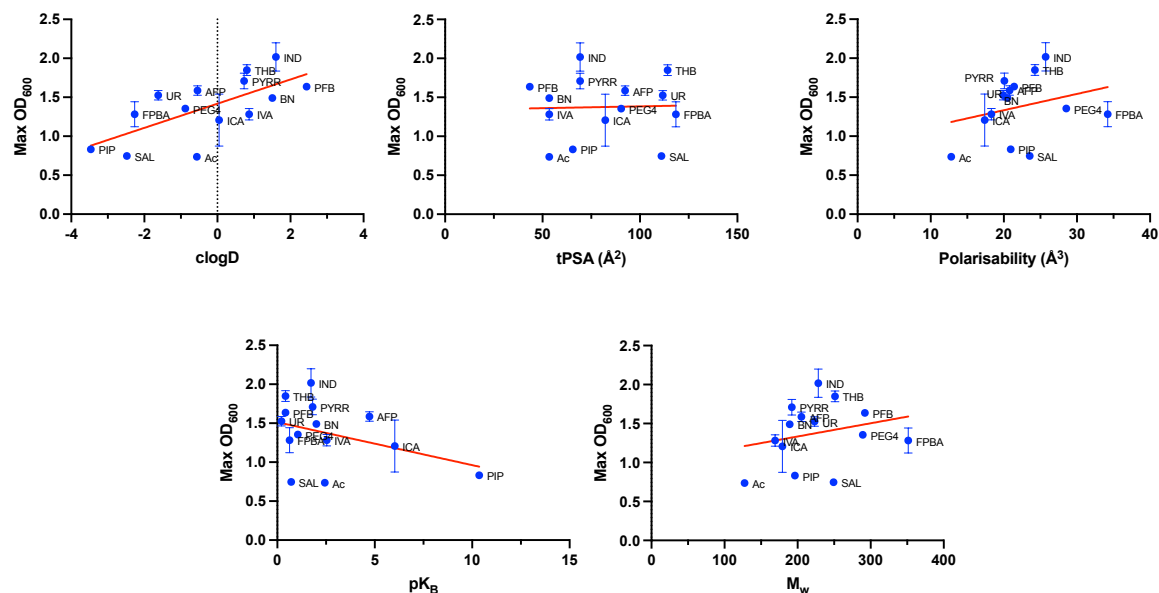


Figure 3.6. Scatter plots of maximum optical density at 600 nm (OD_{max}) as a function of P1 physicochemical properties.

Overall, the data collected from the particle size analyses (Figure 3.2) and turbidimetry experiments (Figure 3.6) suggest that increased **P1** hydrophobicity generally favoured bacterial aggregation due to the increased particle size and OD_{600} . However, as stated prior the particle sizing analysis is limited due to the possible breakdown of aggregates. This has been shown by their exposure to shear during measurements, which likely gives an underrepresentation of the true aggregate sizes. Although the turbidimetry assays are a useful indicator of how the polymer interacts with the bacteria, it is not a direct quantitative measure of aggregate size. Furthermore, absorbance becomes non-linear at high optical densities due to multiple light scattering which limits the accuracy of the measurements. However, it remained a useful tool to probe the aggregation behaviour of the bacteria with the P1 formulations. Thus, with these considerations it is important to probe aggregate formation

with other non-destructive techniques to further corroborate the findings from these initial experiments.

3.2.3 Determining aggregated biomass formation in polymer-treated cultures.

Initial experimentation by Mastersizer analysis and turbidimetry suggested that only polymeric formulations induce bacterial aggregation. However, these experiments are somewhat limited by mechanical breakdown of aggregates in measurement and non-linear absorbance respectively. Therefore, additional experiments were performed to assess polymer-induced aggregation with time using crystal violet (CV) staining. The use of CV staining is justified as it is a standard assay to quantitatively estimate the number of adhered cells to a surface in biofilm research. Thus, using a modified CV staining procedure it was possible to assess aggregate formation in solution following treatment with **P1**. Increased aggregate size causes greater CV uptake which would give a corresponding increase in absorbance when measured by spectrophotometry. In addition, to studying the aggregation formation in solution, the effect of polymer treatment on surface adherence was also tested.

3.2.3.1 Measurement of polymer-microbial aggregates using crystal violet staining

After determining that the polymers alone aggregate bacteria a longitudinal assay over 72h was performed to assess PMC biomass formation in *E. coli* MC4100. At each timepoint bacterial aggregates were washed to remove as many planktonic cells as possible and then stained with 1% CV. Aggregate formation was compared against the solvent treated and untreated controls, however it should be noted that as negligible aggregation occurred in either control, the cultures were centrifuged prior to CV treatment which inflates their value.

For all tested formulations PMC biomass generally increased with time. There a large increase in absorbance for all P1 treated cultures at 1 h post-treatment which agrees with the turbidimetric profiles in 3.2.2. Absorbance further increased between 24 h and 72 h dependent on the formulation in question suggesting increased biomass aggregation with time (**S.I. Figure 3.1**). Interestingly, with **P1-PYRR**, **P1-THB**, and **P1-UR** there is negligible change in biomass after the initial spike 1 h after initial treatment, suggesting possible bacteriostatic properties of these formulations. To simplify statistical analysis the cumulative biomasses were calculated prior, and these values were used in subsequent analyses. Statistical significance relative to the untreated control were calculated using one way-ANOVA with multiple comparisons (**Figure 3.7**). All formulations except the hydrophilic formulations **P1-FPBA** and **P1-SAL** produced a statistically significant increase ($q \leq 0.05$) in cumulative biomass formation relative to the solvent treated cultures. Both **P1-FPBA** and **P1-SAL** contain carboxylate functional groups ($pK_a \sim 6$), thus at pH 7 are deprotonated and anionic. The shared anionic character of the polymer and bacterial cell membrane likely leads to electrostatic repulsion and thus minimal aggregate formation.

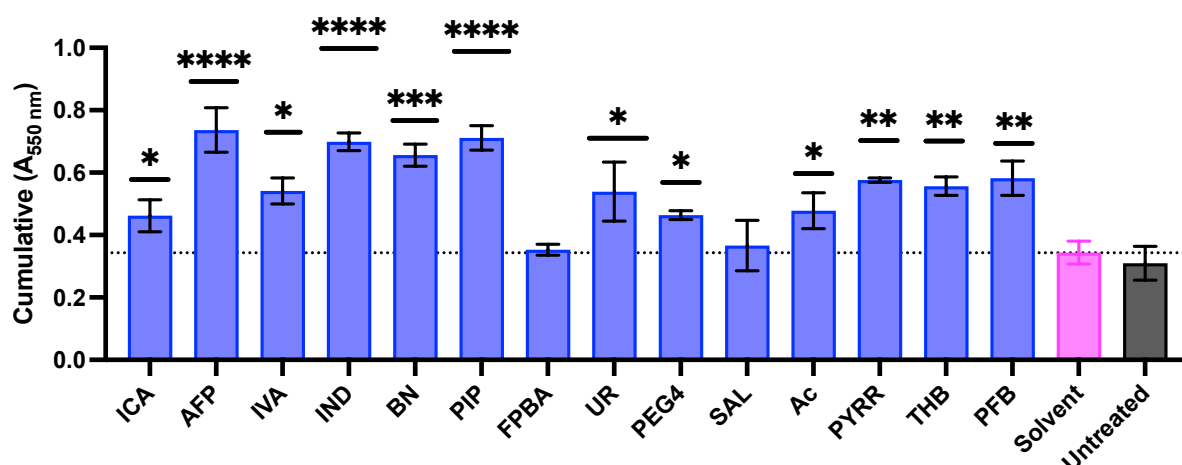


Figure 3.7. Cumulative biomass as measured by crystal violet staining (absorbance @ 550 nm). One-way ANOVA performed for multiple pairwise comparisons between polymer treatment and solvent controls. $q \leq 0.05$ (*); $q < 0.021$ (**); $q < 2 \times 10^{-4}$ (***); $q < 1 \times 10^{-4}$ (****)

The remaining formulations all generated a statistically significant ($q \leq 0.05$) increase in PMC biomass relative to the solvent treated cultures. These other formulations are a range of heterocyclic and aromatic compounds. Initial particle sizing and turbidimetry experiments demonstrated increased PMC aggregate size possibly due to enhanced hydrophobic and/or electrostatic interactions as in agreement with prior literature.¹³ The best candidate was **P1-PIP** which produced the largest mean difference (0.368) in aggregation out of all tested formulations, when compared against the solvent control. As **P1-PIP** is a secondary amine it is protonated at pH 7 and thereby cationic. The permanent cationic charge operates over larger distances than induced dipoles which would also enhance the rate of initial adherence between polymer and bacteria. Furthermore, interaction strength is also a function of charge and so the permanent cationic charge at pH 7 would further potentiate binding between P1-PIP and the cells. Curiously, in contrast to this experiment **P1-PIP** did not induce large aggregate formation compared to other formulations in both the turbidimetry and Mastersizer analyses. However, rapid electrostatic polymer-cell interactions would likely enhance sedimentation rates which would likely result in minimal OD_{max} in turbidimetry.

Likewise, particle size analysis is limited by mechanical shearing of aggregates causing an underrepresentation.

As before, several physicochemical parameters of the polymer formulations were calculated and plotted as functions of cumulative absorbance (**Figure 3.8**). Again, there is a positive and statistically significant correlation between total PMC biomass formation and to clogD when excluding **P1-PIP** ($R^2 = 0.49$) in addition to a positive correlation with basic pK_a ($R^2 = 0.40$). No significant correlation was found with the remaining physicochemical parameters. Basic pK_a is akin to the pK_a of a molecule's conjugate acid. Hence a higher basic pK_a indicates a weaker conjugate acid where the proton is not readily donated. Thus, in the context of this work basic pK_a can be considered a metric of how readily the different **P1** formulations are protonated. The heterocyclic formulations **P1-PIP**, **P1-ICA**, and **P1-AFP** are all expected to be protonated to differing degrees leading to additional electrostatic attraction with the bacteria. At pH 7 **P1-PIP** would be completely protonated and aggregation is strongly favoured due to electrostatic attraction with the bacteria. As electrostatic dipole interactions are stronger and can operate over larger distances than hydrophobic interactions²⁰ this could explain why **P1-PIP** was shown to produce large aggregates in contrast to the other tested formulations.

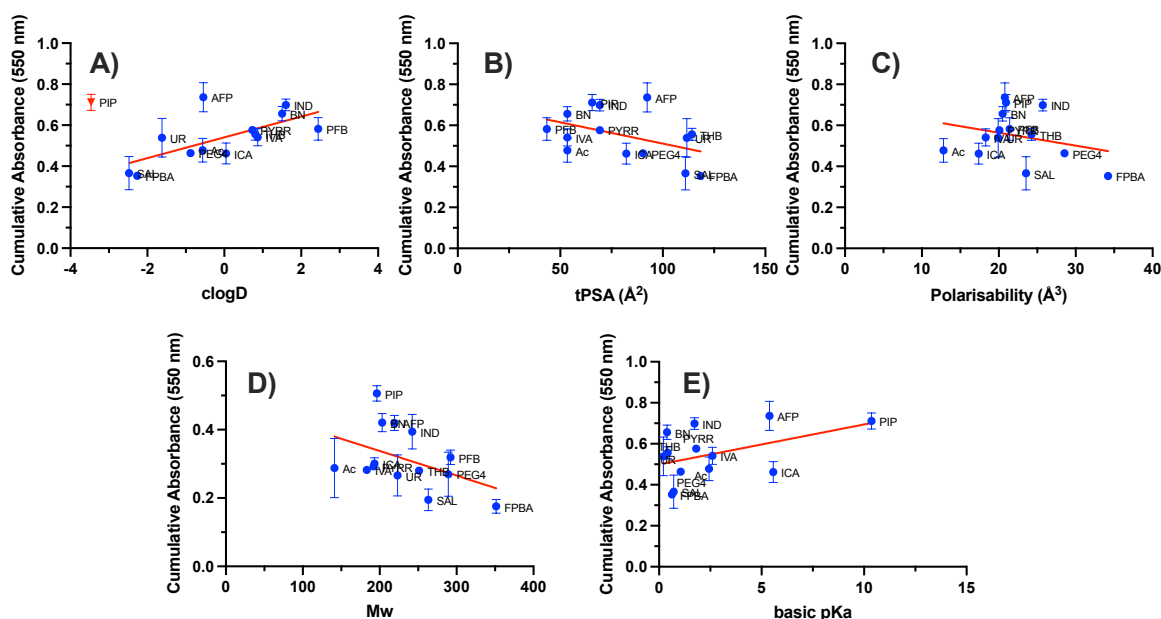


Figure 3.8. Scatter plots of cumulative absorbance at 500 nm as a function of P1 physicochemical properties.

All cell aggregation studies whether by particle sizing analysis, CV staining or turbidimetry suggested that **P1** formulations were critical for induction of bacterial clustering. Of all the calculated physicochemical parameters, hydrophobicity (clogD) frequented as the key parameter driving aggregation. However, there was also indication that electrostatics also aid polymer-driven aggregation. Both polarisability and basic pK_a were identified in different assays as having a significant correlation with aggregation. The lack of consistency in the particle sizing analysis was likely due to vulnerability of the PMCs to hydrodynamic shear, causing aggregate breakdown during measurement. Generally, these findings agreed with the consensus in the literature, that hydrophobic polymers promote bacterial aggregation. One rationale may be that reduced surface energies associated with the hydrophobic formulations increases repulsion with the surrounding water molecules leading to the formation of a clathrate-like structure around the polymer. On adhesion with the bacterial cell surface there would be a large entropic gain from the break-up and ‘release’ of the water molecules

potentially driving the association with the bacteria which promotes aggregation. However, for the hydrophilic formulations like **P1-PEG₄** and **P1-Ac** there would be minimal entropic gain as these polymers more readily interact with the bulk solvent water molecules thereby minimising aggregation in solution. Lack of aggregation in anionic **P1-SAL** and **P1-FPBA** is furthered by electrostatic repulsion due to the shared anionic charge between the polymer and bacteria at pH 7.

3.2.3.2 Testing surface attachment in the presence of polymers

Biofilms adhere to a wide variety of abiotic materials, which is advantageous in biotechnological applications as the microbes are self-immobilised to a particular substrate. Alternatively, for possible biomedical applications it would be useful to sequester bacteria to prevent colonisation of host-tissues as a treatment. This work shows that only polymeric formulations were capable of inducing aggregation in *E. coli* MC4100 in liquid cultures. To expand this, it was of interest to see how the polymers affected surface-attachment. A high-throughput assay was developed in a polypropylene 96-well plate, where *E. coli* MC4100 was cultured statically at 30 °C adhered cell mass was estimated by staining the plates with 0.1% CV. As before higher absorbance values are indicative of increased numbers of surface associated bacteria. In almost all instances except **P1-PEG₄** and **P1-Ac**, supplementation with **P1** formulations hindered bacterial surface attachment, where polymer treatments showed comparable adhered biomass to non-polymer controls. Both **P1-PEG₄** and **P1-Ac** showed a highly statistically significant ($p < 0.001$) increase in attached cells relative to both the untreated, solvent treated and their respective aldehyde controls (**Figure 3.9**). Of further note, both these formulations demonstrated considerably higher attached biomass comparative to

all other **P1** formulations suggesting that these were the best formulations to promote bacterial adherence to abiotic surfaces.

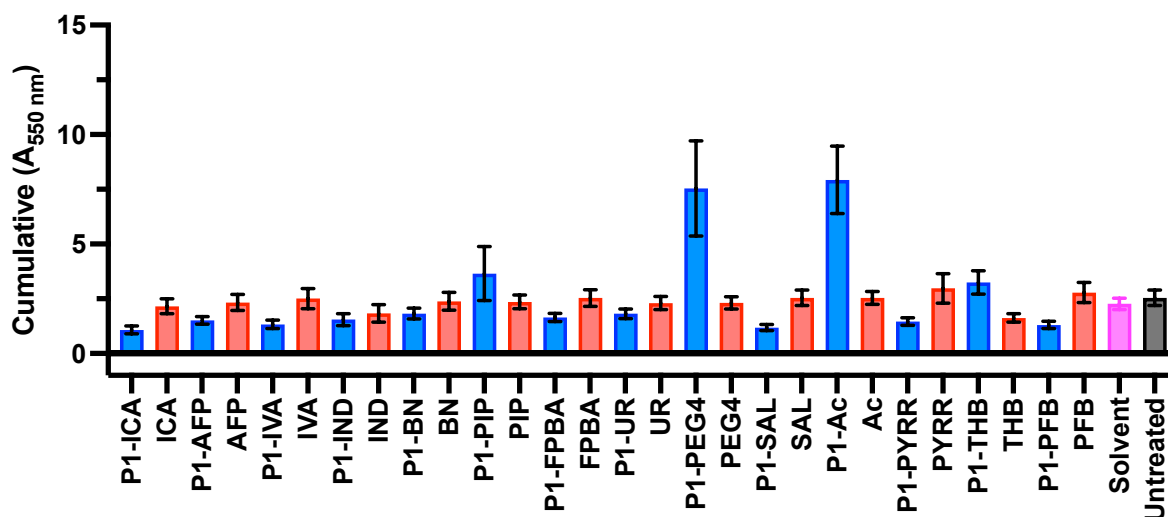


Figure 3.9. Total adhered biomass on polypropylene microwell plate as measured using 0.1% crystal violet.

Previous studies suggested that bacterial colonisation of both biological and synthetic surfaces is significantly reduced in the presence of cationic polymers.^{21–23} In these cases, the bacteria are sequestered by the polymers limiting surface adhesion. Conversely, anionic, and hydrophilic neutral polymers show negligible reduction in bacterial surface attachment and subsequent biofilm formation.²³ Therefore, a similar behaviour likely occurs in this system, where cationic and hydrophobic formulations sequestered *E. coli* thereby limiting surface colonisation (see *S.I. Figure 3.4* at 24h). In contrast, the hydrophilic formulations such as **P1-PEG₄** and **P1-Ac** will not sequester the bacteria causing increased surface colonisation. However, the anionic formulations **P1-FPBA** and **P1-SAL** fail to enhance surface attachment in the same way despite showing the lowest aggregation of all formulations. Hence, bacterial sequestering by **P1** formulations is unlikely to be the sole reason for the observed surface attachment. An additional hypothesis not previously considered in literature is that treatment

by polymers could modulate ECM production which in turn influences surface attachment. Thus, **P1-PEG₄** and **P1-Ac** treatment may significantly enhance ECM production such as curli. Given the significance of curli as a primary adhesin, it would greatly increase surface adhesion in the presence of these polymers. Furthermore, it is possible that in the assay preparation wash steps, the aggregates may have been sloughed from the surface due to hydrodynamic shear which would cause an underrepresentation of the surface bound cells between different treatment types.

3.2.4 Determining biofilm production in polymer-treated cultures

Previous experimentation confirms polymer-dependent bacterial aggregation. Generally, increased aggregation occurred with more hydrophobic and/or cationic formulations. Polymer-induced aggregation does not enhance surface association, which may be due to differing ECM production following treatment with **P1**. In addition, to be considered a biofilm, the bacterial aggregates must produce one or more biopolymers as part of their ECM. To determine whether the bacterial aggregates were biofilms and elucidate differences in surface adhesion, the ECM components poly-*N*-acetylglucosamine (PNAG), colanic acid (CA) and curli were quantified. Curli are the primary adhesin made by *E. coli* K-12 and have roles in attachment to biotic and abiotic surfaces and cell-cell interactions.^{14,24} PNAG and CA are polysaccharides produced during biofilm maturation and are important in biofilm structural development.^{7,8} Previous literature reports suggest that curli production is increased in *E. coli* aggregates either as a pellicle⁵ or when aggregated by polymers¹³. However, to the best of our knowledge there remains no studies conducted to evaluate the effect of polymer-driven aggregation on PNAG or CA production.

3.2.4 Curli expression

3.2.4.1 Experimental design and parameter determination

Curli production was measured using an enhanced green fluorescent protein (eGFP) reporter plasmid (pJLC-A) as described in literature.^{4,5,13} The plasmid pJLC-A contains the gene encoding eGFP under the control of the *csgB* promoter (*csgB::gfp*), which regulates production of the curli structural genes *csgBAC*. Curli is synthesised through the polymerisation of monomeric CsgA by CsgB. Thus, increased *csgB* activity results in increased curli production. Recombinant *E. coli* transformed with pJLC-A would begin to fluoresce, as eGFP is also regulated by the *csgB* promoter. Use of this transformant permits high-throughput quantitative analysis of curli production in real-time. To account for differences between replicates, GFP fluorescence for all treatments were normalised against the maximum GFP fluorescence intensity (GFP_{max}) for the untreated cultures. This normalisation procedure reduced variability between replicate experiments and standardised further analyses. Total increase in *csgB::gfp* fluorescence was calculated as the area under the curve (AUC) of the normalised GFP time-series data. Two-part segmental linear regression was used to estimate the onset of *csgB::gfp* up-regulation (GFP_{on}) and rate of fluorescence increase (k_{GFP}). GFP_{on} was estimated for each biological replicate (of non-normalised data) as the x-axis intercept of the second linear regression (x-axis) corresponding to a time in hours and k_{GFP} was estimated as the gradient of the same line. All calculated parameters were analysed using a one-way analysis of variance (ANOVA) with Tukey's multiple comparison post-hoc analysis to determine any significant differences in multiple pairwise comparisons between the **P1** formulations and the solvent treated cultures as well as **P1** formulations and their respective aldehydes. A false-discovery rate (FDR)

was applied to account for multiple comparisons testing, where an adjusted p-value (q) is used to identify a statistically significant comparison ($q \leq 0.05$).

3.2.4.2 Analysing curli protein production in *E. coli* polymer-induced aggregates

Use of the reporter strain allows in-depth analysis of curli biosynthesis at the transcriptional level. Previous reports of polymer induced aggregation in *E. coli* PHL644 and MC4100 showed that polymer treatment causes an increase in curli production as well as an earlier onset of production (GFP_{on}) in both strains.¹³ Therefore, it was expected that treatment of *E. coli* MC4100 with **P1** formulations would illicit a similar response. However, in contrast to the previously tested poly(acryloyl hydrazide) (pAH), treatment with **P1** formulations did not significantly reduce GFP_{on} (*S.I. Table 3. 1*). For all tested conditions GFP_{on} occurred at approximately 20 h (**Figure 3.10**).

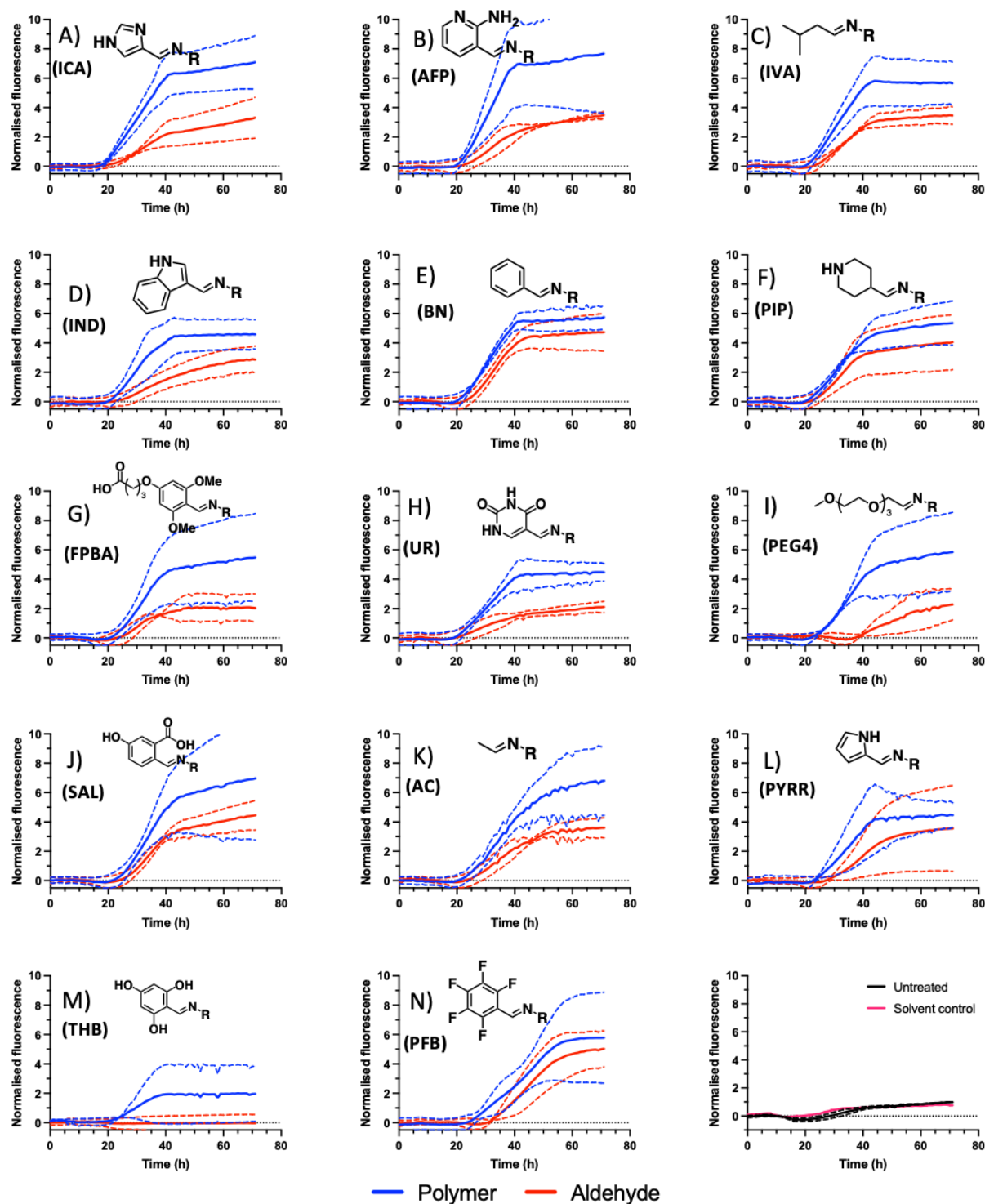


Figure 3.10. A - M Normalised curli production measured in proxy through use of eGFP reporter plasmid pJLC-A in P1 treated (0.05 mg mL⁻¹) *E. coli* MC4100 over 72 h. (blue = polymer & red = aldehyde). Dashed line = SD (n = 3). A = ICA; B = AFP; C = ICA; D = IND; E = BN; F = PIP; G = FPBA; H = UR; I = PEG4; J = SAL; K = AC; L = PYRR; M = THB; N = PFB; O = solvent (pink) & untreated controls (black).

Although **P1** treatments does not shorten GFP_{on}, polymer supplementation enhanced the *csgB* expression rate from 20-40 h. Significantly higher average normalised *csgB* activity was observed relative to the untreated cultures. Increased rate of fluorescence generation indicated higher *csgB* promoter activity, which would result in greater curli expression overall. All formulations except **P1-THB** showed a statistically significant increase in total *csgB* expression relative to the solvent controls (**Figure 3.11**). Interestingly, aldehyde treatments on their own greatly increased *csgB* expression relative to the solvent and untreated controls. Generally, aldehyde treatments induced significantly lower *csgB* production than **P1** formulations, in agreement with prior research.¹³ However, **P1-IND**, **P1-BN**, **P1-PIP**, **P1-PYRR**, and **P1-THB** showed no significant enhancement of total curli production relative to the aldehyde controls. It is generally accepted that indole promotes biofilm formation in *E. coli* where Crl expression is upregulated in response, this promotes σ_s and subsequent downstream biofilm associated genes like *csgD*.²⁵⁻²⁷ In contrast, many indole derivatives including indole-3-carboxaldehyde (as used in this work) showed an 11-fold reduction in biofilm formation in enteroaggregative *E. coli*.²⁸ Therefore, it is possible that **P1-IND** served as an exogenous source of indole-3-carboxaldehyde, causing reduced curli formation despite being highly aggregative. Phenolic benzaldehydes like THB used here are reported to be bactericidal against several Gram-negative bacteria, including *E. coli*.²⁹ Hence, some bactericidal activity may occur with **P1**, which is why little-to-no curli is produced relative to the controls. Similarly, the cationic nature of **P1-PIP** may bestow some bactericidal or bacteriostatic activity. Polymeric quaternary ammonium compounds (polyQACs) are a well-documented class of effective anti-microbial agents;³⁰ however, given that **P1-PIP** still outperformed other formulations this is improbable.

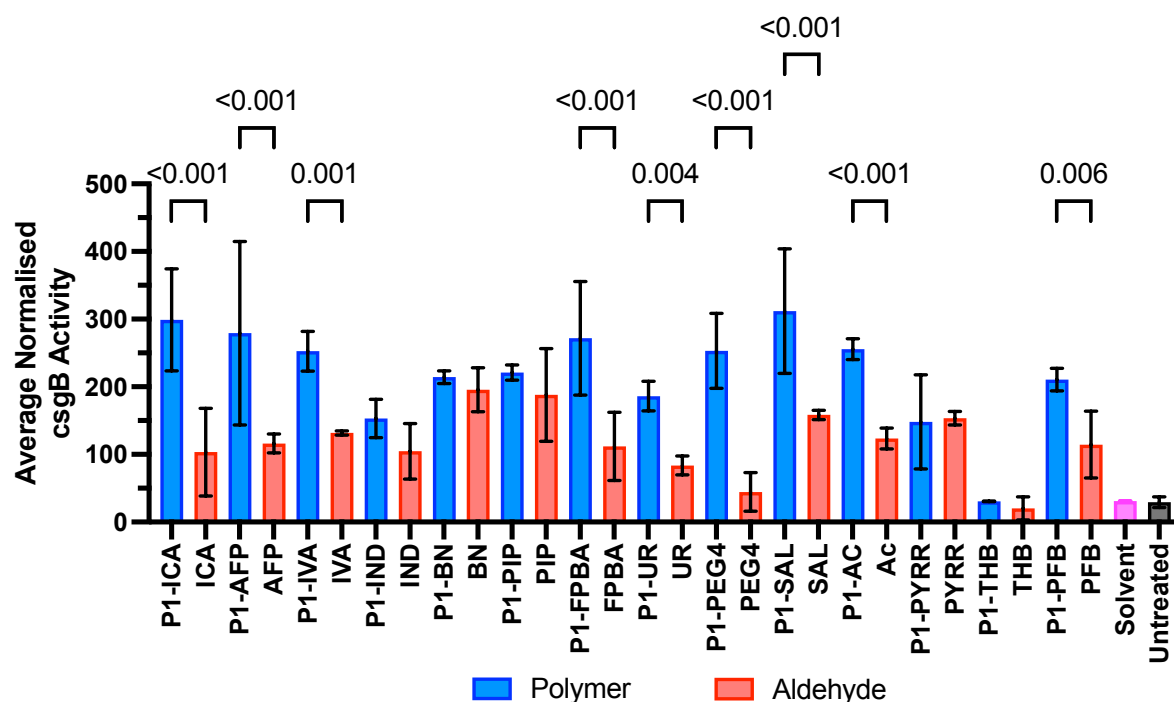


Figure 3.11. Normalised data with average and standard deviation of *csgB* activity determined from the AUC of the GFP fluorescence profiles of the various polymer (blue) and aldehyde (red) treatments. Error bars = S.D. ($n = 3$). Statistical significance tested for with 1-way ANOVA and Tukey's multiple comparisons post-hoc analysis. For clarity only statistically significant ($q \leq 0.05$) pairwise comparisons between the **P1** formulations and their respective aldehydes are shown. All **P1** formulations except **P1-THB** produced a statistically significant increase in *csgB* promoter activity relative to the solvent treated cultures. See appendix for statistical analysis results.

The average normalised *csgB* activity was plotted as a function against several polymer physicochemical properties as done in previous analyses. No significant correlations were identified in any instance (**Figure 3.12**). Surprisingly, *csgB* activity showed a negative correlation with biomass (measured by turbidimetry; $R^2 = 0.44$) suggesting that increased aggregation by **P1** limited curli production. In *E. coli* MC4100, it was recently reported that free-floating pellicles produce more curli than surface adhered biofilm structures.⁵ Similarly, curli production is reportedly lower in sedimented cells compared to planktonic cells across a range of temperatures (like 30 °C as used herein). Whereas comparable *csgB* expression is

only achieved at 37 °C.⁴ The hydrophilic polymers tested here are experimentally shown to cluster a lower proportion of the cells in suspension and produce smaller aggregates. Therefore, reduced aggregation may have enhanced curli production in the hydrophilic P1 formulations.

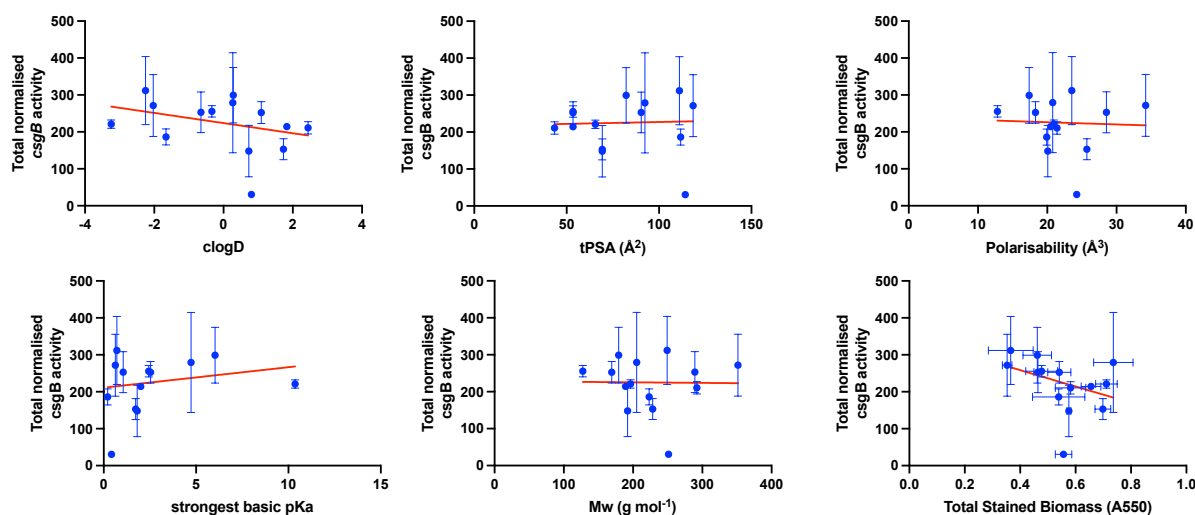


Figure 3.12. Linear regression analyses of total normalised fucose production determined by AUC of the time-series data plotted as a function of several physicochemical parameters of the P1 formulations. A = clogD; B = tPSA; C = polarisability; D = pKb; E = molecular weight (MW). F = Correlation between total normalised csgB activity and total stained biomass (from crystal violet study in 2.2.1).

Moreover, there are numerous environmental stimuli that affect curli expression, as many regulatory pathways and sRNA are shown to influence the activity of the csgD (master biofilm regulator) or its regulator OmpR. Therefore, it is possible that the different formulations may trigger different stress pathways causing a difference in the observed curli expression profiles. A more detailed investigation and discussion of this is given later (see **Section 3.2.6 Probing membrane stress responses in polymer-treated cultures**).

3.2.5 Exopolysaccharide production in bacterial aggregates

As biofilms mature there is increased ECM production, the two major components produced in *E. coli* K-12 biofilms are poly-N-acetyl glucosamine (PNAG) and colanic acid (CA). PNAG is a homopolymer of N-acetyl glucosamine, where partial deacetylation gives the polysaccharide partly cationic charge to aid intercellular adhesion within the biofilm.³¹ Colanic acid is a branched, hydrophilic heteropolymer composed of glucose, galactose, fucose, and glucuronic acid.³² Though it is not essential to biofilm formation it is believed to be critical for the development of 3D structures during biofilm maturation. Extensive literature of ECM production in surface attached *E. coli* biofilms exists; however, to date there remains no reports of PNAG or CA production in polymer-induced aggregates of *E. coli*. Hence, to better understand the roles of the polymer on bacterial physiology it was deemed appropriate to study exopolysaccharide production in the biofilm aggregates.

Unlike curli, neither PNAG nor CA production is primarily transcriptionally regulated³³ preventing the development of a GFP reporter plasmid, as used prior in *csgB* experiments. Therefore, to quantify PNAG and CA, the ECM was extracted from the treated cell cultures and dialysed prior to quantification using chemical assays. Dialysis was performed to remove intracellular contaminants that may interfere in the assay, for example: monosaccharides or aldehydes. Full description of the extraction procedures and quantification assays are outlined in the experimental (see 3.1.7). PNAG and CA production was quantified every 24 h for 3 days. Following ECM extraction, the resultant biomass was pelleted and dried to obtain the dried biomass (DBM). The extracted monosaccharide concentrations were normalised against DBM to account for different aggregate sizes. Originally, it was planned to include an additional

time point, approximately 5 h after initial treatment. Regrettably this could not be performed due to delays in receiving the necessary consumables therefore the later time points were prioritised for quantification.

3.2.5.1 Colanic acid quantification

Colanic acid (CA) is an anionic polysaccharide comprised of glucose, galactose, fucose and glucuronic acid in a 1:2:2:1 ratio.³⁴ Within the ECM of *E. coli*, fucose is unique to CA and so makes a suitable analyte to measure as a proxy for colanic ECM production. Pentose sugars react with cysteine hydrochloride in acidic conditions giving an absorbance peak maximum at 430 nm, whereas hexose-cysteine adducts produce an absorbance maximum at 396 nm. Measurements are performed twice at both wavelengths (pre- and post-cysteine addition) to remove the non-specific hexose sugar interactions allowing direct quantification when compared against a fucose standard. The reported fucose values are normalised to dried biomass (DBM) and calculated according to **Equation 3**. To simplify statistical analysis, the average CA production throughout the duration of the experiment was calculated from the area under the curve in the time-series data. Unlike the curli data, there was far less variability between the replicates no further data pre-treatment was perform prior to statistical analysis.

$$[Fucose](\mu g mL^{-1} mg^{-1}) = \frac{(A_{post}^{430} - A_{post}^{396}) - (A_{pre}^{430} - A_{pre}^{396})}{DBM} \quad (3)$$

In contrast to *csgB* expression, normalised fucose recovery was generally highest at 24 h before a steady decrease for the remainder of the tested time (**Figure 3.13**). The opposite was predicted as CA production is upregulated during biofilm maturation.³⁵ Thus, it is not illogical to expect that recovered fucose would increase with time as the biofilm matures. Yet between 24 and 72 h there is a considerable reduction in measured DBM for all **P1** treated cultures, as

we observe a reduction or minimal change in normalised fucose production throughout. Hence, fucose productivity does not significantly change in this duration as there are less aggregated cells with comparable fucose production from the initial timepoint (24 h). This loss is recovered in DBM with time maybe due to sloughing of the aggregate. Research on *Pseudomonas* biofilms suggest that as nutrient and oxygen limitations occur, biofilms become more susceptible to sloughing (aggregate breakdown due to shear).^{36,37} Hence, a similar phenomenon may have occurred in this system.

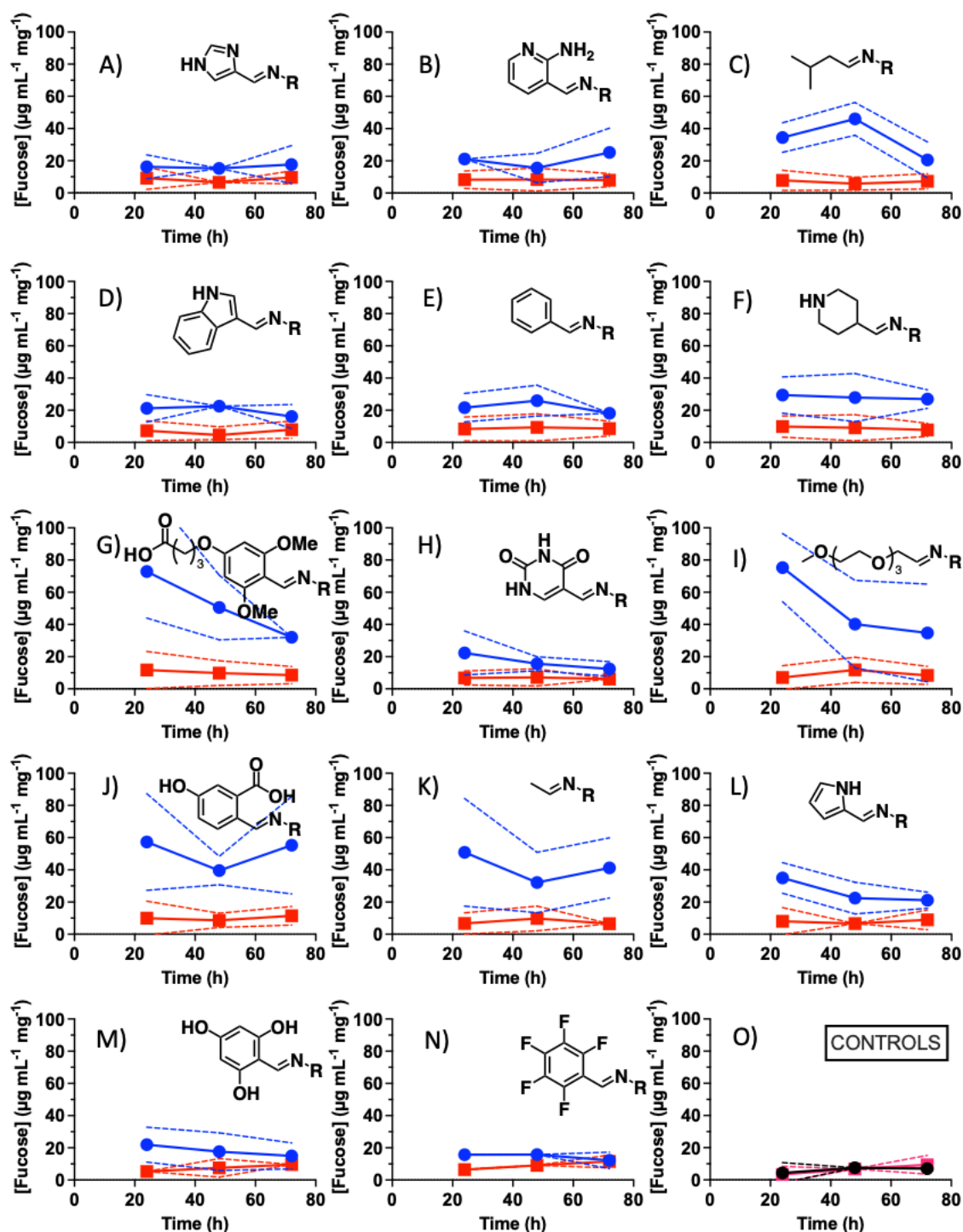


Figure 3.13. A - M Colanic acid production in **P1** treated *E. coli* MC4100 over 72 h (blue = polymer & red = aldehyde). Dashed line = SEM ($n = 3$). A = ICA; B = AFP; C = ICA; D = IND; E = BN; F = PIP; G = FPBA; H = UR; I = PEG4; J = SAL; K = AC; L = PYRR; M = THB; N = PFB; O = solvent (pink) and. Untreated controls (black).

Comparable to the observed effect of **P1** treatment on *csgB* activity, all tested formulations except for **P1-THB** showed a statistically significant increase in recovered fucose compared to the solvent treated cultures. This was indicative of increased CA production following polymer treatment (**Figure 3.14**). Similarly, all polymer treatments except **P1-THB** and **P1-ICA** showed significantly higher averaged fucose concentration compared to their respective aldehydes. This suggests that **P1** formulations enhanced CA production relative to non-polymer control cultures.

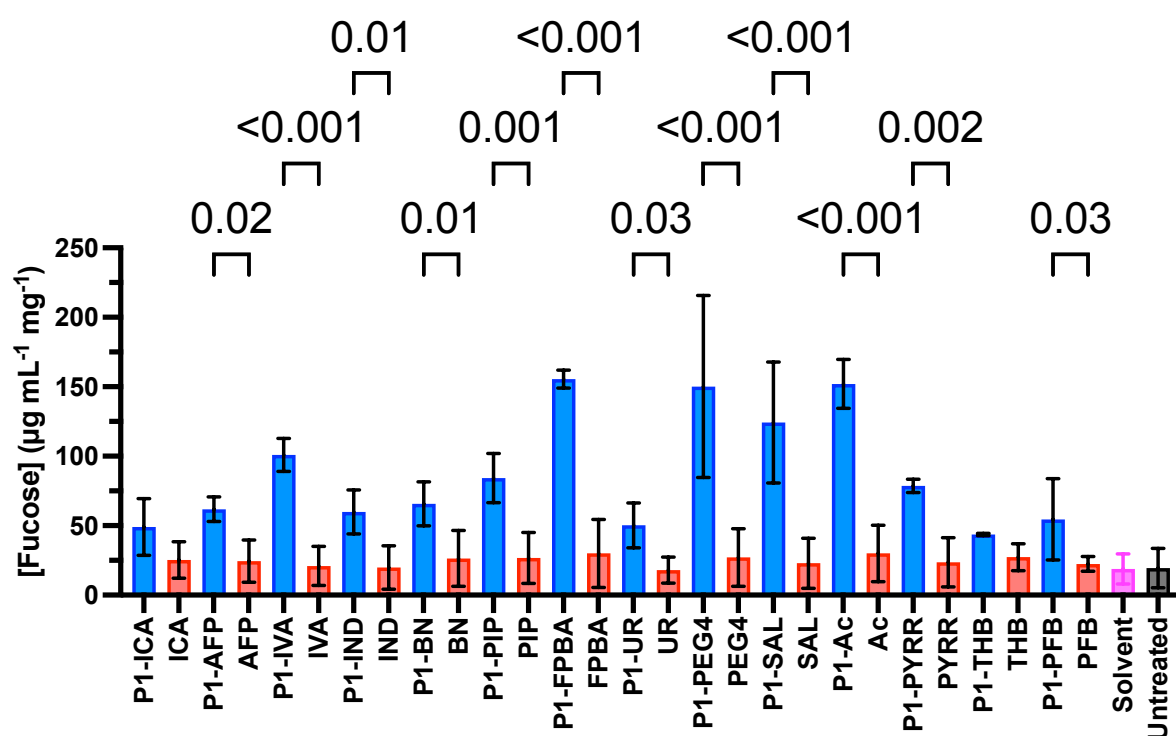


Figure 3.14. One-way ANOVA and Tukey's multiple comparisons post-hoc analysis. For clarity only statistically significant ($q \leq 0.05$) pairwise comparisons between the P1 formulations and their respective aldehydes are shown. All **P1** formulations except **P1-ICA** and **P1-THB** produced a statistically significant increase in total fucose colanic acid production relative to the solvent treated cultures. See appendix for statistical analysis results.

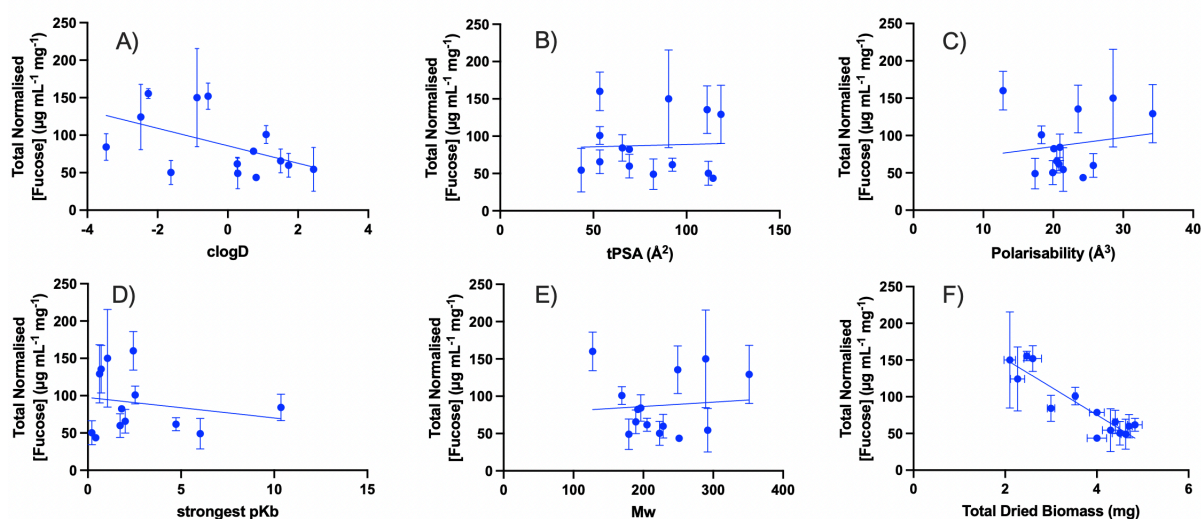


Figure 3.15. Linear regression analyses of total normalised fucose production determined by AUC of the time-series data plotted as a function of several physicochemical parameters of the **P1** formulations. A = clogD; B = tPSA; C = polarisability; D = pKb; E = molecular weight (MW). F = Correlation between total normalised fucose and total dried biomass.

Consistent with the *csgB* analyses, the largest increased fucose production were observed with the hydrophilic formulations. **P1-FPBA**, **P1-PEG₄**, **P1-SAL**, and **P1-AC** produced up to a 10-fold increase in extracted fucose relative to their aldehydes. Furthermore, **P1-FPBA**, **P1-PEG₄**, **P1-SAL**, and **P1-AC** considerably outperformed other polymers as these the only formulations to induce over 40 $\mu\text{g mL}^{-1} \text{mg}^{-1}$ fucose at each timepoint. As with *csgB* promoter activity, aggregation (determined here by total DBM) is negatively correlated ($R^2 = 0.64$) with total normalised fucose (**Figure 3.15**), indicating that smaller aggregates of bacteria produce more ECM. To further explain this this, various linear regressions were performed between the total fucose production and various physicochemical parameters calculated for the **P1** formulations (**Figure 3.15**). For all parameters except clogD, no significant linear or quadratic relationships were observed with total fucose production. Hydrophobicity (clogD) is positively correlated with DBM. This further supports that increased aggregation maybe detrimental to overall curli and CA production when treated with these poly(acetylenic) materials. This is highlighted clearly in **Figure 3.15F**, where there is a strong negative correlation between total normalised

fucose and total DBM. Implying that increased aggregation decreases CA production in *E. coli* MC4100 following treatment with various **P1** formulations.

The negative correlations associated with curli and CA production with biomass was unexpected. It was hypothesised that increased aggregation would increase ECM production possibly through cell density-dependent AI-2 QS.³⁵ Previous reports show that AI-2 concentration is found to be linearly correlated with polysaccharide and protein production in *E. coli* ECM.³⁸ Moreover, clustering of the Gram-negative *V. cholerae* shows an increase in biofilm due to enhanced QS activity following polymer-induced aggregation.^{39–41} On the other hand, in the systems tested herein there are no positive correlations between aggregated biomass and ECM suggesting that there may be no QS induction here. However, as QS has not been monitored in this study it is impossible to definitively conclude the roles of polymer treatment play in QS. To improve the understanding of these results, it would be pertinent to explore this area in future. Alternatively, it is believed that colanic synthesis is regulated by the RcsCDB with auxiliary positive regulator RcsA.⁴² RcsC is a sensor kinase that respond to numerous stimuli like changes in osmotic stress, desiccation, and surface attachment.^{43–45} Within larger aggregates it could be assumed that there is increased solute concentrations entrained within compared to smaller aggregates. Therefore, increased osmolarity within the larger aggregates may lead to upregulation of the Rcs system with a concomitant increase in CA synthesis. Hence, activation of RcsAB may explain why polymer-induced aggregation resulted in significantly higher CA production compared to the aldehyde control cultures. Yet RcsAB activation by osmotic stress likely does not account for the enhanced CA production observed with **P1-FPBA**, **P1-PEG₄**, **P1-SAL**, and **P1-AC**, all of which formed the smallest

aggregates. Therefore, it is possible that these formulations act as a different stimuli thereby upregulating proteins responsible for colanic synthesis.

3.2.5.2 PNAG Quantification by MBTH

PNAG was quantified using 3-Methyl-2-benzothiazolinone hydrazone (MBTH) as described in literature. The concentration of aliphatic aldehydes can be quantified using MBTH to form a Schiff base product which can be quantified by chromatographic or spectroscopic measurements.^{46,47} The MBTH assay has been extended to the quantification of hexose sugars in biological samples such as algae and bacteria.^{48–50} Regarding PNAG, heated acid hydrolysis decomposes the polysaccharide and deacetylates the monomeric units forming glucosamine (GlcN). Reaction with MBTH and subsequent complexation with FeCl_3 yields an intense blue colour which can be used to quantify PNAG against a GlcN standard. Compared to other spectroscopic methods this procedure is reported to be highly selective towards hexosamines with minimal interference from other contaminants, such as amino acids.⁵¹ As performed in the CA quantification assays, all GlcN concentrations were normalised against the total dried biomass (DBM) to account for different degrees of aggregation between the treatments and controls. No formulations were found to induce a statistically significant increase in PNAG production relative to the untreated controls (**Figure 3.16**).

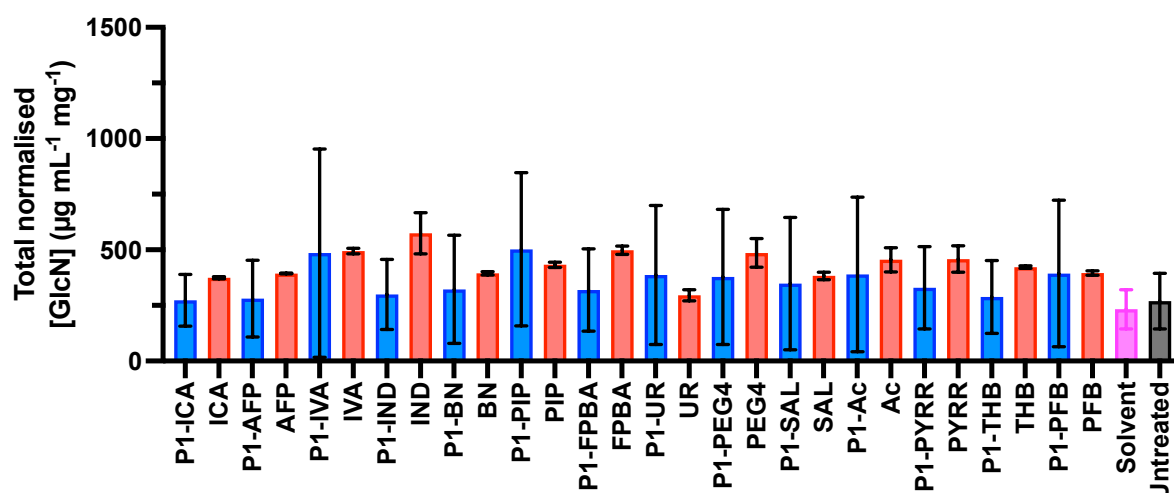


Figure 3.16. Total PNAG production as measured in proxy by glucosamine quantification in the MBTH assays following treatment with **P1** formulations (blue), the respective aldehyde controls (red) and the solvent (pink) and untreated (black) controls. Error bars = s.d. ($n = 3$). One-way ANOVA and Tukey's multiple comparisons post-hoc analysis, showed no statistically significant ($q \leq 0.05$) pairwise comparisons between the P1 formulations and their respective aldehydes.

Studies suggest that production of curli/cellulose and PNAG in biofilms is inversely proportional to one another.⁵² Hence, the ECM of *E. coli* biofilms is dominated by either curli/cellulose or PNAG. Given MC4100 is a K12 strain it is deficient in cellulose, hence its production in the context of this work will not be discussed further. The regulatory processes involved in biofilm formation and maturation are often non-hierarchical, where a myriad of different stimuli can produce one response whilst simultaneously affecting another. Curli production in *E. coli* is further regulated by a series of sRNAs (RprA, OmrA, OmrB, GcvB, McaS, and RydC) which help fine-tune expression within a biofilm.⁵³ One sRNA that plays a regulatory role in both curli and PNAG synthesis is McaS. McaS is activated by cAMP-CRP in response to carbon limitation and is indirectly repressed by RpoS during stationary phase. McaS binds to *csgD* mRNA causing its degradation whilst simultaneously promoting flagella formation by binding *flhDC*.⁵⁴ Under carbon catabolic conditions increased expression of motility genes can be considered a survival strategy regarding possible biofilm dispersal and colonisation of new

environments. Under these same catabolic conditions, McaS binds to *csrA* which derepresses *pgaA* (porin for extracellular PNAG export) translation leading to PNAG synthesis, which indirectly negatively regulates *flhDC* expression. Therefore, simultaneous *pgaA* upregulation and repressed curli production suggests *mcaS* favours PNAG production at the expense of curli.^{55,56} In the context of ECM formation in the polymer-treated cultures compared to the non-polymer controls, it is evident that the aggregates form a curli-dominated complex rather than PNAG dominated. This suggests that McaS repression does not occur under the current tested conditions. Reasons for this remain unclear, though temperature may play a role where PNAG production is more limited at 30 °C compared to 37 °C whilst the opposite is true for curli production *in E. coli* biofilms.

The hypothesis regarding McaS activity on subsequent curli and/or PNAG production in the PMCs, may explain the experimental observations. However, it is important to consider other cellular regulatory mechanisms, like cyclic dimeric guanosine monophosphate (c-di-GMP) that influence ECM formation. c-di-GMP is a secondary messenger ubiquitous in many bacterial species and post-translationally regulates ECM production via allosteric activation of enzymes involved in synthesis and/or export of exopolysaccharides that constitute the ECM.^{33,57} PNAG synthesis is controlled by concentration dependent c-di-GMP formation, where increased c-di-GMP concentrations stabilises the PgaCD complex permitting PNAG synthesis⁵⁸ Therefore, poor PNAG production following **P1** treatment may result from low c-di-GMP activity.

For future work, a more confident conclusion regarding PNAG production and regulation following **P1** treatment may benefit from the development of a *pgaA::gfp*. If there are no

significant changes in PNAG production relative to the untreated controls as found with the MBTH this would greatly increase the confidence in the preliminary results found here. It would also be interesting to study the potential role of c-di-GMP within the polymer treated cultures. Intracellular c-di-GMP concentrations could be measured using a fluorescent-based biosensor as described in literature⁵⁹ that would permit visualisation of cells producing high c-di-GMP concentrations. Furthermore, scrutiny of culture conditions in the presence of polymers and determine how ECM production changes with variables like temperature. To determine whether the phenotype of the polymer-induced aggregates is more strongly controlled by the polymer treatment or the environmental conditions.

3.2.6 Probing membrane stress responses in polymer-treated cultures

As there remained no obvious cause from a physicochemical perspective of the **P1** formulations and their effect on ECM production, an alternative hypothesis was considered. Firstly, the **P1** formulations maybe cytotoxic towards *E. coli*, hence with increased aggregation greater bactericidal activity would occur leading to a reduction in ECM production. Secondly, biofilms are a known stress response in bacteria like *E. coli*. Onset of stationary phase and the switch to a sessile lifestyle is associated with the upregulation of many stress proteins in biofilm development. Therefore, the hydrophilic formulations, whilst being poor bacterial aggregators, may better induce membrane stress in the *E. coli* cultures. Increased cellular stress may upregulate curli and CA production in response. Lastly, these deviations may be a consequence of the polymer topology where a helical polymer is used here. Whereas previous literature reports random-coil polymers. The helical nature of **P1** may alter how it interacts with bacterial cells particularly the potential cytotoxicity or stress induction in the bacteria.

Hence, to probe these hypotheses further experiments were performed to determine the causes of this behaviour, whereby increased aggregation seemingly decreases ECM production. Unfortunately, due to time limitations the role of polymer topology could not be studied.

3.2.6.1. Metabolic activity assays in polymer treated cultures

In **P1** treated cultures, the formulations generally show that curli and CA production is enhanced. Unexpectedly, more hydrophilic formulations such as **P1-SAL**, **P1-FPBA** and **P1-PEG₄** favour ECM production despite forming smaller aggregates compared to more hydrophobic formulations, which disagrees with prior literature research. One possibility is that hydrophobic **P1** formulations are cytotoxic towards *E. coli*. Increased cytotoxicity limits ECM production due to a reduced cell viability following treatment. Helical polymers have been described as effective transfection and anti-bacterial agents. Furthermore, additional bactericidal activity may occur due to increased hydrophobicity which can directly disrupt the cell membranes.^{60,61} Therefore, the bactericidal activity of the **P1** formulations was tested by assessing cellular metabolic activity which is indicative of overall viability. Commonly, cell viability and/or treatment cytotoxicity is measured using the resazurin reduction assay. Metabolically active cells reduce resazurin to the highly fluorescent resorufin via the central metabolic co-enzyme NADH. Hence, greater resorufin formation increases the fluorescence emission intensity (EM) where increased fluorescence infers a higher cell population viability.^{62,63} The percentage of viable cells was calculated as a ratio against the untreated cultures at each time point (assumed to be 100%) and approximated according to **Equation 4** below. This was performed to minimise variance between different experimental repeats.

$$Cell\ viability(\%) = \left(\frac{Em_{polymer}^{584} - Em_{negative\ cont.}^{584}}{Em_{untreated}^{584} - Em_{negative\ cont.}^{584}} \right) \times 100 \quad (4)$$

Cell viability was approximated for all polymers and control treatments every 24 h for 3 days. At each time point there was no statistically significant reduction in cell viability relative to the untreated controls. Furthermore, there was no significant difference in viability between the different formulations except for **P1-FPBA** with **P1-PYRR** and **P1-THB** at 48 h and 72h respectively (**Figure 3.17**). A two-way ANOVA with Dunnet's Post-Hoc analysis was performed to test for any significant differences in cell viability between polymer-treated and untreated cultures. No statistically significant differences were observed signifying that none of the polymers were significantly detrimental to cell viability. However, both time and formulation were identified as statistically significant (but not interaction term). This implied that cell viability is reduced with time relative to untreated controls. As seen in **Figure 3.17** there is a reduction in viability in almost all cases from 24 h, which given the nutrient-limited conditions used for the culture media is unsurprising as from this time-point. the culture environment is likely resource limited, as the cells begin to enter stationary phase.

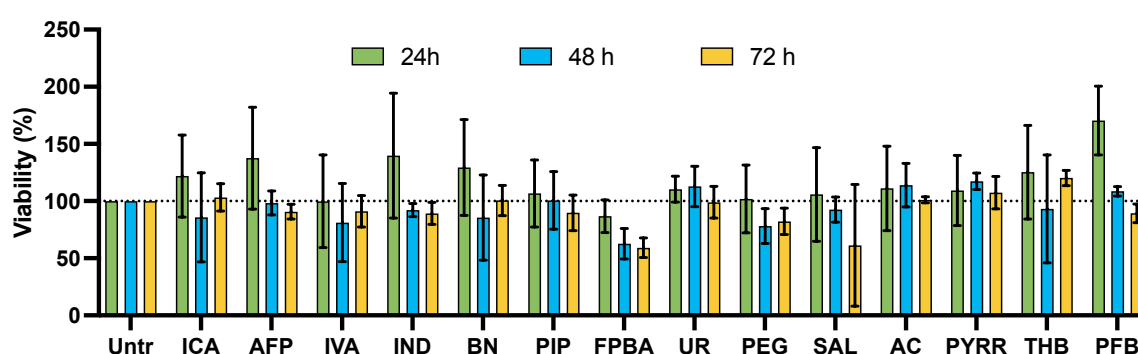


Figure 3.17. Resazurin assay to estimate *E. coli* MC4100 viability in **P1** treated cultures relative to the untreated cell cultures. Error bars = S.D. (n = 3). Statistically significant pairings (*) determined through Tukey's multiple comparisons test.

For all treatments there is an overall reduction in cell viability from 24 h to 72 h. Reduced viability also coincides with reduced CA production noted from 24 – 48 h, where production

was typically highest at 24 h. However, given that curli production continually increased until 48 h the temporal reduction in cell viability does not completely explain the discrepancies with the results found in this experiment compared to prior literature reports. Interestingly, the hydrophilic formulations **P1-FPBA**, **P1-PEG4** and **P1-SAL** all show a large reduction in viability from 24-72 h. This supports the hypothesis that these hydrophilic formulations may be cytotoxic or stressful to the bacteria. Of note, **P1-Ac** shows negligible change in viability, but remained consistently high in *csgB* activity and fucose production. Hence viability or stress may only partly explain the root cause of the inverse relationship between aggregation and ECM production. With that said, care should be taken to not over-analyse the results, though resazurin assays are widely accepted to be suitable indicators of cell viability it is an indirect measure of it, rather than other like colony forming unit (CFU) quantifications.

3.2.6.2 Measuring outer membrane stress in polymer treated *E. coli*

Having assessed that none of the polymeric formulations produced any significant cytotoxicity, additional experimentation was performed to assess potential membrane stress following polymer treatment. In *E. coli* there are several stress response pathways specific to the membrane of the cell: σ^E response, Cpx (conjugative plasmid expression) response, Bae (bacterial adaptive response), Psp (phage shock protein) response and Rcs response (regulator of capsule synthesis).⁶⁴ Production of both curli and CA are reportedly affected by several environmental stimuli and stresses. For instance, RcsA and RcsB expression is upregulated in high osmolarity conditions and/or desiccation forming a heterodimer that transcriptionally activates RcsA-dependent genes and CA synthesis.^{65,66} Similarly, curli production is downregulated by CpxR due to binding to an overlap region of the OmpR recognition site in

csgD.⁶⁷ This exemplifies how both biofilm and external stress responses in bacteria can be heavily intertwined. Therefore, it is an attractive area of investigation to figure the possible mechanisms that underly the polymer-bacteria interaction and subsequent physiological responses. Given that helical polymers are reported to increase pore formation in cell membranes, it is key to explore potential envelope stress induction following treatment by **P1**.

Initial experiments of this focused on investigating the role polymer treatment had on outer membrane porosity with the fluorescent membrane active dye 1-N-phenylnaphthylamine (NPN). NPN has been widely used in the literature to measure membranes permeability in a series of Gram-negative bacteria like *P. aeruginosa* and *E. coli*.^{68–72} NPN fluoresces exclusively within hydrophobic environments, hence no fluorescence is observed in aqueous environments, such as the cell growth media. Due to its hydrophobicity, NPN is unable to penetrate the bacteria's hydrophobic intermembrane space via passive diffusive mechanisms due to the polar cell membrane surface without prior damage to the outer membrane (**Figure 3.18**). Therefore, if treatment of MC4100 by **P1** formulations causes loss of cell membrane integrity then NPN can penetrate the membrane interior producing a subsequent increase in fluorescence emission intensity. Permeability was calculated as a metric of NPN uptake relative to the untreated cultures described in **Equation 5**.

$$NPN\ uptake = \frac{A_{treated}^{420} - A_{negative}^{420}}{A_{untreated}^{420} - A_{negative}^{420}} \quad (5)$$

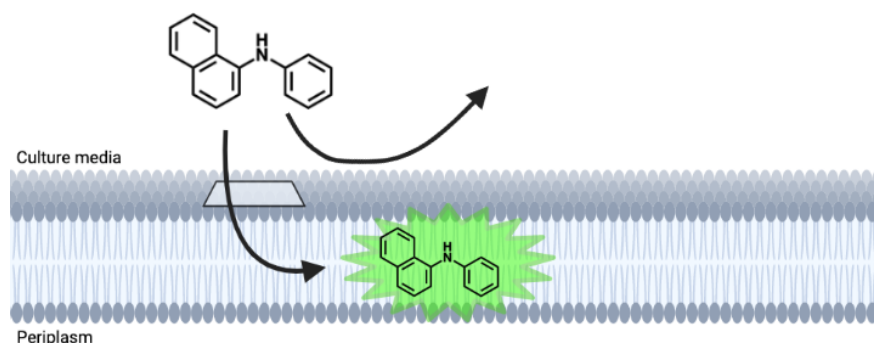


Figure 3.18. Schematic showing the entry of NPN into the hydrophobic intermembrane space causing fluorescence. In the absence of membrane permeation, no fluorescence can occur. Produced in Biorender.

For the experiment, 0.1 mM Ethylenediaminetetraacetic acid (EDTA) was used as a positive control. EDTA chelates divalent cations from the OM (responsible for bridging between anionic LPS monomers) with cationic OM constituents or metal chelating lipids such as N(α),N(α)-Bis[carboxymethyl]-N(ϵ)-[(dioctadecylamino)succinyl]-L-lysine or 1,2-dioleoyl-sn-glycero-3-[N-(5-amino-1-carboxypentyl iminodiacetic acid) succinyl].⁷³ This interaction increases membrane fluidisation and loss of lipopolysaccharides from the OM thereby increasing membrane permeability.^{68,73} Experimental conditions used were a direct replication of the prior ECM experiments. Unfortunately, initial experimental attempts are seemingly limited in scope due to reproducibility issues and large data variance limiting the ability to form a robust conclusion (**Figure 3.19**).

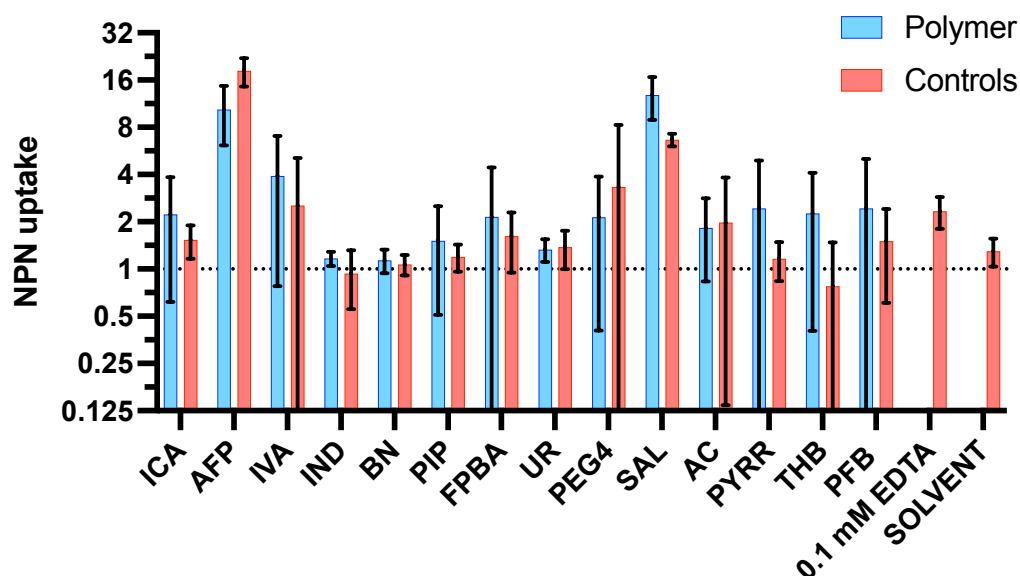


Figure 3.19. NPN uptake in P1 treated cultures (blue) and respective aldehydes (red) relative to untreated *E. coli* MC4100 cultures (black dashed line).

The largest increase in NPN uptake is seen with **P1-AFP** and **P1-SAL**, although control studies showed that **P1-AFP** fluoresces strongly at 420 nm. No confirmation can be made to discern whether the increased fluorescence is due to increased membrane permeation or polymer background fluorescence. Like EDTA, the acidic group in **P1-SAL** is deprotonated at pH 7 allowing it to complex with membrane cations and thus increase permeability, which is reflected by the large NPN uptake. A similarly large increase in uptake is observed with the aldehyde **SAL** treatment which supports this. However, NPN uptake is lower compared to the **P1-SAL** possible due to the polymer inducing some poly-chelate effect. Salicylic acid derivatives have garnered much recent interest as membrane active anti-bacterial agents. Therefore, it is likely that **P1-SAL** may exhibit a similar effect. Interestingly, the other anionic and acidic formulation **P1-FPBA** shows negligible change in NPN uptake relative to the untreated cultures. **FPBA** is an aliphatic acid, whereas **SAL** is aromatic, as such **FPBA** would be expected to have a higher pK_a due to lack of resonance stabilisation. Hence the higher pK_a

would result in a weaker chelation effect which may diminish subsequent membrane permeabilization. All other formulations showed a limited increase in NPN uptake. However, the large variation in the data makes it impossible to conclusively state whether polymer treatment causes membrane permeabilisation.

Caution should be exercised to avoid over analysing these results due to the limited nature of these experiments. A potential caveat in the experimental design may be the low cell densities used. It was deemed necessary to replicate the experimental conditions employed in the ECM quantification studies to ensure the results were translatable. If the initial cell number proved too low then it is possible that insufficient NPN uptake occurs to produce a measurable output. Thus, on repeat experimentation it may be fruitful to increase the initial cell density which may enhance NPN uptake. If no such change occurs then this would further suggest that **P1** formulations do not cause membrane permeation. Unfortunately, time-constraints of the project limited the ability to go back and revisit this as it was deemed more pertinent to focus on other aspects of the project for completeness. In future using alternative membrane active dyes may prove more fruitful than NPN. For instance, 3,3'-diethyloxacarbocyanine iodide [DiOC₂(3)] is a dye that has been used to measure the membrane potential of *E. coli*. Any perturbations to the cell membrane, such as increased porosity can cause a shift in polarisation in the cell membrane. This can be detected using a potential-active dye like DiOC₂(3).^{74–76}

3.2.6.3 Measuring periplasmic membrane stress with SPY::eGFP construct

Given the inconclusive results from the NPN assays an alternative strategy was sought to test membrane stress in *E. coli* MC4100 following treatment with **P1** formulations. Hence, it was

hypothesised that investigation into some of these envelope stress pathways may yield some answers into the possible effect of **P1** formulations on the observed ECM production.

Gram-negative bacteria like *E. coli* contain two membranous bilayers (the outer and inner membrane), the interstitial space between these membranes is known as the periplasm. The periplasm serves many roles, such as: lipoprotein secretion, maintenance of membrane potential, ion transport and osmoregulation.⁷⁷ The periplasm also contains many molecular chaperones, proteins that aid the conformational folding of other proteins.⁷⁸ One periplasmic chaperone that responds to environmental stress is Spheroplast protein Y (SPY).⁷⁹ SPY is strongly repressed in non-stressful conditions but is induced in response to OM stress, such as spheroplasting or protein denaturation, usually following chemical treatment.⁸⁰ It was hypothesised that if **P1** derivatives permeate the OM then expression of the SPY chaperone is upregulated. Therefore, greater SPY activation would indicate increased cell stress. Moreover, SPY is significantly upregulated by two different two-component signal transduction systems, CpxAR and BaeSR as well as RcsB.^{81,82} Therefore, if SPY is upregulated following polymer treatment it may be due to the upregulation in one of these pathways, which would indicate that the increased curli and CA production in polymer-treated cultures may originate from envelope stress. SPY expression in treated cultures of MC4100 was tested using the novel recombinant plasmid³ (pSPY) that contains the eGFP protein under the SPY promoter (*spy::gfp*). Upon increased periplasmic stress SPY expression is strongly upregulated with a concomitant increase in GFP expression and fluorescence emission intensity.

³ Plasmid construct designed, made, and sequenced by AO.

Initial experiments using *E. coli* BL21 in LB media⁴ showed that SPY was strongly upregulated in the presence of 4% EtOH. This was used as the positive control for the stress response experiments in MC4100 following treatment with **P1** formulations. To test the feasibility of using the recombinant pSPY in *E. coli* MC4100 under buffered M63 media, as used in prior polymer aggregation studies. These experiments also probed whether there was minimal autofluorescence from the untransformed (wt) strain both in the presence and absence of EtOH (**Figure 3.20A**). In addition, pSPY has an ampicillin (Amp) resistance marker but as prior biofilm formation experiments have excluded the use of antibiotics to avoid potential interference, the necessity Amp inclusion was also tested for. As shown in **Figure 3.20B** there is limited background fluorescence in untransformed MC4100. The greatest fluorescence was recorded with transformed MC4100 in the presence of Amp which is to be expected given there would minimal plasmid loss in these cultures. Interestingly, both Amp and EtOH and a combination thereof all showed decreased fluorescence when compared to antibiotic treatment on its own and the untreated (transformed) culture. The onset of fluorescence coincides with the onset of the exponential growth phase (see **S.I. Figure 3. 10**), and it can be clearly seen that inclusion of EtOH significantly delays onset of fluorescence, rate of fluorescence generation as well as total fluorescence. Given the low starting cell culture density used in this experiment (0.1 OD), it is possible that the concentration of EtOH is too high causing a cytotoxic effect in the cell populations and preventing cells from growing.

⁴ Initial flow cytometry experiments with EtOH as proof-of-concept were performed by AO. All experiments pertaining to experiment design screening and stress responses in a biofilm environment following polymer treatments were performed personally (ONH).

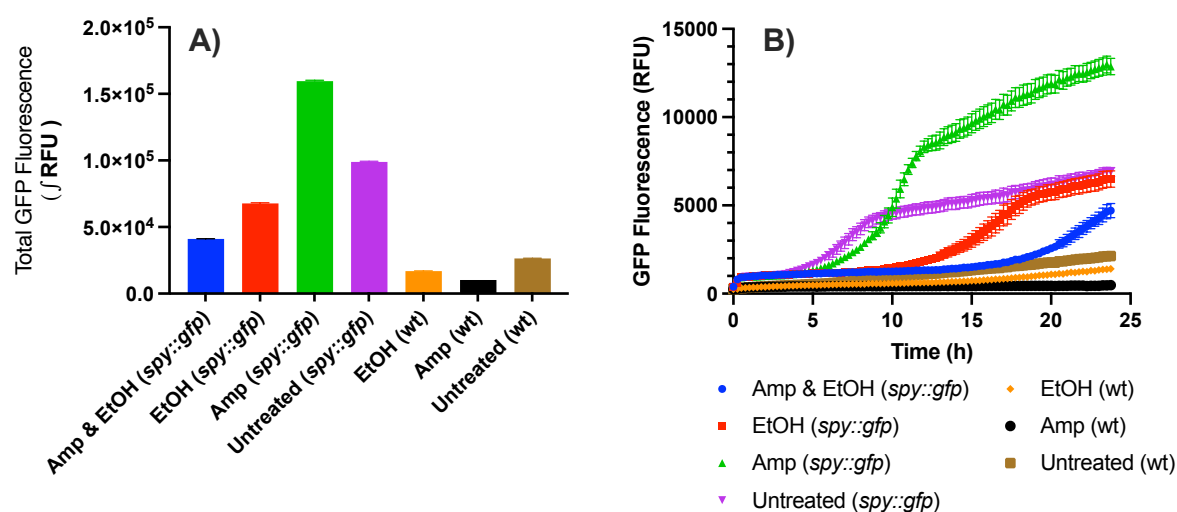


Figure 3.20. Screened conditions for *spy::gfp* construct in *E. coli* MC4100. A = total GFP production calculated as the integral of fluorescence change with time; B = fluorescence change with time. Error bars = SD ($n = 3$).

Given that the combination of Amp and EtOH was seemingly too detrimental to cell growth, Amp was excluded from further experimentation. For determination of stress induction following treatment with **P1**, experiments were performed in identical conditions as before. All polymers and aldehyde treatment showed highly similar fluorescence profiles, though the highest stress was observed with the untreated control cultures. It was suspected that the low cell density and minimal media used in these experiments may restrict growth too much for any appreciable fluorescence to occur. Hence the same experiment was performed with a higher initial cell density (OD = 0.4) in LB media to promote growth in the hopes this may amplify the fluorescence output (**Figure 3.21**).

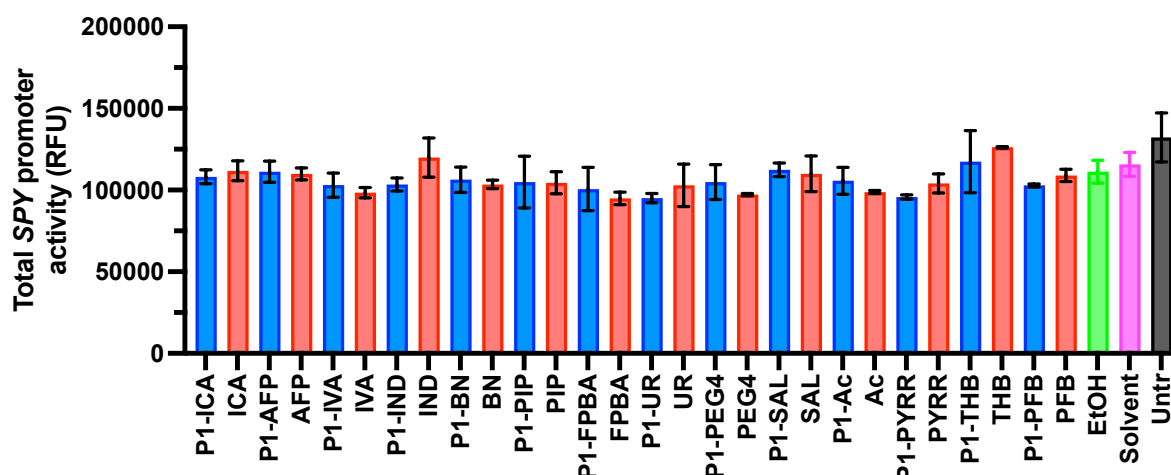


Figure 3.21. Total SPY promoter activity as calculated from the AUC of the change in fluorescence over 24 h for each tested treatment and control. Error bars = S.D. (n = 3).

Fluorescence emission intensity was measured every 30 mins for 24 h to determine the change in SPY expression (if any) following polymer treatment, the area under the curve was calculated for each treatment to determine the total SPY promoter activity in the bacterial cultures. Unfortunately, the experiment remains inconclusive where the polymer treatments show no differences and are all lower than the untreated control. Although this may be a valid result, the possibility where the bacteria within the PMCs are less stressed at this timepoint compared to the untreated planktonic cultures which was seen observed in the viability studies in **Section 3.2.6.1. Metabolic activity assays in polymer treated cultures** However, due to the lack of activity in the positive EtOH control which showed the lowest activity of all the tested cultures once again no definitive conclusions can be made here regarding the role of **P1** formulations and potential stress induction in *E. coli* MC4100.

The lack of success with this experiment may be due to the current experimental designs, which due to time constraints could not be further optimised. Further work development of this assays should find the use of a suitable positive control such as tannins or butanol which

are reported to activate SPY.⁸³ However, it could also indicate that SPY is not activated by the Bae, Cpx, and Rcs pathways following treatment with **P1**. Of these three, BaeR which responds to exogenous cytotoxic compounds is reported to give the largest fold-change in SPY upregulation. The lack of fluorescence between the treatments and control may suggest that neither **P1** nor aldehydes trigger the BaeR response due to lack of toxicity at the concentrations tested. Although it is likely that RcsB is upregulated due to the prior observed increase in CA production at 24 h (**Figure 3.13**), its effect in SPY upregulation may be limited. RcsB dependent upregulation of SPY was shown to only incur a 4-fold increase compared to a 70-fold increase in BaeS dependent activation.⁸² Upregulation of CpxR may result from adhesion to hydrophobic surfaces is detected by NlpE causing upregulation of CpxAR.⁸⁴ CpxP-dependent repression may occur also in response to pilus misfolding.⁸⁵ However, given that MC4100 does not produce type-1 pili, this is unlikely to affect this assay into SPY upregulation. The possible lack of NlpE dependent activation may have resulted from polymer-induced aggregation occurring in solution rather than adherence to a solid substrate despite the polymers' hydrophobicity. Therefore, the forces that arise in the polymer-cell interaction maybe too small to trigger sufficient membrane perturbation, limiting NlpE expression. However, research into CpxR overexpression shows that the induced fold-change in regulated genes is minimal compared to the other stress pathways and there is a degree of redundancy with genes regulated by σ^E and BaeS. It can be argued that CpxR behaves as a modulator of these other pathways rather an independent regulator.⁸² Given that CpxR negatively affects curli production and all cultures except **P1-THB** produced a statistically significant increase in csgB activity. It is unlikely that **P1** treatment upregulated CpxR which may also partly explain the unobserved increase in SPY expression. Literature shows that in CpxR overproducers SPY

is significantly upregulated with no observed increase in *csgDEFG* supporting this observation.⁸¹ With these considerations it is possible that polymer-treated *E. coli* MC4100 experienced minimal SPY upregulation from lack of upregulation of the Cpx, Bae and Rcs pathways.

Due to time constraints no further experiments could be performed to optimise the current experiments nor design additional reporter constructs that could aid in discerning the possible link between polymer-induced stress in *E. coli* on subsequent ECM production within the aggregates. Future work would benefit to produce more specific reporter plasmids e.g., *cpxA::gfp* or *bae::gfp* etc. to probe possible envelope stress pathway responses more precisely. In addition, it would be conducive to study the other stress responses σ^E and Psp to deduce whether these pathways are also affected by polymer treatment. Probing the link between material properties, cellular physiological responses and subsequent biofilm formation will better direct future research regarding novel materials to control biofilm formation.

3.2.7 Probing aggregative mechanism-of-action

Following from previous reports and from other work within the group it was first hypothesised that increased polymer-induced aggregation of the bacteria would show increase biofilm formation characterised by increased ECM production. Consistent with prior literature increased polymer hydrophobicity leads to increased bacterial aggregation (as shown by turbidimetry, CV staining and, PSA).¹³ Conversely, ECM production (CA and curli) in bacteria aggregated by **P1** is negatively correlated with aggregate size. These initial findings

suggested that although increased **P1** hydrophobicity aids aggregation, ECM production is retarded compared to hydrophilic formulations.

Having ruled out polymer cytotoxicity and cell stress (tentatively) as possible causes of the inverse relationship with ECM production and aggregation, other mechanisms were explored. One hypothesis was that different aggregative mechanisms-of-action, for example the depletion or bridging aggregation may produce different physiological responses regarding EPS production. As stated previously, anionic (**P1-FPBA** and **P1-SAL**) and hydrophilic neutral formulations (**P1-PEG4** and **P1-Ac**) may proceed via depletion aggregation. While the remaining cationic and/or hydrophobic formulations likely proceed by bridging aggregation or charge neutralisation. In depleted bacterial aggregates, the individual cells are clustered directly to one another in a lateral arrangement due to exclusion of the polymer chains. Whereas, in bridging aggregation and charge neutralisation the polymer chains directly interact with several cells causing colloidal destabilisation either through direct cross-linking or neutralisation of the shared repulsive charged. Therefore, we hypothesised that if depletion aggregation occurred, then the bacteria would produce more ECM to stabilise the newly formed aggregate. In contrast, bacteria that experience bridging have less requirement to produce EPS relative to their depleted counterparts as the polymer crosslinks the individual cells together acting as an artificial matrix which permits the cells to reallocate cell resources to other less taxing pathways.

To examine this theory, phase diagrams were constructed as described in literature whereby increased cell densities are treated by increasing polymer concentrations. If the polymers follow a bridging aggregation mechanism, one expects the phase diagrams to be positively

correlated, as a higher polymer concentration is required to effectively bridge more cells.⁸⁶ In contrast, if depletion mechanisms occur either a negative or no correlation is observed between polymer and cell concentration, as depletion is due to a crowding effect and as such there is no positive relationship between cell and polymer concentration.^{87,88}

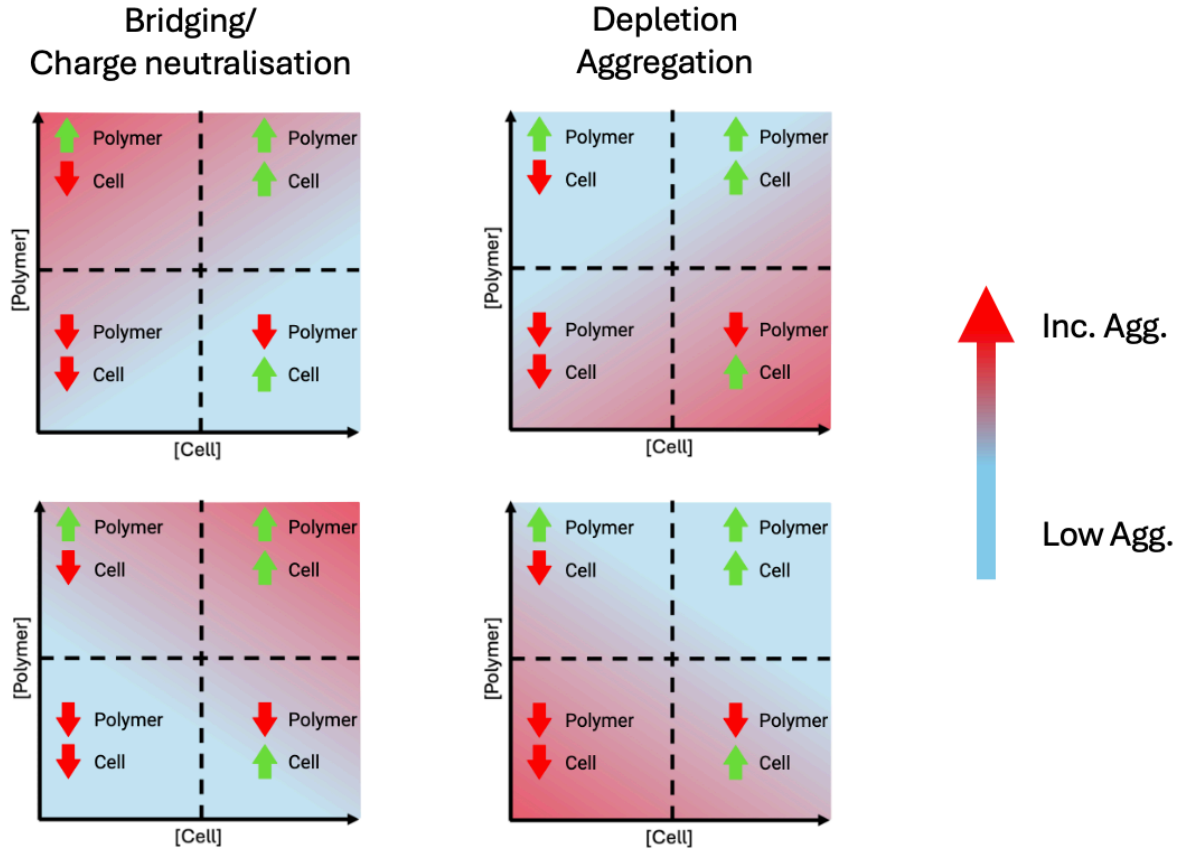


Figure 3. 22. Representation of contour plots with respect to [polymer] (y-axis), cell density (x-axis), and cell aggregation (z-axis) and how it relates to different aggregative mechanisms.

Each formulation was tested at four different polymer concentrations (0.05, 0.25, 0.5 & 1 mg mL⁻¹) with four different cell densities (OD = 0.1, 0.5, 1.0 & 2.0) giving a total of 16 conditions.

The percentage of aggregated bacteria (Agg%) was calculated according to **Equation 6** and plotted as a function of polymer and cell concentrations to give the phase diagram plots in

Figure 3.23.

$$Agg\% = \left[\frac{(OD_{600}^{0h} - OD_{600}^{24h})}{OD_{600}^{0h}} \right] \times 100 \quad (6)$$

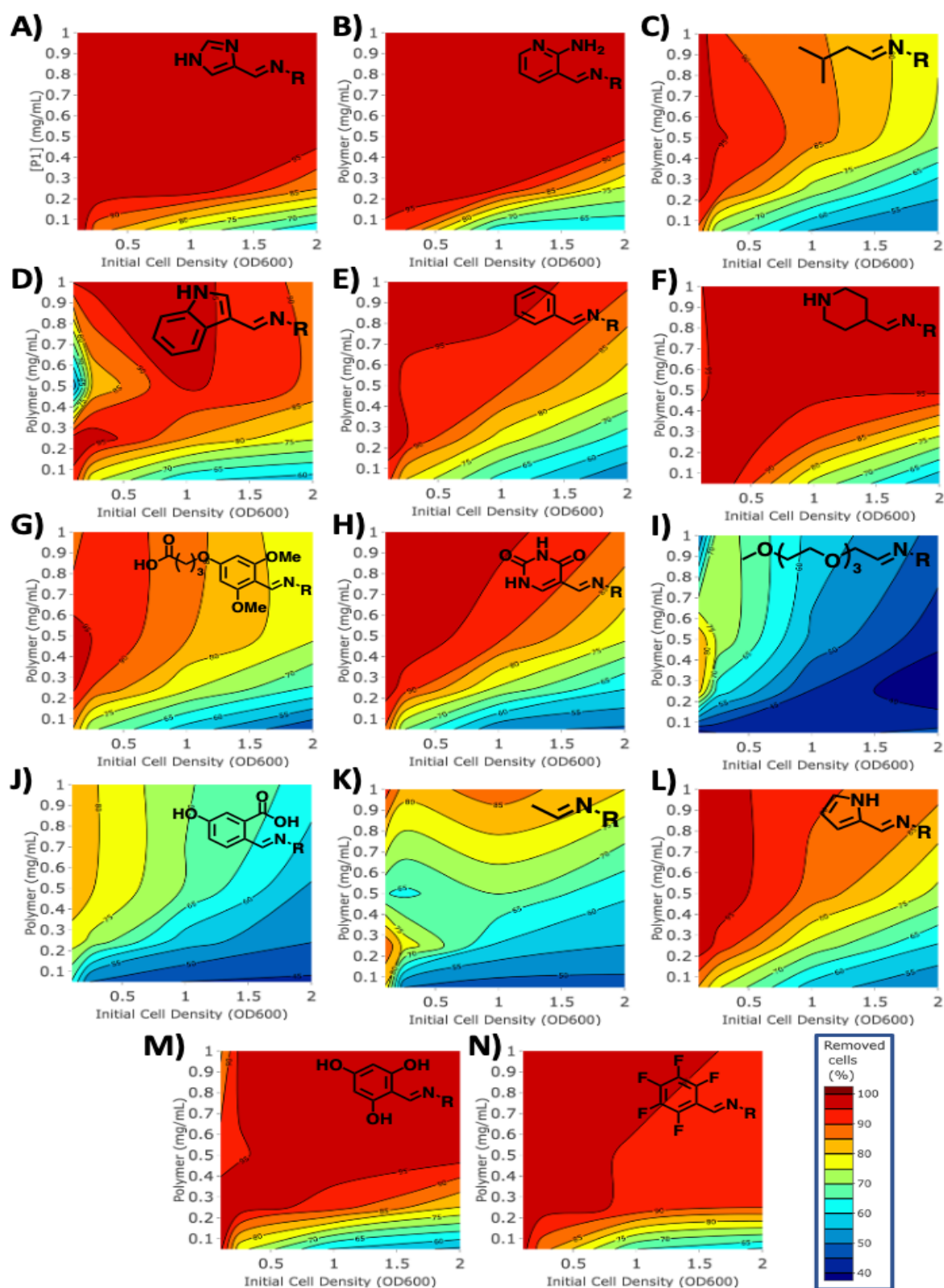


Figure 3.23. Contour plots of *E. coli* MC4100 aggregation (z-axis) at different initial cell densities (x-axis) and polymer concentrations (y-axis) for different **P1** formulations. A = ICA; B = AFP; C = IVA, D = IND; E = BN; F = PIP; G = FPBA; H = UR; I = PEG₄; J = SAL; L = PYRR; M = THB; N = PFB. All **P1** formulations proceed by suspected bridging aggregation mechanism indicated

by regions of low cell aggregation (blue contours) at higher cell density and/or reduced polymer concentrations.

The contour plots show relationship of both polymer concentration (y-axis) and cell density (x-axis) on percentage of cells aggregated (z-axis – represented as the coloured contours). Low aggregation is represented by dark blue colours which transitions to red in conditions that produced high bacterial aggregation. If the contours are positive (blue to red) with respect to the y-axis, this would indicate that aggregation proceeds by non-depletive mechanisms (Figure 3. 22).

Generally, the contours shift from bottom right (low polymer – high cell) to upper left regions (low cell – high polymer). The positive contour indicates that all polymer formulations proceed by polymer bridging mechanisms . High cell densities require increased polymer concentration to achieve sufficient colloidal destabilisation producing greater bacterial aggregation. In agreement with prior experimentation, degree-of-aggregation varied amongst the different formulations. The heterocycles **P1-ICA**, **AFP**, and **P1-PIP** (Figure 3.23A, Figure 3.23B & Figure 2.22F, respectively) seemingly perform the best. The phase diagrams of these formulations are dominated by dark red, showing near 100% aggregation across a broad range of tested polymer and cell concentrations. Therefore, these formulations effectively cluster higher cell densities with a lower effective polymer concentration. Of these three formulations **P1-ICA** and **P1-AFP** performed better as indicated by the steeper contour at low polymer – high cell conditions (bottom right). This was a surprising observation given the cationic character of **P1-PIP**. However as seen in Figure 3.23F at OD = 1, twice the amount of **P1-PIP** is required to achieve the same Agg% as **P1-ICA** and **P1-AFP**. The increased aggregation of these polymers is likely due to electrostatic attraction between the polymer and bacteria. **P1-PIP** is cationic at

pH 7, whereas **P1-ICA** and **P1-AFP** are both partially protonated (2 - 5%) at the same pH. It is interesting to note that both **P1-ICA** and **P1-AFP** both perform slightly better than **P1-PIP** at higher cell densities. This is possibly due to their higher intrinsic hydrophobicity compared to **P1-PIP**. However, it should also be noted that this is only a few percent difference, which may be further resolved to show no difference on further replication of this experiment.

The hydrophobic **P1-THB** (Figure 3.23M) and **P1-PFB** (Figure 3.23N) showed high aggregation across a broad concentration range. Although **P1-THB** could remove nearly 100% of bacteria in all tested cell densities with a lower effective polymer concentration. It should be noted that this difference is marginal. Generally, formulations with increased hydrophobicity show increased aggregation at higher cell densities with the same polymer concentration. The aliphatic **P1-IVA** shows moderate Agg% throughout, however only achieves near complete cell removal at low cell density despite possessing one of the highest calculated clogD. This agrees with prior works, which show that aliphatic derived polymers containing **IVA** or octylaldehyde, were less effective in bacterial clustering compared to their aromatic counterparts.¹³ Aromatic formulations possibly show improved binding due to induced dipole formation between the polymer sidechains and bacterial membrane strengthening the initial interaction.

The initial study performed herein seemingly disprove the hypothesis that hydrophilic polymers such as **P1-FPBA**, **P1-PEG₄**, **P1-Ac**, and **P1-SAL** proceed via depletive mechanisms. All show highly similar contour shapes where increased bacterial aggregation occurs in low cell densities and high polymer concentration. When cell density is high, higher polymer concentrations are required for sufficient aggregation to occur indicative of bridging aggregation. For **P1-FPBA**, **P1-PEG₄**, **P1-Ac**, and **P1-SAL** Agg% ranges from 40-80% across all

tested conditions, whereas many hydrophobic and/or (partially) cationic formulations achieved upwards of 100%. Of the hydrophilic polymers the order of aggregating ability could be estimated as **P1-Ac** > **P1-PEG₄** ~ **P1-SAL** > **P1-FPBA**. This is expected given that both **P1-Ac** and **P1-PEG₄** are non-ionic and will be less repulsive to the bacteria due to the lack of shared charge with the bacterial outer membrane. Both **P1-SAL** and **P1-FPBA** showed the lowest Agg% throughout all tested conditions. Like-charged electrostatic repulsion minimises adhesion between polymer and microbe thereby limiting overall aggregation. Despite the hydrophilicity of these formulations, it is possible that the conjugated backbone is sufficiently hydrophobic to make these formulations amphiphilic. As such the intrinsic hydrophobicity of the poly(acetylenes) may remain too high for a depletion effect to occur and so polymer-induced clustering proceeds by non-depletion mechanisms. This notion is supported by prior studies that showed increased cell surface hydrophobicity in *P. aeruginosa* overcame auto-aggregation by depletion aggregation and instead proceed by non-depletive mechanisms.⁸⁹

All the tested formulations appeared to follow bridging and/or charge neutralisation mechanisms. Although, overall degree-of-aggregation may still affect subsequent ECM formation in the polymer-treated cultures as initial experiments showed reduced curli and CA formation in larger aggregates. One hypothesis is that once the *E. coli* is aggregated by the polymers, minimal ECM components are produced as the **P1** acts as both a substrate for binding and as an artificial matrix. For instance, curli is required for initial and irreversible surface attachment, PNAG in promoting intercellular adhesion and CA for 3D development.^{31,90–98} It is shown here that generally **P1** invokes rapidly aggregates the bacteria (within minutes to hours) likely via a non-depletive mechanism. Aggregates form an irregular

3D structure; akin to the respective roles of curli, PNAG and CA. Production of these biopolymers requires the bacteria to use essential cellular resources that will impart a metabolic burden. Hence, polymer treatment may ameliorate this burden and permit a metabolic shift to other more advantageous pathways for cell proliferation and survival. Where greater aggregation occurs such as with hydrophobic **P1** formulations, there is less of a requirement for the various ECM components to be produced as it is not advantageous to do so. For instance, development of curli $\Delta(csgG-csgC)$, colanic acid $\Delta(wcaL-wza)$, and type-1 pilus $\Delta(fimB-fimH)$ deficient mutants of *E. coli* MG1655 show increased recombinant protein production by 16% in planktonic cultures.⁹⁹ Removal or limitation of these ECM pathways permits greater productivity in the cells due to a reallocation of cellular resources. However, this fails to explain why previous reports of polymer-induced *E. coli* aggregates show a positive relationship with ECM formation.¹³

3.3 Conclusions

The objective of this research was two-fold: (1) can a poly(acetylene) based polymer be used as an effective scaffold for artificial biofilm formation in *E. coli* and (2) attempt to better understand the mechanism-of-action of these polymeric materials on the cell physiology. Following polymer treatment, the original hypothesis of this research is that polymer-induced aggregation would increase biofilm formation through enhanced ECM production.

In this work a library of novel poly(acetylenic) materials (**P1**) was developed and tested as materials to nucleate biofilm growth in the biotechnologically relevant but poor biofilm producing strain *E. coli* MC4100. Fourteen formulations with a range of physicochemical properties were screened to test aggregation formation and surface attachment in the presence of **P1** formulations. In consensus with prior literature reports, increasing the **P1** hydrophobicity increased bacterial aggregation in the liquid phase but not surface attachment. **P1-PEG₄** and **P1-AC** were the only formulations to induce significant surface colonisation. Both **P1-PEG₄** and **P1-AC** provoked the greatest increase in curli and colanic acid production. Therefore, increased surface adherence is likely due enhanced ECM production and negligible aggregation. Polymer formulations were critical to macroscopic aggregate formation which cannot occur in the absence of polymer from the lack of intercellular bridging. All polymer treatments except **P1-THB** produced a statistically significant increase in curli and CA production (as measured in proxy by *csgB* activity and fucose concentrations) relative to the respective aldehyde, solvent, and untreated controls. Hence, polymer formulations were essential to both aggregation and ECM formation which could not be achieved in the absence of **P1**. These findings suggested that **P1** is a suitable scaffold for

nucleating biofilm growth in *E. coli* MC4100. Interestingly, no significant increase in PNAG production is observed in the microbial aggregates, possibly due to lack of *csgD* repression by McaS sRNA.

Unexpectedly, both curli and CA production was inversely proportional to aggregate formation in polymer-treated cultures. Although the underlying mechanisms behind this remained elusive. Cell viability suggested negligible cytotoxicity of the polymer formulations negating the likelihood of this as a cause. The OM and PM stress assays using NPN and *spy::gfp* respectively remain inconclusive and a possible explanation may reside here. Future work would benefit using alternative membrane responsive dyes such as DiOC₂(3). In addition, the creation of more specific plasmid reporter constructs of alternative stress pathways would permit a more direct investigation into the possible role of polymer-induced stress and subsequent ECM production.

Though full mechanistic understandings could unfortunately not be resolved within the timeframe of this project, the research had still yielded positive results. Therefore, given that **P1** formulations were essential to both aggregate and ECM formation it can be concluded that **P1** is a suitable scaffold for biofilm nucleation in *E. coli* MC4100.

3.4 Bibliography

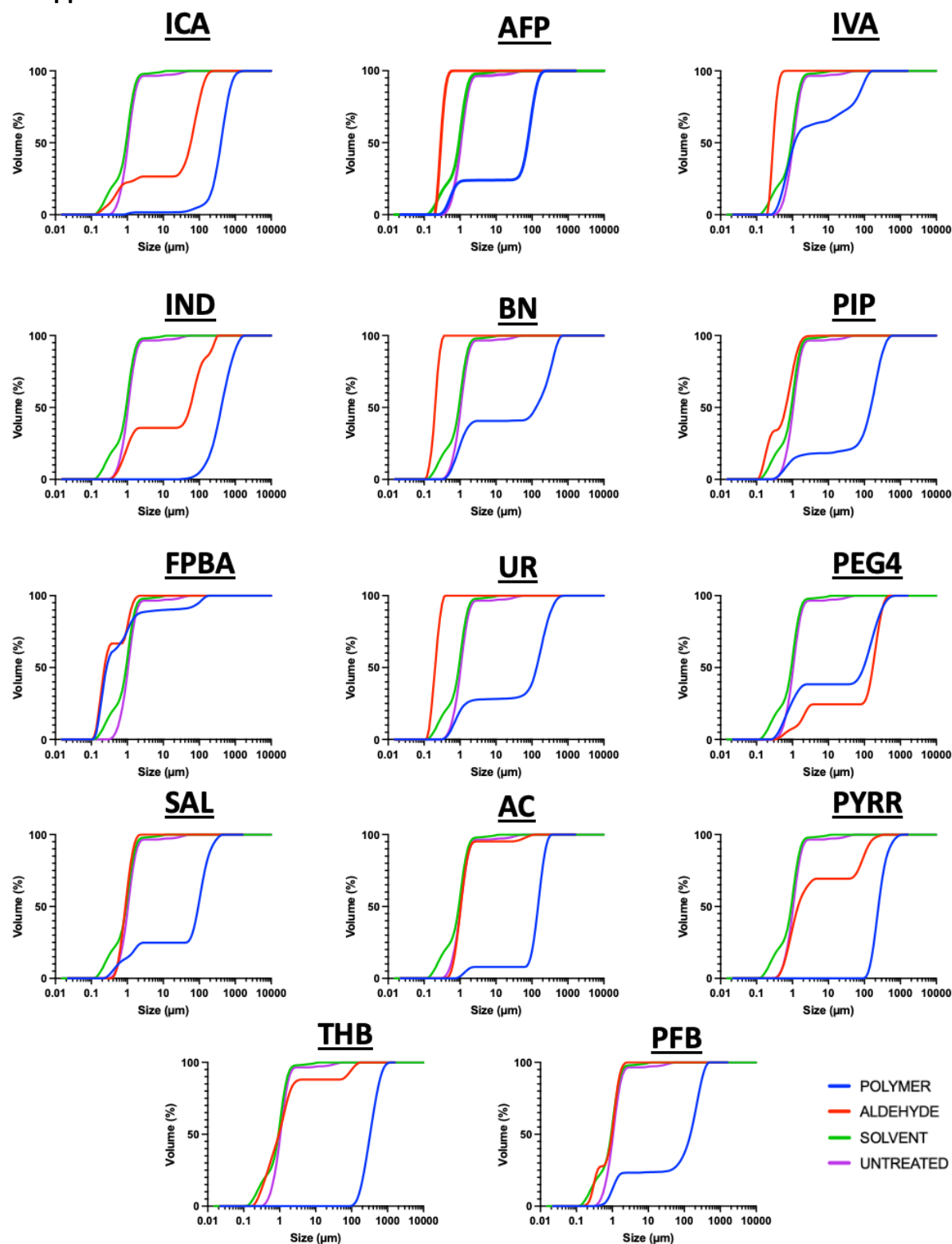
- 1 Biotechnology Market Report 2022-2030: Industry Growth, Top Companies Share, Size, and Forecast.
- 2 G. Walsh and E. Walsh, *Nat Biotechnol*, 2022, **40**, 1722–1760.
- 3 J. E. Cronan, *eLS*, , DOI:10.1002/9780470015902.a0002026.pub2.
- 4 J. Leech, S. Golub, W. Allan, M. J. H. Simmons and T. W. Overton, *Arch Microbiol*, 2020, **202**, 1517–1527.
- 5 S. R. Golub and T. W. Overton, *J Biosci Bioeng*, 2021, **131**, 381–389.
- 6 A. N. Tsoligkas, M. Winn, J. Bowen, T. W. Overton, M. J. H. Simmons and R. J. M. Goss, *ChemBioChem*, 2011, **12**, 1391–1395.
- 7 C. C. Goller and T. Romeo, *Curr Top Microbiol Immunol*, 2008, **322**, 37–66.
- 8 C. Beloin, A. Roux and J.-M. Ghigo, *Curr Top Microbiol Immunol*, 2008, 249–289.
- 9 D. O. Serra, A. M. Richter and R. Hengge, *J Bacteriol*, 2013, **195**, 5540–5554.
- 10 J. E. Peters, T. E. Thate and N. L. Craig, *J Bacteriol*, 2003, **185**, 2017–2021.
- 11 C. Peng, A. Vishwakarma, S. Mankoci, H. A. Barton and A. Joy, *Biomacromolecules*, 2019, **20**, 1675–1682.
- 12 N. Cerca, G. B. Pier, M. Vilanova, R. Oliveira and J. Azeredo, *Res Microbiol*, 2005, **156**, 506–514.
- 13 P. Adoni, A. Romanyuk, T. W. Overton and P. Fernandez-Trillo, *Mater Horiz*, 2022, **9**, 2592–2602.
- 14 O. Vidal, R. Longin, C. Prigent-Combaret, C. Dorel, M. Hooreman and P. Lejeune, *J Bacteriol*, 1998, **180**, 2442–2449.
- 15 R. Acharya, in *Satellite Signal Propagation, Impairments and Mitigation*, Elsevier, 2017, pp. 57–86.
- 16 E. Leire, S. P. Amaral, I. Louzao, K. Winzer, C. Alexander, E. Fernandez-Megia and F. Fernandez-Trillo, *Biomater Sci*, 2016, **4**, 998–1006.
- 17 Y. Tsuchido, R. Horiuchi, T. Hashimoto, K. Ishihara, N. Kanzawa and T. Hayashita, *Anal Chem*, 2019, **91**, 3929–3935.
- 18 J. J. C. Martín, M. Assali, E. Fernández-García, V. Valdivia, E. M. Sánchez-Fernández, J. M. G. Fernández, R. E. Wellinger, I. Fernández and N. Khier, *J Mater Chem B*, 2016, **4**, 2028–2037.
- 19 A. T. Poortinga, R. Bos, W. Norde and H. J. Busscher, *Surf Sci Rep*, 2002, **47**, 1–32.
- 20 *Intermolecular and Surface Forces*, Elsevier, 2011.
- 21 N. Perez-Soto, O. Creese, F. Fernandez-Trillo and A.-M. Krachler, *ACS Chem Biol*, 2018, **13**, 3021–3029.
- 22 N. Perez-Soto, L. Moule, D. N. Crisan, I. Insua, L. M. Taylor-Smith, K. Voelz, F. Fernandez-Trillo and A. M. Krachler, *Chem Sci*, 2017, **8**, 5291–5298.
- 23 L. L. Foster, S. Yusa and K. Kuroda, *Antibiotics*, 2019, **8**, 61.
- 24 C. Prigent-Combaret, E. Brombacher, O. Vidal, A. Ambert, P. Lejeune, P. Landini and C. Dorel, *J Bacteriol*, 2001, **183**, 7213–7223.
- 25 C. Lelong, K. Aguiluz, S. Luche, L. Kuhn, J. Garin, T. Rabilloud and J. Geiselmann, *Molecular & Cellular Proteomics*, 2007, **6**, 648–659.
- 26 A. Bougdour, C. Lelong and J. Geiselmann, *Journal of Biological Chemistry*, 2004, **279**, 19540–19550.
- 27 L. Gualdi, L. Tagliabue and P. Landini, *J Bacteriol*, 2007, **189**, 8034–8043.
- 28 R. J. Melander, M. J. Minvielle and C. Melander, *Tetrahedron*, 2014, **70**, 6363–6372.

- 29 M. Friedman, P. R. Henika and R. E. Mandrell, *J Food Prot*, 2003, **66**, 1811–1821.
- 30 D. Zubris, K. Minbiole and W. Wuest, *Curr Top Med Chem*, 2016, **17**, 305–318.
- 31 Y. Itoh, J. D. Rice, C. Goller, A. Pannuri, J. Taylor, J. Meisner, T. J. Beveridge, J. F. Preston and T. Romeo, *J Bacteriol*, 2008, **190**, 3670–3680.
- 32 I. W. Sutherland, *Biochemical Journal*, 1969, **115**, 935–945.
- 33 S. Steiner, C. Lori, A. Boehm and U. Jenal, *EMBO J*, 2012, **32**, 354–368.
- 34 C. Wang, H. Zhang, J. Wang, S. Chen, Z. Wang, L. Zhao and X. Wang, *Microbiol Res*, 2020, **239**, 126527.
- 35 J. Domka, J. Lee, T. Bansal and T. K. Wood, *Environ Microbiol*, 2007, **9**, 332–346.
- 36 S. M. Hunt, E. M. Werner, B. Huang, M. A. Hamilton and P. S. Stewart, *Appl Environ Microbiol*, 2004, **70**, 7418–7425.
- 37 D. Applegate and J. Bryers, in *Physiology of Immobilized Cells (Proceedings of an International Symposium held at Wageningen, Netherlands, 10-13 Dec 1989)*, eds. J. de Bont, J. Visser, B. Mattiasson and J. Tramper, Elsevier Publishers, Amsterdam, 1990.
- 38 H. Chen, C.-H. Yan, Y.-F. Zhan, L.-T. Geng, L.-L. Zhu, L.-C. Gong and J. Wang, *Int J Mol Sci*, 2022, **23**, 8059.
- 39 H. D. Lu, A. C. Spiegel, A. Hurley, L. J. Perez, K. Maisel, L. M. Ensign, J. Hanes, B. L. Bassler, M. F. Semmelhack and R. K. Prud'homme, *Nano Lett*, **15**, 2235–2241.
- 40 N. Perez-Soto, O. Creese, F. Fernandez-Trillo and A.-M. Krachler, *ACS Chem Biol*, 2018, **13**, 3021–3029.
- 41 N. Perez-Soto, L. Moule, D. N. Crisan, I. Insua, L. M. Taylor-Smith, K. Voelz, F. Fernandez-Trillo and A. M. Krachler, *Chem Sci*, 2017, **8**, 5291–5298.
- 42 N. Majdalani and S. Gottesman, *Annu Rev Microbiol*, 2005, **59**, 379–405.
- 43 T. Ophir and D. L. Gutnick, *Appl Environ Microbiol*, 1994, **60**, 740–745.
- 44 D. D. Sledjeski and S. Gottesman, *J Bacteriol*, 1996, **178**, 1204–1206.
- 45 L. Ferrières and D. J. Clarke, *Mol Microbiol*, 2003, **50**, 1665–1682.
- 46 F. S. de Oliveira, B. C. O. Leite, M. V. A. S. de Andrade and M. Korn, *J Braz Chem Soc*, 2005, **16**, 87–92.
- 47 M. A. Eberhardt and J. M. Sieburth, *Mar Chem*, 1985, **17**, 199–212.
- 48 S. Van Wycken, W. Long, S. K. Black and L. M. L. Laurens, *Anal Biochem*, 2017, **518**, 90–93.
- 49 M. Schneider, G. F. Zimmer, E. B. Cremonese, R. de C de S Schneider and V. A. Corbellini, *Waste Management & Research: The Journal for a Sustainable Circular Economy*, 2014, **32**, 653–660.
- 50 Y.-S. Cheng, Y. Zheng, J. M. Labavitch and J. S. VanderGheynst, *Process Biochemistry*, 2011, **46**, 1927–1933.
- 51 A. TSUJI, T. KINOSHITA and M. HOSHINO, *Chem Pharm Bull (Tokyo)*, 1969, **17**, 1505–1510.
- 52 S. Lo Svenningsen, in *Regulating with RNA in Bacteria and Archaea*, ASM Press, Washington, DC, USA, 2018, pp. 283–304.
- 53 A. Boehm and J. Vogel, *Mol Microbiol*, 2012, **84**, 1–5.
- 54 F. Mika and R. Hengge, *RNA Biol*, 2014, **11**, 494–507.
- 55 M. K. Thomason, F. Fontaine, N. De Lay and G. Storz, *Mol Microbiol*, 2012, **84**, 17–35.
- 56 M. G. Jørgensen, M. K. Thomason, J. Havelund, P. Valentin-Hansen and G. Storz, *Genes Dev*, 2013, **27**, 1132–1145.
- 57 M. B. Poulin and L. L. Kuperman, *Front Microbiol*, , DOI:10.3389/fmicb.2021.730980.
- 58 A. Boehm, S. Steiner, F. Zaehring, A. Casanova, F. Hamburger, D. Ritz, W. Keck, M. Ackermann, T. Schirmer and U. Jenal, *Mol Microbiol*, 2009, **72**, 1500–1516.

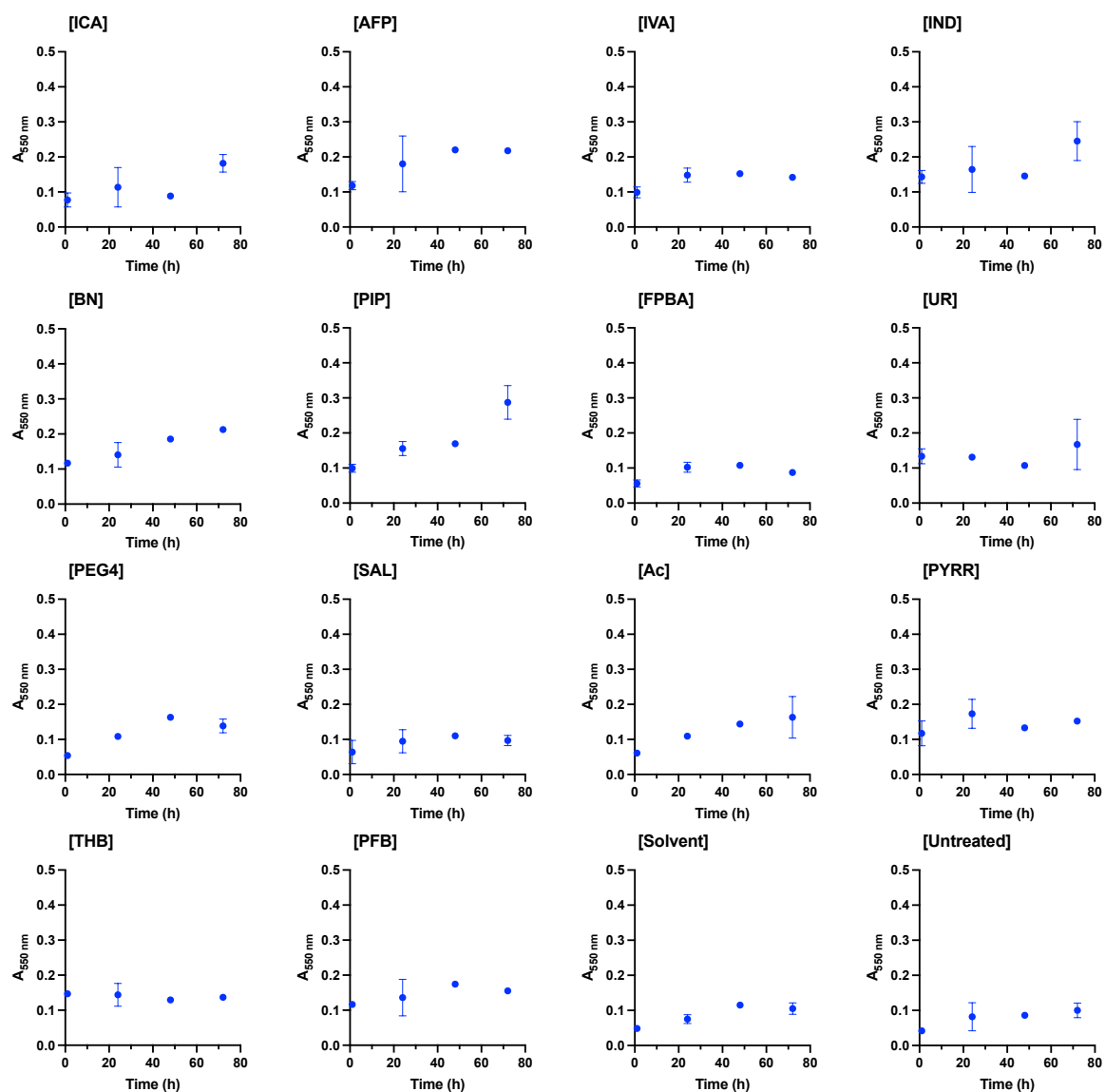
- 59 A. M. Vrabioiu and H. C. Berg, *Proceedings of the National Academy of Sciences*, , DOI:10.1073/pnas.2116830119.
- 60 T. Leigh and P. Fernandez-Trillo, *Nat Rev Chem*, 2020, 1–20.
- 61 N. P. Gabrielson, H. Lu, L. Yin, K. H. Kim and J. Cheng, *Molecular Therapy*, 2012, **20**, 1599–1609.
- 62 P. Costa, A. T. P. C. Gomes, M. Braz, C. Pereira and A. Almeida, *Antibiotics*, 2021, **10**, 974.
- 63 S. D. Sarker, L. Nahar and Y. Kumarasamy, *Methods*, 2007, **42**, 321–324.
- 64 A. M. Mitchell and T. J. Silhavy, *Nat Rev Microbiol*, 2019, **17**, 417–428.
- 65 M. Wehland and F. Bernhard, *Journal of Biological Chemistry*, 2000, **275**, 7013–7020.
- 66 D. Hagiwara, M. Sugiura, T. Oshima, H. Mori, H. Aiba, T. Yamashino and T. Mizuno, *J Bacteriol*, 2003, **185**, 5735–5746.
- 67 G. Jubelin, A. Vianney, C. Beloin, J.-M. Ghigo, J.-C. Lazzaroni, P. Lejeune and C. Dorel, *J Bacteriol*, 2005, **187**, 2038–49.
- 68 H.-L. Alakomi, A. Paananen, M.-L. Suihko, I. M. Helander and M. Saarela, *Appl Environ Microbiol*, 2006, **72**, 4695–4703.
- 69 I. M. Helander and T. Mattila-Sandholm, *J Appl Microbiol*, 2000, **88**, 213–219.
- 70 I. M. Helander, H.-L. Alakomi, K. Latva-Kala and P. Koski, *Microbiology (N Y)*, 1997, **143**, 3193–3199.
- 71 I. M. Helander, E.-L. Nurmiäho-Lassila, R. Ahvenainen, J. Rhoades and S. Roller, *Int J Food Microbiol*, 2001, **71**, 235–244.
- 72 D. M. Livermore, *Clinical Infectious Diseases*, 1988, **10**, 691–698.
- 73 V. Prachayasittikul, C. Isarankura-Na-Ayudhya, T. Tantimongcolwat, C. Nantasenamat and H.-J. Galla, *Acta Biochim Biophys Sin (Shanghai)*, 2007, **39**, 901–913.
- 74 M. A. Hudson, D. A. Siegele and S. W. Lockless, *Antimicrob Agents Chemother*, , DOI:10.1128/AAC.00910-20.
- 75 J. B. Parsons, J. Yao, M. W. Frank, P. Jackson and C. O. Rock, *J Bacteriol*, 2012, **194**, 5294–5304.
- 76 M. Yang, A. S. Jalloh, W. Wei, J. Zhao, P. Wu and P. R. Chen, *Nat Commun*, 2014, **5**, 4981.
- 77 S. I. Miller and N. R. Salama, *PLoS Biol*, 2018, **16**, e2004935.
- 78 L. Breydo, J. M. Redington and V. N. Uversky, 2017, pp. 145–185.
- 79 H. Kim, K. Wu and C. Lee, *Front Mol Biosci*, 2021, **8**, 678697.
- 80 S. Hagenmaier, Y. D. Stierhof and U. Henning, *J Bacteriol*, 1997, **179**, 2073–2076.
- 81 T. L. Raivio, S. K. D. Leblanc and N. L. Price, *J Bacteriol*, 2013, **195**, 2755–2767.
- 82 S. Bury-Moné, Y. Nomane, N. Reymond, R. Barbet, E. Jacquet, S. Imbeaud, A. Jacq and P. Boulloc, *PLoS Genet*, 2009, **5**, e1000651.
- 83 H. Kim, K. Wu and C. Lee, *Front Mol Biosci*, , DOI:10.3389/fmolb.2021.678697.
- 84 K. Otto and T. J. Silhavy, *Proceedings of the National Academy of Sciences*, 2002, **99**, 2287–2292.
- 85 Y. M. Lee, P. A. DiGiuseppe, T. J. Silhavy and S. J. Hultgren, *J Bacteriol*, 2004, **186**, 4326–4337.
- 86 N. Nazeer and M. Ahmed, *Eur Polym J*, 2019, **119**, 148–154.
- 87 J. Schwarz-Linek, A. Winkler, L. G. Wilson, N. T. Pham, T. Schilling and W. C. K. Poon, *Soft Matter*, 2010, **6**, 4540–4549.
- 88 J. Schwarz-Linek, G. Dorken, A. Winkler, L. G. Wilson, N. T. Pham, C. E. French, T. Schilling and W. C. K. Poon, *EPL (Europhysics Letters)*, 2010, **89**, 68003.
- 89 S. Azimi, J. Thomas, S. E. Cleland, J. E. Curtis, J. B. Goldberg and S. P. Diggle, *mBio*, , DOI:10.1128/mBio.00860-21.

- 90 E. A. Epstein and M. R. Chapman, *Cell Microbiol*, 2008, **10**, 1413–1420.
- 91 L. Gualdi, L. Tagliabue, S. Bertagnoli, T. Ieranò, C. De Castro and P. Landini, *Microbiology (N Y)*, 2008, **154**, 2017–2024.
- 92 C. Prigent-Combaret, G. Prensier, T. T. Le Thi, O. Vidal, P. Lejeune and C. Dorel, *Environ Microbiol*, 2000, **2**, 450–464.
- 93 M. M. Barnhart and M. R. Chapman, *Annu Rev Microbiol*, 2006, **60**, 131–147.
- 94 C. Goller, X. Wang, Y. Itoh and T. Romeo, *J Bacteriol*, 2006, **188**, 8022–8032.
- 95 G. Stevenson, K. Andrianopoulos, M. Hobbs and P. R. Reeves, *J Bacteriol*, 1996, **178**, 4885–4893.
- 96 W. D. Grant, I. W. Sutherland and J. F. Wilkinson, *J Bacteriol*, 1969, **100**, 1187–1193.
- 97 B. Obadia, S. Lacour, P. Doublet, H. Baubichon-Cortay, A. J. Cozzone and C. Grangeasse, *J Mol Biol*, 2007, **367**, 42–53.
- 98 T. May and S. Okabe, *J Bacteriol*, 2008, **190**, 7479–7490.
- 99 B. H. Sung, C. H. Lee, B. J. Yu, J. H. Lee, J. Y. Lee, M. S. Kim, F. R. Blattner and S. C. Kim, *Appl Environ Microbiol*, 2006, **72**, 3336–42.

3.5 Appendix



S.I. Figure 3.1. Cumulative volume distributions of *E. coli* MC4100 following treatment with P1 formulations (blue), aldehydes (red), solvent (green) and untreated cultures (purple).



S.I. Figure 3.2. Time series data for aggregated biomass measurements by crystal violet staining. Error bars = s.d. ($n = 3$).

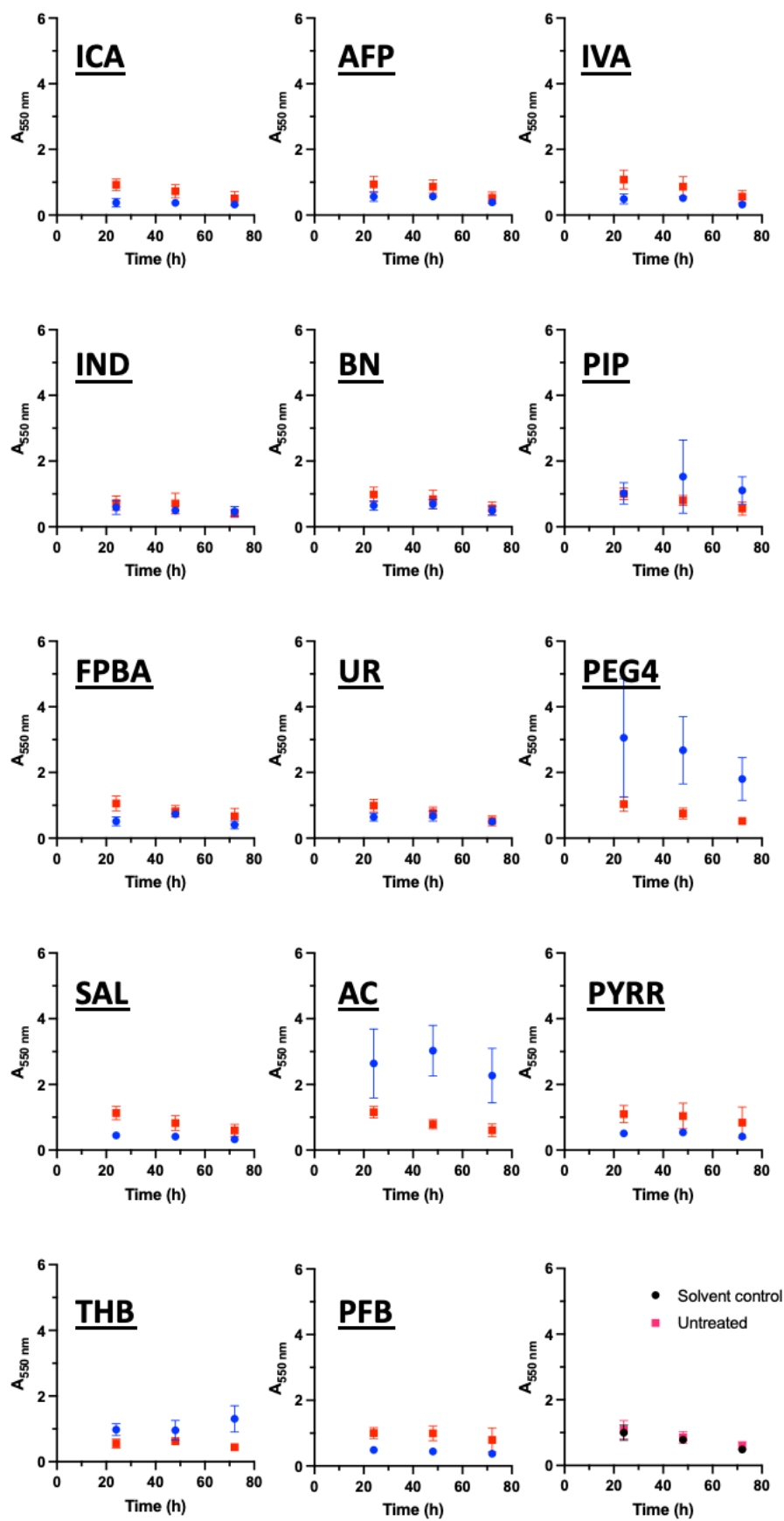
ANOVA & Normality test results

4	ANOVA summary					
5	F	14.60				
6	P value	<0.0001				
7	P value summary	****				
8	Significant diff. among means (P < 0.05)?	Yes				
9	R squared	0.9319				
10						
11	Brown-Forsythe test					
12	F (DFn, DFd)	4.622e+029 (15, 16)				
13	P value	<0.0001				
14	P value summary	****				
15	Are SDs significantly different (P < 0.05)?	Yes				
16						
17	Bartlett's test					
18	Bartlett's statistic (corrected)					
19	P value					
20	P value summary					
21	Are SDs significantly different (P < 0.05)?					
22						
23	ANOVA table	SS	DF	MS	F (DFn, DFd)	P value
24	Treatment (between columns)	0.5558	15	0.03705	F (15, 16) = 14.60	P<0.0001
25	Residual (within columns)	0.04060	16	0.002537		
26	Total	0.5964	31			
27						
28	Normality of Residuals					
29	Test name	Statistics	P value	Passed normality	P value summary	
30	D'Agostino-Pearson omnibus (K2)	4.271	0.1182	Yes	ns	

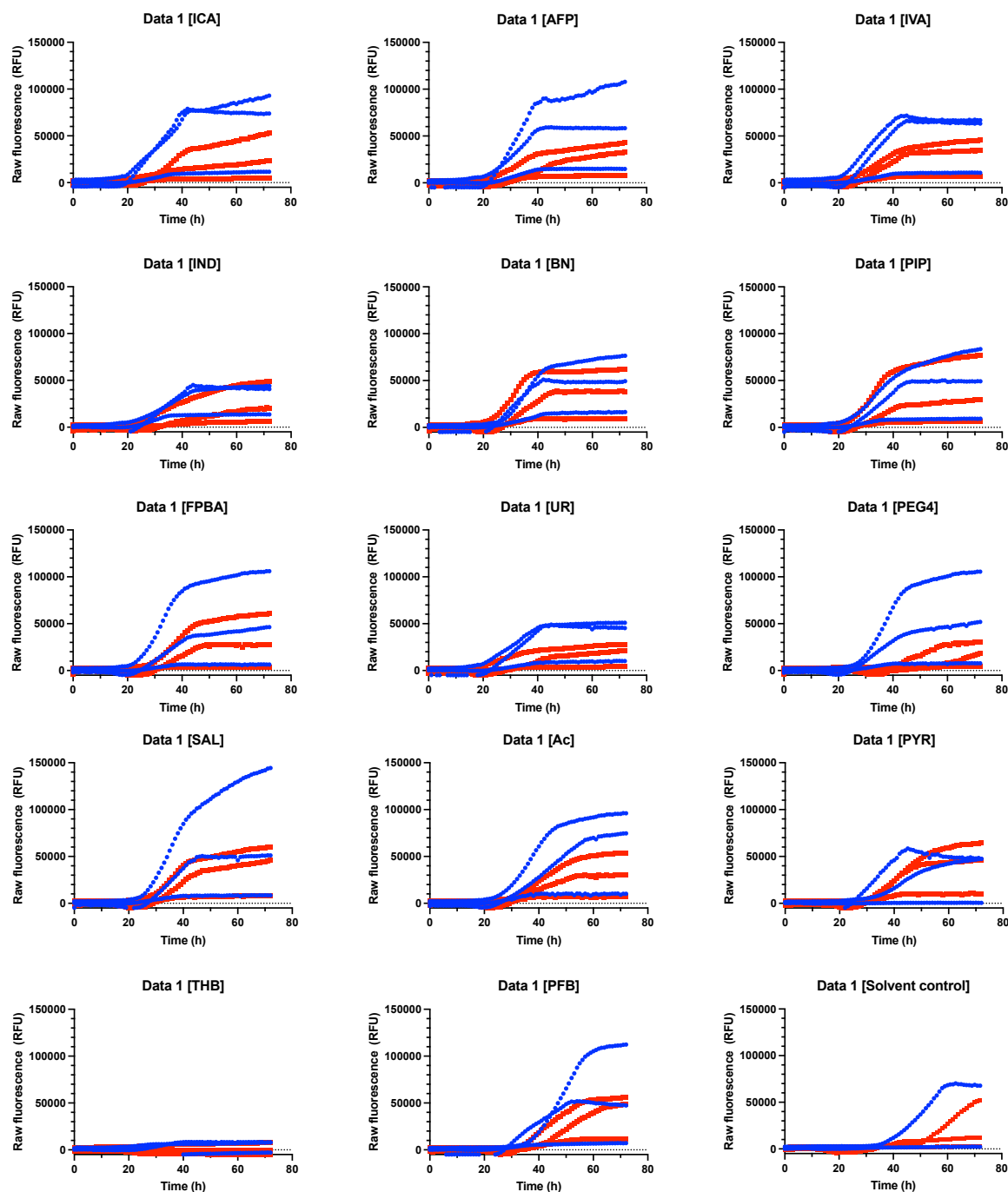
Post-hoc analysis for pairwise comparisons

1	Number of families	1			
2	Number of comparisons per family	15			
3	Q	0.05			
4					
5	Two-stage linear step-up procedure of Benjamini, Krieger and Yekutieli	Mean Diff.	Discovery?	q value	Individual P Value
6	ICA vs. Solvent	0.1178	Yes	0.0086	0.0326
7	AFP vs. Solvent	0.3925	Yes	<0.0001	<0.0001
8	IVA vs. Solvent	0.1975	Yes	0.0005	0.0012
9	IND vs. Solvent	0.3545	Yes	<0.0001	<0.0001
10	BN vs. Solvent	0.3120	Yes	<0.0001	<0.0001
11	PIP vs. Solvent	0.3675	Yes	<0.0001	<0.0001
12	FPBA vs. Solvent	0.009166	No	0.1802	0.8579
13	UR vs. Solvent	0.1952	Yes	0.0005	0.0013
14	PEG4 vs. Solvent	0.1200	Yes	0.0086	0.0300
15	SAL vs. Solvent	0.02217	No	0.1498	0.6658
16	Ac vs. Solvent	0.1338	Yes	0.0054	0.0172
17	PYRR vs. Solvent	0.2322	Yes	0.0002	0.0003
18	THB vs. Solvent	0.2127	Yes	0.0003	0.0006
19	PFB vs. Solvent	0.2380	Yes	0.0001	0.0002
20	Untreated vs. Solvent	-0.03433	No	0.1224	0.5052

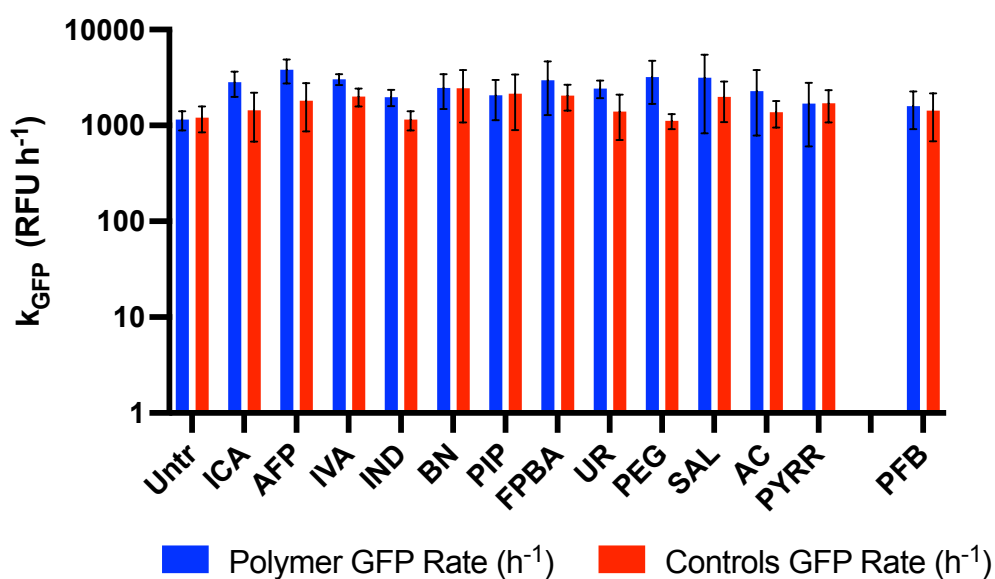
S.I. Figure 3.3. Results of 1-way ANOVA data for aggregated biomass measurements by crystal violet staining. Analysis performed in GraphPad 9.



S.I. Figure 3.4. Time series data for surface bound E.coli MC4100 measurements by crystal violet staining. Blue circle = polymer treated; red square = aldehyde treated. Error bars = s.d. (n = 3).



*S.I. Figure 3.5. Non-normalised data for *csgB::gfp* data. Each line represents an individual biological control. Blue lines = polymer & red lines = aldehyde controls.*



S.I. Figure 3.6. Exponential GFP production rates for polymer treatment (blue) and controls (red), calculated from two-part segmental regression analysis (taken as gradient of second line). No regression analysis could be performed on THB data due to poor data fit in regression.

S.I. Table 3. 1. Onset of GFP production following treatment. Calculated from two-part segmental regression analysis (where GFP_{on} taken as the x-intercept of the 2nd). No regression analysis could be performed with THB, so these values was estimated manually.

Sample	Polymer GFP_{on} (h) \pm s.d.	Controls GFP_{on} (h) \pm s.d.
ICA	21.9 \pm 4.80	25.9 \pm 6.90
AFP	24.9 \pm 4.90	27.0 \pm 5.50
IVA	25.0 \pm 5.60	27.1 \pm 4.00
IND	25.1 \pm 4.90	29.3 \pm 6.60
BN	25.9 \pm 6.70	28.1 \pm 4.00
PIP	26.4 \pm 6.40	27.4 \pm 6.10
FPBA	26.4 \pm 5.80	28.8 \pm 2.20
UR	23.3 \pm 5.70	23.7 \pm 8.10
PEG4	27.5 \pm 4.10	19.2 \pm 2.20
SAL	28.8 \pm 5.70	29.9 \pm 4.80
AC	28.3 \pm 6.40	29.8 \pm 4.40
PYRR	29.3 \pm 6.40	29.4 \pm 3.20
THB	5.40 \pm 6.00	17.8 \pm 7.20
PFB	28.9 \pm 5.40	32.4 \pm 2.40
AcOH/DMSO	N/A	28.2 \pm 7.80
Untreated	N/A	19.9 \pm 4.70

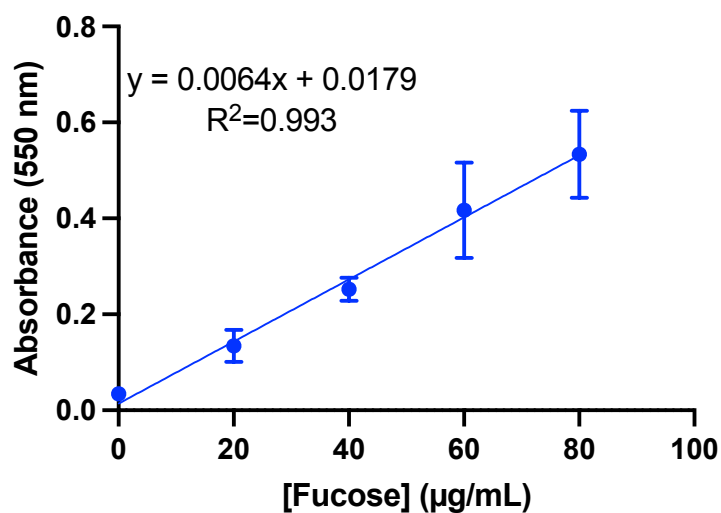
1-way ANOVA & Normality test results (Total csgB Fluorescence Anal.)

Ordinary one-way ANOVA ANOVA results					
3					
4	ANOVA summary				
5	F	4.134			
6	P value	<0.001			
7	P value summary	***			
8	Significant diff. among means (P < 0.05)?	Yes			
9	R squared	0.6740			
10					
11	Brown-Forsythe test				
12	F (DFn, DFd)	0.8044 (29, 58)			
13	P value	0.74			
14	P value summary	ns			
15	Are SDs significantly different (P < 0.05)?	No			
23	ANOVA table	SS	DF	MS	F (DFn, DFd) P value
24	Treatment (between columns)	436137	29	15039	F (29, 58) = 4.1 P<0.001
25	Residual (within columns)	210989	58	3638	
26	Total	647126	87		
27					
28	Normality of Residuals				
29	Test name	Statistics	P value	Passed normality	P value summary
30	D'Agostino-Pearson omnibus (K2)	5.205	0.07	Yes	ns

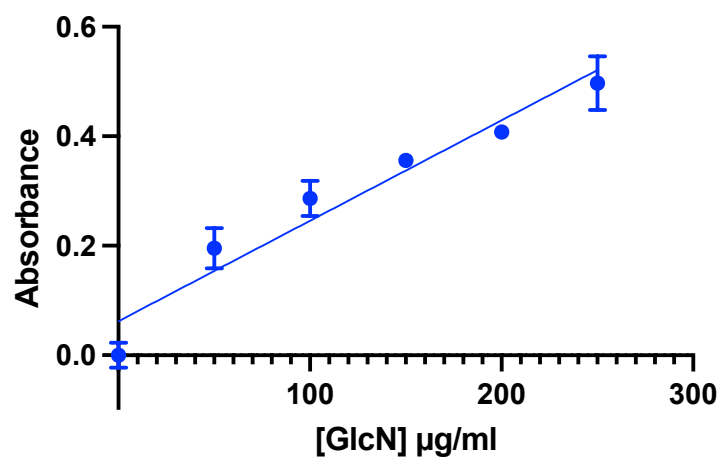
Post-hoc analysis for pairwise comparisons

5	Two-stage linear step-up procedure of Benjamini, Krieger and Yekutieli	Mean Diff.	Discovery?	q value	Individual P Value	
6	P1-ICA vs. ICA	166.1	Yes	0.002	0.001	A-B
7	P1-AFP vs. AFP	178.2	Yes	0.002	<0.001	C-D
8	P1-IVA vs. IVA	105.9	Yes	0.02	0.04	E-F
9	P1-IND vs. IND	97.52	Yes	0.03	0.05	G-H
10	P1-BN vs. BN	52.57	No	0.15	0.29	I-J
11	P1-PIP vs. PIP	50.63	No	0.15	0.31	K-L
12	P1-FPBA vs. FPBA	120.0	Yes	0.01	0.02	M-N
13	P1-UR vs. UR	104.6	Yes	0.02	0.04	O-P
14	P1-PEG4 vs. PEG4	147.6	Yes	0.005	0.004	Q-R
15	P1-SAL vs. SAL	91.33	Yes	0.04	0.07	S-T
16	P1-AC vs. Ac	104.2	Yes	0.02	0.04	U-V
17	P1-PYRR vs. PYRR	57.84	No	0.13	0.25	W-X
18	P1-THB vs. THB	62.83	No	0.14	0.26	Y-Z
19	P1-PFB vs. PFB	43.29	No	0.18	0.38	AA-AB
20	Solvent vs. Untreated	5.583	No	0.40	0.92	AC-AD
21	P1-ICA vs. Solvent	236.3	Yes	<0.001	<0.001	A-AC
22	P1-AFP vs. Solvent	257.1	Yes	<0.001	<0.001	C-AC
23	P1-IVA vs. Solvent	194.3	Yes	0.002	<0.001	E-AC
24	P1-IND vs. Solvent	150.3	Yes	0.008	0.008	G-AC
25	P1-BN vs. Solvent	190.4	Yes	0.002	0.001	I-AC
26	P1-PIP vs. Solvent	160.0	Yes	0.005	0.005	K-AC
27	P1-FPBA vs. Solvent	163.7	Yes	0.005	0.004	M-AC
28	P1-UR vs. Solvent	143.7	Yes	0.01	0.01	O-AC
29	P1-PEG4 vs. Solvent	161.3	Yes	0.005	0.005	Q-AC
30	P1-SAL vs. Solvent	199.2	Yes	0.002	<0.001	S-AC
31	P1-AC vs. Solvent	186.3	Yes	0.002	0.001	U-AC
32	P1-PYRR vs. Solvent	128.2	Yes	0.02	0.02	W-AC
33	P1-THB vs. Solvent	45.53	No	0.20	0.45	Y-AC
34	P1-PFB vs. Solvent	137.7	Yes	0.01	0.02	AA-AC

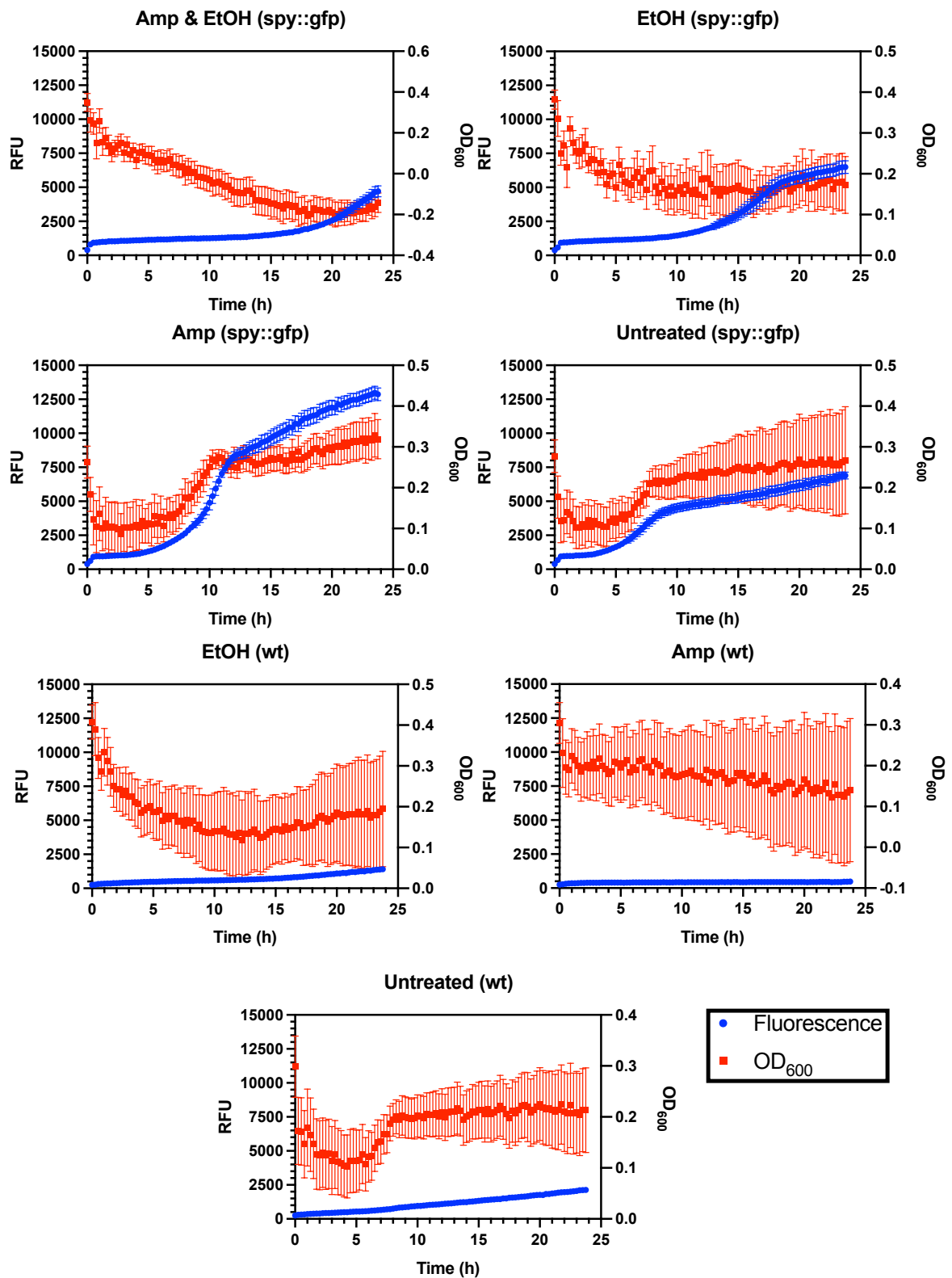
S.I. Figure 3.7. Results of 1-way ANOVA for total measured fluorescence in *csgB::gfp* experiments (AUC) measurements. Analysis performed in GraphPad 9.



S.I. Figure 3.8. Linear calibration plot used to calculate fucose concentration from absorbance.



S.I. Figure 3.9. Linear calibration plot used to calculate glucosamine (GlcN) concentration from absorbance.



S.I. Figure 3. 10. Individual growth curves (red squares) and GFP expression (blue dots) in *E. coli* MC4100 transformed with *pSPY*, grown in LB media for 24 h, 30 °C, 150 rpm. Error bars = s.d. ($n=3$)

Chapter 4 – Testing biocatalytic formation of 5-fluoro-L-tryptophan with recombinant polymer-induced biofilms

4.0 Introduction

Many metal catalysts are transition and/or precious metals are non-renewable sources. In addition, chemocatalysts suffer from low activity and often require high temperatures, pressures, and pH extremes to achieve sufficient product formation.¹ Furthermore, many chemocatalytic reactions require oxygen free conditions and so catalytic activity is often lost compromised from oxidation. Metal catalysts in chiral synthesis often use bulky hydrophobic ligands limiting catalysts to organic solvents. The harsher conditions employed by traditional chemocatalysis inflicts a large environmental burden from harmful waste in addition to increased process costs from increased energy consumption and control measures.²⁻⁴

Production of fine chemicals using biocatalysis is highly attractive as it circumvents the need for non-sustainable practices such as precious metal catalysts, organic solvents, high-pressures and temperatures. Biocatalysis can be defined as the use of an organism or its components (enzymes) to catalyse a chemical reaction. Biocatalytic reactions are performed using purified enzymes in solution, immobilised enzymes, or whole-cell biocatalysis. Although enzymes have been successfully applied in an array of different chemical reactions they are frequently limited by their ease of denaturation. Enzyme denaturation occurs when changes to protein folding causes a structural change to the enzyme active site, as it is no longer complementary to its substrate the catalytic activity is compromised.⁵ Denaturation often occurs when the enzyme is subject to atypical environmental conditions such as extreme temperature, pH, ionic strength, and organic solvents.⁶ Though enzyme immobilisation can improve stability, catalytic activity may be compromised due to detrimental alterations to the protein structure.⁷ Adsorptive methods are less denaturing; however, immobilised biocatalysts are prone to leaching into the reaction media.⁸ Therefore, biocatalyst recyclability is reduced,

compromising process longevity which limits long-term process economics. Furthermore, a critical factor not considered is that many 'industrially relevant' biocatalysts e.g., ketoreductases (KRED) or alcohol dehydrogenases (ADH) are redox reactions^{9,10}. Biocatalytic redox reactions necessitate stoichiometric co-factor supplementation to act as an electron source e.g. NADPH. This becomes economically unfeasible due to the extremely high costs associated with co-factor synthesis. Costs can be mitigated with the design of an enzyme cascade capable of co-factor regeneration (**Figure 4.1**). However, this remains a laborious, time-consuming, and expensive strategy due to the requirement of multiple purified enzymes.¹¹ For 'greener' chemical technologies like biocatalysis to become more widely adopted in industry, it is critical that its process economics surpass those of traditional chemical-based methods.

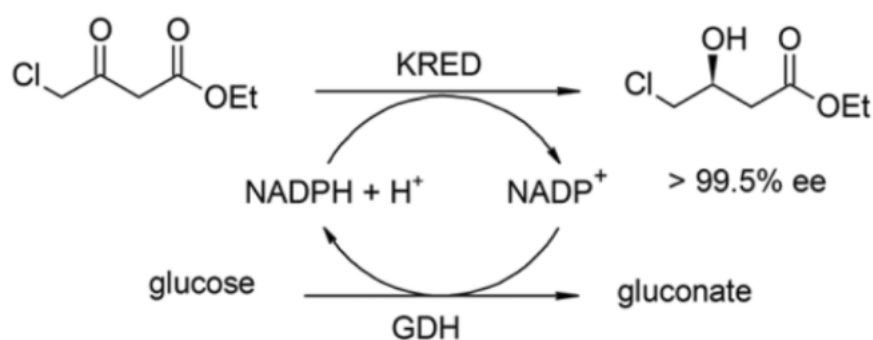


Figure 4.1. NADPH-dependent reduction of ethyl-4-chloroacetoacetate by a ketoreductase (KRED). NADPH co-factor regeneration by the secondary enzyme glucose dehydrogenase (GDH)³

An alternative to using immobilised enzymes is to utilise whole-cells as the functional catalyst. The combination of a catalytic and living system encompassed by whole-cell biocatalysis provides considerable advantages as the enzyme is protected from external stresses by the cell membrane/ cell envelope. Additionally, the organism can continually produce the biocatalytic enzyme and any necessary co-factors, simplifying process design.¹² *In vivo*

synthesis negates downstream purification and formulation of the enzyme product, further reducing processing costs. It is estimated that the cost of a whole-cell biocatalytic process is approximately 10% of that of a purified enzyme.¹¹ Costs are further minimised as whole-cell biocatalytic processes generally bypass the need for co-factor supplementation as the enzymatic reaction occurs as part of the cells' metabolism.

Whole-cell biocatalysis have already been successfully applied in industrial processes. For instance, expression of nitrile hydratase in *Rhodococcus rhodochrous* enables the industrial synthesis of acrylamide from acrylonitrile. Extremely high yields and productivity (99.99%, $\leq 2 \text{ kg L}^{-1} \text{ d}^{-1}$ respectively) in the biocatalytic process far surpass the efficiency of Cu catalyst-based syntheses.² Biocatalytic industrial scale production of acrylonitrile by *R. rhodochrous* now measures in at approximately 650 000 tonnes per annum.^{2,13} However, like enzymes non-native pH, temperature, or organic solvents maybe cytotoxic. This reduces catalytic activity due to a decline in viable cell numbers and metabolic activity of individual cells.¹¹ As with purified enzymes, conditions for whole-cell biocatalysis are dependent on cell viability. Although bacterial immobilisation in polymeric substrates like sodium alginate, agar, and hyaluronic acid^{14,15} can counteract potentially deleterious conditions, whole-cell immobilisation suffers from mass-transfer limitations reducing process efficiency.¹⁶ Moreover, continued cell growth can compromise the immobilisation material negating its use as cells become exposed to the culture milieu.

Recently, the potential application of biocatalytic biofilms has been explored as an alternative strategy to overcome the issues experienced with free-enzyme and whole-cell based

biocatalysis. The biofilm ECM helps protect the cells from the environmental stresses such as pH and temperature extremes as well as increased tolerance of organic solvents. Channelled mushroom-like structures and high local cell density promotes mass-transfer due to the establishment of large diffusion gradients within the biofilm.¹⁷ Moreover, due to the self-immobilisation and slow growth rates, biofilms are well adapted for applications in continuous processing greatly improving process economy and scalability.¹⁸

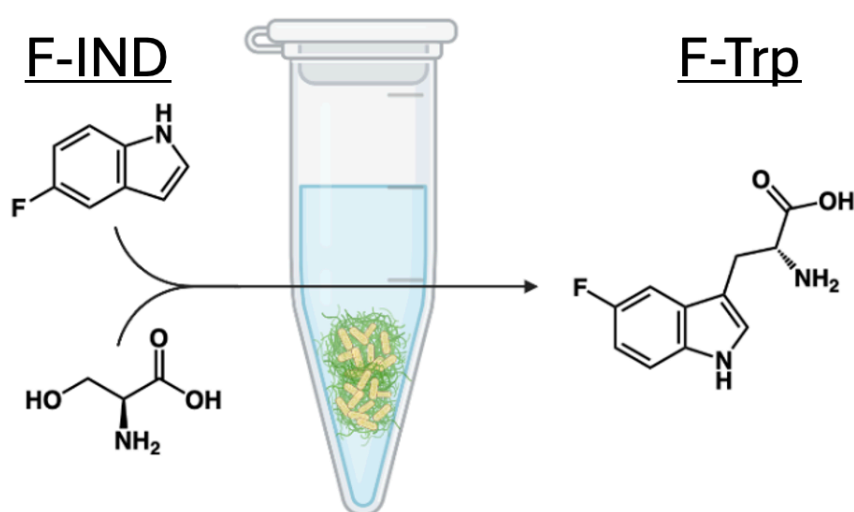


Figure 4.2 Schematic showing biocatalytic reaction of 5-fluoroindole and L-serine to form 5-fluorotryptophan by polymer microbial complexes of *E. coli* MC4100

In the previous chapter it was shown that poly(*N*-acetylene hydrazinecarboxamide) (P1) could successfully nucleate biofilm growth in *E. coli* MC4100 by induced aggregation and ECM production. To continue this work, we looked whether the resultant polymer-microbial complexes (PMC) could be applied in the sphere of biocatalysis. To test catalytic activity the synthesis of 5-fluorotryptophan (5F-Trp) from 5-fluoroindole (5F-Ind) and serine was chosen as the model reaction (**Figure 4.2**). Halotryptophans are an important precursor in medicinal chemistry for the synthesis of anti-tumour agents like rebeccamycin or the development of modified peptides for NMR analysis.^{19,20} *E. coli* MC4100 was transformed with the

recombinant high-copy number plasmid pSTB7 encoding for constitutive expression of tryptophan synthase (TrpBA) native to *Salmonella enterica*.^{21–24} Previous in-group research demonstrated that biocatalytic transformation of 5-halotryptophans (F, Cl, and Br) is possible in *E. coli* biofilms.^{22,24} Initial studies utilised 7-day old mature *E. coli* biofilms adhered to poly-L-lysine spin coated glass slides. The recombinant biofilms considerably outperformed the cell-free lysate and planktonic cultures in both halotryptophan formation and catalytic longevity. The long-term performance of *E. coli* biocatalytic biofilms was due to constant regeneration of the recombinant enzyme over several days.²² Further developments of this research first saw the use of recombinant polymer-induced aggregates of *E. coli* PHL644 and MC4100 expressing TrpBA. MC4100 showed similar efficiency in 5F-Trp formation to PHL644 despite its lower metabolic activity.²³

As a proof-of-concept cultures of *E. coli* MC4100-pSTB7 were treated with P1 formulations to induce aggregation and EPS formation. The PMCs were cultured for 48h in 1× M63/ phosphate buffer before removal of culture media and gentle washing to remove planktonic cells, the cell media was replaced with a reaction buffer containing 1 mM 5-fluoroindole and 7 mM serine and cultured for a further 24h. Given that no aggregation is observed in non-polymer treatments all planktonic cultures were centrifuged prior to the media exchange. The biocatalytic activity of the PMCs were determined by the quantitative consumption of 5F-Ind and formation of 5F-Trp via HPLC.

4.1 Experimental

4.1.1 Bacterial strains and plasmids

E. coli K-12 strains MC4100: araD139 Δ (argF-lac)U169 rpsL150 relA1 flbB5301 deoC1 ptsF25rbsR.²⁵ Recombinant pSTB7, a pBR322-based plasmid containing the *Salmonella enterica* serovar Typhimurium TB1533 *trpBA* genes and encoding ampicillin resistance, was purchased from the American Type Culture Collection (ATCC 37845).²⁶ *E. coli* strains were transformed with plasmids using the standard heat shock method.

4.1.2 Culture set-up

General cell treatment performed as described in **Section 3.1.1**. Growth media was supplemented with 10 μ g/mL tetracycline. *E. coli* MC4100 pSTB7 was cultured in 1:1 (v/v) 0.1 M $\text{KH}_2\text{PO}_4/\text{K}_2\text{HPO}_4$ (1mL) and 1 \times M63 at 30 $^{\circ}\text{C}$, 150 rpm for 24 h.

4.1.3 Biocatalytic Screening

Method taken from literature.²³ After 24h, for the polymer-treated cultures the planktonic cells were removed by supernatant was removed by pipetting and then replaced carefully with sterile 0.1M $\text{K}_2\text{HPO}_4/\text{KH}_2\text{PO}_4$. This washing step was performed twice to maximise planktonic cell removal before addition of 1mL reaction buffer (100 mM KH_2PO_4 , 15 mM $(\text{NH}_4)_2\text{SO}_4$, 1 mM MgSO_4 , 1.8 μ M FeSO_4 , 10mM glucose, 0.5% thiamine (w/v), 40 $\mu\text{g mL}^{-1}$ L-cysteine adjusted to pH 7 with 5M KOH). As there was no aggregate formation in the planktonic cultures, no washing steps were performed and the cultures were centrifuged (1 min @ 14000 $\times g$), the supernatant removed and then replaced with the reaction buffer. The biocatalytic reaction was then performed for an additional 24 h, incubated at 30 $^{\circ}\text{C}$ at 150 rpm for 24h. After an additional 24 h, all cell cultures were centrifuged (5 min @ 14000 $\times g$) after which the supernatant was removed and filtered through a 0.22 μm PTFE filter to remove any cellular contaminants and stored at -20 $^{\circ}\text{C}$ prior to analysis.

4.1.4 HPLC Analysis of Reaction Buffer Supernatant

Method taken from literature.²³ The relative concentrations of 5-fluoroindole were measured using HPLC by monitoring the decrease in sample peak integral corresponding to 5-fluoroindole from a 1 mM 5-fluoroindole control sample, and the relative increase in sample peak integral corresponding to 5-fluorotryptophan by comparing with the peak integral corresponding to 1 mM 5-fluorotryptophan sample in the reaction buffer (theoretical maximum yield from 1 mM 5-fluoroindole). Samples were analysed using a Shimadzu HPLC with a C-18 column at 0.7 mL min⁻¹. A UV detector was used for the analysis. Gradient: Solvent A (Water 0.1% formic acid), Solvent B (Methanol 0.1% formic acid). 10% Solvent B, 30 s; 10-90% Solvent B over 12 min, hold 90% Solvent B for 2.5 min, 90-10% Solvent B over 1 min, hold 10% Solvent B for 5 min.

4.2 Results and Discussion

To probe the efficiency of the PMCs as biocatalysts three metrics were calculated; indole depletion (D), 5F-Trp yield (Y) and the reaction efficiency (E) as described by **Equations 1 – 3**.²⁴

$$D = 1 - \left(\frac{[5F - Ind]_{24}}{[5F - Ind]_0} \right) \times 100 \quad (1)$$

$$Y = \left(\frac{[5F - Trp]_{24}}{[5F - Ind]_0} \right) \times 100 \quad (2)$$

$$E = \left(\frac{Y}{D} \right) \times 100 \quad (3)$$

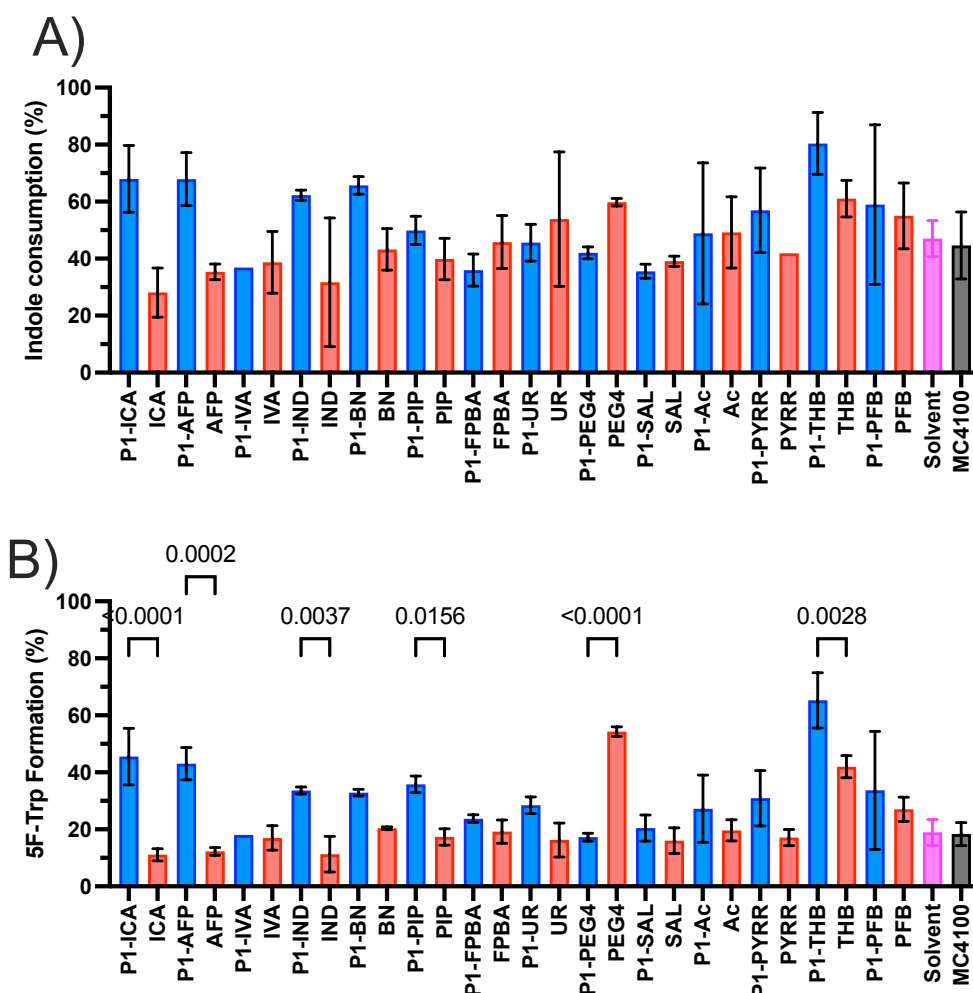


Figure 4.3 Plot of 5-fluoroindole conversion of polymer treated cultures and non-polymer controls. B) Plot of 5-fluorotryptophan conversion of polymer treated cultures and non-polymer controls. Statistical analysis performed using one-way ANOVA with Tukey's multiple comparisons post-hoc analysis with a false-discovery rate applied for multiple comparisons.

Statistically significant results marked on plots ($q \leq 0.05$). All significant polymer-aldehyde comparisons also showed a statistically significant difference from the untreated controls, though these have been omitted from the plots for clarity. No statistically significant difference in 5F-IND consumption was noted for any of the tested conditions.

Despite greatly enhanced 5F-Trp formation, none of the P1 formulations produced any statistically significant increase in indole consumption relative to the aldehyde or untreated controls (**Figure 4.3A**). However, many polymeric formulations readily showed a large increase in consumed 5F-Ind relative to their aldehyde controls. Moreover, several aldehyde-treated cultures showed poorer 5F-Ind uptake compared to the untreated controls. This suggested that these aldehydes proved detrimental to cell uptake of 5F-Ind. The largest observed difference in 5F-Ind uptake between polymer and aldehyde occurred with **P1-ICA**, **P1-AFP**, **P1-Bn** and **P1-THB** where total 5F-Ind consumption ranged between 60 – 80%. All non-polymer controls whether aldehyde (except for PEG₄), solvent, or untreated cultures showed comparable 5F-Ind ranging from 30 – 50% consumption. 5F-Ind consumption in the planktonic cultures is much higher in this work compared to prior research (~20%). Different reagent consumption in this work maybe due to the planktonic cultures being centrifuged prior to the biotransformation assay here. It was previously shown that reaction rates in planktonic whole-cell biocatalysis were initially faster than biofilms due to the reduced mass-transfer limitations.²⁴ In these previous experiments, haloindole and halotryptophan concentrations were measured at multiple points across the timescale of the experiment rather than just the endpoint as here. Therefore, it is reasonable to suggest that the comparably high 5F-Ind consumption in the planktonic cultures may be due to the increased reactant diffusion rates relative to the biofilm aggregates. Cellular indole uptake is believed to primarily occur via diffusion through the cell membrane.²⁷ Organic solvents like DMSO are shown to increase

membrane permeability,^{27,28} this could enhance 5F-Ind uptake due to increase diffusion rates. However, the effect of organic solvent may be more limited in the biofilm cultures due to enhanced aggregation and ECM production. Lower permeation from solvents would further reduce relative 5F-Ind diffusion. However, given that this is a single time-point measurement it cannot be clearly concluded on the role of 5F-Ind diffusion into the PMC. Future works would benefit from performing multiple samplings to generate kinetic profiles which would give better indication of how the different physiological states affect 5F-Ind uptake.

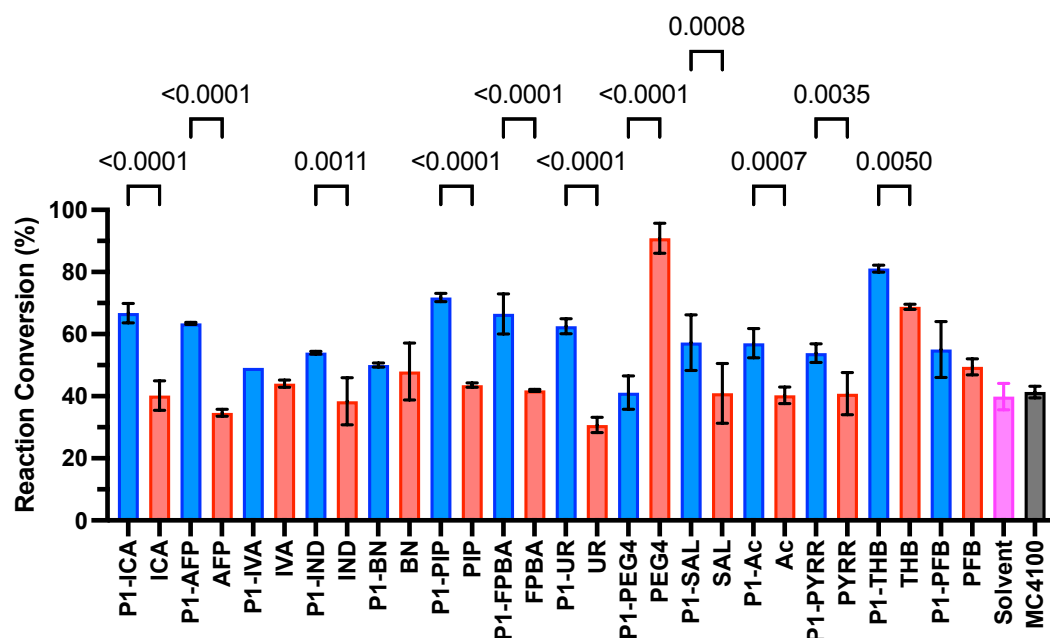


Figure 4.4 Plot of reaction conversion of polymer treated cultures and non-polymer controls. Statistical analysis performed using one-way ANOVA with Tukey's multiple comparisons post-hoc analysis with a false-discovery rate applied for multiple comparisons. Statistically significant results marked on plots ($q \leq 0.05$). All significant polymer-aldehyde comparisons also show a statistically significant difference from the untreated controls, though these have been omitted from the plots for clarity. No statistically significant difference in indole consumption was noted for any of the tested conditions.

Although planktonic and biofilm cultures alike showed comparable 5F-Ind consumption, several polymer-treated cultures (**P1-ICA**, **P1-AFP**, **P1-IND**, **P1-PIP**, and **P1-THB**) produced a statistically significant increase in 5F-Trp formation relative to the planktonic cultures (**Figure**

4.3B). Furthermore, all PMC cultures except **P1-IVA**, **P1-BN**, **P1-PEG₄**, and **P1-PFB** showed significantly higher yields compared to the respective aldehyde-treated cultures (**Figure 4.4**). Aggregate size, biomass (by crystal violet and turbidimetry) and metabolic activity were all positively correlated with 5F-Ind consumption and 5F-Trp conversion (**Figure 4.5**).

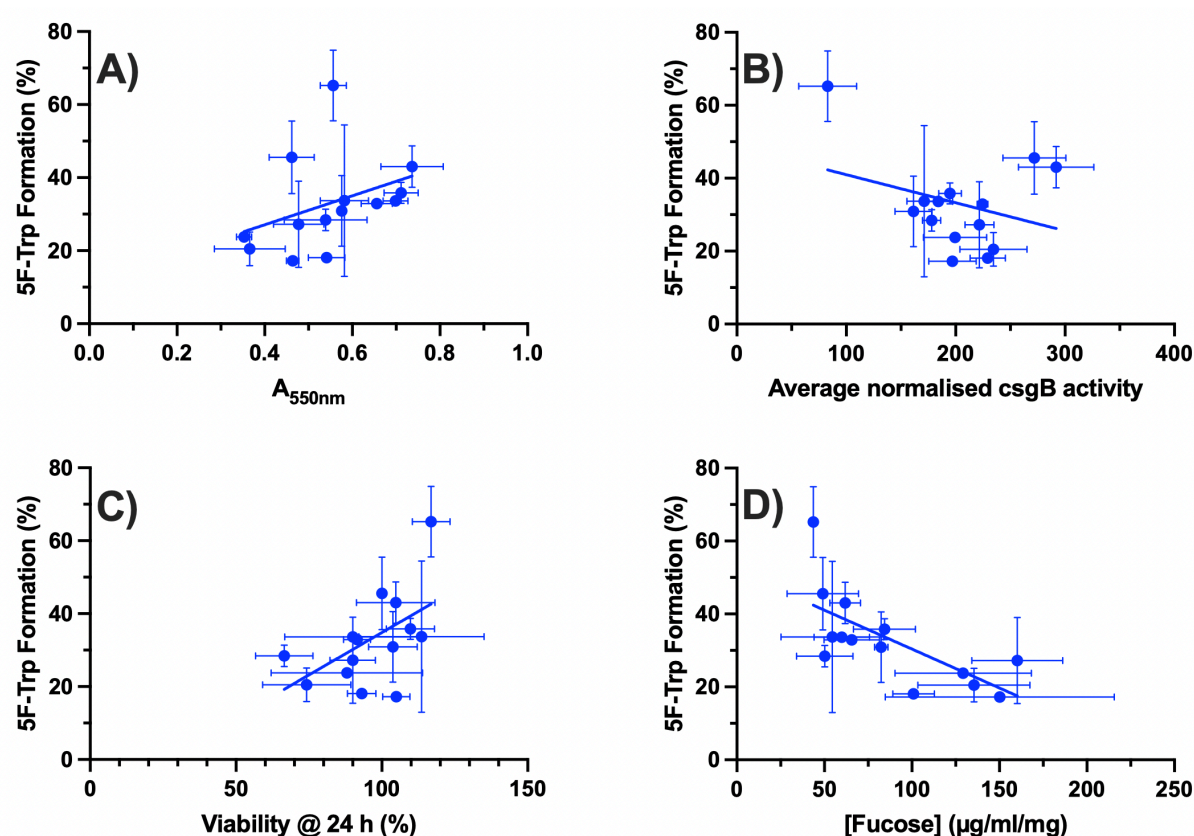


Figure 4.5. Correlations of 5F-Trp formation with measured biological parameters following treatment with P1 formulations. A) Aggregate sizing by crystal violet staining; B) csgB expression; C) cell viability/metabolic activity; D) colanic acid production.

Logically, with increased aggregation there are more metabolically active cells present to catalyse the conversion of 5F-Ind, overall increasing yields. Alternatively, increased aggregation may cause a shift in Trp metabolism due to a biofilm-like response (see later). Increased aggregation better protects the cells against chemical treatment from the reaction buffer. In contrast, total colanic acid (as measured in proxy) was negatively correlated with 5F-Trp

formation. There is no obvious correlation with curli expression, due to the extremely high productivity of the **P1-THB** cultures and the very low curli production by the same treatment. If **P1-THB** is removed as an outlier, and a linear regression analysis is performed there shows a slight positive correlation with *csgB* expression although it is not statistically significant. However, in this context ECM production is negatively co-correlated with aggregated biomass i.e. lower ECM was observed with larger bacterial aggregates. Hence, it is impossible to distinguish whether differences in catalytic activity arise from increased biomass or reduced ECM. However, it is likely that ECM production is only partly responsible for the observed trends in the biotransformation. Limited ECM synthesis may facilitate reagent/product diffusion between the cells and reaction media whilst still promoting a biofilm phenotype. Large clusters of metabolically active cells can more effectively utilise 5F-Ind as lower relative ECM formation promotes reactant diffusion into the cell. Increased substrate uptake would likely improve product formation. These results are consistent with previous literature, where larger MC4100 aggregated biomass induced by hydrophobic aromatic polymers produced the highest yields of 5F-Trp.²³ In contrast to surface-adhered biofilms, the **P1**-induced aggregates of *E. coli* MC4100 used in this work performed noticeably better.²⁴ The glass adhered MC4100 biofilms reported by Perni *et al.* exhibited moderate 5F-IND consumption (~40%) but very poor 5F-Trp yields and reaction selectivity (~20% and 10% respectively) after 24 h.²⁴ In this work the top 5 performing formulations showed 5F-IND consumption ranged from 60-80%. Furthermore, 5F-Trp yields, and reaction efficiencies reached 35-60% and 50-80% respectively. As the PMCs are suspended in solution rather than fixed to a surface this may enhance reactant diffusion due to improved mixing compared to surface adhered cells.

The major exception to the biofilm cultures out-performing the planktonic cultures in the above reaction parameters is PEG₄-aldehyde. In all tested metrics, PEG₄-aldehyde significantly out-performed **P1-PEG₄** and all other polymer formulations. Increased 5F-Ind uptake by PEG₄-aldehyde may be due to possible chelation and sequestration of cations within the bacterial outer membrane (OM). Chelation with OM constituents would likely increase membrane porosity like DMSO treatment, facilitating 5F-Ind ingress. However, the considerable increase in 5F-Trp formation and reaction yields by PEG₄-aldehyde relative to the other treatments is unlikely to be explained by greater 5F-Ind uptake alone. It is more plausible that differences in 5F-Ind conversion likely arise due to shifts in cell metabolism due to the relative intracellular concentrations of 5F-Ind and 5F-Trp which would in turn influence the respective permeases responsible for their import and export (see next). PEG₄-aldehyde may promote conversion due to an effect within any of these possible mechanisms. However, a mechanistic understanding remained outside the scope of this project and so a conclusion cannot be made.

Although we can only speculate on the different 5F-Trp yields between planktonic cultures and the PMCs, it is improbable that these differences are due to reduced viability. Previous data showed no significant reduction in cell viability following polymer treatment (see **3.6.1**). Therefore, differences in biocatalytic performance are potentially due to different protein expression profiles of membrane proteins involved in indole and tryptophan import/export. *E. coli* produces native tryptophanase (TnaA) which hydrolyses tryptophan into pyruvate and ammonia. Previously, planktonic *E. coli* cultures were demonstrated to upregulate TnaA expression in the presence of exogenous tryptophan devoid of catabolic repression.²⁹ TnaA expression is also induced at the onset of stationary phase dependent σ_s and Crl activity.^{30,31}

Further evidence suggests that TnaA is additionally regulated by CRP-cAMP in response to nutrient-limited conditions;³² upregulated TnaA expression permits tryptophan catabolism for ATP generation. Therefore, an excess of intracellular tryptophan in conjunction with starved conditions could prove detrimental to reaction yields due to a metabolic shift favouring indole reformation via increased TnaA expression.

Intracellular tryptophan levels in *E.coli* are maintained by several permeases (membrane transport proteins) (Figure 4.6). Mtr, TnaB, and AroP are responsible for the import of aromatic amino acids including tryptophan,^{33,34} whereas YddG exports tryptophan.³⁵ In the presence of tryptophan, cellular Mtr is repressed by TrpR,³⁶ whilst AroP repression occurs via TyrR³⁷ protein preventing further tryptophan influx. Although Mtr and AroP participate in tryptophan transport, TnaB is considered the most essential permease for tryptophan import from its necessity regarding catabolic growth on tryptophan. As TnaB is within the *tnaAB* operon it is under the same regulatory mechanisms as TnaA.³⁸ Similarly, active indole efflux from the cell is performed by Mtr again and AcrEF.^{39,40} One hypothesis is that differential expression of indole and/or tryptophan permeases between biofilms and planktonic cultures alter intracellular indole and/or tryptophan concentrations. Therefore, altered permease activity and relative changes in intracellular indole and tryptophan would influence the catalytic performance of biofilm and planktonic cultures. In the absence of tryptophan efflux, increased TnaA expression would favour 5F-Ind reformation. Domka *et al.*, found that AcrEF and YddG were significantly upregulated in mature biofilms compared to planktonic cultures and early biofilms,⁴¹ where the authors argue that an accumulation of intracellular indole hinders biofilm formation.^{41,42} Furthermore, the same study showed that TrpBA is upregulated in developing

and mature biofilms, whereas TnaAL expression is reduced compared to the early biofilm (~4 h)⁴¹. Given that TnaB is under the same transcriptional regulation as tnaA, it would be expected that TnaB expression is also repressed within the biofilm. To the best of our knowledge there are no reports on differential AroP expression between planktonic and biofilm cultures. Therefore, potential increased YddG expression in the PMCs would prevent intracellular accumulation of 5F-Trp. Limited intracellular 5F-Trp concentrations would minimise induction TnaA expression thereby favouring product formation.

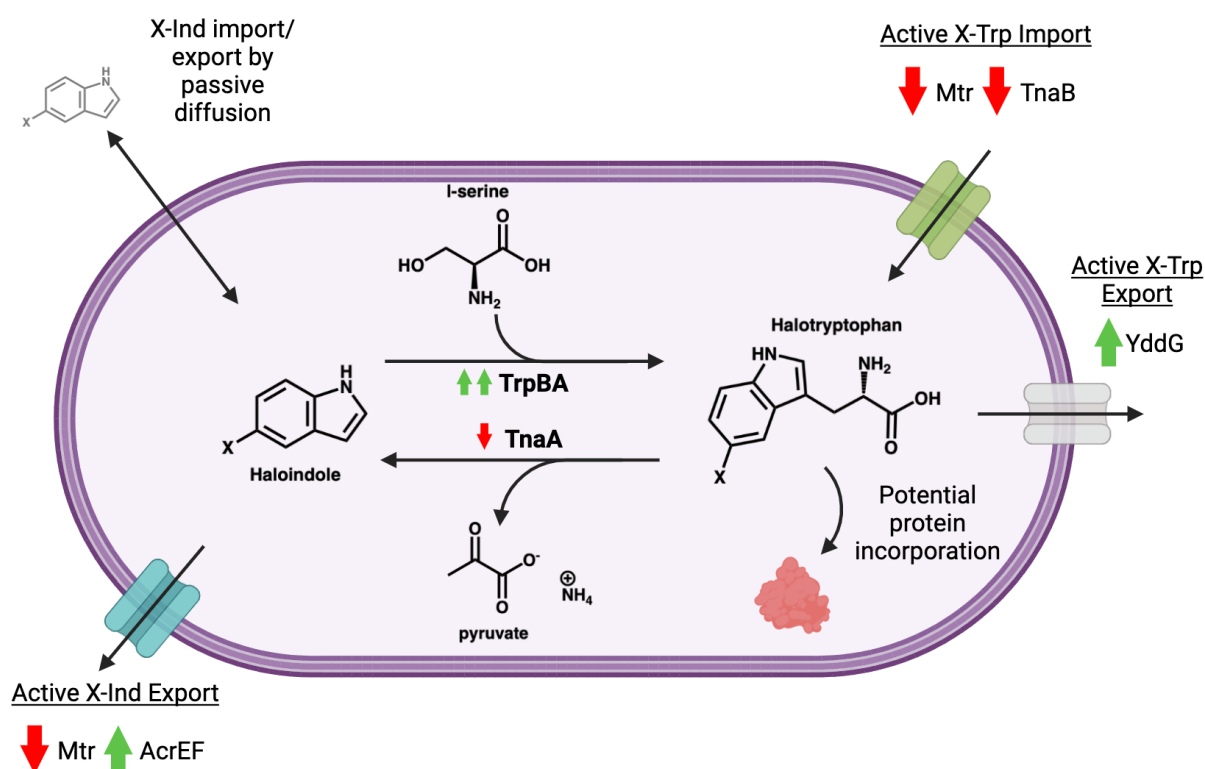


Figure 4.6. Overview of possible indole and tryptophan import and export mechanisms in *E. coli*. Arrows represent whether the protein is up- (green arrow) or down-regulated (red arrow) within a biofilm relative to planktonic cultures. The double green arrow adjacent to TrpBA represents constitutive overexpression by recombinant pSTB7. Produced in Biorender.

If we review our tested system conditions, the biocatalytic reaction is performed in stationary phase cultures with no additional carbon source for growth (e.g., glucose). Under these conditions, it would be reasonable to expect that TnaA is upregulated favouring 5F-Ind

formation. However, given that TrpBA is constitutively overexpressed this theoretically should favour the 5F-Trp formation. Over the course of this experiment, it is reasonable to consider that the reversibility of this reaction is highly dynamic due to fluctuations in relative intracellular concentrations of 5F-Ind and 5F-Trp. In this case L-serine is reduced as it is not reformed in the 5F-Trp \rightarrow 5F-Ind reaction, which would likely diminish the observed yields. On the other hand, for the polymer-treated cultures 5F-Trp export and import is respectively up and downregulated due to increased expression of YddG and repression of TnaB/Mtr. Therefore, accumulation of intracellular 5F-Trp concentrations compared to the planktonic cultures. Within the biofilm, reduced intracellular accumulation of 5F-Trp would minimise relative TnaA expression favouring product formation due to more effective utilisation of L-serine. This theory is somewhat substantiated given that reaction efficiency (E) was significantly higher in 70% of the polymer-treated cultures. Future work should investigate the mechanistic principles of these systems, possibly via transcriptomic analysis of various permeases involved.

Potential disparities in recombinant plasmid stability between the biofilm and planktonic cultures may have affected catalytic activity and subsequent product titres. Recombinant biofilms are shown to possess increased plasmid stability compared to planktonic bacteria in the absence of any selective pressure.^{43,44} It is postulated that diminished grow rates in biofilm cultures reduce the metabolic burden of plasmid maintenance in recombinant cultures compared to planktonic cells. Therefore, biofilms act as a plasmid 'sink' due to greater retention.⁴³ For example, robust biofilm forming strain like *E. coli* ATCC 33456 expressing recombinant eGFP displayed increased plasmid retention after 6 days (90% positive) whereas

50% of cells had lost the plasmid by 48h in the planktonic chemostat cultures.⁴⁴ Similar findings were also observed in *P. aeruginosa* biofilm that again showed minimal plasmid loss after 4 days in the absence of any antibiotic selection.⁴³ No antibiotics are included in the reaction buffer; hence, it is plausible that plasmid retention is favoured in the PMCs. Higher plasmid retention would likely give higher catalytic activity from increased intracellular TrpBA expression. Given the culture longevity and glucose-limited conditions, it is likely that σ_s /CRP-cAMP mediated upregulation of TnaA occurs in both PMCs and planktonic cultures. However, constitutive overexpression of TrpBA by pSTB7 positive bacteria likely exceeds elevated TnaA expression favouring 5F-Trp formation. Hence, if plasmid retention is higher in the PMCs, recombinant TrpBA expression is increased favouring product formation compared to planktonic cultures. Therefore, higher yields obtained in biofilms may be a combination of increased TrpBA expression and increased 5F-Trp efflux which limits TnaA-mediated catabolism.

Differences in performance between the polymer formulations would likely result from one or more of the above transport mechanisms and/or plasmid stability being affected in a currently unknown way. Likewise, this could explain why PEG₄-aldehyde treated cultures were the most productive, although no clear conclusion can be made it is likely that one of the above mechanisms is greatly altered by this treatment. In future, to distinguish possible effects of the polymer and/or aldehyde treatment on the bacterial genotype it would be useful to conduct genomic testing following polymer treatment and compare between the different treated cultures. This would permit a better mechanistic understanding between the effect of the material on the bacterial phenotype/genotype and the subsequent effect on catalytic activity.

Additional future work regarding biocatalytic optimisation would benefit from the development of various knockout strains which alter the 5F-Trp membrane transport and minimise its intracellular accumulation. For instance, a Δmtr or $\Delta aroP$ strain would limit 5F-Trp import into the bacteria which should help minimise relative TnaA expression. Conversely, a YddG overexpresser strain could export 5F-Trp more effectively which simultaneously minimises intracellular accumulation and improves product recovery. It is possible to develop a $\Delta tnaA$ strain, however given that TnaA is demonstrated to play a role in *E. coli* biofilm formation use of any knockout strains would likely greatly compromise the ability to form biofilms in these knockout strains.^{24,45}

4.3 Conclusions

Using a variety of P1 formulations, *E. coli* MC4100 was aggregated into biofilm-like structures that effectively catalysed the synthesis of 5-fluoro-L-tryptophan from 5-fluoroindole. The biocatalytic ability of the biofilms is dependent on the number of aggregated cells and their metabolic activity (indicated by cell viability). In general, much higher yields were achieved in the PMCs compared to planktonic cultures. The increased productivity of biofilm cultures may result from increased plasmid retention producing higher TrpBA expression driving product formation. Furthermore, product efflux is promoted whilst the influx is reduced likely due to differential gene expression in biofilms.

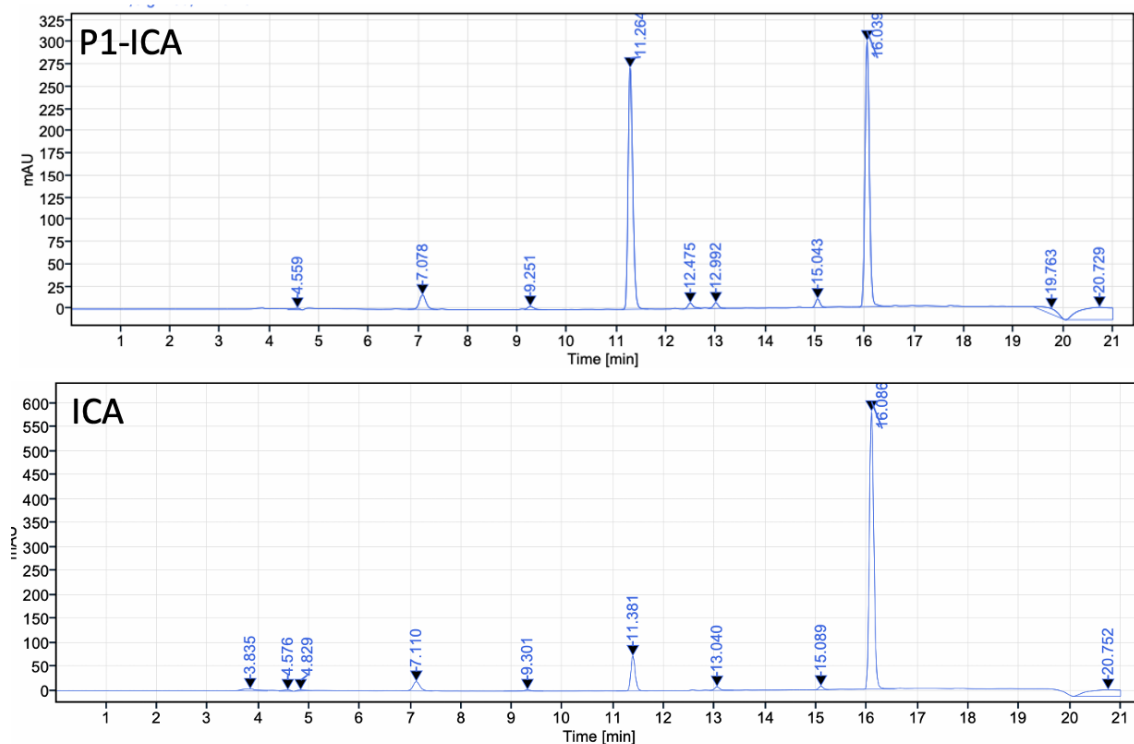
After this initial proof-of-concept it would be beneficial to expand the scope of biocatalytic reactions tested in future. There exist many examples of different industrially relevant biocatalytic enzymes like alcohol dehydrogenases, nitro reductases and transaminases to name but a few. Any of which could be easily applied in our system here through simple genetic manipulation. The system shown here could also be tested for more complex biocatalytic reactions e.g. biocatalytic multi-step one-pot synthesis. Furthermore, a considerable advantage to biocatalytic biofilms is their catalytic longevity compared to their planktonic counterparts. Therefore, expanding the duration of the biocatalytic reaction would be interesting to see whether these polymer-driven biofilms also possess the same catalytic longevity as traditional surface-adhered biofilms.

4.4 Bibliography

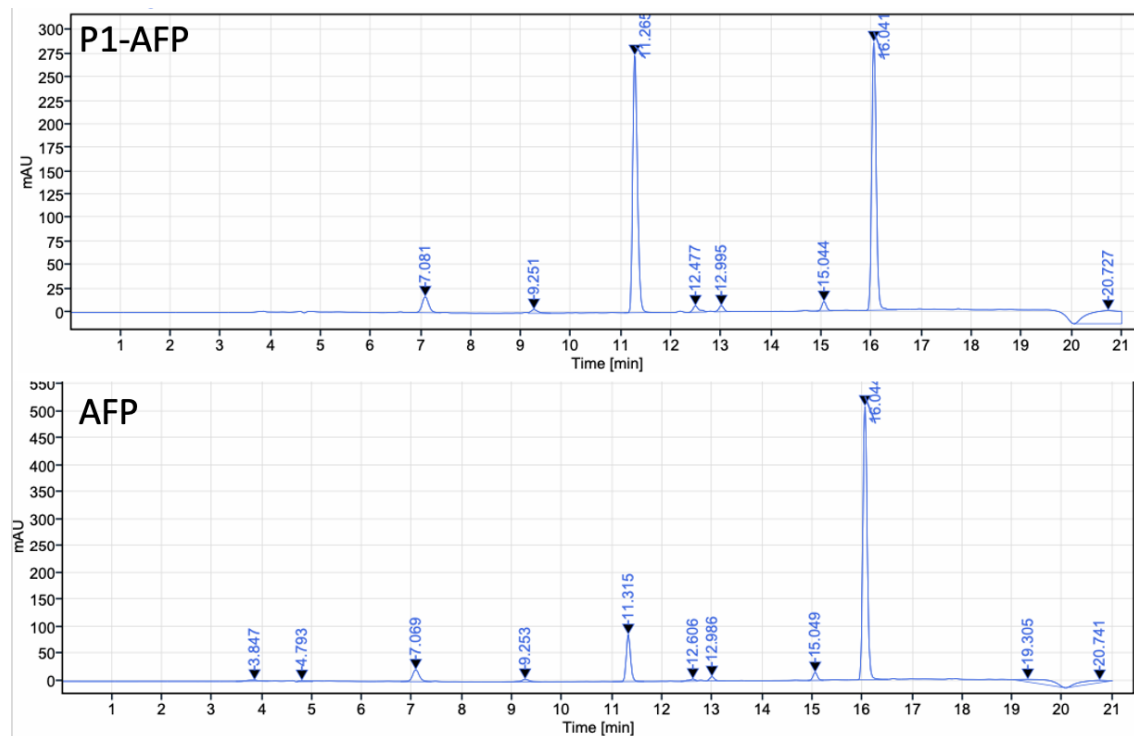
- 1 B. Hauer, *ACS Catal*, 2020, **10**, 8418–8427.
- 2 E. M. M. Abdelraheem, H. Busch, U. Hanefeld and F. Tonin, *React Chem Eng*, 2019, **4**, 1878–1894.
- 3 R. A. Sheldon and J. M. Woodley, *Chem Rev*, 2017, **118**, 801–838.
- 4 P. N. Devine, R. M. Howard, R. Kumar, M. P. Thompson, M. D. Truppo and N. J. Turner, *Nat Rev Chem*, 2018, **2**, 409–421.
- 5 P. E. V. Paul, V. Sangeetha and R. G. Deepika, in *Recent Developments in Applied Microbiology and Biochemistry*, Elsevier, 2019, pp. 107–125.
- 6 J. Ge, D. Lu, M. Yan and Z. Liu, in *Comprehensive Biotechnology*, Elsevier, 2011, pp. 925–932.
- 7 S. S. Nadar and V. K. Rathod, *Int J Biol Macromol*, 2020, **152**, 1108–1112.
- 8 M. L. Ferreira, in *Biocatalyst Immobilization*, Elsevier, 2023, pp. 365–401.
- 9 D. Kalaitzakis, J. D. Rozzell, I. Smonou and S. Kambourakis, *Adv Synth Catal*, 2006, **348**, 1958–1969.
- 10 A. S. de Miranda, C. D. F. Milagre and F. Hollmann, *Frontiers in Catalysis*, , DOI:10.3389/fcrls.2022.900554.
- 11 R. A. Sheldon and D. Brady, *Chemical Communications*, 2018, **54**, 6088–6104.
- 12 M. Schrewe, M. K. Julsing, B. Bühler and A. Schmid, *Chem Soc Rev*, 2013, **42**, 6346–6377.
- 13 H. Gröger, Y. Asano, U. T. Bornscheuer and J. Ogawa, *Chem Asian J*, 2012, **7**, 1138–1153.
- 14 J. Lu, W. Peng, Y. Lv, Y. Jiang, B. Xu, W. Zhang, J. Zhou, W. Dong, F. Xin and M. Jiang, *Ind Eng Chem Res*, 2020, **59**, 17026–17034.
- 15 D. Berillo, A. Al-Jwaied and J. Caplin, *Polymers (Basel)*, 2021, **13**, 1073.
- 16 J. M. Radovich, *Biotechnol Adv*, 1985, **3**, 1–12.
- 17 C. Beloin, A. Roux and J.-M. Ghigo, *Curr Top Microbiol Immunol*, 2008, 249–289.
- 18 M. Winn, J. M. Foulkes, S. Perni, M. J. H. Simmons, T. W. Overton and R. J. M. Goss, *Catal Sci Technol*, 2012, **2**, 1544.
- 19 E. Yeh, S. Garneau and C. T. Walsh, *Proceedings of the National Academy of Sciences*, 2005, **102**, 3960–3965.
- 20 X. Wang, P. Mercier, P.-J. Letourneau and B. D. Sykes, *Protein Science*, 2005, **14**, 2447–2460.
- 21 A. N. Tsoligkas, M. Winn, J. Bowen, T. W. Overton, M. J. H. Simmons and R. J. M. Goss, *ChemBioChem*, 2011, **12**, 1391–1395.
- 22 X. Tong, T. T. Barberi, C. H. Botting, S. V Sharma, M. J. H. Simmons, T. W. Overton and R. J. M. Goss, *Microb Cell Fact*, 2016, **15**, 180.
- 23 P. Adoni, A. Romanyuk, T. W. Overton and P. Fernandez-Trillo, *Mater Horiz*, 2022, **9**, 2592–2602.
- 24 S. Perni, L. Hackett, R. J. Goss, M. J. Simmons and T. W. Overton, *AMB Express*, 2013, **3**, 66.
- 25 O. Vidal, R. Longin, C. Prigent-Combaret, C. Dorel, M. Hooreman and P. Lejeune, *J Bacteriol*, 1998, **180**, 2442–2449.
- 26 H. Kawasaki, R. Bauerle, G. Zon, S. A. Ahmed and E. W. Miles, *Journal of Biological Chemistry*, 1987, **262**, 10678–10683.
- 27 S. Pinero-Fernandez, C. Chimerele, U. F. Keyser and D. K. Summers, *J Bacteriol*, 2011, **193**, 1793–1798.
- 28 B. Gironi, Z. Kahveci, B. McGill, B.-D. Lechner, S. Pagliara, J. Metz, A. Morresi, F. Palombo, P. Sassi and P. G. Petrov, *Biophys J*, 2020, **119**, 274–286.
- 29 K. Gish and C. Yanofsky, *J Bacteriol*, 1993, **175**, 3380–3387.

- 30 S. Lacour and P. Landini, *J Bacteriol*, 2004, **186**, 7186–95.
- 31 C. Lelong, K. Aguiluz, S. Luche, L. Kuhn, J. Garin, T. Rabilloud and J. Geiselmann, *Molecular & Cellular Proteomics*, 2007, **6**, 648–659.
- 32 P. Di Martino, R. Fursy, L. Bret, B. Sundararaju and R. S. Phillips, *Can J Microbiol*, 2003, **49**, 443–449.
- 33 C. Yanofsky, V. Horn and P. Gollnick, *J Bacteriol*, 1991, **173**, 6009–6017.
- 34 G. Li and K. D. Young, *Microbiology (N Y)*, 2013, **159**, 402–410.
- 35 V. Doroshenko, L. Airich, M. Vitushkina, A. Kolokolova, V. Livshits and S. Mashko, *FEMS Microbiol Lett*, 2007, **275**, 312–318.
- 36 J. P. Sarsero, P. J. Wookey and A. J. Pittard, *J Bacteriol*, 1991, **173**, 4133–4143.
- 37 P. Wang, J. Yang, B. Lawley and A. J. Pittard, *J Bacteriol*, 1997, **179**, 4213–4218.
- 38 C. Yanofsky, V. Horn and P. Gollnick, *J Bacteriol*, 1991, **173**, 6009–6017.
- 39 V. M. Heatwole and R. L. Somerville, *J Bacteriol*, 1991, **173**, 3601–3604.
- 40 K. Kawamura-Sato, K. Shibayama, T. Horii, Y. Iimura, Y. Arakawa and M. Ohta, *FEMS Microbiol Lett*, 1999, **179**, 345–352.
- 41 J. Domka, J. Lee, T. Bansal and T. K. Wood, *Environ Microbiol*, 2007, **9**, 332–346.
- 42 J. Domka, J. Lee and T. K. Wood, *Appl Environ Microbiol*, 2006, **72**, 2449–2459.
- 43 H. L. Røder, U. Trivedi, J. Russel, K. N. Kragh, J. Herschend, I. Thalsø-Madsen, T. Tolker-Nielsen, T. Bjarnsholt, M. Burmølle and J. S. Madsen, *NPJ Biofilms Microbiomes*, 2021, **7**, 78.
- 44 H. A. O’Connell, C. Niu and E. S. Gilbert, *Biotechnol Bioeng*, 2007, **97**, 439–446.
- 45 J. Shimazaki, S. Furukawa, H. Ogihara and Y. Morinaga, *Biochem Biophys Res Commun*, 2012, **419**, 715–718.

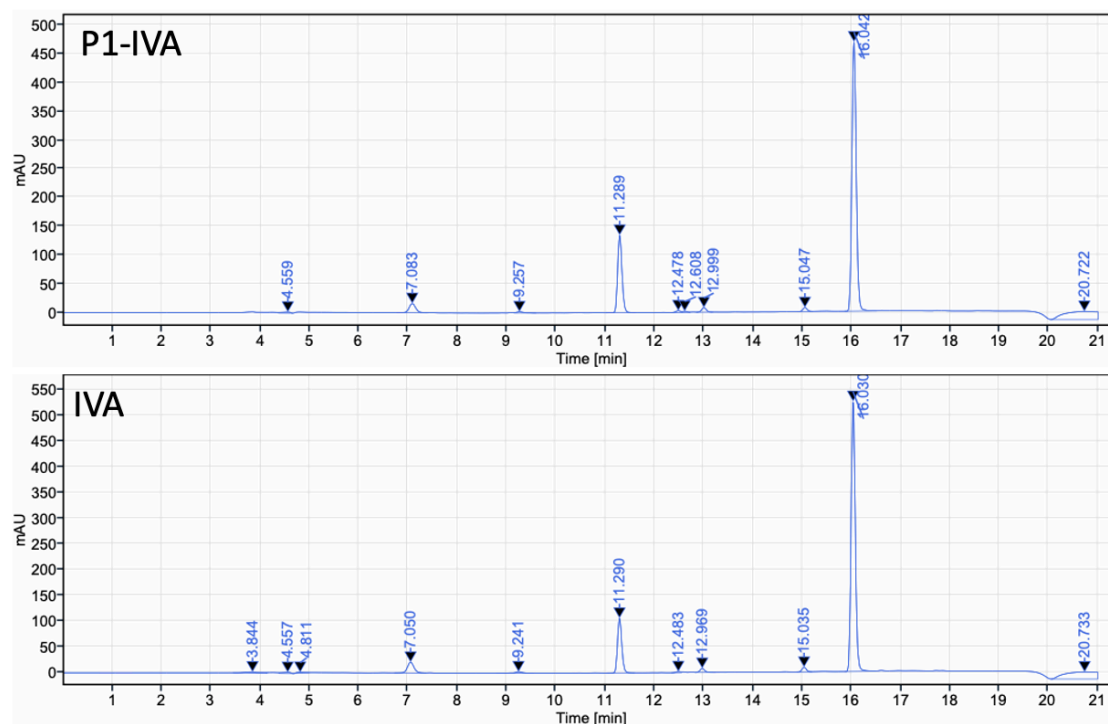
4.5 Appendix



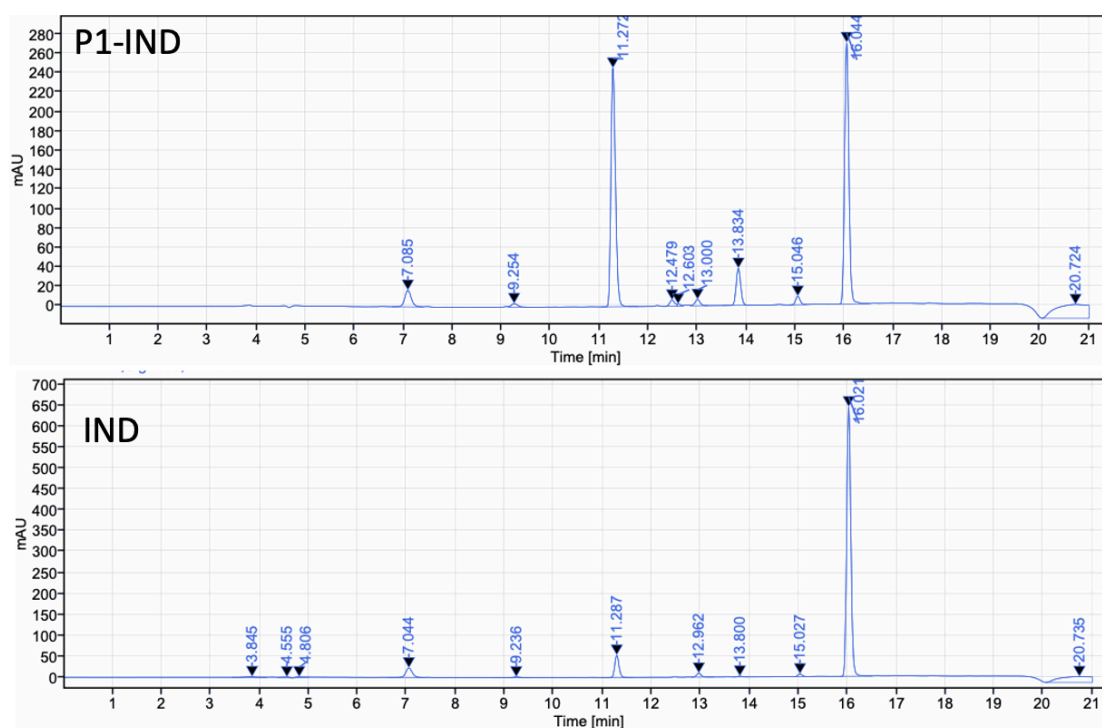
S.I. Figure 4.1 HPLC chromatogram of filtered supernatant for *E.coli* MC4100 pSTB7 cultures following incubation in the presence of 0.42 μ M P1-ICA (top) and 0.42 μ M ICA (bottom) for 24h, followed by incubation in the reaction buffer for an additional 24 h.



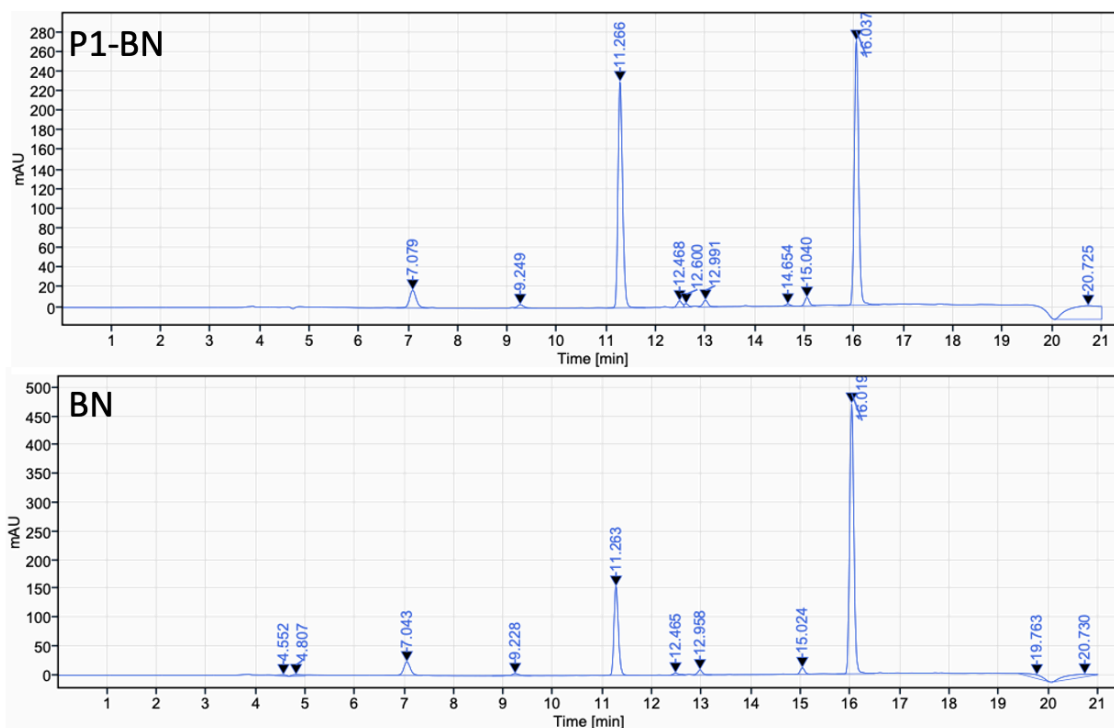
S.I. Figure 4.2 HPLC chromatogram of filtered supernatant for *E.coli* MC4100 pSTB7 cultures following incubation in the presence of 0.42 μ M P1-AFP (top) and 0.42 μ M AFP (bottom) for 24h, followed by incubation in the reaction buffer for an additional 24 h.



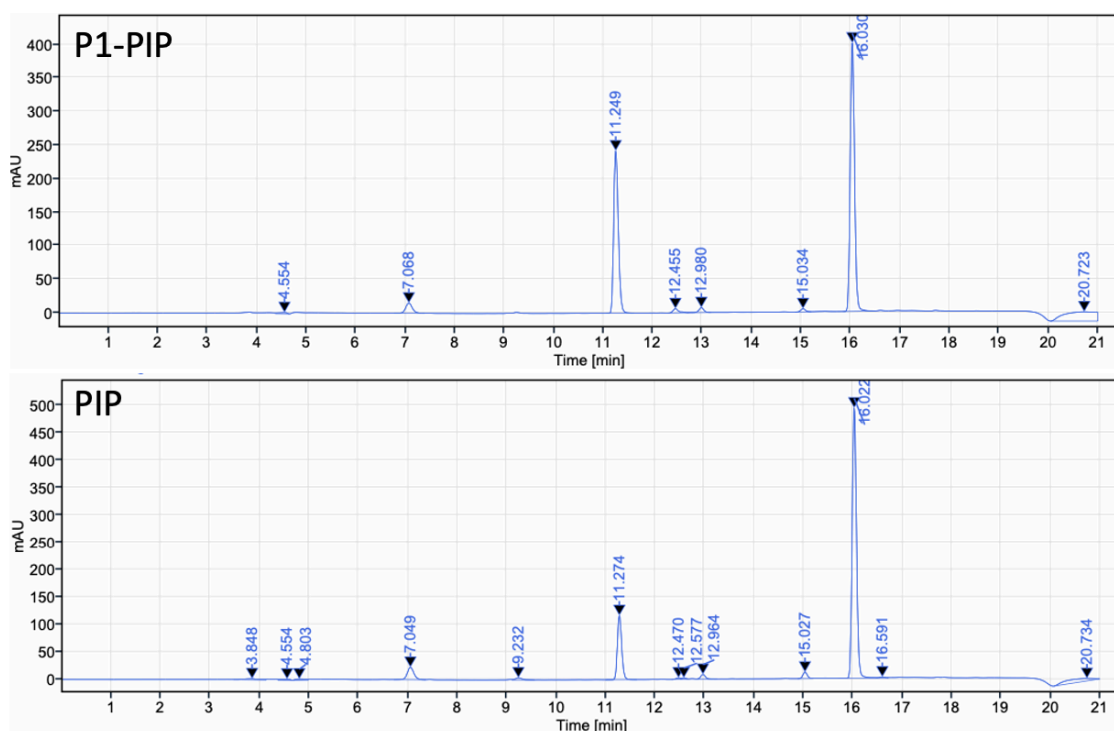
S.I. Figure 4.3 HPLC chromatogram of filtered supernatant for *E. coli* MC4100 pSTB7 cultures following incubation in the presence of 0.42 μ M P1-IVA (top) and 0.42 μ M IVA (bottom) for 24h, followed by incubation in the reaction buffer for an additional 24 h.



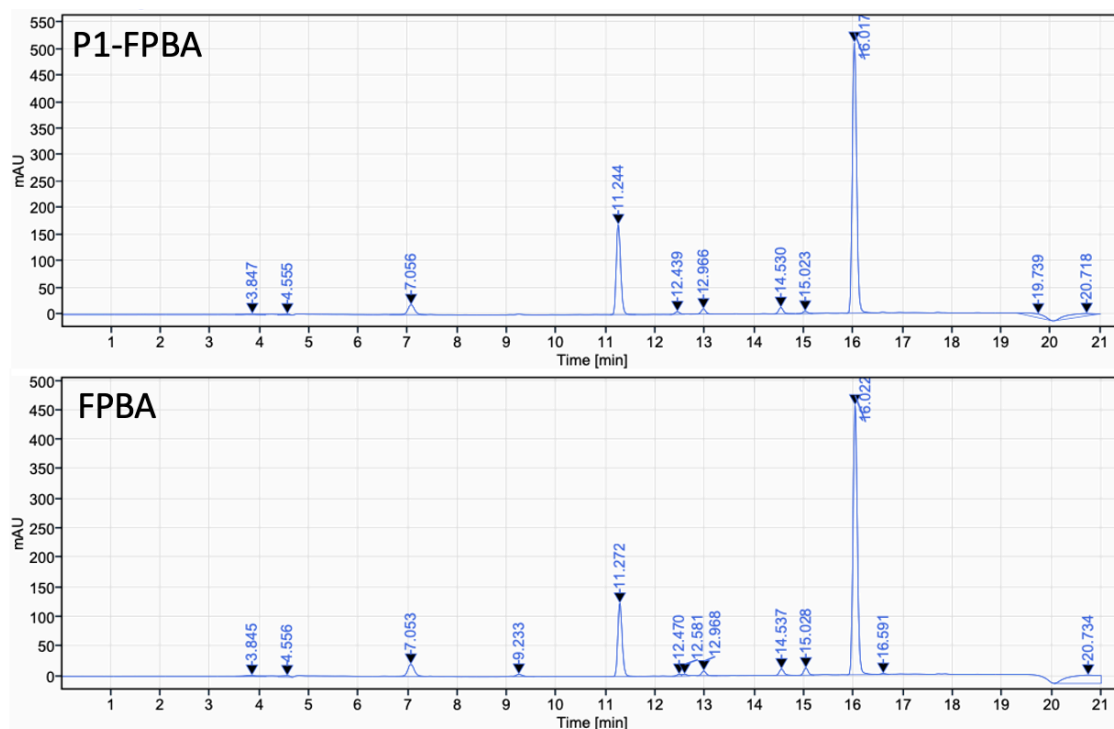
S.I. Figure 4.4 HPLC chromatogram of filtered supernatant for *E. coli* MC4100 pSTB7 cultures following incubation in the presence of 0.42 μ M P1-IND (top) and 0.42 μ M IND (bottom) for 24h, followed by incubation in the reaction buffer for an additional 24 h.



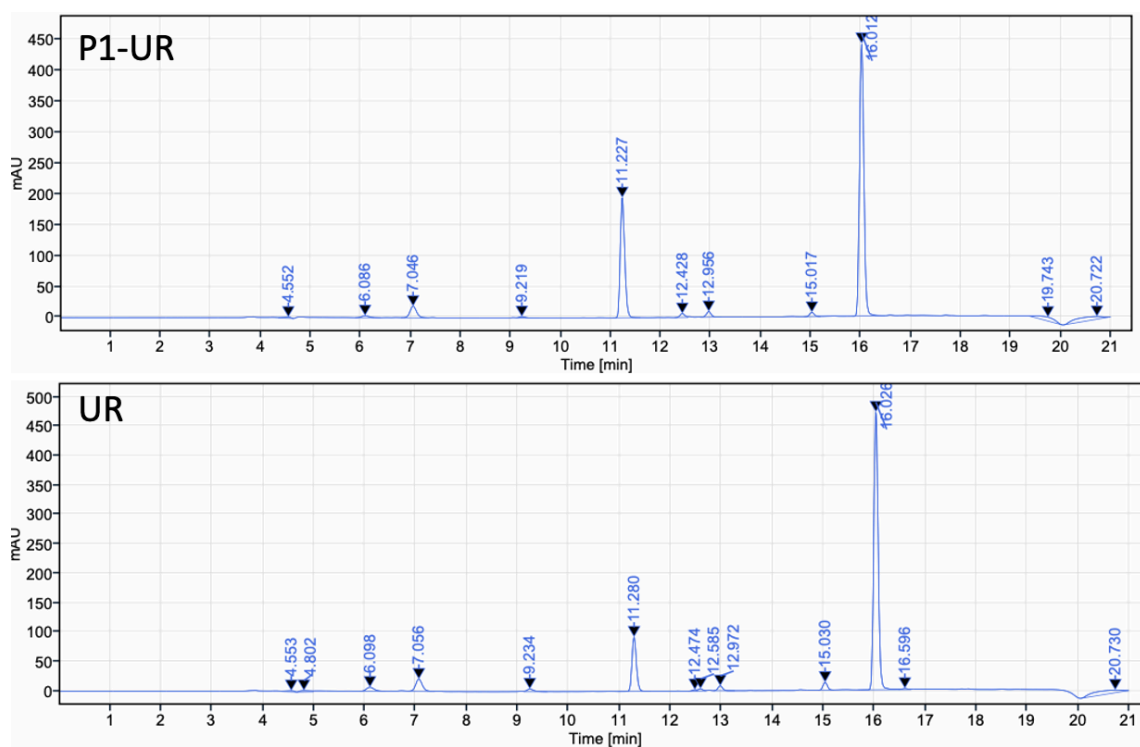
S.I. Figure 4.5 HPLC chromatogram of filtered supernatant for *E.coli* MC4100 pSTB7 cultures following incubation in the presence of 0.42 μ M P1-BN (top) and 0.42 μ M BN (bottom) for 24h, followed by incubation in the reaction buffer for an additional 24 h.



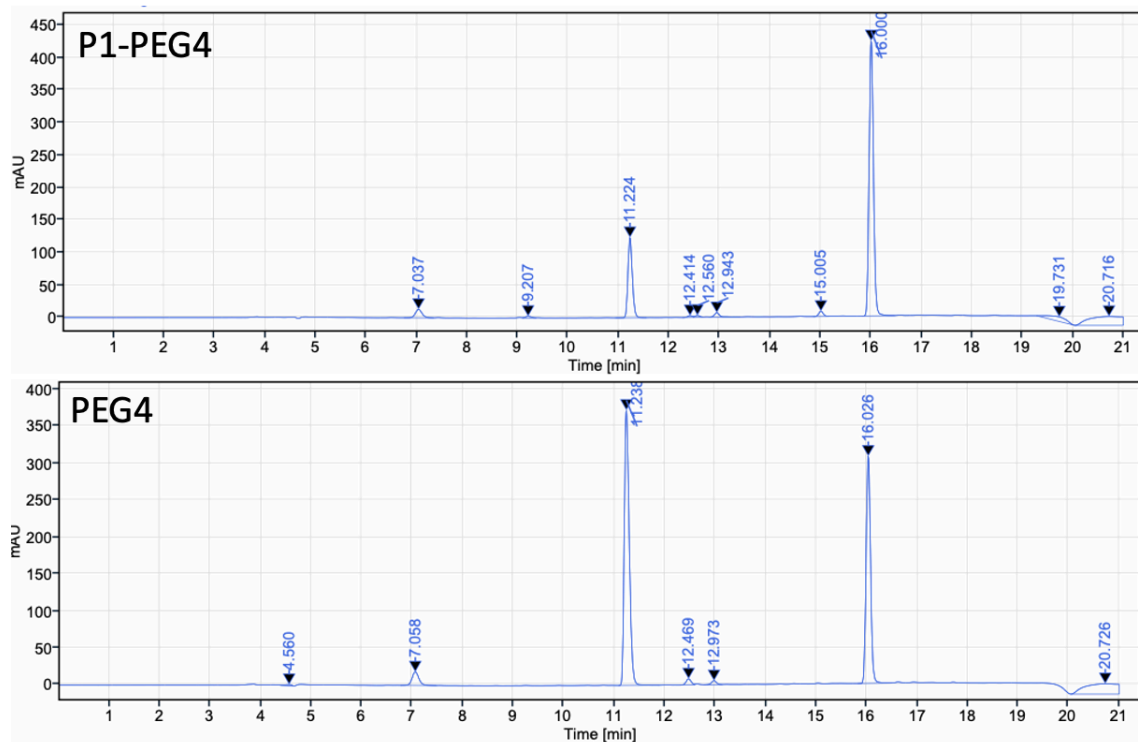
S.I. Figure 4.6 HPLC chromatogram of filtered supernatant for *E.coli* MC4100 pSTB7 cultures following incubation in the presence of 0.42 μ M P1-PIP (top) and 0.42 μ M PIP (bottom) for 24h, followed by incubation in the reaction buffer for an additional 24 h.



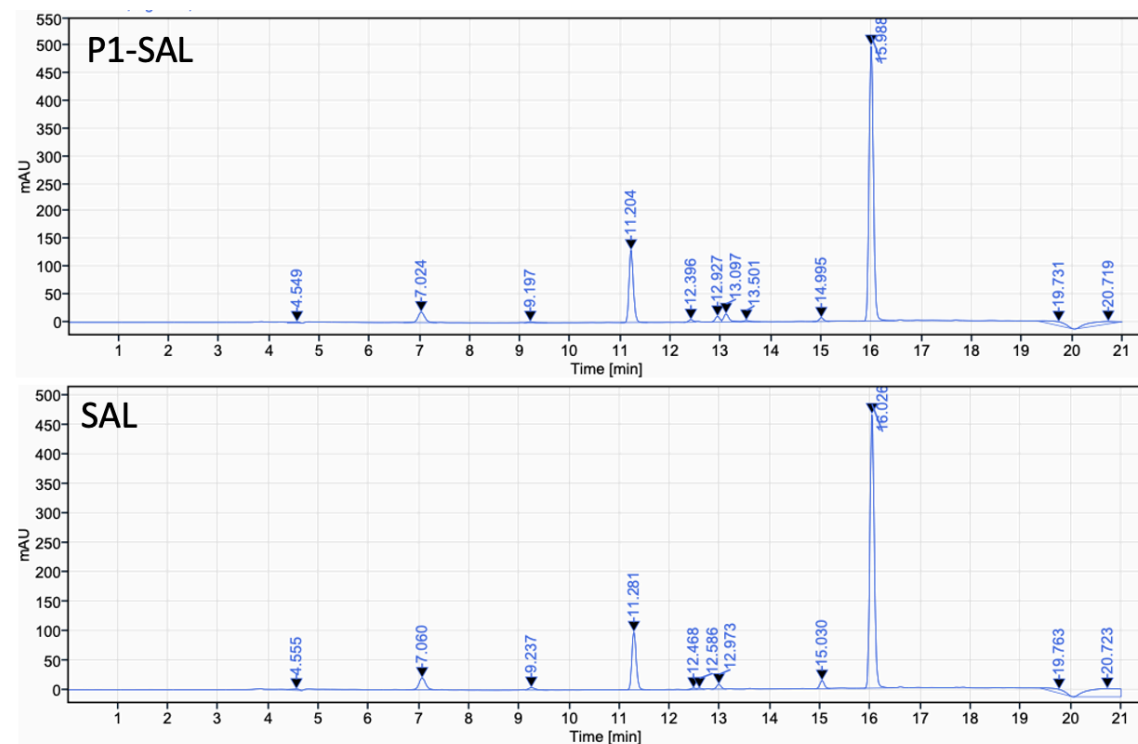
S.I. Figure 4.7 HPLC chromatogram of filtered supernatant for *E. coli* MC4100 pSTB7 cultures following incubation in the presence of 0.42 μ M P1-FPBA (top) and 0.42 μ M FPBA (bottom) for 24h, followed by incubation in the reaction buffer for an additional 24 h.



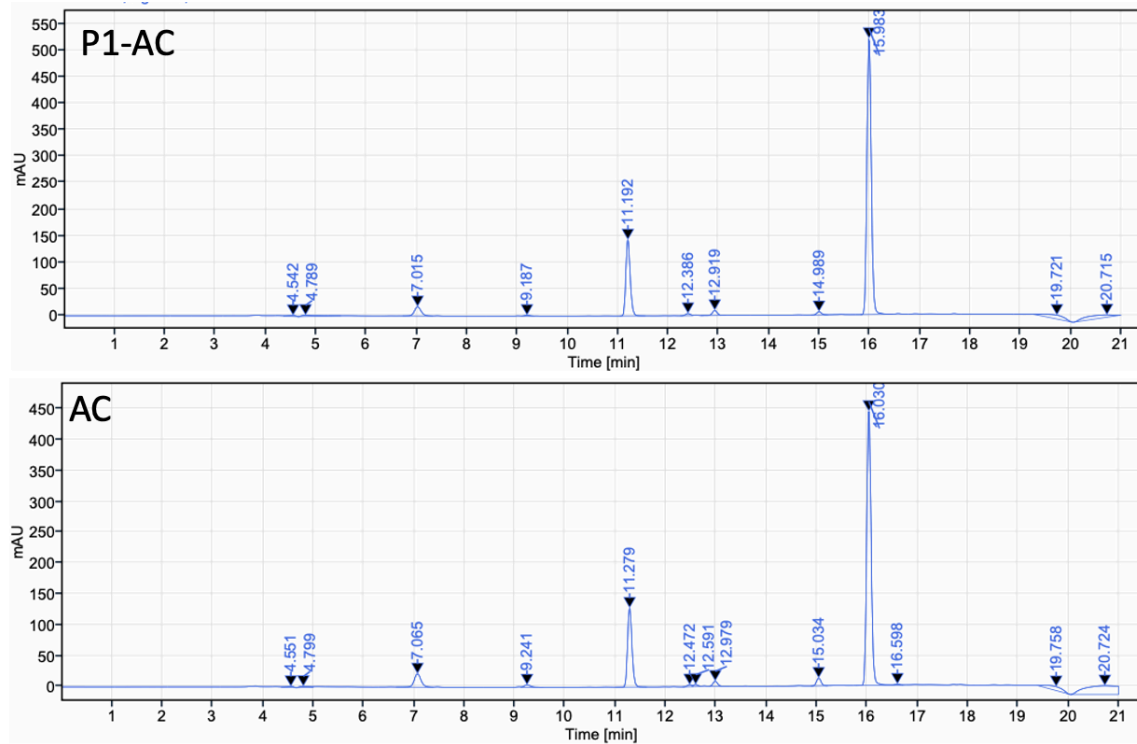
S.I. Figure 4.8 HPLC chromatogram of filtered supernatant for *E. coli* MC4100 pSTB7 cultures following incubation in the presence of 0.42 μ M P1-UR (top) and 0.42 μ M UR (bottom) for 24h, followed by incubation in the reaction buffer for an additional 24 h.



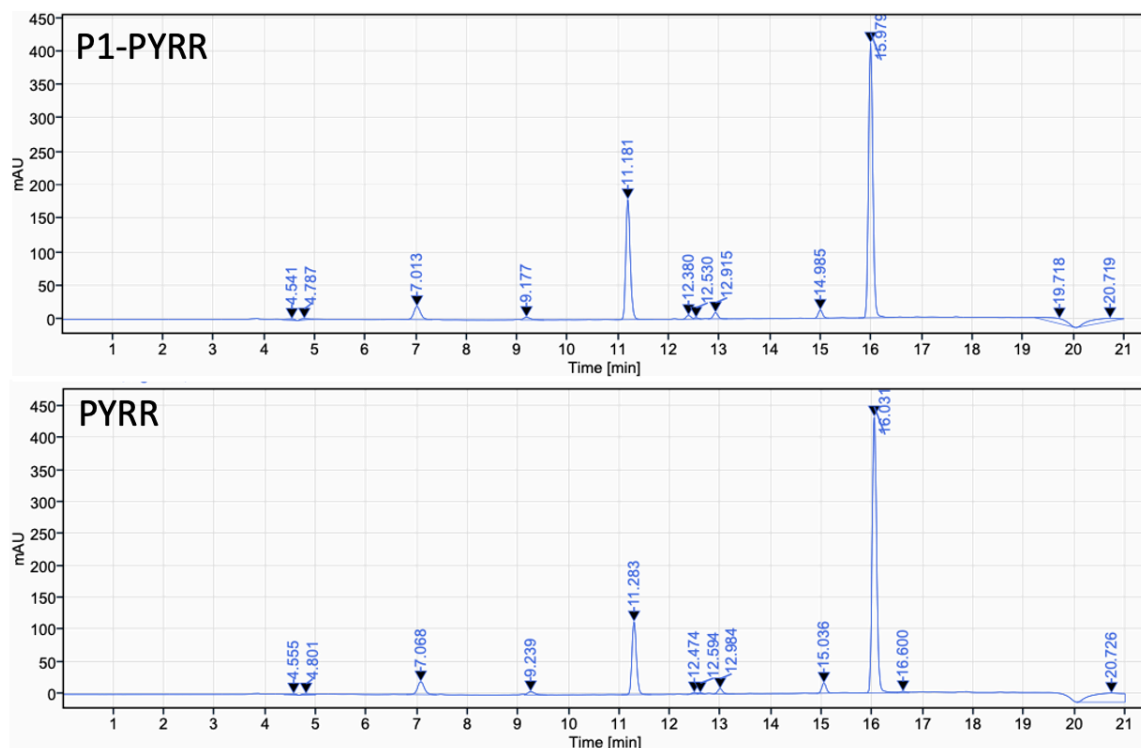
S.I. Figure 4.9 HPLC chromatogram of filtered supernatant for *E.coli* MC4100 pSTB7 cultures following incubation in the presence of 0.42 μ M P1-PEG₄ (top) and 0.42 μ M PEG₄ (bottom) for 24h, followed by incubation in the reaction buffer for an additional 24 h.



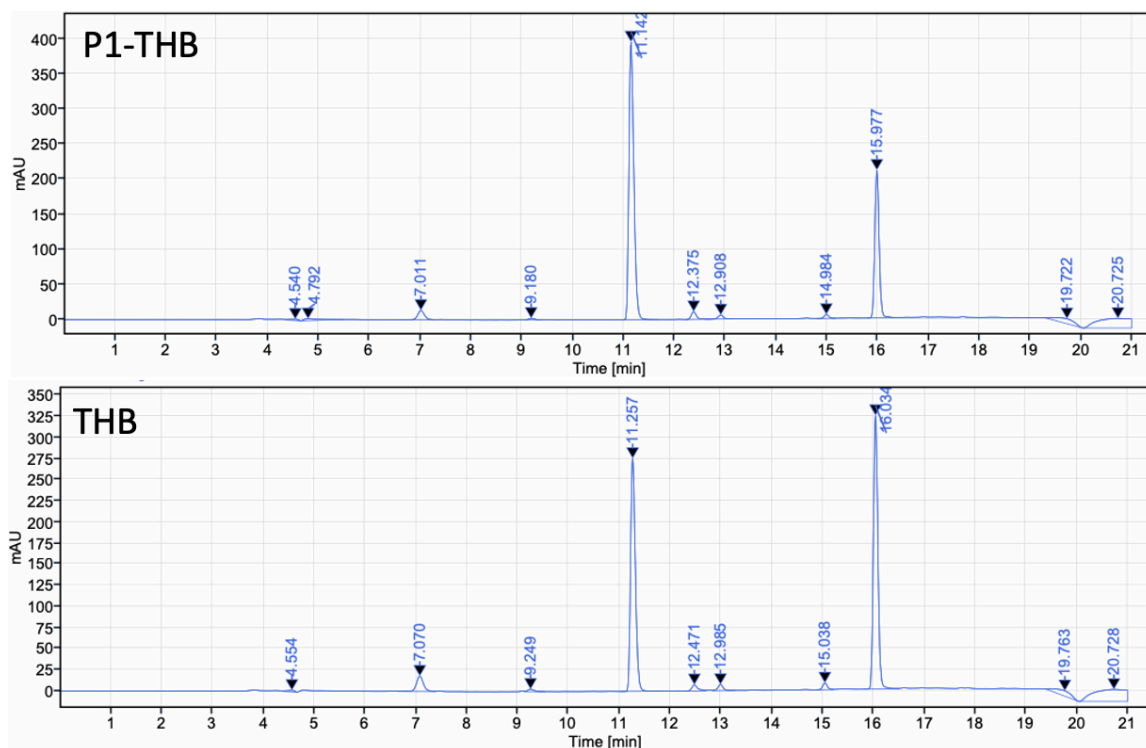
S.I. Figure 4.10 HPLC chromatogram of filtered supernatant for *E.coli* MC4100 pSTB7 cultures following incubation in the presence of 0.42 μ M P1-SAL (top) and 0.42 μ M SAL (bottom) for 24h, followed by incubation in the reaction buffer for an additional 24 h.



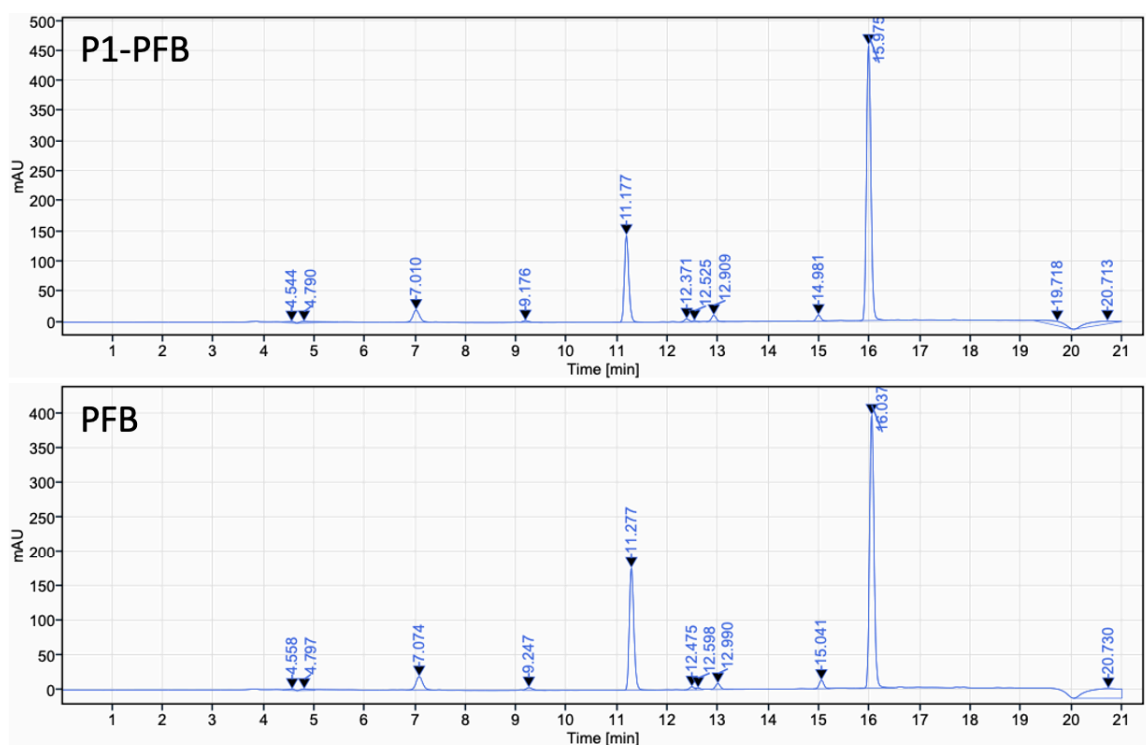
S.I. Figure 4.11 HPLC chromatogram of filtered supernatant for *E.coli* MC4100 pSTB7 cultures following incubation in the presence of $0.42 \mu\text{M}$ P1-AC (top) and $0.42 \mu\text{M}$ AC (bottom) for 24h, followed by incubation in the reaction buffer for an additional 24 h.]



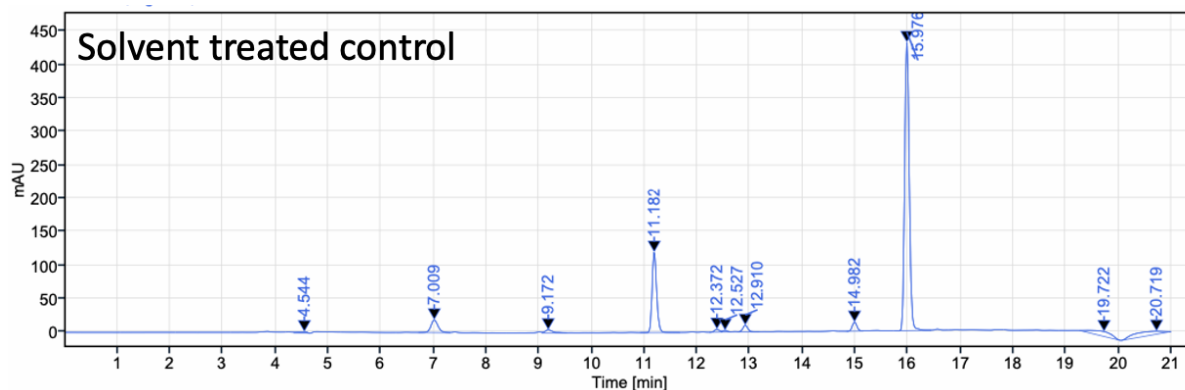
S.I. Figure 4.12 HPLC chromatogram of filtered supernatant for *E.coli* MC4100 pSTB7 cultures following incubation in the presence of $0.42 \mu\text{M}$ P1-PYRR (top) and $0.42 \mu\text{M}$ PYRR (bottom) for 24h, followed by incubation in the reaction buffer for an additional 24 h.



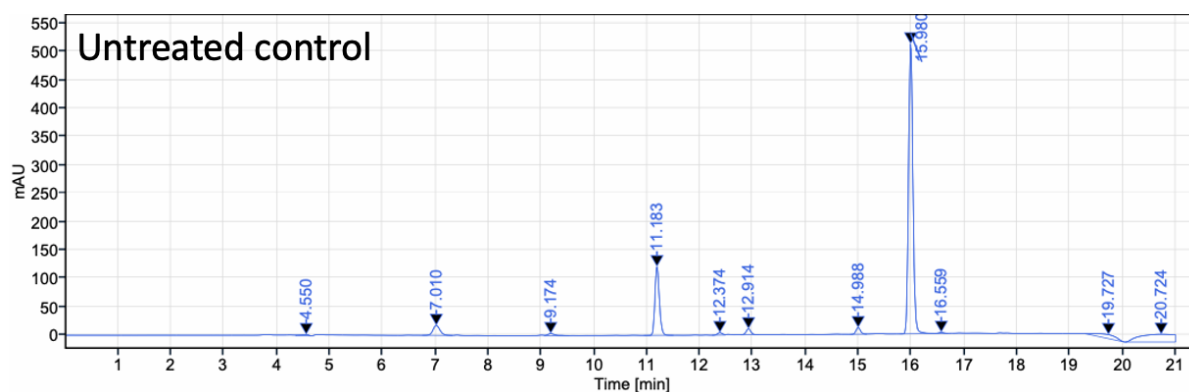
S.I. Figure 4.13 HPLC chromatogram of filtered supernatant for *E.coli* MC4100 pSTB7 cultures following incubation in the presence of 0.42 μ M P1-THB (top) and 0.42 μ M THB (bottom) for 24h, followed by incubation in the reaction buffer for an additional 24 h.



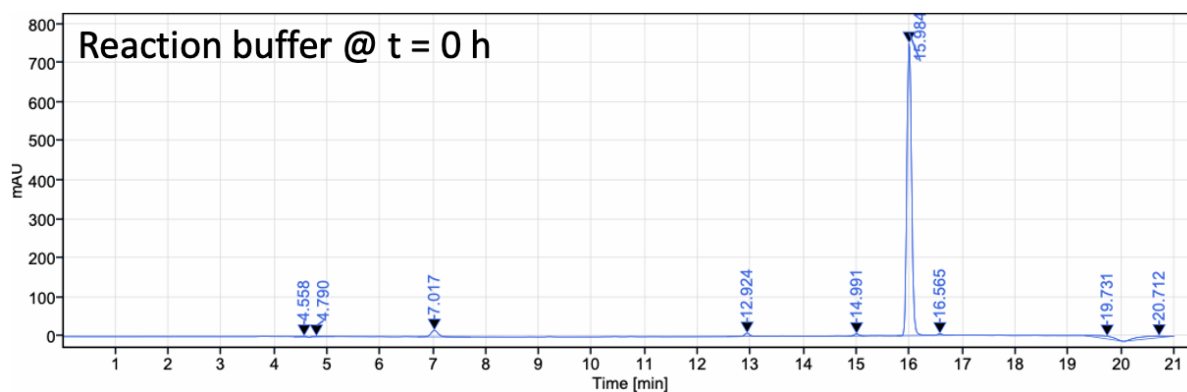
S.I. Figure 4.14 HPLC chromatogram of filtered supernatant for *E.coli* MC4100 pSTB7 cultures following incubation in the presence of 0.42 μ M P1-PFB (top) and 0.42 μ M PFB (bottom) for 24h, followed by incubation in the reaction buffer for an additional 24 h.]



S.I. Figure 4.15 HPLC chromatogram of filtered supernatant for *E. coli* MC4100 pSTB7 cultures following incubation in the presence of 1:1 DMSO/0.2M AcOH (10 μ L), followed by incubation in the reaction buffer for an additional 24 h.



S.I. Figure 4.16 HPLC chromatogram of filtered supernatant for untreated *E. coli* MC4100 pSTB7 cultures incubated for 24h, followed by incubation in the reaction buffer for an additional 24 h.



S.I. Figure 4.17 HPLC chromatogram of filtered fresh reaction buffer in the absence of *E. coli*.

Chapter 5 – Conclusions & Future Work

The aim of this thesis was to test the feasibility of helical polymer materials as nucleating agents for biofilm formation in *E. coli*. The initial stages of this project focussed on the development of a novel poly(acetylene) scaffold – poly(propargyl hydrazine carboxamide) (P1) that was capable of post-polymerisation to allow for easy generation of a material library. To the best of our knowledge, it is the first example of a post-polymerisation modification of a poly(acetylene) that utilised hydrazone click chemistry. The monomer was synthesised in good yields (60%) in a one-pot synthesis, and polymerisation of M1 showed quantitative yields with quantitative cis-character. Post-polymerisation modification was successful with a broad range of chemical substrates. Furthermore, spectroscopic studies suggested that P1 may adopt a helical conformation following functionalisation.

The material library derived from P1 was used to treat the biotechnologically relevant strain *E. coli* MC4100. Biofilm formation was assessed with respect to polymer-induced aggregation and subsequent extracellular matrix (ECM) formation where temporal production of curli, PNAG and colanic acid were all measured following polymer treatment. Polymer treatment was essential to aggregate formation, where increased polymer hydrophobicity induced greater aggregation in the bacteria. Construction of phase diagrams suggested that polymer-induced aggregation proceeded by bridging aggregation in all formulations. Generally, polymers significantly increased curli and colanic acid production, but there was no significant change in PNAG production. Surprisingly, ECM production showed a negative correlation with aggregation where diminished colanic acid and curli production was observed in formulations that were strong aggregators. In conclusion, given the necessity of P1 formulations to form aggregates and the significant increase in curli and colanic acid it can be concluded that P1 is

a suitable scaffold for biofilm engineering in *E. coli* MC4100. However, the mechanisms behind this currently remain unknown as reduction in cell viability was ruled out and investigation into potential stress mechanisms were inconclusive. Polymer-induced aggregation may circumvent the requirement for ECM production as the polymers could act as an artificial ECM allowing the bacteria to 'reallocate' metabolic resources. Although conclusions regarding the mechanisms are beyond the scope of this project, it opens exciting avenues to explore. Future work would strongly benefit from transcriptomics analyses in polymer-treated cultures to help identify the role of formulation at the gene level. Furthermore, if automation is possible then the number of polymer formulations could be greatly increased. Increasing the formulations tested would greatly increase the statistical power of these studies. In conjunction with transcriptomics, a QSAR type analysis could be performed to determine possible structure-activity relationships regarding biofilm formation. This would be highly useful in the development of both pro- and anti-biofilm materials, regardless of the potential application.

The final objective of this thesis was to test the polymer-induced biofilms within the sphere of biocatalysis. The model biocatalytic reaction to produce 5-fluorotryptophan (5F-Trp) from 5-fluoroindole was tested in *E. coli* MC4100 recombinantly overexpressing TrpBA. Performance between the cultures varied, though several formulations showed appreciable 5F-Trp formation after 24h. Potential differences in product yields may result from differing expressions of native indole and tryptophan permeases following polymer treatment. In future, the development of TrpBA (tryptophan permease) overexpression strains would promote product egress and likely enhance observed yields. Additionally, expanding the scope of tested biocatalytic reactions would also be useful to exemplify the potential this technology

has as a 'plug and play' system. Here different recombinant enzymes can be expressed to perform different biocatalytic reactions, or even a reaction cascade for potential one-pot multistage syntheses. From a process engineering stand-point it would be interesting to see how this technology can be scaled. Currently it is likely limited due to the susceptibility of the aggregates to hydrodynamic shear. Therefore, different reactor designs such packed-bed, trickle-bed, fluidised-bed, and air-lift reactors could all be tested as potential low shear environments to scale-up this technology.

This page is left intentionally blank.